UNIVERSITY OF SOUTHAMPTON

FACULTY OF NATURAL AND ENVIRONMENTAL SCIENCES

School of Ocean and Earth Science

The role of the seagrass *Zostera noltii* on sand transport across an intertidal sand flat in Ryde, Isle of Wight

by

Mohamad Anas Mohamad Annuar

Thesis for the degree of Doctor of Philosophy

April 2021

Supervisors:

Dr. Charlotte Thompson, NOC

Prof. Steve Hawkins, FNES

Chair of the Advisory Panel:

Dr. Ivan Haigh, NOC

UNIVERSITY OF SOUTHAMPTON

ABSTRACT

FACULTY OF NATURAL AND ENVIRONMENTAL SCIENCES

Doctor of Philosophy

THE ROLE OF SEAGRASS *ZOSTERA NOLTII* ON SAND TRANSPORT ACROSS THE INTERTIDAL FLAT IN RYDE, ISLE OF WIGHT

Mohamad Anas Mohamad Annuar

Seagrass meadows are known to buffer wave energy, reduce current velocities and hence can provide stability to the coasts. The presence of seagrass on the seabed modifies the dynamics of the benthic boundary layer and thus the sediment transport. The overall aim of this project is to address the limited knowledge on the interactions between seagrass, seabed and the counteracting sedimentary processes by investigating interactions between the intertidal seagrass *Zostera noltii* and the surrounding sediments. Specifically, I am investigating how this species affects the mean flow, the turbulence in the canopy, and the resulting sediment mobilisation. *Zostera noltii* shows a strong seasonality, therefore the intertidal area of Ryde, Isle of Wight was monitored monthly over two annual cycles to assess the effect of seasonal changes on sediment characteristics and bed morphology. Grain size trend analysis was carried out in order to investigate the sand transport pathways on the intertidal flat in the region of seagrass. Sediment transport patterns were defined using Grain Trend Analysis. The Ryde intertidal flat is composed mainly of fine, well sorted and positively skewed sand. The transport vectors suggest a westward transport on the west side of Ryde Pier and an on-offshore transport on the east side of Ryde Pier. Gradients in sediment texture and composition were related to the season and influenced by meadow distribution and density. This was attributed to the mechanical trapping of particles and enhanced deposition due to dampening of current and wave action in the meadows. Locations inhabited by seagrass showed less change in bed morphology compared to bare sand areas. The tidal flat was found to be stable or exhibited minor bed accretion (cms) along vegetated profiles. Laboratory experiments carried out in a recirculating and annular flume on *Zostera noltii* showed that turbulence and mean flow were reduced within the canopy indicating low sediment transport in the region of the seagrass. Seagrass increases deposition in summer by modifying the boundary layer through its above-ground biomass and resists erosion in winter by increasing cohesiveness of the bed through its below-ground biomass (roots and rhizomes). Despite the reduction in seagrass canopy influence on the hydrodynamic forcing, the persistent presence of below-ground biomass all year round reduces sediment transport hence providing stability to the bed.

Table of Contents

List of Tables

List of Figures

DECLARATION OF AUTHORSHIP

I, Mohamad Anas Mohamad Annuar declare that this thesis and the work presented in it are my own and has been generated by me as the result of my own original research.

The role of the seagrass *Zostera noltii* on sand transport across an intertidal sand flat in Ryde, Isle of Wight

I confirm that:

1. This work was done wholly or mainly while in candidature for a research degree at this University;
2. Where any part of this thesis has previously been submitted for a degree or any other qualification at this University or any other institution, this has been clearly stated;
3. Where I have consulted the published work of others, this is always clearly attributed;
4. Where I have quoted from the work of others, the source is always given. With the exception of such quotations, this thesis is entirely my own work;
5. I have acknowledged all main sources of help;
6. Where the thesis is based on work done by myself jointly with others, I have made clear exactly what was done by others and what I have contributed myself;
7. None of this work has been published before submission

Signed:

Date: 15 April 2021

Acknowledgements

Praise to Allah S.W.T by whose grace and blessing, I have successfully completed my research. Thanks for His greatest love and blessing.

I would also like to express my heartfelt appreciation to my supervisors, Dr. Charlotte Thompson and Professor Steve J. Hawkins for their guidance throughout this project especially during my writing process. They have been source of valuable guidance, feedback and advice. I am also very grateful to Professor Carl L. Amos for supervising me through most part of this research. His expertise in field observation and unbounded enthusiasm for science are invaluable.

My special thanks go to my family. I am indebted to my beloved mother, Hjh. Zanariah, my father, Hj. Annuar and all my siblings, Asma', Alyaa and my late sister, Amirah. Even though you are not here with us, you are such an inspiration and motivation to me.

I would like to acknowledge the Ministry of Higher Education and Universiti Malaysia Terengganu (UMT) for the scholarship received for this research. The field and laboratory work involved in this project could not have been successfully completed without the vital assistance of Hachem Kassem, Matthias Thomsen, Oliver Hogg, Clementine Chirol, Izwan, Hilman, Syarawi, Sanusi, Amer, Adull, Fisham and the rest of Keluarga Southampton guys, and all those who helped me during my monthly survey. Without these guys, field data collection, processing and analysis would have been virtually impossible.

Finally, my very special thanks goes to my wife, Sofia Shahir. Thank you for your patience, care, support and for always being there for me during this tough times and always filling me with love. And to the apple of our eyes, my daughter Maryam. Thank you for bringing me more joy than I could ever have imagined possible.

Chapter 1: Introduction

1.1 General context of the study

The worlds coasts are under pressure from the landward side due to development stemming from human population growth much of which is concentrated at coastlines (Nicholls et al., 2007; Ruberti et al., 2018). From the seaward side, they are also subject to a variety of human impacts associated with coastal development and resource exploitation (Meinesz et al., 1991; Sundblad & Bergström, 2014; Thompson et al., 2002). They are also under increasing threat from climate change leading to greater storminess (Lowe & Gregory, 2005; Messori et al., 2016) and sea level rise (Möller et al., 2014; Valle et al., 2014), with the risks of coastal flooding and erosion accelerating (McNinch, 2004). Natural habitats are thus under multiple pressures which can compromise delivery of a variety of valuable ecosystems services such as natural coastal protection and carbon sequestration (Costanza et al., 1997)). Previously, hard engineering approaches (i.e. rock revetments, groynes, breakwaters) were used extensively as coastal defence solutions to erosion (Liu et al., 2019). In recent years, however, coastal engineers have been exploring soft engineering solutions (i.e. vegetation planting, reef restoration) to mimic natural defence processes (Ferrario et al., 2014; Narayan et al., 2016). These forms of protection are not suitable for all coastal areas, but where applicable such an approach is generally more cost effective and environmentally sustainable (Airoldi et al., 2005; Arkema et al., 2013; Firth et al., 2016).

Coastal natural habitats such as seagrass meadows (Potouroglou et al., 2017), salt marshes (Möller et al., 2014), coral reefs (Ferrario et al., 2014), and mangroves (Montgomery et al., 2018) are regarded as natural defences for the shoreline (Arkema et al., 2013). These habitats act as buffers to incoming large waves and currents especially during stormy seasons (Rupprecht et al., 2017). Seagrass meadows in particular offer coastal protection by promoting deposition of particles (Gacia & Duarte, 2001; Gacia et al., 1999), reducing the hydrodynamic forces of waves (Fonseca & Cahalan, 1992; Manca et al., 2012; Paul & Amos, 2011; Stratigaki et al., 2011), currents (Lefebvre et al., 2010; Nepf, 1999) and reducing sediment re-suspension (Cabaço et al., 2008; Gacia & Duarte, 2001; Ganthy et al., 2015; Ward et al., 1984). Seagrass abundance, particularly in temperate regions, generally has a unimodal seasonal development, peaking in the dry season/ summer when the temperature and light are more favourable (Bargain et al., 2013; Ganthy et al., 2013; Hillman et al., 1995; Paul & Amos, 2011).

The food, shelter and habitat provided by seagrasses, as in other biogenic natural habitats (i.e salt marshes, mangrove forests, coral reefs), provide ideal breeding and feeding areas for many species including those commercially exploited (Lugendo et al., 2006; Polte & Asmus, 2006). They can be particularly important nursery grounds for commercial fish species (Cullen-Unsworth et al., 2014). The slow decomposition rates in seagrass sediments leads to accumulation of carbon, making these habitats a large carbon sink (Duarte et al., 2013; Fourqurean et al., 2012). Thus they provide many ecosystem services in addition to coastal protection (Nordlund et al., 2018).

Seagrasses are under threat (Terrados et al., 1999; Valle et al., 2014). They are declining due to both anthropogenic pressures such as habitat loss through coastal development (Short et al., 2014; Waycott et al., 2009) and eutrophication (van Katwijk et al., 2009). They can also be impacted by natural phenomena (Cabaço et al., 2008; Dolch et al., 2013; Rasheed et al., 2014). These include sediment burial and siltation triggered by storms and river inflows, occurring mostly during winter affecting seagrass mortality and growth (Cabaço et al., 2008; Han et al., 2012). Changes in such processes may in some cases be ultimately be linked to climate change leading to greater precipitation (Cloern et al., 2016) and stormier seas (Lowe & Gregory, 2005).

The hydrodynamics over a seagrass bed are commonly assessed in two separate forms: wave and steady flow dynamics. Under unidirectional flow, the additional drag exerted by plants reduces the mean flow within vegetated areas compared to the unvegetated ones (Kadlec, 1990; Shi et al., 1995). The energy transfer produces turbulence above the canopy that promotes sediment accumulation by reducing near bed stresses, therefore promoting deposition (Leonard & Luther, 1995; Nepf, 1999; Ward et al., 1984) and decreasing the re-suspension of sediment (Neumeier & Amos, 2006). On the other hand, wave dissipation in the vegetated canopy depends on the ratio of water depth to canopy height (Chen et al., 2007). A wave energy reduction of approximately 40% per metre of seagrass bed was found in four different seagrass species, *Halodule wrightii, Syringodium filiforme, Thalassia testudinum and Zostera marina* (Fonseca & Cahalan, 1992), with reductions of up to 80% by a single species (*Thalassia testudinum*) having been observed in the field (Prager & Halley, 1999). Furthermore, interaction of different seagrass species with hydro-sedimentary process differs, as shown by Fonseca & Cahalan (1992). The leaf-length, stiffness and motion are unique characteristics of each species. Paul & Amos (2011) compared drag coefficients induced by *Zostera noltii* with a *Thalassia testudinum* meadow (Bradley & Houser, 2009) and kelp mimics (Kobayashi et al., 1993; Mendez et al., 1999) and found that vegetation stiffness was the main parameter controlling drag.

Despite recognition of the important role vegetation plays in flow dynamics and how it affects sediment transport, work focusing on the direct morphodynamic evolution of sediment beds in response to vegetation has been lacking (Yager & Schmeeckle, 2013). It is essential to understand how seagrass meadows change the dynamics in the benthic boundary layer, where most of sediment transport is taking place, as these changes will have implications for coastal protection, shoreline management and coastal construction.

In the remainder of this introductory chapter, I justify my study and then review the literature before giving the overall aims and specific objectives of the thesis and the structure of the thesis.

1.2 Justification of this study

Increased awareness on the importance of seagrass beds for both coastal protection and nature conservation has prompted various conservation and restoration projects on this habitat (van Katwijk et al., 2009). Previous research has shown the effectiveness of seagrass in attenuating waves (Chen et al., 2007; Paul & Amos, 2011) and modifying steady flows (Fonseca et al., 2007; Lefebvre et al., 2010). The reduction of turbulence and shear velocity within a seagrass canopy indicates a reduction in the transfer of momentum to the bed, which should reduce sediment transport (Ganthy et al., 2015). Nevertheless, sand mobilisation within and around a seagrass bed remains unquantified. Field studies on a seasonal scale of sediment transport around seagrass meadows are rarely conducted. It is important in particular to have field measurements to validate the findings gathered through flume experiments. Moreover, most studies on seagrass have focused on the subtidal species, which tend to be larger, taller and present all year round. These includes species like *Posidonia oceanica* (Gacia & Duarte, 2001; Manca et al., 2012; Stratigaki et al., 2011) and *Zostera marina* (Fonseca et al., 1982; Lefebvre et al., 2010).

The emphasis of my study will be the smaller and shorter leafed species, *Zostera noltii*. This species grows on intertidal flats and shallow subtidal banks (Ondiviela et al., 2014). Compared to other, larger species, there is limited knowledge on the influences of *Zostera noltii* on hydro-sedimentary processes (Ganthy et al., 2013). The study site, Ryde, Isle of Wight was chosen as the test site for work on the intertidal *Zostera noltii* beds. Previous work carried out in the area has focused on wave attenuation by *Zostera noltii* (Paul & Amos, 2011). My work will focus on the sediment transport under unidirectional flow. The study area is also the subject of a long-term monitoring programme by the Channel Coastal Observatory (CCO) (accessible at http://www.channelcoast.org/), providing a context for my shorter-term study.

1.3 Coastal stability provided by vegetation

The coastal zone is characterised by a wide range of natural habitats including wetlands, tidal flats, sandy beaches and rocky headlands (Raffaelli & Hawkins, 1996). Vegetation in these habitats plays an important role in supporting biodiversity and commercial fisheries (Nordlund et al., 2018), improving water clarity (Bulmer et al., 2018) and sequestering carbon dioxide from the atmosphere and generating oxygen through photosynthesis (Dennison, 1987; Hendriks et al., 2014). Coastal vegetation such as seagrasses, mangroves and saltmarsh plants consist of above-ground biomass (i.e. shoots and leaves) that interact with the flow (Hendriks et al., 2010; Montgomery et al., 2018) and below-ground biomass (i.e. roots and rhizomes) that binds the bed (Christianen et al., 2013; Duarte et al., 1998). Consequently, such vegetation provide various physical ecosystem services including protection against coastal threats such as erosion by wind and waves especially during storm surges (Rupprecht et al., 2017) (Figure 1.1). Comparing vegetated and unvegetated plots across the globe, Potouroglou et al., (2017) found that seagrass meadows facilitate sediment surface elevation and reduce erosion. They reported an average increase of 31 mm per year in surface elevation. Surface elevations were found to fluctuate during the year with particle trapping and centrimetric accretion dominating the colonised area during the seagrass growing time (Ganthy et al., 2013). Erosion was recorded during degeneration period, however, it was less compared to the unvegetated area and overall net sediment accretion were recorded per year. Eroded sediment during the reduced seagrass density period were mostly finer particles that were resuspended (Ganthy et al., 2013; Wilkie et al., 2012).

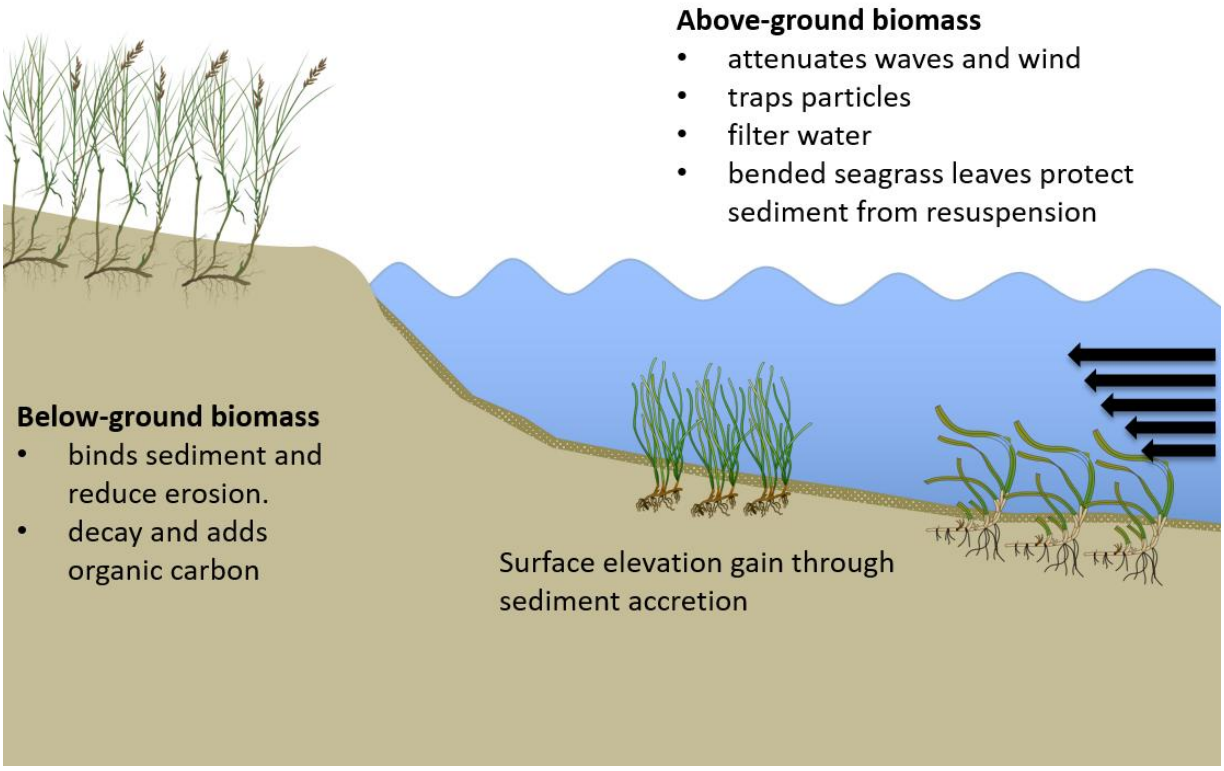

Figure 1.1: Physical services provided by coastal vegetation summarised from different sources (Charbonneau et al., 2016; Hendriks et al., 2010; Manca et al., 2012; Potouroglou et al., 2017).

Plants are able to alter the physical properties of a seabed in two ways; firstly through its extensive roots and rhizomes network and secondly by changing the sediment composition. The roots and rhizome helps to bind sediment (den Hartog, 1970). The leaves traps organic matter and finer sediment particles and thus increase the particle cohesion (Feagin et al., 2015).

The low energy and safe environment provided by vegetation attracts fishes and small invertebrates (Lugendo et al., 2006; Whitfield, 2017). In turn, microorganisms in this habitat generate biologically cohesive extracellular polymeric substances (EPS) that help to improve the cohesiveness of sediment with its surficial biofilm (Malarkey et al., 2015). They suggested that biological cohesion caused by the EPS is far stronger than physical cohesion. EPS increases the time of bedforms development by two orders of magnitude.

The efficiency of coastal vegetation reducing currents and waves and stabilising the sediment is related to ecosystem, the hydrodynamics and biological features of plants. Larger seagrass species in particular, are observed to offer a greater variety of ecosystem services compared to the smaller seagrass species (Nordlund et al., 2016). Nevertheless, smaller seagrass species offer important services, as it tends to have faster growth and turnover as compared to the larger seagrass species (Duarte, 1991).

1.4 Description of seagrass *Zostera noltii*

Zostera noltii, commonly known as dwarf eelgrass, is a common intertidal seagrass species in temperate European and African coasts. The distribution stretches from the shores of southern Norway to Mauritania (Auby & Labourg, 1996; Borum et al., 2004). In the UK, *Zostera noltii* populations occur on all of the coasts with higher concentrations in the south and west of England, eastern England and Scotland (Marsden & Chesworth, 2015) (Figure 1.2). The living biomass can be described as above-ground (leaves and shoots) and below-ground biomass (roots and rhizomes) (Figure 1.3). Each shoot of *Zostera noltii* generally has 2 to 5 narrow leaves that are attached to a horizontal rhizome by a short branch. The ribbon like, dark-green leaves are 5 to 27 cm long and 0.5 to 2 mm wide. The rhizome segments can be from 5 to 35 mm long and 0.5 to 2 mm thick. There are 1-4 roots attached to the internodes between the rhizome segments. The morphological variability of this seagrass species is highly dependent on sea bed morphology, light availability, sediment texture and chemical composition as well as the hydrodynamics of the environment (Peralta et al., 2000). Shorter leaves (17-22 cm) tend to develop in shallower and more dynamic waters, longer leaves (up to 45 cm) generally occur in more sheltered and deeper waters (Auby & Labourg, 1996; Paul & Amos, 2011; Peralta et al., 2000). Small leaf size is often proportional to high shoot density (Peralta et al., 2000).

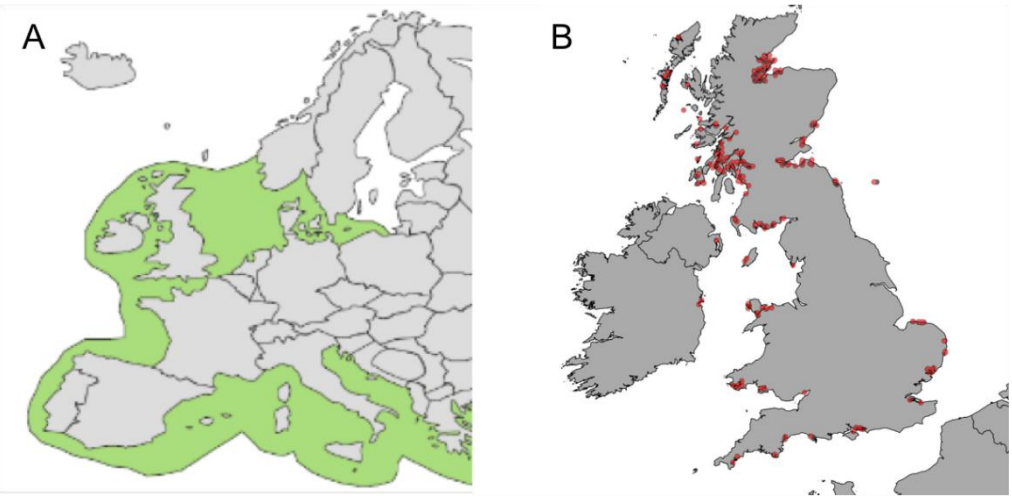

Figure 1.2: *Zostera noltii* distribution A) in Europe, source: (Borum et al., 2004) and B) around the United Kingdom, source:("National Biodiversity Network," 2017).

Seagrass abundance shows a cyclic, seasonal pattern. The shoot density increases from spring to summer and decreases from autumn to winter (Paquier et al., 2014; Paul & Amos, 2011; Vermaat & Verhagen, 1996). In the Mediterranean and Southwest of Netherlands, shoot densities are high (4000 - 22000 m^{-2}; Auby & Labourg, 1996) and (1000 – 23000 m^{-2};

Vermaat & Verhagen, 1996), respectively. These values are very high compared to shoot densities observed in lagoonal environments (536±182 m^{-2} in winter and 1037±480 m^{-2} shoots in summer).

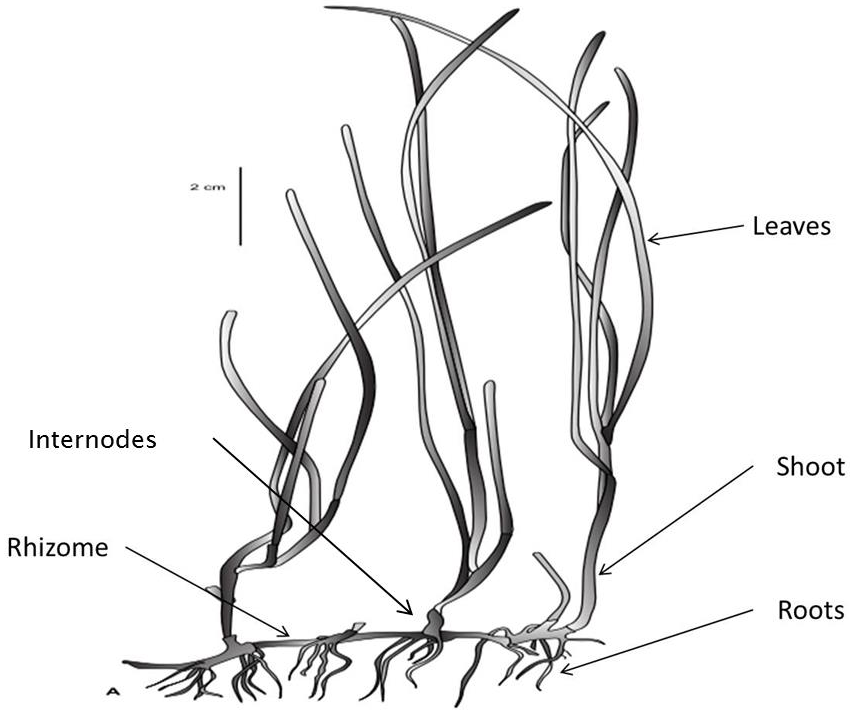

Figure 1.3: Schematic diagram of *Zostera noltii* morphology (modified from Borum et al. 2004).

In general, seagrass beds play an important role in ecosystem functioning (Bos et al., 2007; Bouma et al., 2005; Peralta et al., 2008). The existence of seagrass plants changes habitat complexity as the sheltered environment provides protection from predators, offers safe spawning areas and also a rich food supply (McMahon et al., 2014; Polte & Asmus, 2006). Moreover, seagrass sequestration of carbon makes it a major carbon sink (Duarte et al., 2013; Fourqurean et al., 2012).

Growing mainly in the intertidal area, *Zostera noltii* meadows are vulnerable to increases of sea level and temperature (Valle et al., 2014). It is also sensitive to sediment burial and erosion (Cabaço & Santos, 2007; Cabaço et al., 2008). This species is listed in the IUCN Red List of Threatened Species as having a decreasing population trend and has a 'Least Concern' status (IUCN, 2016). In the UK, it is listed as Nationally Scarce (only present in 16 - 100 of the UK's ten km square units, Marsden & Chesworth, 2015). Declining *Zostera noltii* populations have an adverse effect on organisms relying on the seagrass (Cardoso et al., 2008). The declining trend has prompted rehabilitation and restoration programmes to be conducted as knowledge on its stabilizing effects on the sea bed increases (Bos & van Katwijk, 2007; van Katwijk et al., 2009). Hence, it is important to understand the interaction between this

particular seagrass with hydro-sedimentary processes to ensure successful restoration programs.

1.4.1 Previous work on *Zostera noltii*

While studies on the influence of vegetation on channel flows have been executed in many research centres, most of these were done using structures mimicking vegetation properties (Anderson & Smith, 2014; Augustin et al., 2009; Manca et al., 2012; Paul et al., 2016). Moreover, little work has been done on *Zostera noltii* in particular. Studies on sediment transport within and around this seagrass species are even scarcer. In-situ experiments carried out by Thompson et al. (2004) investigated the role of *Zostera noltii* on flow dynamics and seabed erosion under unidirectional flow. They found that the presence of the seagrass reduced the bed shear stress and bed erosion by creating a closed canopy relative to a bare mud bed. The closed canopy produced reduced roughness and faster flow above the meadow, known as skimming flow. This investigation was conducted in February during the seasonal minimum seagrass density. The meadow is likely to grow to its full extent during summer and so does its influence on the sea bed. Another study was carried out at Ryde, Isle of Wight measuring wave attenuation by *Zostera noltii* (Paul & Amos, 2011). The results show that *Zostera noltii* effects the wave attenuation and the effect corresponds to the shoot density. There is a minimum amount of seagrass shoot density before the meadow can caused wave attenuation. They also found that the drag coefficient by the plant was not related to its seasonal parameters (i.e. height and density), but rather corresponded to hydrodynamic conditions. Ganthy et al. (2015) carried out the most recent study on the influence of *Zostera noltii* in a recirculating flume to investigate the impact of the shoots on the flow and sediment transport. Their experiment using real seagrass found the presence of skimming flow over the bended meadow similar to the study of Thompson et al. (2004) in the field. They also showed the importance of shoot density on flow modification and sediment erosion. Moreover, higher flow velocity resulted in higher attenuation. The highest shoot density (±18230 shoots/ m^2) resulted in 81 % flow attenuation whilst the lowest density (±7960 shoots/ m^2) caused 50 % flow attenuation at 0.4 m/s, respectively. Even though there is fundamental understanding on the effect of vegetation on flow dynamics and to a limited extent, suspended sediment transport, until now there have been no studies carried out to quantify bed load sediment transport in a natural *Zostera noltii* bed and the role of the below-ground biomass in sediment stabilisation.

1.5 Research aim and objectives

The overall aim of my study was to investigate the effect of seagrass, *Zostera noltii* on sediment transport and stabilisation across a sandy intertidal flat. In order to achieve this, the following three objectives were addressed by a combination of field measurements and laboratory experiments:

1. To provide understanding on the spatial changes of the intertidal flat and characterize the seagrass, sediment distribution, trends, and transport pathways. The determination of sand transport pathways was undertaken by means of grain-size trend analysis (GSTA). The effectiveness of GSTA technique over a vegetated bed was tested (Chapter 3).

2. To examine the temporal impact of *Zostera noltii* on intertidal flat stability in Ryde, Isle of Wight. Intertidal flats are subject to changes in water depth and tidal current flow speed. Moreover, the seagrass distribution varies greatly throughout the year (peak seagrass density during summer). Therefore, it was assumed that seagrass provides varied amounts of protection to the intertidal flat that is seasonal in frequency (Chapter 4).

3. To investigate the role of *Zostera noltii* on sand transport under unidirectional flow under laboratory (controlled) conditions. The presence of flexible vegetation will modify the flow structure thus affecting the benthic boundary layer and sediment transport rates. The impacts of plant density and height with flow structure, shear stress and sand transport will be evaluated (Chapter 5).

1.6 Thesis structure

This thesis consists of six chapters. This introductory (Chapter 1) provides an overview on the importance of studying the complex relationship between flow, seagrass and sediment transport. This chapter explains basic ecology of *Zostera noltii* and its distribution before elaborating on the flow behaviour involved in vegetated beds. Chapter Two describes the study area, which is the Ryde intertidal flat located at the northeast of the Isle of Wight. The methods used to analyse sediment and seagrass samples are also presented. In Chapter Three, I first explain the dynamics of a tidal flat. Then sediment transport pathways on the intertidal flat of Ryde, Isle of Wight determined using the Grain Size Trend Analysis is presented. It is backed by the analysis of LIDAR images. Chapter four describes the impact of *Zostera noltii* spatial and temporal impact of *Zostera noltii* intertidal flat stability. The environmental conditions of Ryde were characterised. It is then followed by discussion on the short-term and long-term evolution of the intertidal flats. Chapter Five presents a laboratory experimental study of small-scale influences of a *Zostera noltii* canopy on sediment mobilisation under the unidirectional flow. Investigations on the influence of seagrass towards unidirectional flow and sediment mobilisation were made using *Zostera noltii* mimics as well as real *Zostera noltii* with a sand bed. The flow dynamics and sand transport from the laboratory experiment are presented here. The report concludes with general discussion and a synthesis of the conclusions from all the chapters in Chapter Six, putting the work into a wider context.

Chapter 2: Study area and general methods

2.1 Study area

The *Zostera noltii* meadow covers approximately 5 hectares of the Ryde intertidal sand flat located on the northeast coast of the Isle of Wight (Figure 2.1). This area is sheltered from waves propagating up the English Channel, therefore the incoming waves are small with little influence of swell (Figure 2.2). It is a main route for passenger ferries and hovercrafts from Portsmouth to Ryde. Thus, the region is subject to the effects of boat wakes and the disruptive effect of the hovercraft at low tide. The hovercraft pathway cuts through a seagrass meadow on the east side of the Ryde Pier and appears to show an impact on the seabed (Figure 2.2 A). The area is subject to a semi-diurnal tide, and the tidal range is between 2 m during neap tides and 4 m during spring tides.

The most prominent artificial structure in the study region is the Ryde Pier, which extends approximately 700 m seawards and divides the study area into east and west flats. The pier was built on 25 cm diameter stilts (Figure 2.2 D). Parallel to the pier, there is a railway connecting Ryde to other parts of the island. The railway was built on square stilts with a dimension of 30 cm x 30 cm. New stilts (diameter: 45 cm) were recently added to support the railway. *In situ* observation suggests that refraction and reflection by the stilts were not evident. Thus they are not considered to have a huge influence on the hydrodynamics over the sand flats (Paul & Amos, 2011). However, there was scour-pits (holes diameter: ±30 cm) observed around the stilts suggesting minor, local morphological influence of the pier on sediment transport. Seawalls and revetments cover most of the shoreline along the landward margin of the coast.

Figure 2.1: Location of the study area, Ryde, Isle of Wight highlighted in the white box.

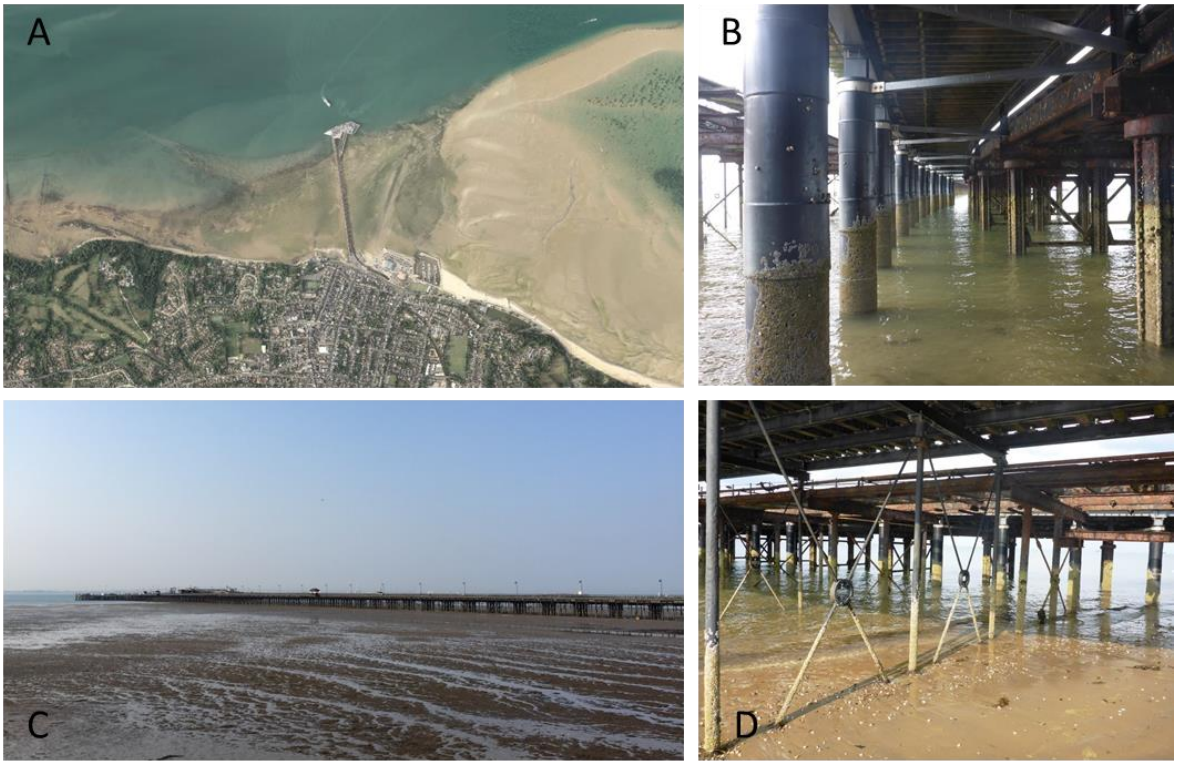

Figure 2.2: (A) The whole study area Ryde (source: CCO). A hovercraft pathway can be seen on the east side of Ryde Pier. (B) New stilts supporting the railway. (C) Ryde tidal flat during a spring low tide. (D) Stilts supporting the pier.

The seagrass meadows are exposed during low tides and occur between 0.6 m and 2.3 m below Mean Sea Level (MSL), slightly changed from what was recorded by Paul (2011) which was between 0.7 m and 2.7 m below MSL. The Hampshire and Isle of Wight Wildlife Trust has identified that this site should be designated as a Marine Conservation Zone due to its importance environmentally as a food source, nursery ground and sheltered habitat to a host of marine and coastal species (Marsden & Scott, 2015). The study area is divided into "Ryde East" and "Ryde West", referring to the east and west side of Ryde Pier.

Three types of *Zostera* species were recorded in the intertidal region of Ryde (Figure 2.3) in a report produced by the Hampshire and Isle of Wight Wildlife Trust. They are *Zostera marina, Zostera angustifolia* and *Zostera noltii*. *Zostera noltii* meadows colonize a major part of Ryde Sands. The shoot density of this species varies between 316±113 shoots m^{-2} in February 2009 and 2318±429 m^{-2} shoots in August 2009. Leaf lengths have an annual average value of 13±3 cm (Paul & Amos, 2011).

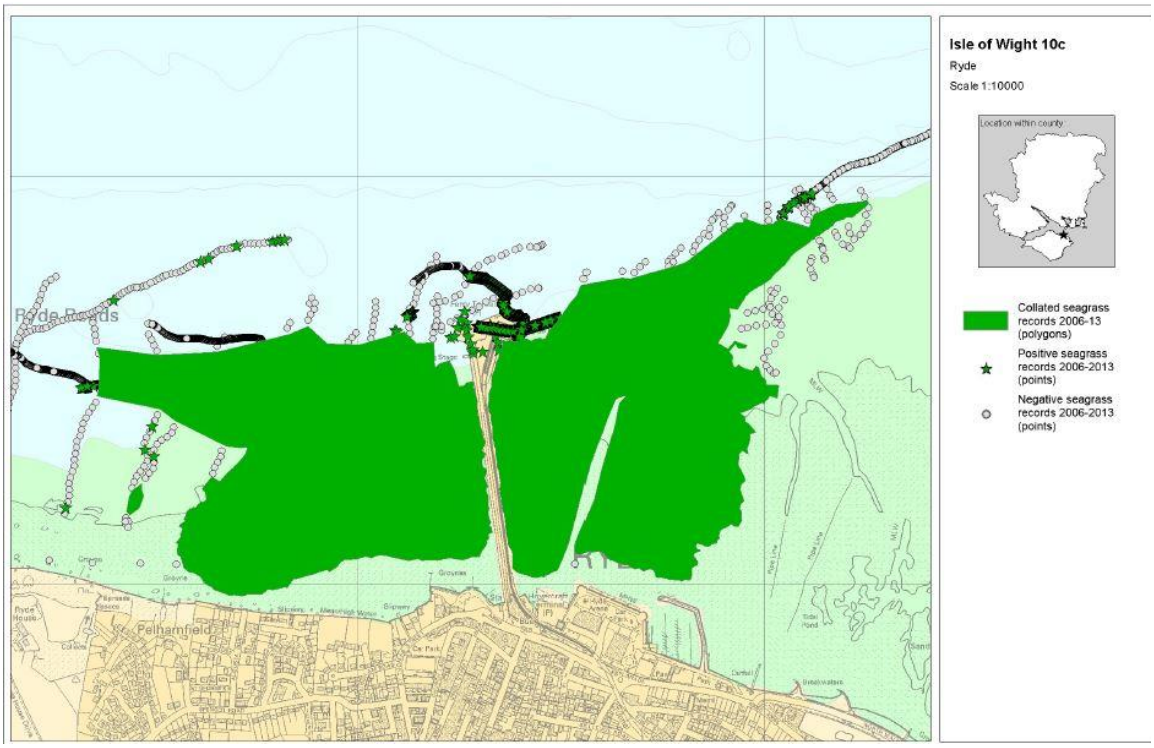

Figure 2.3: Seagrass distribution in Ryde, Isle of Wight (from Marsden & Scott, 2015).

2.2 Field methods

A pressure transducer (RBRduo by RBR Ltd.) was deployed from 20 April 2015 – 20 May 2015 to gather tide information in the study area. The pressure transducer was fixed on one of the pier stilt and positioned 0.5 m above the seabed, measured from the pressure sensor. It was set to measure continuously at 4 Hz. Two Electromagnetic Current Meters with an integrated Optical Backscatter Sensor, OBS (EMCM, Valeport Model 808) were deployed from 31 August – 4 September 2015 to monitor water depth and two-dimensional horizontal flow velocities. The current meters were mounted on quadropods and positioned 0.15 m above the bed measured from the central line of the current sensor. They were set to sample at 4 Hz in bursts of 20 minutes every hour. The tide was manifested as a progressive wave with maximum values (0.3 m s^{-1}) during high and low water and generally lower flow velocities closer to the shore.

A total of 160 sediment samples (100 g) were collected in March 2015 across the intertidal sand flats of Ryde (Figure 2.4). Sampling was undertaken on a regular grid, of 75 m x 75 m on the west of Ryde Pier and 100 m x 100 m on the east side of Ryde Pier. A surficial layer (upper 3 cm) of the sediment was sampled which is considered representative of recent processes (Plomaritis et al., 2008).

The study site has been visited monthly from August, 2015 until October 2017 to measure the distribution of seagrass and to collect sediment samples at four key sites along a reference

transect. 100 g of surficial layer of sediment were collected at these locations (Figure 2.4). Seagrass density was measured within a 0.5 x 0.5 m quadrat (Figure 2.5) at the key sites. In addition, the length of five randomly chosen leaves was measured at each station to record leaf length and width variation over the growth cycle. Five photos of seagrass within the quadrat were captured around the designated sites to estimate the seagrass cover and its variation. Intertidal profiles were recorded along two lines (RYD19 and RYD23) across the intertidal flat using a Real Time Kinematic (RTK) Global Positioning System (GPS) produced by Trimble. The instrument has an accuracy of 1-2 cm horizontally and twice that vertically.

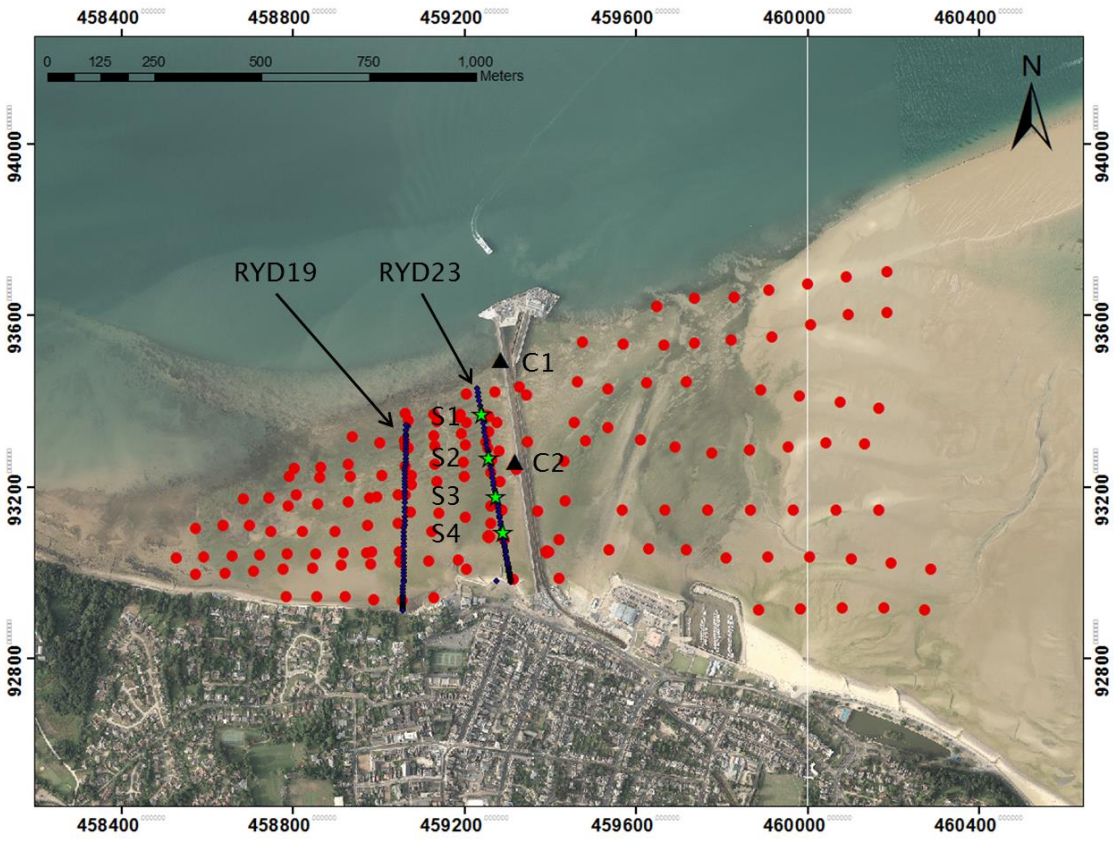

Figure 2.4: Transect lines, RYD19 and RYD23, sites visited monthly (green stars) and sediment sampling points during March 2015 visit (red dots).

Figure 2.5: Measuring *Zostera noltii* shoot density within a 0.5 m x 0.5 m quadrat during a visit to Ryde in January, 2016.

Table 2.1: Locations of surficial sediment and seagrass measurements carried out monthly from August, 2015 to October, 2017

STATION I.D.	LATITUDE	LONGITUDE	OSGB36 National Grid	
	Decimal degrees	Decimal degrees	Easting	Northing
RYD23_S1	N 50.73443	W 1.16124	459287.46	93093.78
RYD23_S2	N 50.73518	W 1.16144	459272.58	93177.02
RYD23_S3	N 50.73600	W 1.16167	459255.32	93268.02
RYD23_S4	N 50.73692	W 1.16190	459237.93	93370.14

2.2.1 Sediment analysis

Sediment samples were wet sieved at 63 μm with freshwater to separate sand from clay and mud. Sand fractions were dried in an oven at 60˚C and weighed. Sands were sub-sampled using a splitter to ensure random division of the sediment sample and burnt in a furnace at 550˚C for 4.5 hours. The loss on ignition (LOI) was used to measure the organic matter content by measuring the sample weight before and after combustion.

The grain size ranges were determined by means of a 2 m settling tower available in the National Oceanography Centre Southampton (NOCS). The settling tower is 0.15 m in diameter, filled with freshwater and works by measuring the cumulative weight of sample settling time over 200 seconds, over a length of 1.73 m. Sediment samples are launched into the column using a trigger mechanism. A single layer of sand grains is adhered to the base of

the wetted plate of the trigger mechanism. The plate and the logging device were triggered simultaneously to record the velocity of sediment settling. The weight of the sediment accumulating on the balance at the base of the apparatus was recorded using the TOWER2© program. The temperature of the water in the column varied between 19-23 ºC and was recorded using a thermometer for settling velocity calculation.

The use of settling velocities to determine grain size provides a more accurate interpretation compared to a mechanical procedure such as dry sieving as it provides a higher resolution grain size distribution and takes into account the shape, density and hydraulic behaviour of the grains (Plomaritis et al., 2008). Approximately 1 g of sub-sample was released in a single run and at least three replicates were undertaken for each sample. The analysis was repeated when any mechanical error was detected. The grain sizes were calculated from the settling velocity using a Matlab script written for the NOCS settling column by Neumeier (unknown) following equation formulated by Soulsby (1997).

$$w_s = \frac{v}{d_{50}}[(10.36^2 + 1.049D_*^3)^{0.5} - 10.36]$$

Equation 2.1

Where w_s is the settling velocity, v is the kinematic viscosity (1.36×10^{-6} m^2 s^{-1}), d_{50} is the median grain size (m) and D* is the dimensionless grain diameter defined as:

$$D_* = \left[\frac{g(s-1)}{v^2}\right]^{\frac{1}{3}} d_{50}$$

Equation 2.2

Where g is acceleration due to gravity = 9.81m/s^2, s is the grain density minus water density.

Chapter 3: Sediment transport pathways and seagrass distribution on the intertidal flat of Ryde, Isle of Wight

3.1 Abstract

Sediment characteristics including grain size are important factors governing beach slope and influencing sediment transport rates. They are key to understanding transport patterns and a crucial criterion in selecting the appropriate fill material for beach nourishment. However, little is known about how grain size and sorting varies spatially and temporally on an intertidal flat with seagrass cover. This study focuses on sediment transport on the intertidal flat at Ryde, north east of Isle of Wight. Sediment transport directions were estimated by the means of Grain Size Trend Analysis (GSTA), a statistical model developed to determine sediment transport direction based on spatial distribution patterns of sediment characteristics (mean grain size, sorting and skew). Sediments on the intertidal flat were composed of very fine sand. There was a clear change of sediment characteristics with location on the intertidal flats. Coarser sediment were recorded at the east side of Ryde Pier on the sand bank, while sediments were finer on areas associated with seagrass. Sediments were very well sorted and positively skewed. GSTA indicate a strong east to west sediment transport direction on the west side of the Ryde Pier. This finding does adhere to SCOPAC (2012), which suggested Ryde Sands is an area of convergence of littoral drift from both easterly and westerly directions. Grain size parameters suggest the presence of two distinct sediment populations with significant different grain size distributions: (1) Ryde sand bank to the hovercraft path; and (2) west side of Ryde Pier. A dense canopy of the seagrass, *Zostera noltii* occupied most of the survey area during its peak summer cover, whereas some areas were characterised by more patchy seagrass. The distribution of *Zostera nolttii* was only limited to the intertidal zone to a depth of -1.5 m Ordnance Datum (OD) where the intertidal flats are only exposed during the Lowest Astronomical Tide.

3.2 Introduction

Coasts are facing the threat of sea level rise (Pethick, 2001) coupled with stormier seas (Lowe & Gregory, 2005) and greater frequency extreme events (Mitchell et al., 2006; Scott et al., 2016; Sillmann & Roeckner, 2008), all ultimately driven by anthropogenic climate change. Human society contributes directly and indirectly towards these changes by globally changing the climate regionally and locally, altering the nutrient inputs and influencing sediment transport (Cloern et al., 2016; Kirwan & Megonigal, 2013; Ruberti et al., 2018). Intertidal sand flats play an important role in ecological functioning of coastal ecosystems and provide protection to the coast against storm events.

As a result of its important ecological role, preservation and restoration of seagrass beds are important in managing a sustainable coastal environment (Mcskimming et al., 2016; Rodríguez-Salinas et al., 2010). Therefore, the ability to accurately map and monitor seagrass meadows is crucial in order to safeguard their habitat. Knowledge of the extent, density and the canopy height may also help in assessing the hydrodynamics and sediment transport in the area (Koch et al., 2006; Lefebvre et al., 2009). The intertidal flats at Ryde on the Isle of Wight have extensive cover of the seagrass, *Zostera noltii*, and have been chosen as a model study system to understand the influence of seagrass beds on sedimentary processes.

Sediment transport in coastal environment plays a crucial role in regulating the morphology, hydrological processes as well as playing ecological roles over different spatial and temporal scales. Regular and detailed scientific studies on intertidal flats behaviour are necessary, since changes to the coastal processes may have significant impact on local residents, economic activities and resource management. One of the simplest and most cost effective way to study the movement of sediment is through the analysis of spatial changes in grain-size parameters (mean, sorting and skewness)(Le Roux & Rojas, 2007). The study of grain characteristics are significant in the understanding of transport process pattern because grain-size trends are the natural result of dynamic sediment transport processes (McLaren & Bowles, 1985). Sediment pathways derived by this method are, however, usually made without consideration of hydrodynamic conditions of an area (Hughes, 2005).

In this chapter my aims were to provide understanding of the sediment processes and their relationship to distribution and abundance of seagrass distribution on Ryde Sands using spatial distribution patterns, grain size trend analysis and image analysis. The study will also improve the understanding of the application of grain size trend analysis on sand flats.

Most attention has been given to the influence of subtidal seagrass beds on sediment characteristics and dynamics (*Zostera marina* by Lefebvre et al. (2010) and van Katwijk et al.

(2010); *Posidonia oceanica* by De Falco et al. (2003) and Hendriks et al. (2008) and *Cymodocea nodosa* by Hendriks et al. (2010)). In contrast much less attention has been given to intertidal beds with *Zostera noltii* (but see, Ganthy et al. (2015) and Wilkie et al. (2012). The intertidal is often subject to greater wave action than subtidal environments. Intertidal seagrasses are usually smaller and show greater seasonality in abundance and cover than those in the subtidal zone (Park et al., 2016). Thus my work explores a dynamic environment with complex interactions with seagrass. The study location is of considerable conservation importance (Marsden & Chesworth, 2015), thereby warranting further investigation.

The specific objectives of this study were to:

- identify the composition of sediment on Ryde Sands intertidal flat;

- determine the spatial distribution pattern of sediments on Ryde Sands intertidal flat;

- determine the net sediment pathways of Ryde Sands using grain size trend analysis;

- determine the spatial distribution of seagrass from aerial photography.

3.3 Material and methods

3.3.1 Intertidal flats

Tidal flats are highly important ecosystems that provide services including protection to the coastal zone (Salvador de Paiva et al., 2018; Temmerman et al., 2013) and provide habitat for plants and wildlife (Ganthy et al., 2013; Passarelli et al., 2014). They are generally characterised by accumulation of fine-grained sediment and gentle bed slopes. The gentle bed slope of intertidal flats dissipate wave energy and protect coastlines from erosion.

Tidal flats are formed in areas where the currents are strong enough to move sediments. Their generation requires a source of mobile sediment, usually fine-grained either delivered from the rivers, erosion of the coasts and seabed or from cliff recession (Gao, 2019). Tidal currents are usually the dominant force over other hydrodynamic forces. High amount of fine-grained sediment supply reduces the bed slope over the intertidal area. The reduction of bed slope will enhance tidal currents and reduce wave breaking due to bed friction. In a typical tidal flats system where there is an abundance of sand supply and the tidal currents dominates, sand flats are formed. Strong tidal currents during the late stage of the ebb prevent fine-grained sediment from settling on the bed. During the flood slack, the material settled tends to be suspended (Gao, 2019).

Intertidal flats act as sediment sinks and are generally stable long term (Kakeh et al., 2015). The stability allows the development of vegetation and other organisms in the area and thus provide further protection to the coasts (Neumeier & Ciavola, 2004; Potouroglou et al., 2017; Schanz & Asmus, 2003). Furthermore, vegetation patches of *Spartina sp.* on intertidal flats have been observed to induce high accretion rates (Ward et al., 2003)and reduce erosion (Lo et al., 2017). Despite their stability, changes in the morphology of tidal flats do happen in both the short and long-term. Bed-levels fluctuate under the influence of mainly tidal currents, waves and storm events (Hu et al., 2018, 2017; Wang et al., 2012). The individual or combination of these processes will affect the sediment movement on the tidal flat over different timescales both seasonal and longer term (Gao, 2019; Gong et al., 2017).

It is crucial to understand the physical processes of accretion, erosion and reworking on intertidal flats as they are very important for coastal planning, engineering, and ecosystem maintenance.

3.3.2 Grain size trend analysis

Grain size trend analysis is an empirical technique quantifying changes in grain size distribution to estimate sediment transport and behaviour. Spatial variations in mean grain-size parameters have long been used to explain the fining or coarsening of sediment in the direction of transport (McCave, 1978; Pettijohn & Ridge, 1932).

As a fundamental property of sediment particles, grain size was used to determine the source of sediment, transport history and understand depositional processes (Folk & Ward, 1957; Krumbien, 1938). Analyses of grain size distributions are normally described by their deviation from the prescribed ideal distribution (Blott & Pye, 2001). In sedimentological studies, geometric rather arithmetic scaling is usually employed to prevent imbalance in emphasize of coarse and fine sediment. Logarithmic Udden-Wentworth grade scales were adopted where the grain size of one size class differ to the following class by a factor of two. Krumbien (1934) introduced the class scaling based on phi (ϕ) values and this scale has been widely used since (McCave, 1978; Pedreros et al., 1996; Plomaritis et al., 2008).

Four parameters are typically used to describe the grain-size distributions, these are: a) mean, the average grain size, b) sorting, the spread of the sizes around the average, c) skewness, the symmetry of preferential spread to one side of the average and d) kurtosis, the degree of concentration of the grains relative to the average. These parameters can be obtained through graphical and mathematical methods, such as the 'method of moments'. The analysis of spatial changes in grain-size parameters (mean, sorting and skewness) is a standard approach for the identification of sediment transport patterns, especially in complex

systems due to its simplicity and cost effectiveness. Hence, it can be a useful tool in situations where more complicated and expensive process of direct measurements of sediment movement are not feasible.

The approach of describing transport pathway by combining aforementioned parameters was introduced by McLaren (1981) and subsequently by McLaren & Bowles (1985). This method assesses sediment transport pattern in relation to deposited grain size by means of three textural parameters; mean, sorting and skewness. The basis of the theory lies in the assumption that finer sediment are lighter and bound to travel further under lower energy, and coarser sediment are easier to deposit (McLaren & Bowles, 1985). GSTA was developed by McLaren & Bowles (1985) as a one-dimensional statistic technique. The theory demonstrates two acceptable trends out of possible eight (Figure 3.1) that are, i) grain size should be coarser, better sorted and more positively skewed or ii) finer, better sorted and more negatively skewed in the direction of transport (McLaren & Teear, 2013). In order to reduce the bias induced by a one-dimensional approach, Gao and Collins (1992) developed this into a two-dimensional technique and derived a mathematical model that described another two cases that can occur. These are the sediment can become, i) finer, better sorted and positively skewed and ii) coarser, better sorted and negatively skewed. These two cases summarise the net sediment transport patterns of a site, however they do not imply that it is definitive.

This technique has been applied in various marine environments such as sand banks (Poulos & Ballay, 2010), estuaries (McLaren & Teear, 2013), beaches (Plomaritis et al., 2008; Poizot et al., 2013; Van Lancker et al., 2004) and exposed continental shelf (Balsinha et al., 2014).

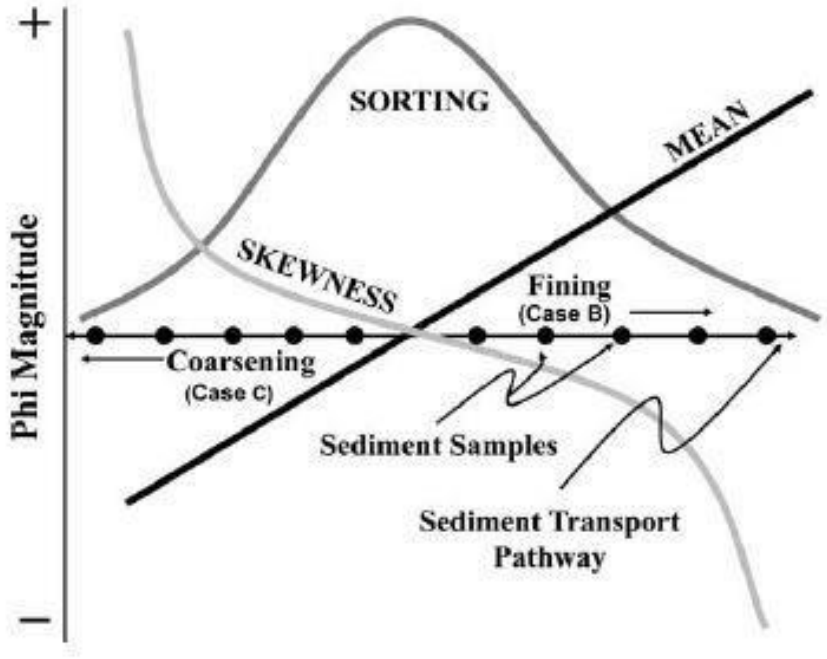

Figure 3.1: Two accepted cases to define sediment transport pathway using grain-size trend analysis (Adapted from McLaren & Bowles (1985).

The method uses a regular grid as the grain size parameters of each sample are compared with the parameters of the same number of the neighbouring sites, therefore removing bias in residual trends and ensuring the results to have the same statistical weight. To use this method, an essential input is the nearest neighbouring cells of a sample grid. A pair of neighbours cells are defined when the distance between the two is shorter than, for example, the maximum sampling interval or a geostatistical distance (Gao & Collins, 1992; Poizot et al. 2006). Then, GSTA calculates trend vectors for every site by comparison with its neighbours.

3.3.3 Uncertainties of GSTA

Grain size trend analysis has been widely used to describe sediment distribution in various sedimentary environments (Plomaritis et al., 2008; Poizot et al., 2013; Zhang et al., 2013), however there are a number of uncertainties that needs to be considered to ensure reliable GSTA results.

The prediction of sediment transport using this method was built upon the ease of sediment grains to be transported (i.e., the probability of fine grains sediment to be transported is greater than coarser grained sediment). The model also assumes that the transport of one particular grain size is independent of any other grain transportation. In the events that

particles flocculate, the transport behaviour is altered thus having different rates of settling and therefore not being accounted for by GSTA.

GSTA indicates the average sediment transport of an area. It does not account the transport caused by any individual events such as storms, surges and tides. During storm events, increased wave heights generally leads to higher sediment transport (Boudet et al., 2017).

Another important factor that can determine the accuracy of the GSTA is the spacing of sample collection. Large spacing of samples can result in transport patterns determined by GSTA not being related to each other thus comprising the accuracy of the conclusions being made. Furthermore, the sedimentological environments and geographic shape of an area should be considered in sample collection planning (Poizot et al., 2008). Samples in Ryde were collected in a fairly regular grid to minimise edge effect (Poizot et al., 2006) at a high sampling density to represent all of the different observed Ryde morphology.

Lastly, the sediment trend patterns are also influenced by the depth of the sediment sampling. If the sampling depth is too great then past events could be captured and represented in the results (Gao & Collins, 1992). As an example, sampling depth of 5 to 10 cm could be associated with a time-scale of 1 to 10 years in Yangpu Harbour (Gao & Collins, 1992). The depth of the sample should be taken to represent the time that it takes for the sediment trend to accumulate (Poizot et al, 2008). Therefore in Ryde, only the surficial layer (upper 2 cm) of the sediment were sampled.

In short, the limitations of GSTA models include not identifying transport mechanisms, transport events or changes in transport patterns due to storm events.

3.3.4 Sediment Characteristics

Sand found on beaches is mostly the result of weathering of rocks, therefore the composition of the sediment can be related to its source. In the UK, beaches are mostly composed of quartz with a density of 2650 kg/m^3 and sizes varying from boulders to muds. This led to classification of sediments by size (Table 3.1). The statistical parameters of the grain size distributions (mean grain size, sorting, skew and kurtosis) were calculated following the graphical method defined by Folk & Ward (1957).

Table 3.1: Grain size classification previously used by (Udden, 1914), (Wentworth, 1922) and (Friedman & Sanders, 1978). Phi scale is based on negative logarithm (to base 2) of the particle diameter in millimetres [φ = log2D].

Grain size range		Aggregate name	
φ scale	(metric)	Udden (1914) and Wentworth (1922)	Friedman and Sanders (1978)
< −8	> 256 mm		Boulders
−7 to −8	128 - 256 mm	Cobbles	Large cobbles
−6 to −7	64 -128 mm		Small cobbles
−5 to −6	32 - 64 mm		Very coarse pebbles
−4 to −5	16 - 32 mm	Pebbles	Coarse pebbles
−3 to −4	8 - 16 mm		Medium pebbles
−2 to −3	4 - 8 mm		Fine pebbles
−1 to −2	2 - 4 mm	Granules	Very fine pebbles
0 to −1	1 - 2 mm	Very coarse sand	Very coarse sand
1 to 0	½ - 1 mm	Coarse sand	Coarse sand
2 to 1	250 - 500 µm	Medium sand	Medium sand
3 to 2	125 - 250 µm	Fine sand	Fine sand
4 to 3	63 - 125 µm	Very fine sand	Very fine sand
8 to 4	4 - 63 µm	Silt	Silt
> 8	< 4 µm	Clay	Clay

Modified from (Blott & Pye, 2001)

3.3.4.1 Mean

Mean grain size is an index of grain measurement due to its size. Increase of mean value (in phi scale) indicates a decrease in grain size and vice versa. Mean value is obtained from the calculation of the gravity centre under the grain size curve or the gravity centre of the cumulative distribution curve. The mean value was obtained by using the following formula;

$$M_z = \frac{\phi_{16} + \phi_{50} + \phi_{84}}{3}$$

Equation 3.1

Where the ϕ_{16} represents the median of the coarsest third of the sample, ϕ_{50} represents the median of the middle third and ϕ_{84} the median of the finest third.

Mean size gives an indication of the magnitude of force applied by water or wind that is responsible for moving the grains. It tells either the competence of the process (i.e., can move a certain size of sediment) or the fall velocity below which that sediment can no longer remain in transport. The characterisations of sediment sizes in accordance to its size range are given above (Table 3.1).

3.3.4.2 Sorting

Sorting is a measure of standard deviation. It is the range of grain sizes in a sediment sample and indicates how widely the grain sizes are scattered, with regard to the mean. This indicates the range of forces which determine the sediment size distribution. Standard deviation is computed with the following formula:

$$\sigma_I = \frac{\phi_{84} - \phi_{16}}{4} + \frac{\phi_{95} - \phi_5}{6.6}$$

Equation 3.2

The characterisations of sediment sizes in accordance to its standard deviation are given in (Table 3.2) below.

Table 3.2: Standard deviation of sediment

σφ, Standard deviation	
< 0.35	Very well sorted
0.35 – 0.50	Well sorted
0.50 – 0.71	Moderately well sorted
0.71 – 1.00	Moderately sorted
1.00 – 2.00	Poorly sorted
2.00 – 4.00	Very poorly sorted
> 4.00	Extremely poorly sorted

3.3.4.3 Skewness

Skewness measures the degree of symmetry that determines the tendency of the data to spread preferentially to one side of the average. It can be an indication of mixing of sediment sources or removal of fractions and sorting during transport and deposition. Positive skewness is the mode of coarser sediments, with a tail of finer sediments, which suggests the

distribution is skewed towards positive phi values. This indicates a depositional environment (Tucker, 2009). The value of skewness is obtained with the following formula:

$$Sk_I = \frac{\phi_{16} + \phi_{84} - 2\phi_{50}}{2(\phi_{84} - \phi_{16})} + \frac{\phi_5 + \phi_{95} - 2\phi_{50}}{2(\phi_{95} - \phi_5)}$$

Equation 3.3

The characterisations of sediment sizes in accordance to its skewness are given in (Table 3.3) below.

Table 3.3: Skewness of sediment

Skφ, Skewness	
> 0.3	Very positively skewed
0.3 – 0.1	Positively skewed
0.1 – - 0 .1	Symmetrical
-0.1 – -0.3	Negatively skewed
< -0.3	Very negatively skewed

3.3.4.4 Kurtosis

Kurtosis measures the ratio of the sorting in the extremes compared to the sorting in the central section or how peaked grain size distribution is. The value of kurtosis is obtained with the following formula:

$$K_G = \frac{\phi_{95} - \phi_5}{2.44(\phi_{75} - \phi_{25})}$$

Equation 3.4

The characterisations of sediment kurtosis are given as in (Table 3.4).

Table 3.4: Kurtosis of sediment

φ, Kurtosis	
< 0.67	Very platykurtic
0.67 – 0.90	Platykurtic
0.90 – 1.11	Mesokurtic
1.11 – 1.50	Leptokurtic
> 1.50	Very leptokurtic

3.3.5 Seagrass cover by Normalized Difference Vegetation Index (NDVI)

The seagrass distribution was analysed from a series of aerial photography acquired from the Channel Coastal Observatory (CCO) using the Normalized Difference Vegetation Index (NDVI). NDVI is generally used to monitor crop health and photosynthetic activity. The NDVI, originally introduced by Rouse et al., (1974) to assess green biomass, remains a reliable tool in dealing with agricultural, semi-natural and natural vegetation monitoring (Gomes et al., 2017; Sholihah et al., 2016) as well as assessing vegetation health and density (Cheikh et al., 2018; Kinyanjui, 2011). This is mainly due to its ability to discriminate vegetation from other element in multispectral images. The index is quantified by measuring the difference in two spectral bands, between near-infrared (NIR) and red light (VIS). NIR is reflected while VIS is absorbed by vegetation. The formula can be written mathematically as:

$$\mathrm{NDVI} = (\mathrm{NIR} - \mathrm{VIS})/(\mathrm{NIR} + \mathrm{VIS})$$

Equation 3.5

The spatial distribution of intertidal *Zostera noltii* seagrass beds were studied with false colour infrared (FCIR) aerial photography in Ryde over two years, 2013 and 2016 during the peak seagrass growth. The images were mosaicked and processed with the Normalized Difference Vegetation Index (NDVI) function in ArcGIS.

3.3.6 Study site setting and environmental context

Ryde is located at the north-eastern coast of the Isle of Wight in the eastern Solent. According to the Sediment Transport Study by SCOPAC (2012), it has been suggested that sediment is transported along the beaches from Seaview on the east side and from Fishbourne on the west side and converges at Ryde Sands (Figure 3.2). Westward drift was observed from Seaview to Ryde Pier as indicated by the accumulation of sands on groynes along the beaches.

The first direction of transport is northwestward transport from the east side of the island, due to exposure to wind waves from the southeast. This is supported by mineralogical analysis of sediments at Ryde Sands which revealed a high quantity of limonite, a sand mineral derived from the Lower Greensand, abundant on Sandown Bay, southeast of the Isle of Wight (Dyer, 1980).

The second direction of transport from the west side of Ryde towards the Ryde Pier is driven by local waves in the Solent created by westerly winds. Sediment between Old Castle Point and Ryde is largely muddy (silt + clay). The tidal currents from the Eastern Solent transport

the muds from the south and west of Isle of Wight or from Bracklesham Bay in Chichester (Dyer, 1980; Algan *et al* 1994).

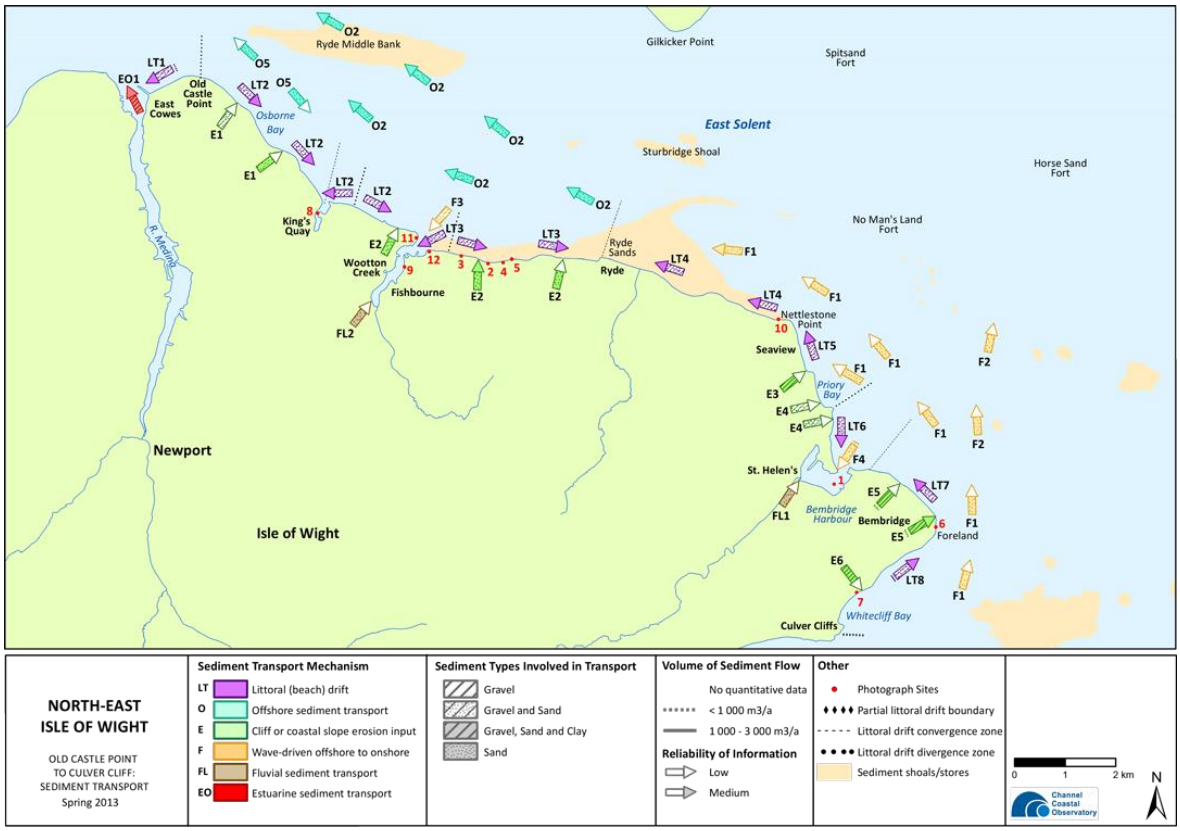

Figure 3.2: Sediment transport pathways in the North East Isle of Wight suggested by SCOPAC sediment transport study (source; SCOPAC, 2012).

3.3.7 Study area

A total of 170 sediment samples were collected across Ryde intertidal sand flat (Figure 3.3). Sampling was undertaken on a regular grid, 75 m x 75 m on the west of Ryde Pier (referred as Ryde West) and 100 m x 100 m on the east of Ryde Pier (referred as Ryde East). This covers an area of approximately 2000 m long and 700 m wide. In order to gain an understanding of recent and local transport rate, only the surficial layer (upper 2 cm) of the sediment were sampled (Plomaritis et al., 2008). The surficial layer of sediment was collected using a scope during low tide, when the tidal flats is exposed.

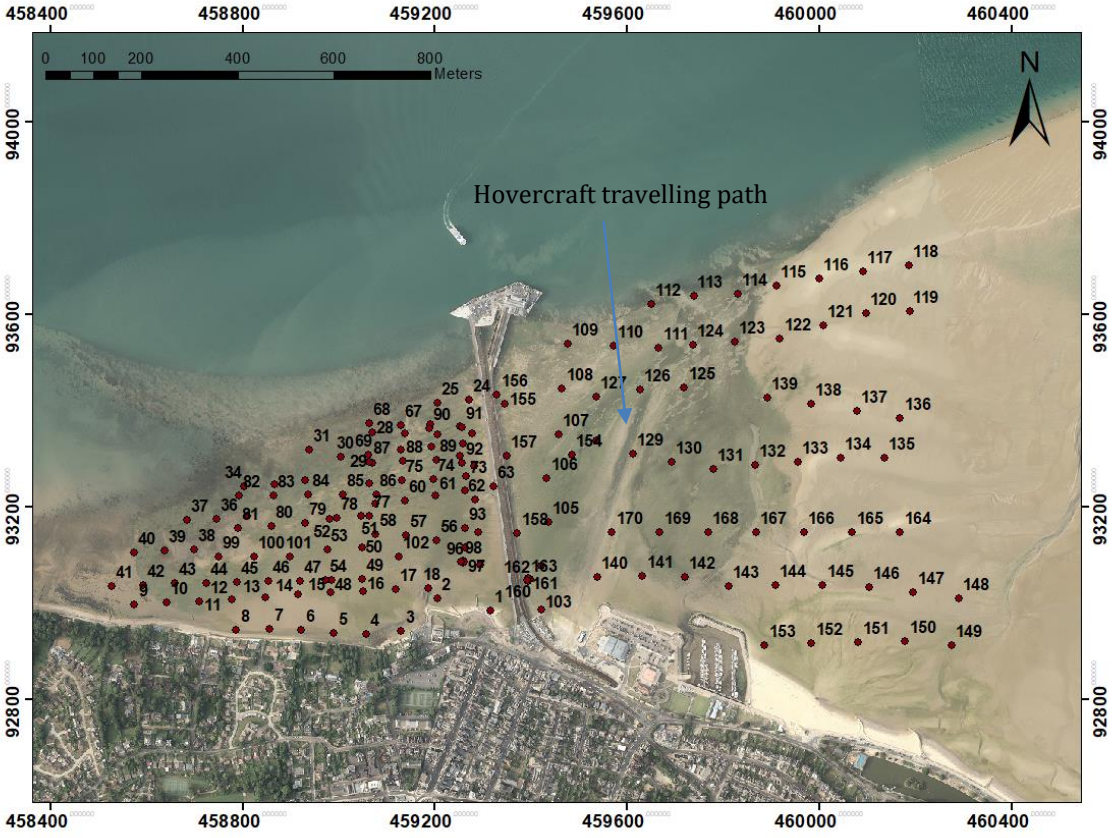

Figure 3.3: Sampling sites visited in March 2015. Stations 1 - 102 are located on the west side of the pier while stations 103 – 170 are on the east side of the pier.

3.3.8 Sediment analysis

Sediment samples were wet sieved at 63 µm with water to separate sand from clay and mud. The sand fraction were dried in an oven at 60˚C and weighed. Sands were sub-sampled using a splitter and burnt in a furnace at 450˚C for 6 hours to eliminate the organic content through loss on ignition (LOI).

The grain size ranges were determined by means of settling velocity using a 2 m tall settling tower. The settling tower is 0.15 m in diameter, filled with freshwater and logs based upon a balance accumulation system. The use of the settling velocity technique for grain size analysis provides more accurate interpretation compared to mechanical procedure such as dry sieving as it provides continuous grain size distribution and takes into account the shape, density and hydraulic behaviour of the grains (Plomaritis et al., 2008).

Approximately 1g of sub-sample was measured in a single run and at least 3 measurements were taken for each sample. The analysis was repeated when there is obvious error in the resulting grain size distribution curve such as negative weight being recorded. This can happen when there are too much sediments accumulating on the weigh scale at the bottom of

the settling tower. A Matlab routine *Cal_settling* written by Neumeier was used to calculate the settling velocities of grains and convert it to grain diameter (d_{50}) using equation formulated by Soulsby (1997) as detailed in Chapter 2. The statistical parameters were used to generate the mean grain size, sorting, skew and kurtosis values for each sample using the graphical method (Folk & Ward, 1957).

3.3.9 Grain size trend analysis

Grain size trend analysis was formulated using a program developed by Gao (1996) to define the net sediment transport pathways. The program analyses the samples using mean grain size, sorting and skewness. The results allow analysis of length and direction of the trend vectors.

The data required for the model include the total number of sampling stations *(N),* a scaling factor for *X* data *(A),* the characteristic distance *(DC),* sampling station numbers, location of samples and grain size parameters. The first line of the model includes the total number of sampling sites, scaling factor and characteristic distance. The second line and the rest include the location of the sample, mean grain size, sorting and skewness.

3.3.10 Other methods of data collection

3.3.10.1 LiDAR Data

LiDAR (Light Detection and Ranging) data was acquired from Channel Coastal Observatory (CCO). The LiDAR data acquired are filtered data containing true height of the land with all buildings and other structures filtered out. The LiDAR surveys are flown at an elevation of approximately 800 m which produces a swath 700 m wide. The bathymetry of Ryde Sands had a 1 m horizontal spatial resolution with a vertical accuracy of 0.15 m.

Four sets of LiDAR data acquired in May 2007, February 2008, March 2013 and March 2014 were analysed. Image files in ASCII format were processed in ArcGIS where the different image tiles were mosaicked using the mosaic to new raster function with the details in Table 3.5.

Table 3.5: GIS Input Data.

Coordinate system	British National Grid
Cell size	0.1
Pixel type	32 bit unsigned

The nibble function was used to fix the erroneous area (such as areas without data), making sure values are assigned to the NoData locations. Floated values were converted into metres by dividing them by 1000. Mosaic was cropped into the required area by using a masking technique.

3.4 Results

3.4.1 Bathymetry

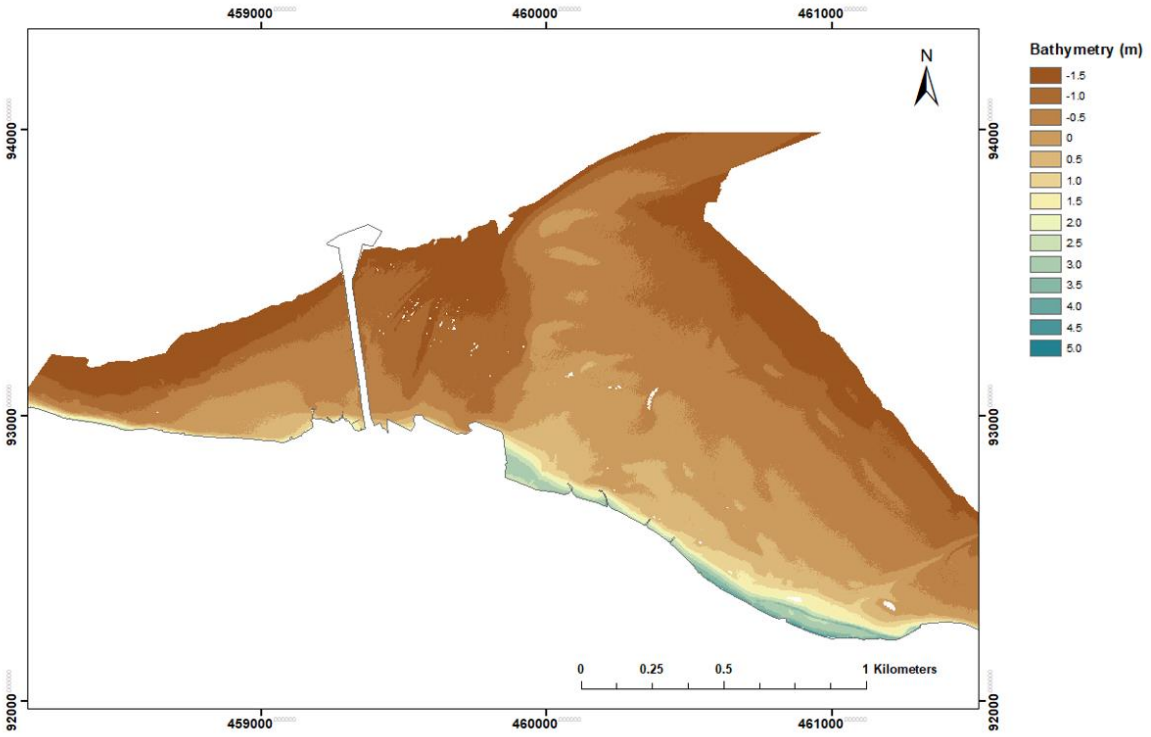

Figure 3.4: Bathymetry (colour scale in m) of Ryde Sands in March 2015.

The bathymetry values of Ryde intertidal sand flats (Figure 3.4) are given in meters and the datum used is Ordnance Datum (OD at Newlyn). The depth of the sand flat is between 4.5 and -2.5 m but majority of the area measures between 1 and -1.5 m.

The sand bank on the east side had a gentle slope with a gradient of 1 in 213. On the west side of the pier, the slope was steeper at 1 in 148 and the sand flat got steeper further to the west. On the east side of Ryde Pier, a spit was formed at the edge of the sand flat.

3.4.2 Sediment composition

The main sediment type on the sand flat was sand ranging from 2.05 to 2.91 phi. All of the samples were formed of greater than 95 % sand. Finer sediments (> 4.0 phi/ 63 µm) were also found in most of the samples however the amount was small. The median grain size of Ryde (Figure 3.5) is between 2.02 to 2.92 phi.

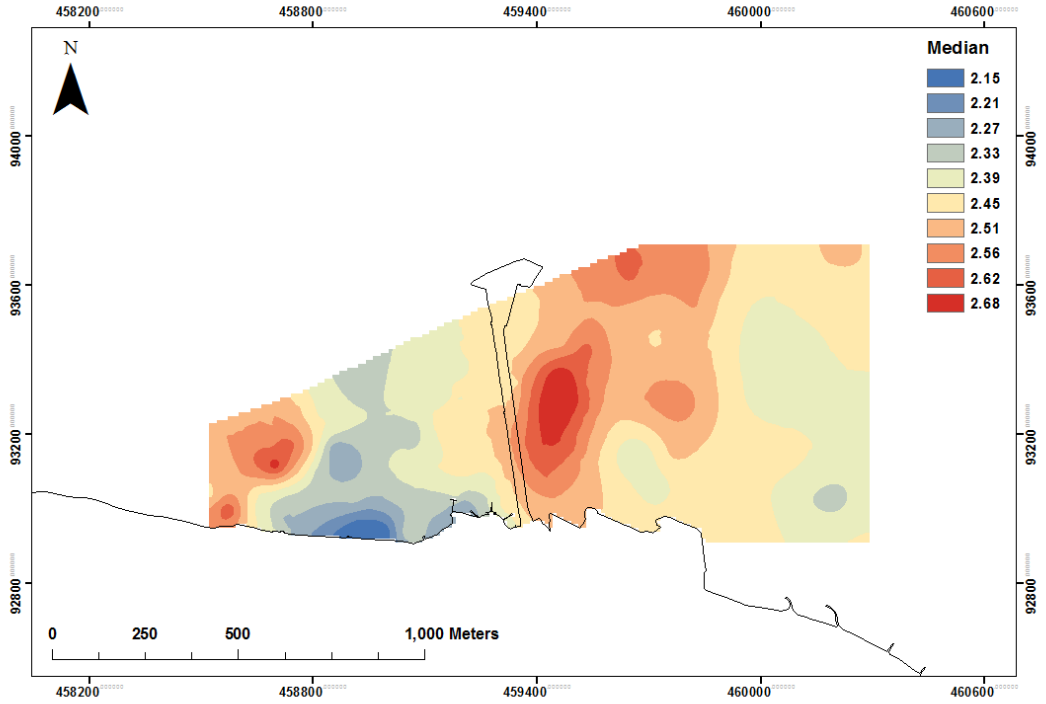

Figure 3.5: Median grain size in phi of Ryde Sands in March 2015. Blue indicates coarser while red indicates finer grains.

3.4.3 Spatial distribution patterns

Sediment characteristics of Ryde Sands were calculated following the settling rate analysis using the settling column. The mean size, standard deviation (sorting), skewness and kurtosis are subdivided in the subsequent section to allow the results of each statistical parameter to be discussed individually. All of the samples indicate a normal (bell-shaped) distribution.

3.4.3.1 Mean grain size

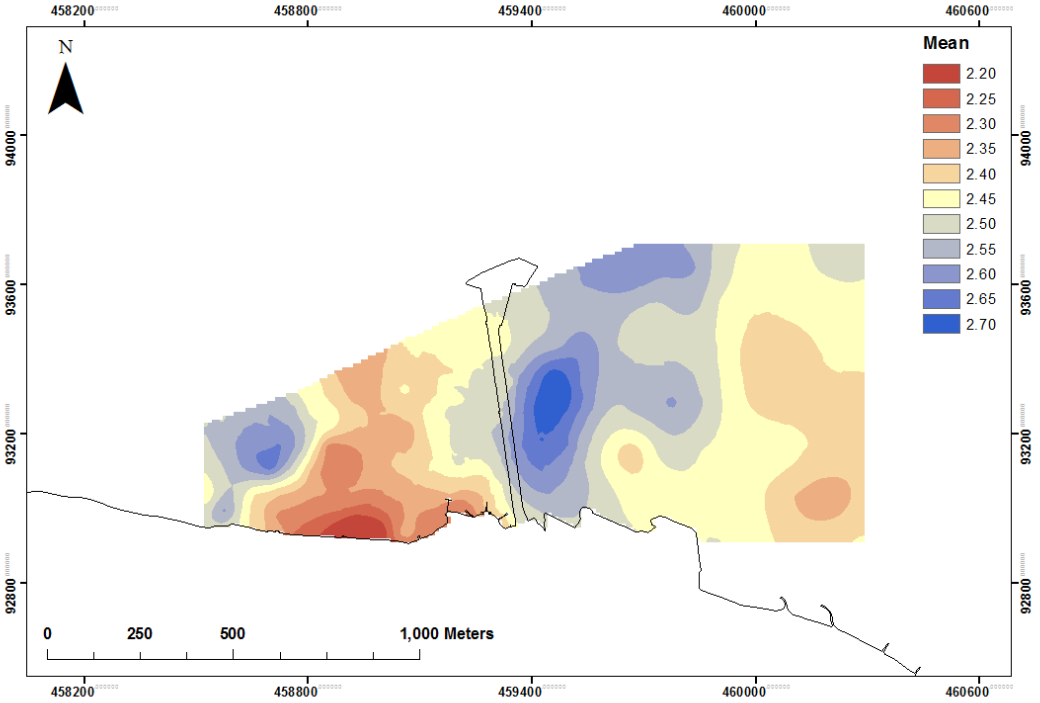

Figure 3.6: Mean grain size in phi in March 2015. Blue indicates finer grains while red indicates coarser grains.

Overall, the mean grain size indicated generally fine sand over the intertidal flat (Figure 3.6). The sediment on both Ryde East and Ryde West (location in relation to Ryde Pier) show a westward fining trend indicating longshore transport. Mean grain size ranged between 2.05 to 2.89 phi. Patches of finer sediment were found furthest west of the study site on the east side of Ryde Pier where seagrass meadows are dense. In Ryde West, samples closest to the land (site 4 to 8 in Figure 3.3) showed coarser sediment. The mean grain size pattern in this area was less obvious. However mean grain size was found to be finer in the area of dense seagrass meadows.

On Ryde East, grain size was recorded to be coarser on the sand bank (2.31 – 2.56 phi). In the seagrass area (sites 105 and 106), finer sediments were present (2.79 and 2.85 phi, respectively). The area around where there was a hovercraft travelling, a channel which cut across the seagrass meadows showed a coarser grain size (2.50 – 2.59 phi). No samples were collected directly over the hovercraft travel path due to safety reasons.

Coarser sediment found on some areas of the sand flat led to the production of Figure 3.7. Mean grain size plotted against the elevation shows a coarsening of sand as the elevation of sand flat gets higher where seagrass was also absent with a weak but statistically significant negative correlation ($r= -0.4$, $p < 0.001$).

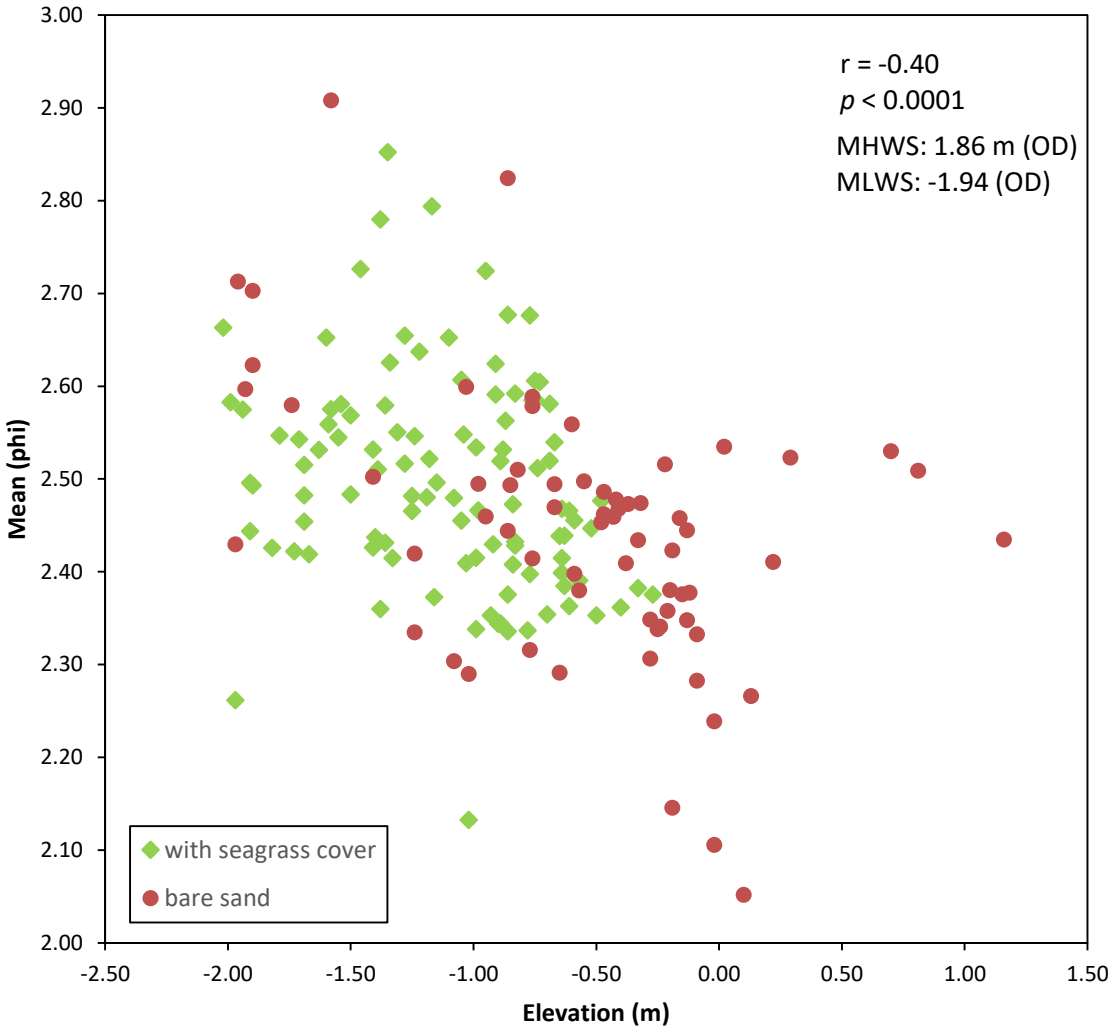

Figure 3.7 :Mean particle size against versus elevation. Higher mean values indicate finer sediment.

3.4.3.2 Sorting

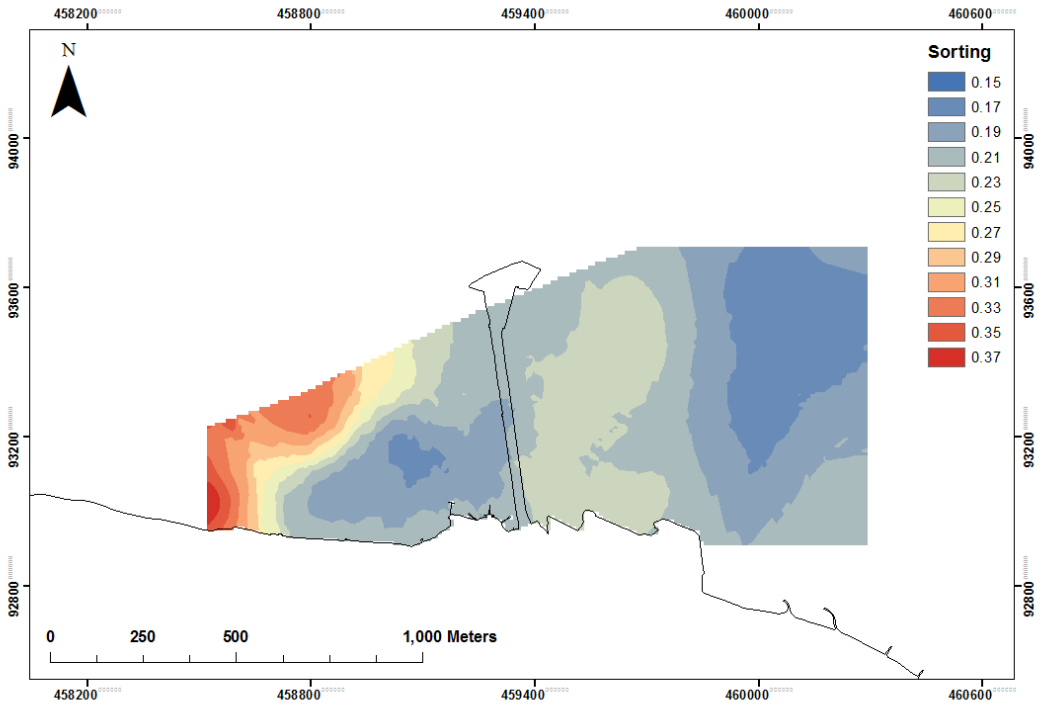

Figure 3.8: Sorting grain size in phi in March 2015. Blue indicates poorer sorting while red indicates better sorting.

The sorting of sediments (Figure 3.8) ranged from 0.12 to 0.53 phi and were classed as very well sorted to well sorted. The general trend of sorting on the sand flat can be divided into two parts, one to the east of the pier and the other to the west. On both sides, sorting improves in a west to east direction.

On the east side of the pier, sediment sorting ranged between 0.13 to 0.26 phi and were classed as very well sorted. Sediment on the sand bank was better sorted than areas where seagrass is present. The sample inside the seagrass area had a sorting value of 0.25 compared to the sand bank with a sorting value of 0.15. On Ryde West, sediment sorting ranges between 0.12 to 0.53 phi and were classed as very well sorted to well sorted. Less well sorted areas were localised to the furthest west of the study area. These areas were close to dense seagrass meadows.

3.4.3.3 Skewness

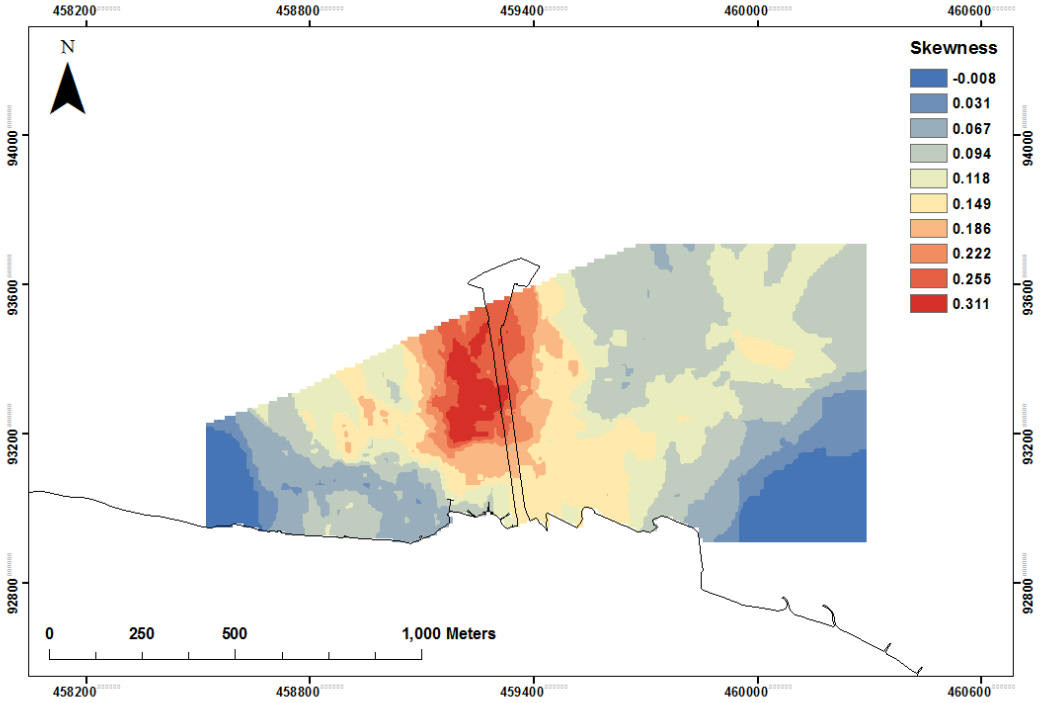

Figure 3.9: Skewness grain size in phi in March 2015. Blue indicates symmetrical distribution while red is more positively skewed.

Figure 3.9 indicates the skewness trends over the sand flat. Skewness ranged from -0.29 (negatively skewed) to 0.57 phi (very positively skewed). The map of skewness shows a gradual change from the east and west to the centre, from symmetrical to positively skewed. Most samples taken on the area where seagrass was abundance were positively skewed. On the sand flat, sediment sorting were mostly symmetrical.

3.4.3.4 Kurtosis

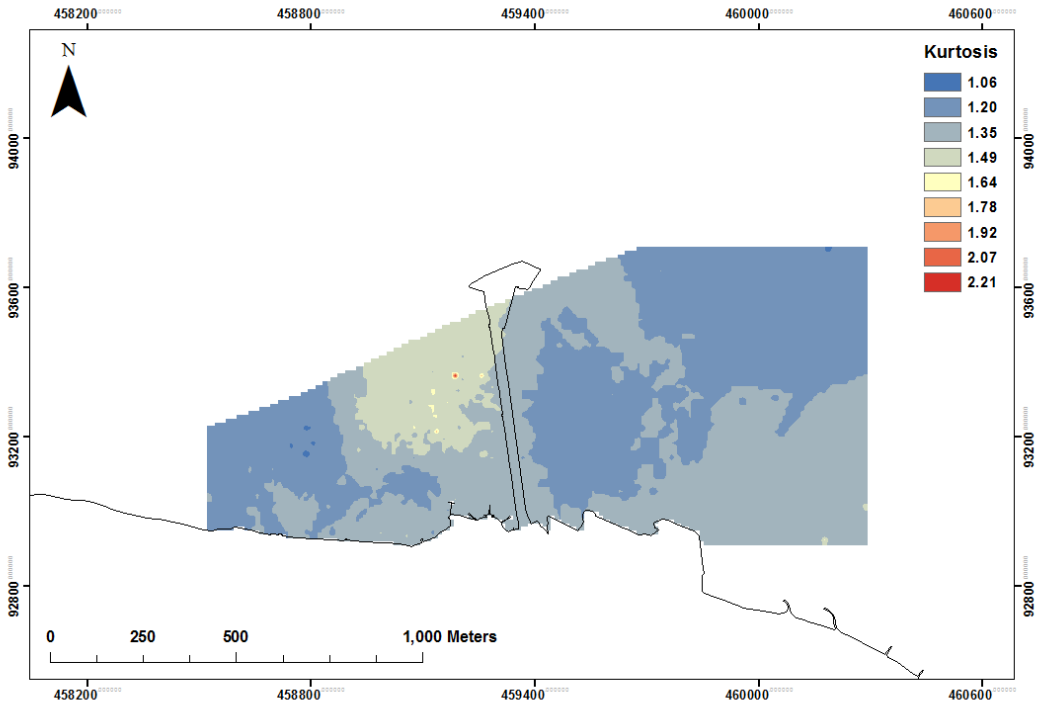

Figure 3.10: Kurtosis of grain size in March 2015. Blue indicates platykurtic distribution while red indicates very leptokurtic distribution.

Kurtosis ranged from 0.81 (platykurtic) to 2.32 phi (very leptokurtic) (Figure 3.10). Generally, the sampling area had a mesokurtic to leptokurtic (normal to peaky curve) sediment distribution. On Ryde West, a peakier curved sediment distribution was observed where the seagrass was most abundant, as compared to the rest of the area. On this side, the map of kurtosis showed a gradual east to west change from mesokurtic to leptokurtic. On Ryde East, the kurtosis trend was less defined with a leptokurtic sediment distribution throughout the area.

3.4.4 Sediment transport directions

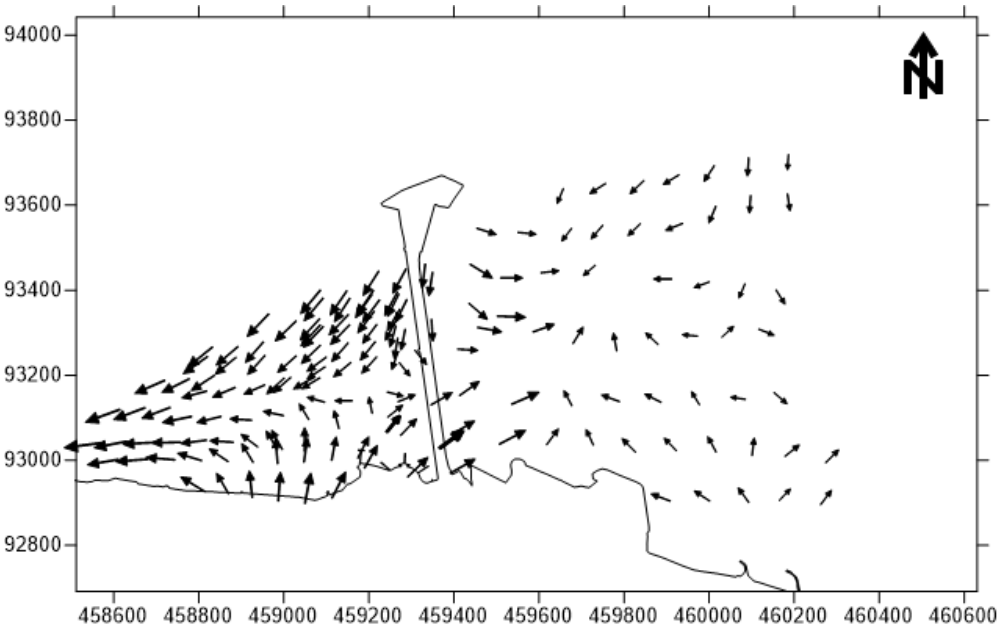

Figure 3.11: Sediment transport direction. Arrow length indicates the confidence of the transport directions.

Derived sediment transport directions are shown in Figure 3.11. The trend vectors show the direction of sediment transport with the arrow size indicating the confidence of transport direction (small arrows indicate a low reliability while bigger arrow represents a high reliability). The reliability of the results is dependent on the number of surrounding samples to compare data with. The vectors that have low reliability (small arrows) appear to have fewer surrounding samples than high reliability vectors (big arrows). The vectors on the east side of the pier show a lower reliability compared to the west as the spacing of the sampling was bigger.

The overall transport direction suggested by GSTA is towards the West. The trend was more complex and less clear over the east side of Ryde Sands further away from Ryde Pier. Despite the lower reliability vectors on this side, aerial photographs and LiDAR analysis verified the direction of transport. Figure 3.12 shows the movement of the sand bank on the east side of the pier from 2007 to 2016. The sand bank is moving westward towards the seagrass area.

Closer to the seawall, the sediment transport direction was seaward as current competence decreased and sediment load became coarser grained. The result also shows that Ryde Pier may have an effect to the sediment transport, as the westward fining of sediment seems to be disrupted by the pier. This may be due to the scouring around the pier stilts and the lack of vegetation observed below the pier.

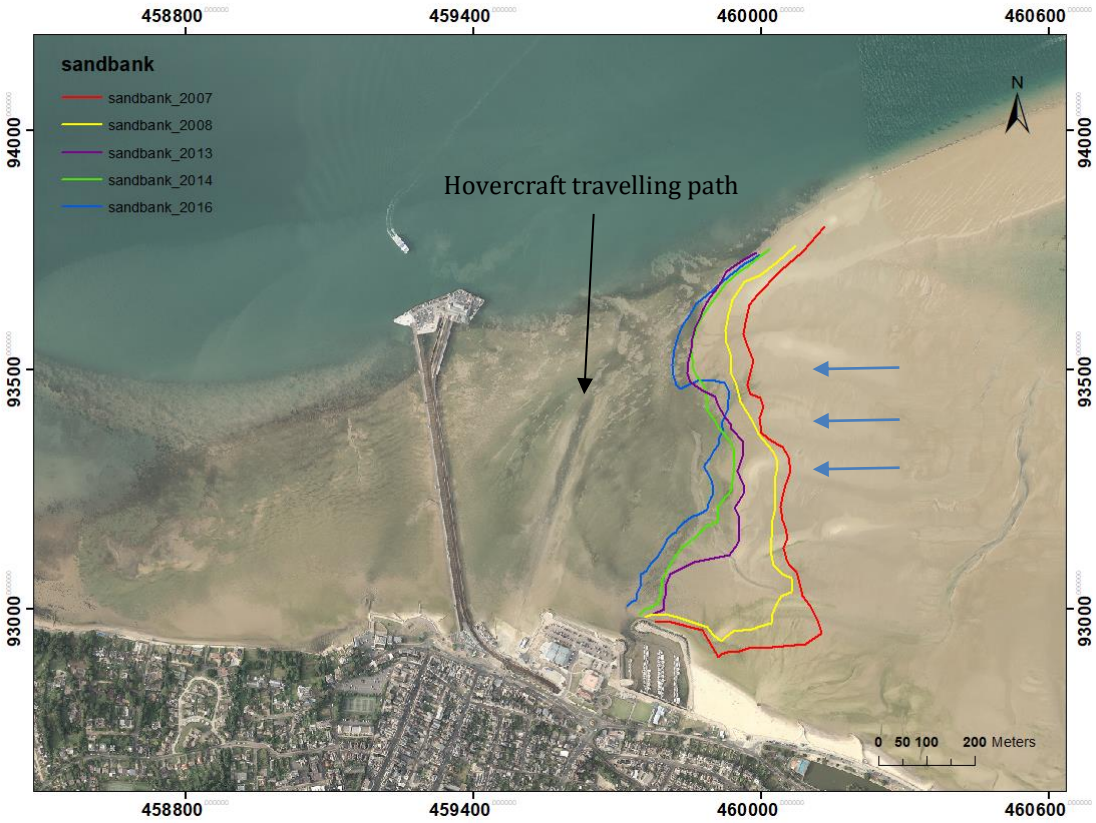

Figure 3.12: The movement of the unvegetated part of Ryde Sands (direction depicted in blue arrows) on the east side of Ryde Pier over the period of 10 years from 2007 to 2016. Background image was from August 2013.

3.4.5 Seagrass distribution detected by remote sensing: Normalised Difference Vegetation Index (NDVI)

Figure 3.13 and Figure 3.14 show aerial images of Ryde intertidal flats indicating the areas of ground, overlaid upon this are the NDVI readings of each pixel from the FCIR. These pixels are coloured depending upon the NDVI reading: 0.05–0.1 NDVI for sparse vegetation, 0.1 -0.2 for dense and over 0.2 for very dense vegetation. NDVI values of above 0.2 corresponds with a dense *Zostera noltii* vegetation. All NDVI readings in the area corresponded with areas identified as vegetation during the ground-truthing survey.

A steady and linear increase in meadow areas was observed between 2013 and 2016 with total surfaces colonized by *Zostera noltii* increasing from 54.56 to 61.95 ha, respectively. The NDVI recorded on both images ranged from 0.05 to 0.4. The densest part of the meadow has the NDVI of more than 0.2. A greater increase in the densest part of the meadow (NDVI > 0.2) was observed. From the 2013 image, the NDVI values are below 0.2. In 2016, the densest meadow represented 35% of total meadow surfaces. The seagrass expansion took place

mainly towards the upper part of the intertidal zone on the west side of Ryde Pier and along the pier on the east side.

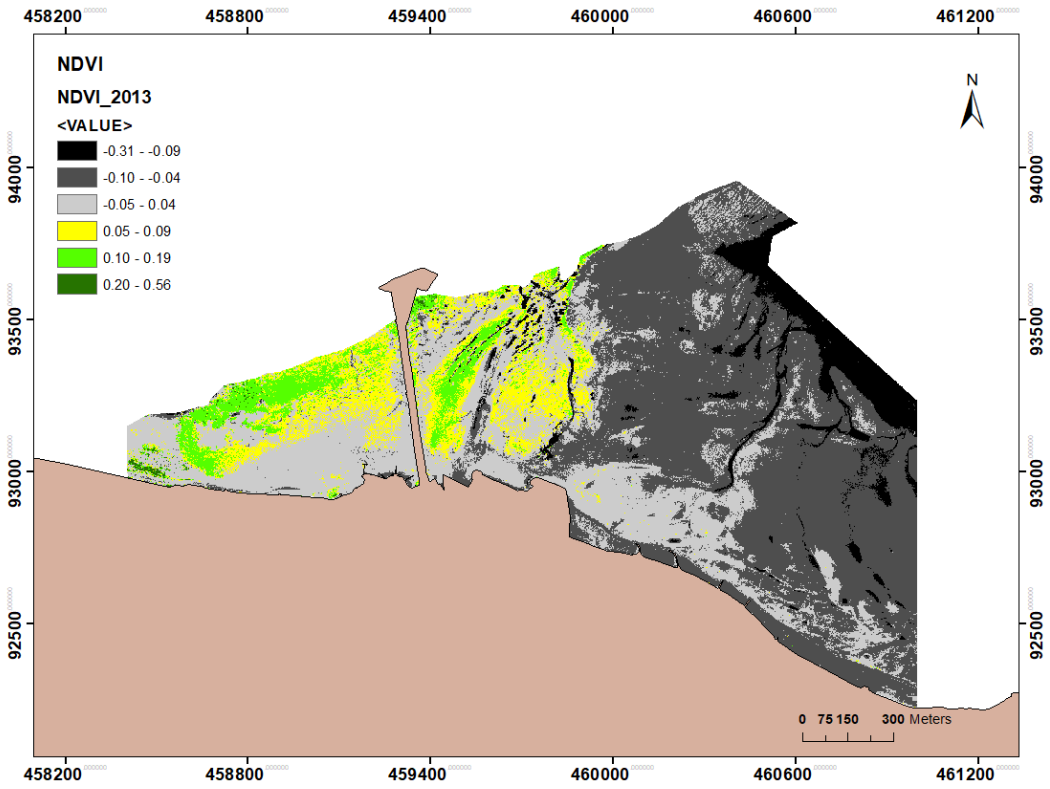

Figure 3.13: Vegetated areas in Ryde Sands in 2013 calculated using the three NDVI thresholds: Yellow denotes areas of probable vegetation but sparse coverage, light green equates moderate coverage, and dark green is area of vegetation with dense coverage.

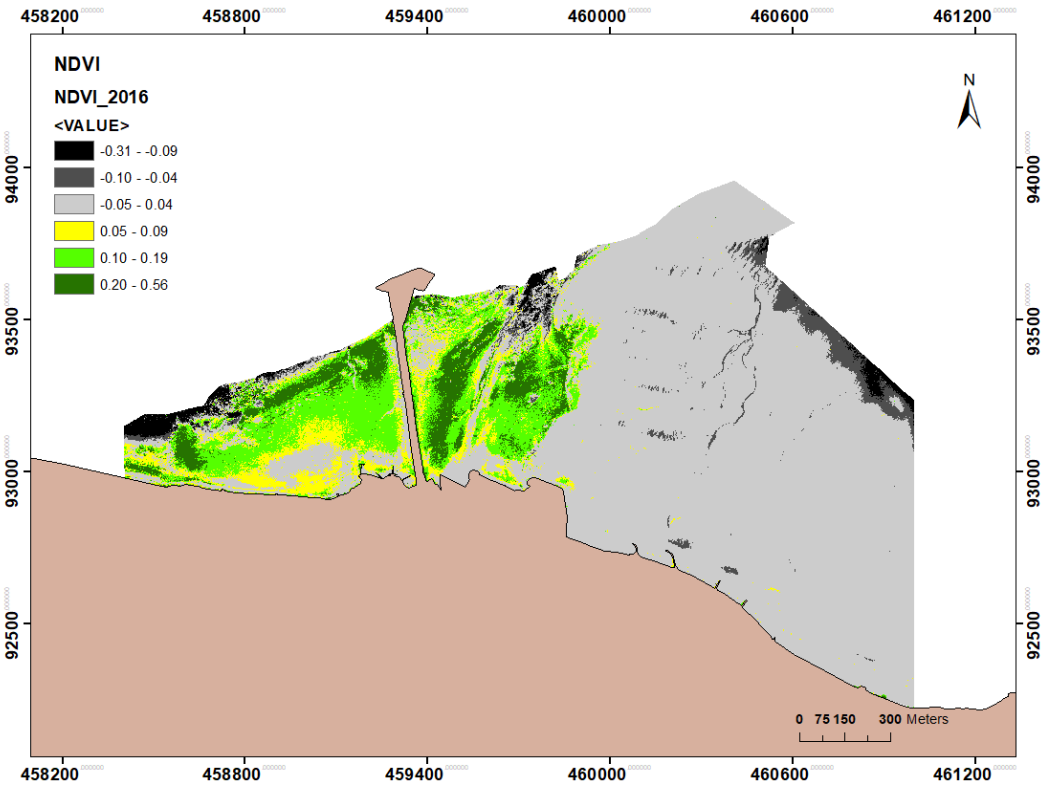

Figure 3.14: Vegetated areas in Ryde Sands in 2016 calculated using the three NDVI thresholds: Yellow denotes areas of probable vegetation but sparse coverage, light green equates moderate coverage, and dark green is area of vegetation with dense coverage.

3.5 Discussion

This section is divided into three parts. The first discusses the results related to the sand flat composition and the features found on the sand flat. The second part relates to the transport directions that could occur on the sand flat in relation to the statistical parameters. The third is on the detection of seagrass distribution by spatial remote sensing.

3.5.1 Ryde Sands sediment composition and morphology

Ryde intertidal sand flat is a relatively flat feature with a height mainly between 1 and -1 m Ordnance Datum, as shown from the bathymetric survey. The composition of Ryde Sands is of fine sands (0.13 to 0.24 mm) with very little silt, clay or gravels present. The lack of very fine material on the sand flat is likely due to the wave action being strong enough not to deposit the finer grained sediments. To the west of the sand flat, the bed is sheltered by seagrass meadows and contains finer sediments. The *Zostera noltii* patches accumulated finer sediment underneath their canopies compared to the adjacent bare sites. The dampening of waves (Paul & Amos, 2011; Reidenbach & Thomas, 2018) and reduced current flow (Lefebvre et al., 2010) inside the seagrass meadow allowed finer particles to settle from the water

column. Elevation of the sandflat appears to be related to the mean sediment grain size that is deposited in the area. The mean grain size indicates a fining of sediment in the longshore drift direction from east to west on the east side of the pier. The fine-grained material moves in suspension following the residual water flow.

Generally, sediment on the intertidal sand flat were very well sorted. Sorting is relatively better on the unvegetated bed of Ryde East and decreases in the dense seagrass meadow. The sorting of sediment grains is mainly governed by the hydrodynamic conditions. Poor sorting is normally associated with areas or seasons with high energy conditions (Abuodha, 2003; Bramha et al., 2017). However, poorer sorting of sediment in seagrass meadows as compared to their adjacent areas has been reported before (De Falco et al., 2000; Grady, 1981). This can be the result of continuous addition of finer or coarser materials due to particle trapping. Seasonal variation will also occur as the seagrass growth varies with season being greatest in summer (Hendriks et al., 2008) as I found at Ryde (see also Paul & Amos (2011)).

The sediment was predominantly positively skewed on the seagrass area and symmetrical on the rest of the sand flat. The fine skew on the seagrass areas can be considered to be due to the admixture of fine grained particles caused by the trapping of particles by *Zostera noltii* above ground biomass (Wilkie et al., 2012). Skewness responds to transport direction and supply sources (Román & Achab, 1999). The very positively skewed and positively skewed sediments (which are dominant in this study) usually suggest the introduction of fine material or removal of coarser fraction (Friedman, 1961) or winnowing of sediments (Duane, 1964). The sign of skewness can be related to environment energy where energy levels are low are characterized by positive skewness, and indicates a depositional environment (Duane, 1964).

Overall, the kurtosis did not indicate any definite patterns on Ryde intertidal sand flat. Leptokurtic sediments on the intertidal flats indicate a stable depositional environment. Fine sediment size and dominant leptokurtic nature of sediments typically reflect maturity of the sand (Nagalakshmi et al., 2018; Román & Achab, 1999).

It can be concluded, from the analysis of the sediment parameters, that there is a slight difference between the characteristics of sediment found on the seagrass area, and the sediment in the sand bank area. It is not possible to deduce whether these differences are caused by the sediments coming from two different sources or not. However, it is more likely to be the effect of seagrass and the hydrodynamics on the intertidal flat (see also Grady (1981); Heiss et al. (2000)).

3.5.2 Sediment transport patterns on Ryde Sands intertidal flat

Sediment transport patterns have been evaluated through GSTA and image analysis. The GSTA suggests that the general movement of sediment is towards the west. High reliability of transport was recorded on the west side of the pier due to a denser sampling stations as compared to the east side. The sediment transport pathways on the sand flat were analysed in separate sections as pointed out by letters in Figure 3.15.

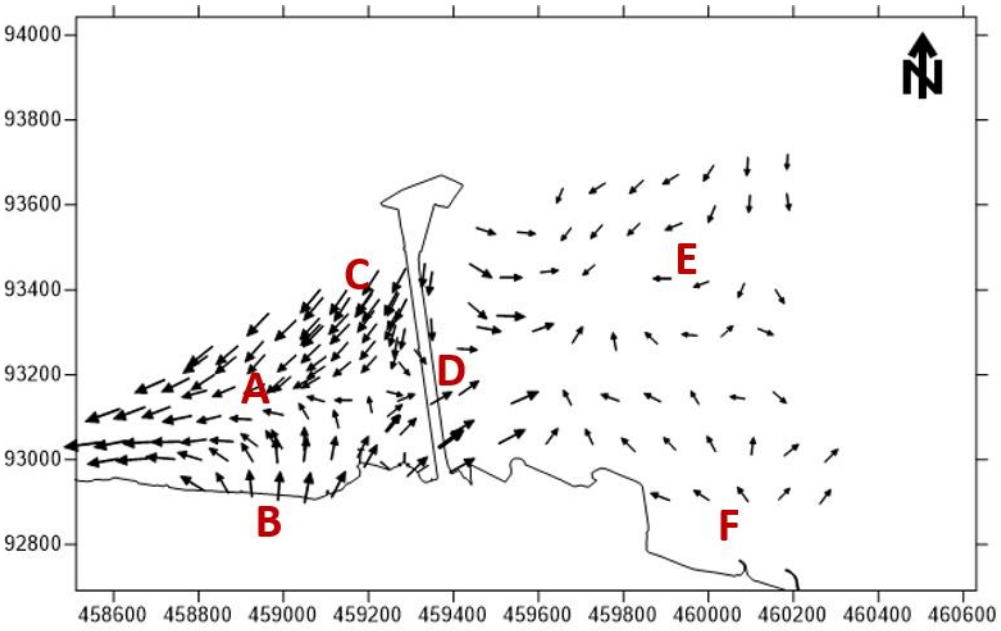

Figure 3.15: Areas of sediment transport pathway.

At area on the west of the pier where seagrass is the most extensive (Area C), it was seen that there was a sediment transport pathway that goes towards the southwest. This transport direction has a high reliability and is in accordance to a previous study in the same area by Tonks (2008). Further west (Area A), the transport pathway continues in a westward direction. The transport direction is influenced by the tidal current direction from east to west during the flood tide (i.e. peak current). On Ryde East close to the pier (Area D), the seagrass area shows transport towards the east and south east. The general transport on the sand bank is towards the west (Area E). Despite a lower reliability of transport vector in this area, probably due to not enough sample points in the area, the analysis of LiDAR data and satellite images from 2007 to 2016 verifies this direction of transport. The westward movement of the sand bank over the 10 years was recorded to be over 300 m. The model showed a possible convergence zone between Area D and E, as suggested by SCOPAC (2012), indicating the zone as the area near a sand spit on the east side of the pier head. In the areas close to the seawalls (Area B and F), the sediments are transported towards the sea. These areas are considerably steeper than to the rest of the sand flat.

Analysis of LiDAR data and aerial photographs indicated that the spit formed in a north east direction. Tonks (2008) reported that the end of the spit has remained stable from 1975 to 1995, whereas the west side is growing further offshore. At the top of area D, there is a sediment transport pathway that goes towards the east. This transport direction has a low reliability, however it could provide an explanation for the spit location and growth on this side.

3.5.3 Seagrass distribution on Ryde Sands intertidal flat

Ryde intertidal sand flat is a suitable place for comparison of seagrass distribution change using high resolution aerial photograph, for *Zostera noltii* was almost the exclusive living macrophyte in the mapped intertidal area. There was a larger species of seagrass, *Zostera marina* present in Ryde, however this species occupies the subtidal area rather than the intertidal area. A few senescent drifting macroalgae were occasionally present.

Seagrass distribution have been evaluated using NDVI from aerial images captured during the peak distribution of seagrass in the summer of 2013 and 2016. The results were able to detect seagrass distribution and giving estimates of the density. An increase in meadow areas was observed from 2013 to 2016 with total surfaces colonized by *Zostera noltii* increasing by 13.5 % from 55 to 62 ha, respectively. There was also an increase in the densest part of the meadow (NDVI > 0.2). In 2013, the densest part of the meadow represented only 2 % of total meadow surfaces, compared to 35 % in 2016. The seagrass expansion took place mainly towards the lower part of the intertidal zone. On the west side of Ryde Pier, the densest meadows were observed on the lower intertidal zone whilst on the east side, the densest meadows extent covers the whole intertidal zone. The meadow is separated by a bare sand section which is the pathway for hovercraft service.

The expansion of the seagrass beds can possibly be linked to the tidal flat accretion. The escalation of bed level increases the duration of emersion, thus allowing the seagrass to be exposed to light for a longer duration of time (Barillé et al., 2010; Madsen et al., 2001). Vermaat & Verhagen (1996) have reported that *Zostera noltii* photosynthesis is largely limited to low tide daylight especially in a turbid estuary. The increase of biomass can also reduce resuspension of sediment resulting clearer water (Gacia et al., 1999).

3.6 Conclusions

Surficial sediment and seagrass distribution of Ryde intertidal sand flat were analysed in this study. The general distribution of sediment on the sand flat showed a domination of fine sand. There are differences in the characteristics of sediment in the sand flat, in agreement

with the different environments in the study zone. The areas where seagrass meadows were present contain finer and less well sorted sand as compared to the sand bank.

The grain size statistics suggest a fining of grain size towards west in the direction of sediment transport as predicted by GSTA. Sediment becomes less sorted in this direction. Dominance of positive skewed sediment in the study area indicates the prevalence of low energy and depositional environment. Relatively high fraction of leptokurtic sediment in the tidal flat also depicted that the area has a largely uniform energy environment.

The results from my study shows that the GSTA provides meaningful sediment transport pathways over Ryde Sands intertidal flat including the vegetated area. GSTA indicates transport on sand flat occurs mainly to the west due to longshore currents generated by waves travelling north-east. The reliability of the transport vectors varied depending on the closeness of the surrounding sample sites. Low reliability of sediment transport pathway by GSTA in the sand bank area was due to lower sampling resolution. This method is without any consideration of known hydrodynamic conditions that could potentially influence sediment pathways and therefore doesn't give an answer to the transport pathways. However, the transport path inferred is consistent with both, peak tidal current and local longshore current generated by waves.

The formation of spit on the edge of the sand bank, however, suggests a second longshore transport current generated by waves travelling south-east. Previous studies discussed in the literature (SCOPAC, 2012; Tonks, 2008) indicated a convergence zone was to be on the west side of the pier. However, it would appear that the convergence zone could be on the east side of the pier in a north-east direction along the edge of the sand flat to the end of the spit. The accumulation of sand that forms the spit is most likely originating from the transport of sediment from the west of Ryde. Furthermore, analysis of the aerial images indicate a westerly movement of the sand bank. The west edge of the sand bank which is also the head of the spit has moved more than a 100 m to the left. The shift of sand bank towards the seagrass area may pose a risk of sediment burial to the seagrass meadow.

The use of aerial photographs and vegetation index for seagrass detection provided a preliminary mapping of the seagrass bed in Ryde. The NDVI provided the distribution extend as well as density of seagrass. The seagrass, *Zostera noltii* distribution area increased in the span of 3 years and there were large areas of dense meadows detected in 2016. Seagrass was found only at depths shallower than -1.5 m but not on the sand bank area on Ryde East. There was an increase in seagrass distribution where the meadows expanded towards the upper intertidal zone. 21 hectares of the survey area were classified as dense meadow with average densities of 2000 shoots m^{-2} and reaching local maxima of approximately 4000 shoots m^{-2}.

The seagrass area covers 62 ha of the total 285 ha of the intertidal sand flat. The reasons for seagrass distribution growth can be attributed to the increase in bed elevation, thus increasing light availability and low amount of human activities allowing the seagrass to grow.

Chapter 4: Spatial and temporal impact of Zostera noltii on intertidal flat stability in Ryde, Isle of Wight

4.1 Abstract

Seagrasses are known for their wave attenuating and sediment trapping ecosystem services, however, the extent of their influences on the morphology differ from one location to the other. Long-term observational datasets that record and quantify variability, changes and trends in intertidal flat morphology inhabited by seagrass are rare. In this study, I investigated the morphological changes that occur on intertidal flats in Ryde, Isle of Wight due to the presence of the seagrass, *Zostera noltii* with consideration to varying plant cover and sediment composition and the interaction between them. Detailed seasonal observations were made for two years along two shore profile. These were put into context by analysis of longer-term observations made by the Channel Coast Observatory between 2005 -2017.

Gradients in sediment texture and composition were related to meadow distribution and density. This was attributed to the mechanical trapping of particles and enhanced deposition due to dampening of wave action in the meadows. Erosion and accretion varies over short time intervals. However, over longer time scales the sand flat is generally stable. At the eastern and western extents of the study area accretion occurred while the middle parts were undergoing erosion. Locations inhabited by seagrass showed less change compared to bare sand profiles. The tidal flat was found to be stable or exhibited minor bed accretion (cms) along vegetated profiles. Furthermore, accretion was related to seasonal growth patterns of the meadows. The presence of *Zostera noltii* meadow stabilised the intertidal flat during the peak summer growth season as well as providing erosion control during the winter months, despite losing most of its above-ground biomass during this season. Even during the winter seasonal decrease of biomass, the meadow reduced erosion of the tidal flat.

Overall, these results provide a baseline understanding for ecosystem management aimed at affecting sediment dynamics, thereby contributing to a better understanding of nature-based solutions to address coastal erosion. In addition, the present study highlights the important role of even small intertidal seagrasses as ecosystem engineers.

4.2 Introduction

Seagrass meadows are important for sediment trapping (Gacia et al., 1999; Hendriks et al., 2010) and sediment stabilisation (Fonseca, 1989; Potouroglou et al., 2017). Seagrasses, especially large subtidal species like *Zostera marina*, *Thalassia testudinum* and *Posidonia oceanica* affect coastal water quality by absorbing nutrients and trapping sediments (Adriano et al., 2005; Bulmer et al., 2018; Manca et al., 2012). Moreover, seagrass meadows have the ability to reduce wave action consequently modifying the energy regimes of their environments (Heiss et al., 2000; Manca et al., 2012), helping to stabilise sediments by trapping and binding the sediment through their vast root system that takes up nutrients from the sand and provided anchorage from the plants themselves (Fonseca, 1989). The sediment-trapping ability of seagrass can lead to an equilibrium between deposition and erosion to maintain a relatively constant sea bed (Koch, 1999).

The effects of vegetation on sediment properties occur via complex interactions among the plants, suspended sediments in the water and hydrodynamics (Wilkie et al., 2012). Fine sediment and organic matter accumulation in a dense seagrass bed is caused by promotion of trapping of sediment, and by reduction of resuspension, shown to be caused by wave and current reduction in *Posidonia oceanica* (Gacia & Duarte, 2001; Manca et al., 2012; Jorge Terrados & Duarte, 2000). Previous studies have identified shoot density and flexibility as important factors in sediment trapping (Bouma et al., 2005; Hendriks et al., 2008; Peralta et al., 2008). It has been demonstrated in flume studies that sediment trapping and deposition in seagrass beds were positively related to plant density in *Zostera noltii* and *Spartina anglica* (Bouma et al., 2005; Peralta et al., 2008) and *Posidonia oceanica* meadows (Hendriks et al., 2008), as well as shown in my laboratory experiment in Chapter 5. Densely covered beds of *Zostera marina* at sandy sites showed a significant increase of fine sediment fractions and organic matter in vegetated patches as compared to the unvegetated areas (van Katwijk et al., 2010). However, it has also been shown in flume studies that above certain plant densities in a *Zostera noltii* meadow (Ganthy et al., 2015; Peralta et al., 2008) and at the leading edge of the meadow in *Zostera marina* (Fonseca & Koehl, 2006) and *Posidonia oceanica* (Manca et al., 2012) mimics, that these effects might differ due to the bending of the shoots. Whilst the combined interpretation of these studies provides a better understanding of the effect of changes in vegetation on particle trapping and deposition, none of them includes the winter state when above-ground plant density and biomass are significantly reduced. Stabilising effects on the seabed are also different depending on plant morphology, therefore it is essential to evaluate each species individually.

The focus of my work was to evaluate the relationships in spatial and temporal variations in bed profiles with occurrence, density and morphology of *Zostera noltii*. This seagrass species

is smaller compared to those cited earlier and occurs intertidally. It is characterized by a unimodal seasonal development, with leaf density showing a summer maximum and a winter minimum as revealed by variations in its above-ground cover and biomass, losing more than 86% of its above-ground biomass during its seasonal decline (Paul & Amos, 2011).

4.2.1 Aim and objectives

Sand flats are known to be dynamic and complex environments that are influenced by physical and biological processes. The shore at Ryde is an example of a sand flat with intertidal seagrass beds creating a biologically diverse environment (Marsden & Chesworth, 2015). Regular and detailed scientific studies on shore behaviour are key coastal management tools, since changes to coastal processes may have significant impact on coastal populations, economic activities and resource management as outlined in the Shoreline Management Plan, SMP (Isle of Wight Council & Haskoning, 2010). The sand flats do not only serve as natural defence against erosion, they are also used as feeding grounds for birds and provide a sheltered habitat with rich food supply and protection from predators (Marsden & Chesworth, 2015). Recently, there has been progress towards the integration of nature-based solutions such as coastal vegetation to protect the coast (Morris et al., 2019); therefore it is important to properly understand the environment and know its limitation before this solution can be implemented widely. Therefore, investigations of the shore in terms of changes to the depth and gradient, as well as to sediment characteristics are of significant scientific value as they reflect the geomorphologic response in the coastal area. This may be of particular relevance as adaptation approaches become more widely used as management tools (Ondiviela et al., 2014). As part of the long-term management of the coast, a beach profile survey programme commenced in 2004 by Channel Coastal Observatory (CCO) at Ryde located on the northeast of the Isle of Wight. This was chosen as one of the sites surveyed as part of the National Network of Regional Coastal Monitoring Programmes of England where ongoing and uninterrupted beach monitoring now spans more than 14 years. This programme enables the study of long-term changes of vegetated bed in the field.

The overall aim of my study was to investigate the spatial and temporal influence of seagrass, *Zostera noltii* on intertidal flat morphology at Ryde, Isle of Wight in order to better understand the extent of any stability afforded the sand flat (i.e. erosion and deposition) through the presence of the seagrass in the area.

The objectives of this study were to:

1) determine the spatial and temporal distribution of sediment and seagrass on Ryde Sands intertidal flat over seasonal (2015-2017) time scales;

2) determine the morphological evolution of the intertidal flat on Ryde Sands intertidal flat over seasonal (2015-2017) and longer time scales (2004-2017);
3) identify the spatial and temporal relationships between sediment characteristics, sand flat morphology and seagrass distribution.

4.3 Material and methods

4.3.1 Study area

The 4.5 km-long Ryde intertidal flats are situated at the northeast region of the Isle of Wight, off the south coast of England. The intertidal flats have a triangular shape and the central part extends approximately 2 km into the East Solent with a total area of approximately 340 ha. The prominent feature in the area is a 700 m long pier separating two sides of the sand flat into Ryde West and Ryde East. Seagrass, *Zostera noltii* covers approximately 30 ha of the sand flat in the west and 35 ha in the east. Another seagrass species, *Zostera marina* was observed at the lower boundary below -2.73 m Ordnance Datum (OD) but its extent is unknown. Detailed description of the study area can be found in Chapter 2.

4.3.2 Sediment and seagrass sampling

A total of 104 sediment samples were collected across four stations over profile RYD23 on the intertidal flats (Figure 4.1:). Sampling was undertaken over 26 months (August 2015 – October 2017). In order to gain an understanding of recent and local transport rates, only the surficial layer (upper 3 cm) of the sediment were sampled (Plomaritis et al., 2008). The surficial layer of sediment was collected using a trowel during low tide, when the tidal flat is exposed. Analysis of sediment is described in Chapter 2.

At each sampling location, the structural parameters of the meadow were characterised. Shoot density was counted in one 0.5 x 0.5 m quadrat and 5 randomly chosen replicates were taken at each station to estimate the percentage cover in each quadrats. To determine biomass and Leaf Area Index (LAI), ten shoots were randomly collected at each sampling site. The length and width of the leaves were measured, and the mean total leaf area per shoot multiplied by the shoot density to obtain the LAI (m^2 leaves m^{-2}).

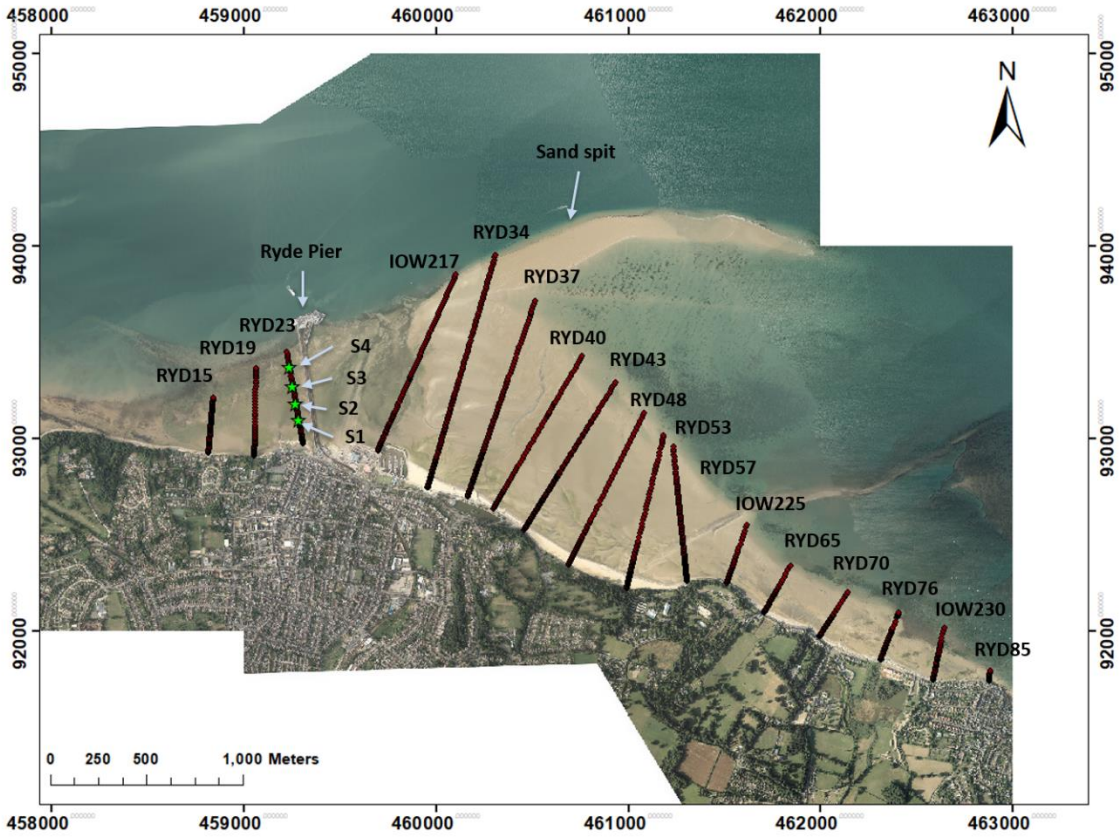

Figure 4.1: Profile names (RYD15 – RYD85) and locations from CCO. S1 – S4 marks my sediment and seagrass sampling between 2015 and 2017 (see Table 4.1 for further details). Area on the east and west side of Ryde Pier was referred as Ryde West and Ryde East, respectively.

4.3.3 Beach profile

Beach profile analyses were made from monthly surveys and data obtained from the CCO website. CCO beach profile surveys were carried out bi-annually in late winter/early spring and late summer/early autumn using Real Time Kinematic (RTK) Global Positioning System (GPS) produced by Trimble and supplied by KOREC Group, United Kingdom. Additional monthly surveys were carried out in accordance to the CCO survey format (available on www.channelcoast.org) using the same equipment. The positional accuracy of the data used in this study was ± 15 mm and elevational accuracy of ± 20 mm.

Profiler 3.2 XL program (Cohen, 2014) was used to analyse the profiles. Cross-sectional areas and slope values were obtained to examine the evolution of the morphology of the intertidal flat. The data were collected from autumn 2004 to spring 2017. The data from each of the years was compared to each other by plotting the profiles and using the extrapolated cross-

sectional area as a proxy for beach volume. The annual evolution rates of the profiles were measured by calculating the slope of the regression line.

The change in cross-sectional area was calculated as the difference in Cross-sectional Area (CSA) between two surveys at a same profile limit, expressed as a percentage change compared to the earlier CSA using the following equation.

$$\%\ change = \frac{CSA_1 - CSA_2}{CSA_2} \text{x } 100$$

Equation 4.1

where CSA_1 = was the area of the previous survey and CSA_2 was the recent survey. Therefore, a change of –10% represents erosion of 10% of the area of last survey. The results allowed the percentage of erosion and accretion to be analysed for certain time periods.

4.3.3.1 Monthly profiles

The site was visited monthly during spring low tides over a 26 month period from August 2015 to October 2017. Two lines, RYD19 and RYD23 (Figure 4.1) on Ryde West were recorded using the same RTK GPS used in CCO surveys to investigate the monthly changes on the intertidal flats profile.

4.3.3.2 Channel Coastal Observatory (CCO) beach profiles

CCO surveys included 3 lines on the east of Ryde Pier (Ryde East) namely RYD15, RYD19 and RYD23 and 14 lines on the west part (Ryde West) namely IOW217, RYD34, RYD37, RYD40, RYD43, RYD48, RYD53, RYD57, IOW225, RYD65, RYD70, RYD76, IOW230 and RYD85 in that order to the east (Figure 4.1). The profile survey dates are listed in Table 4.1.

.

Table 4.1: Profile sampling dates.

	Profile name					
	RYD15-57	**IOW217**	**IOW225**	**RYD65**	**RYD70,76, IOW230**	**RYD85**
Profile 1	14/10/2004	14/10/2004	14/10/2004	02/09/2004	09/02/2004	02/09/2004
Profile 2	24/05/2005	24/05/2005	24/05/2005	10/01/2005	10/01/2005	10/01/2005
Profile 3	15/11/2005	26/05/2006	26/05/2006	15/03/2006	22/08/2005	22/08/2005
Profile 4	26/05/2006	09/10/2006	09/10/2006	14/08/2006	15/03/2006	15/03/2006
Profile 5	09/10/2006	21/03/2007	21/03/2007	22/03/2007	14/08/2006	12/09/2006
Profile 6	21/03/2007	07/04/2008	07/04/2008	22/01/2008	22/03/2007	22/03/2007
Profile 7	07/04/2008	15/10/2008	15/10/2008	18/08/2008	22/01/2008	22/01/2008
Profile 8	15/10/2008	26/03/2009	26/03/2009	26/11/2008	18/08/2008	18/08/2008
Profile 9	26/03/2009	07/09/2009	07/09/2009	22/04/2009	26/11/2008	02/09/2008
Profile 10	07/09/2009	29/03/2010	29/03/2010	19/10/2009	22/04/2009	26/11/2008
Profile 11	29/03/2010	26/08/2010	26/08/2010	26/04/2010	19/10/2009	22/04/2009
Profile 12	26/08/2010	18/02/2011	18/02/2011	06/10/2010	26/04/2010	19/10/2009
Profile 13	18/02/2011	02/08/2011	02/08/2011	19/04/2011	06/10/2010	26/04/2010
Profile 14	02/08/2011	06/08/2012	06/08/2012	27/10/2011	19/04/2011	06/10/2010
Profile 15	06/08/2012	11/02/2013	11/02/2013	06/08/2012	27/10/2011	19/04/2011
Profile 16	11/02/2013	23/08/2013	23/08/2013	11/02/2013	06/08/2012	27/10/2011
Profile 17	23/08/2013	27/02/2014	27/02/2014	23/08/2013	11/02/2013	06/08/2012
Profile 18	27/02/2014	26/08/2014	26/08/2014	27/02/2014	23/08/2013	11/02/2013
Profile 19	26/08/2014	05/03/2015	05/03/2015	26/08/2014	27/02/2014	23/08/2013
Profile 20	05/03/2015	17/08/2015	17/08/2015	05/03/2015	26/08/2014	27/02/2014
Profile 21	17/08/2015	07/03/2016	07/03/2016	17/08/2015	05/03/2015	26/08/2014
Profile 22	07/03/2016	16/09/2016	16/09/2016	07/03/2016	17/08/2015	05/03/2015
Profile 23	16/09/2016	14/03/2017	14/03/2017	16/09/2016	07/03/2016	17/08/2015
Profile 24	14/03/2017			14/03/2017	16/09/2016	07/03/2016
Profile 25					14/03/2017	16/09/2016
Profile 26						14/03/2017

4.3.4 Tidal characteristics

Ryde is subject to a semi-diurnal tide (Figure 4.2 A), and the tidal range is between 2 m during neap tides and 4 m during spring tides. Ryde experiences an extended high-water with slight double peaks on some tides; the ebb stage of the tide is shorter than the flood. The tidal flow showed that the tide was a progressive wave type over the tidal flats. The results from an electromagnetic current meter (EMCM) deployed in September 2015 (details in Chapter 2) showed the maximum depth averaged current velocities were around 0.2 m s^{-1} and took place over high water and low water (Figure 4.2 B). The flow velocities were generally lower closer to shore. The main flow was from East to West during flood tide and West to East during the ebb tide (Figure 4.2 C). The tidal flow rotates clockwise over the flats

during tidal inundation. Mean High Water Spring (MHWS) in Ryde is 1.86 m and Mean Low Water Spring (MLWS) is -1.94 m OD (Tonks, 2008).

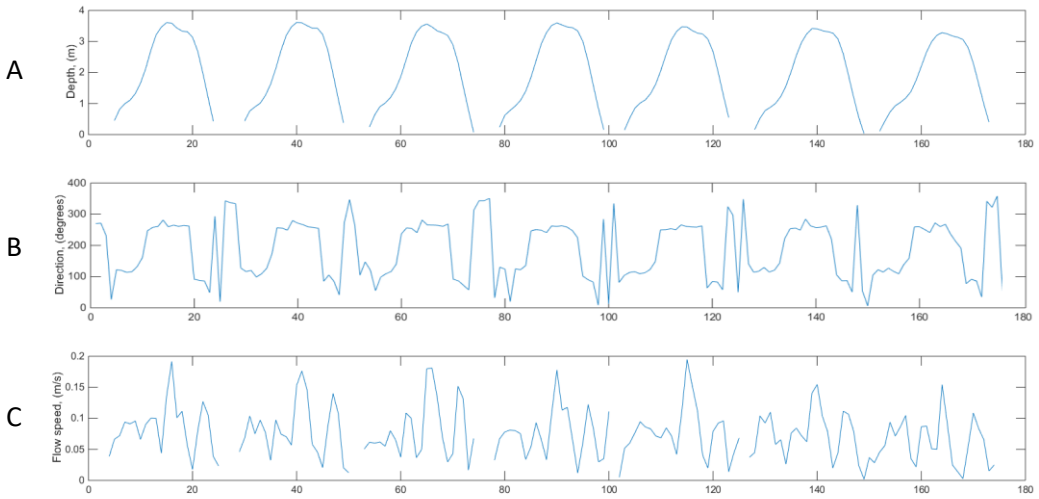

Figure 4.2: Tidal flow conditions measured in September 2015 representing A) the tidal elevation, B) the direction, where 0 degrees is north and C) flow speed.

4.4 Results

4.4.1 Seagrass and sediment composition

4.4.1.1 Monthly surveys of RYD23

Figure 4.3 shows the *Zostera noltii* shoot density at four stations (S1 - S4) along the RYD23 survey line depicted in Figure 4.1. S1 was located towards the upper shore, while S4 was closest to the mean low water line. Seagrass growth was strongly seasonal over the 26 month period. Shoot densities (Figure 4.3) showed a distinct variation over the growth cycle with maximum shoot densities in summer and minimum values in winter. Shoot density also varied with location with sparser density closest to the upper backshore and denser shoot density on the lower foreshore. The average density was 1182 shoots/ m^2 with a minimum of 40 shoots/ m^2 in January 2017 and a maximum of 4360 shoots/ m^2 in June 2017. Peak seagrass distribution differed between years as seagrass density was most abundant in September in 2015, August in 2016 and June in 2017.

Leaf lengths averaged 16.8 cm with a minimum of 10 cm in January 2017 and a maximum of 30 cm in October 2016. The variation of leaf length throughout the year was similar to that recorded in other *Zostera noltii* meadows in the Arcachon Bay, France (Auby & Labourg, 1996) and in Venice Lagoon, Italy (Curiel et al., 1996). Values recorded in Ryde were based on

a smaller sample populations where longest leaves of a shoot are recorded which may have led to an over-estimation of the leaf length.

As the seagrass meadows varied in leaf length, width and density over the different seasons, a parameter that includes these values was used to better represent the meadow. Therefore, the 1-sided leaf area index (LAI = leaf length × leaf width × density, $m^2\ m^{-2}$) was calculated and used in the following analyses. The average LAI was 0.28 $m^2\ m^{-2}$ with a minimum of 0.002 $m^2\ m^{-2}$ in January 2017 and a maximum of 1.34 $m^2\ m^{-2}$ in September 2015 (Figure 4.5). Average seagrass percentage cover showed similar trends (Figure 4.4).

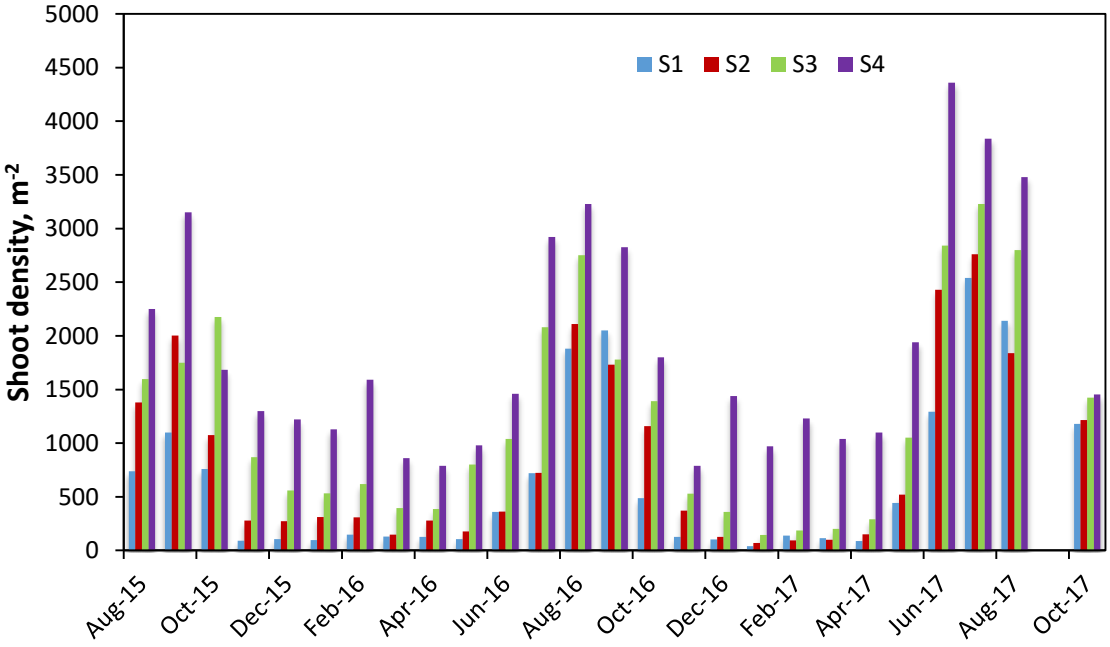

Figure 4.3: Monthly shoot density from August 2015 to October 2017 at Station 1 -4 (S1 highest, S4 lowest) along RYD23 line.

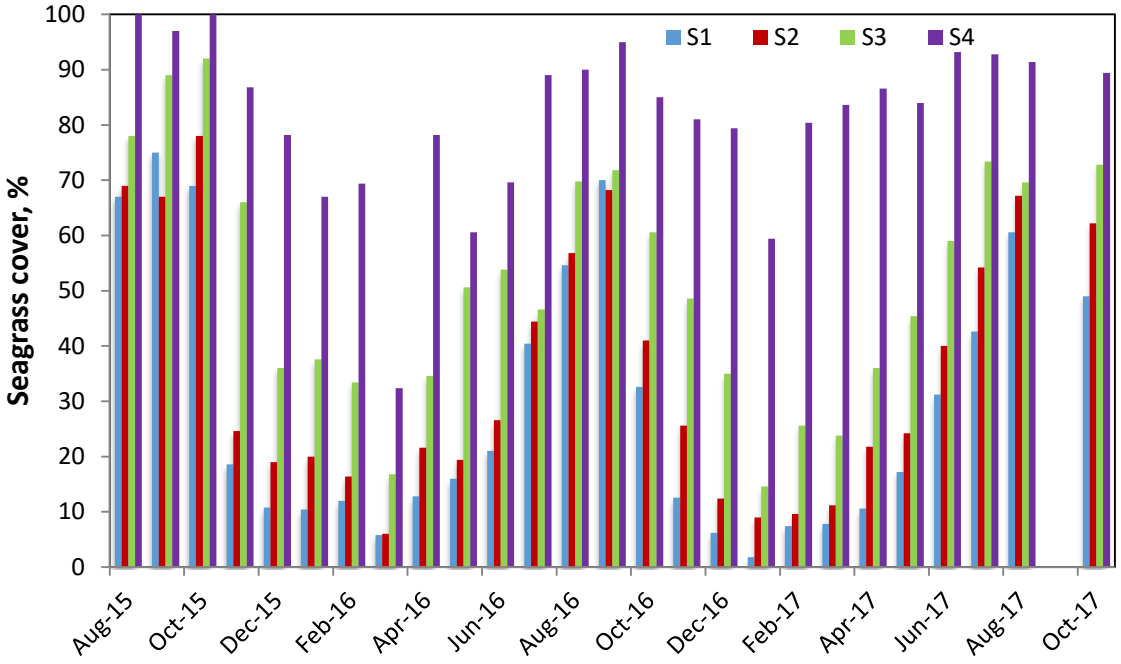

Figure 4.4: Monthly seagrass percentage cover from August 2015 to October 2017 at Station 1 - 4 (S1 highest, S4 lowest) along RYD23 line.

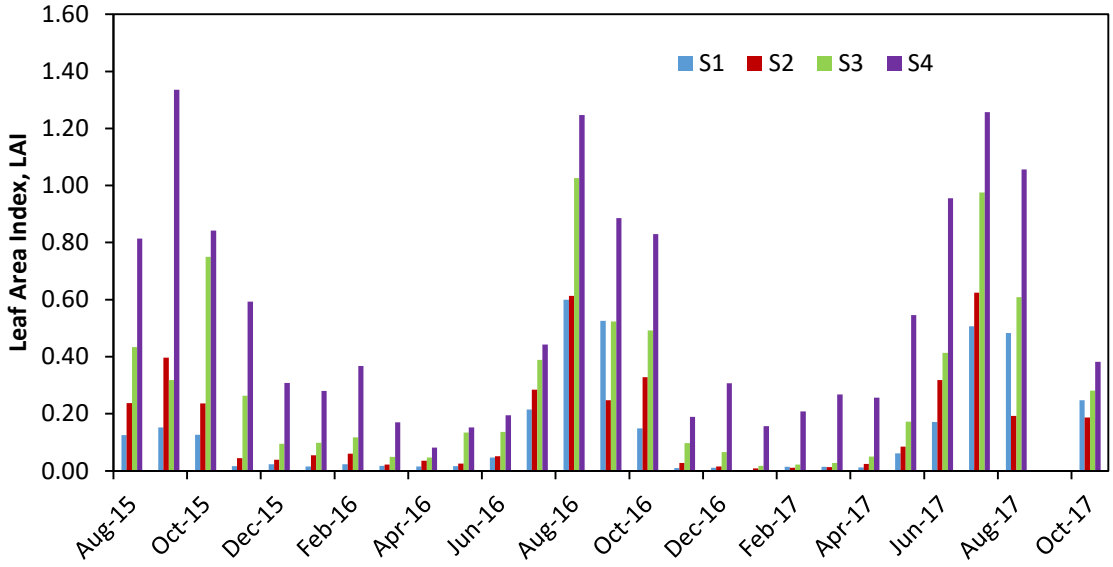

Figure 4.5: Monthly leaf area index from August 2015 to October 2017 at Station 1 -4 (S1 highest, S4 lowest) along RYD23 line.

4.4.2 Spatial and temporal sediment distribution patterns

The sediment characteristics of Ryde Sand were calculated following settling rate analysis using a settling column (detailed in Chapter 2). All of the samples showed a normal (bell-shaped) size distribution. The sieved samples of sediment indicate that the predominant sediment type on the flat was sand (-1 to 4 phi). All of the samples were formed of greater than 95 % sand. The mean grain size, standard deviation (sorting), skewness and kurtosis of

Ryde are given in Figure 4.6 A to Figure 4.6 D following the graphical method. The samples show a mean of between 2.40 to 2.69 phi (Figure 4.6 A). The mean grain size was reasonably uniform over the sand flat with a small trend of fining towards the foreshore. There were no clear trend of mean size variation between the seasons except for at the middle station (S2), where the winter and spring sediments were slightly coarser as compared to during summer and autumn. The average mean grain size in both winter and spring at S2 were 2.51 phi while in summer and autumn, both averaged at 2.55 phi. All of the sediments collected were very well sorted with values between 0.15 to 0.27 phi. The average sorting of sediments (Figure 4.6 B) were 0.18, 0.19 and 0.18 phi in the seaward direction (S1-S3), while the sorting were slightly poorer (0.20 phi) in the most seaward station in the area with thickest seagrass density (S4). Sorting values of the collected sand flat samples revealed that sediments were generally better sorted during the winter months, especially at S4 where sorting values improved from 0.22 phi in the summer to 0.19 phi in the winter.

Across the study area, skewness ranged from 0.08 to 0.39 phi (Figure 4.6 C). 72% samples were very finely skewed, 25% samples were finely skewed and 3% were symmetrical. Sediment were finer skewed with increasing seaward distance across the sand flat with an average of 0.18, 0.20, 0.27 and 0.30 phi from S1 to S4 respectively. During summer months, sediment were also more finely skewed compared to during winter months at all stations except at the most landward station (S1), which had a near symmetrical distribution in summer 2015 (0.08 phi). Values of kurtosis (Figure 4.6 D) along the transect ranged from mesokurtic or normal distribution (10%) to a leptokurtic or peaked distribution (90%), with distributions from 0.98 to 1.41 phi, with 70 % of the mesokurtic sediment recorded on the foreshore (S4). Lowest kurtosis value, 0.98 phi (mesokurtic) was at S4 in spring 2017 while the highest value, 1.41 phi (leptokurtic) was at S2 in autumn 2016. The midshore (S2 and S3) had on average, a more peaked distribution as compared to above and below (S1 and S4). Values of kurtosis did not show any seasonal trend. Two landward stations showed a more peaked distribution in the summer while the other two seaward stations were more leptokurtic during the winter seasons.

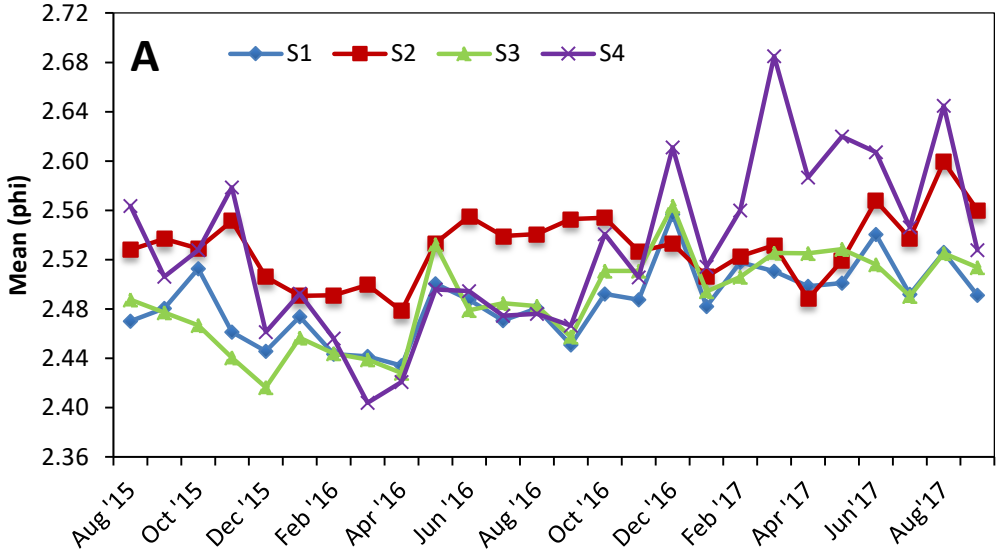
A
S1
S2
S3
S4
Mean (phi)
2.72
2.68
2.64
2.60
2.56
2.52
2.48
2.44
2.40
2.36
Aug '15
Oct '15
Dec '15
Feb '16
Apr '16
Jun '16
Aug '16
Oct '16
Dec '16
Feb '17
Apr '17
Jun'17
Aug'17

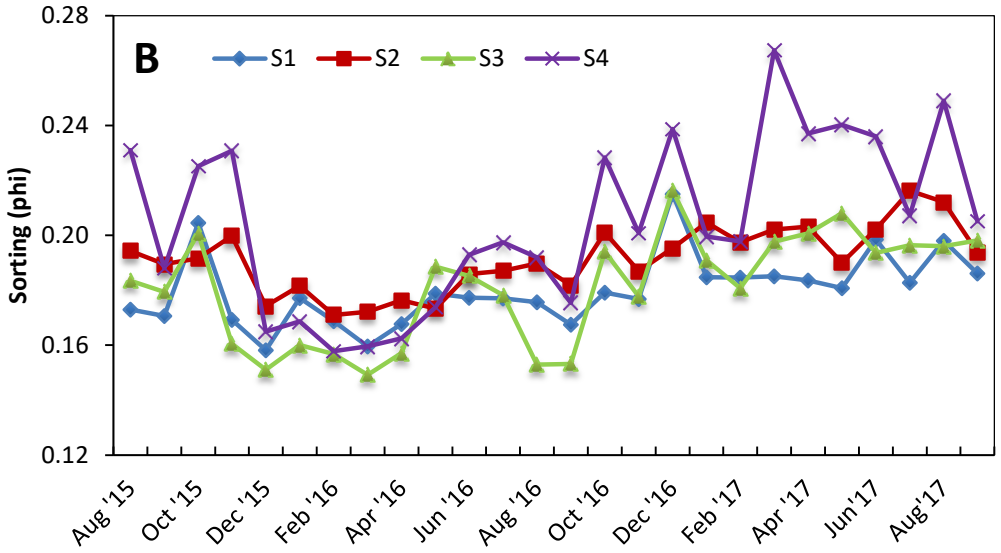
B
S1
S2
S3
S4
Sorting (phi)
0.28
0.24
0.20
0.16
0.12
Aug '15
Oct '15
Dec '15
Feb '16
Apr '16
Jun '16
Aug '16
Oct '16
Dec '16
Feb '17
Apr '17
Jun'17
Aug'17

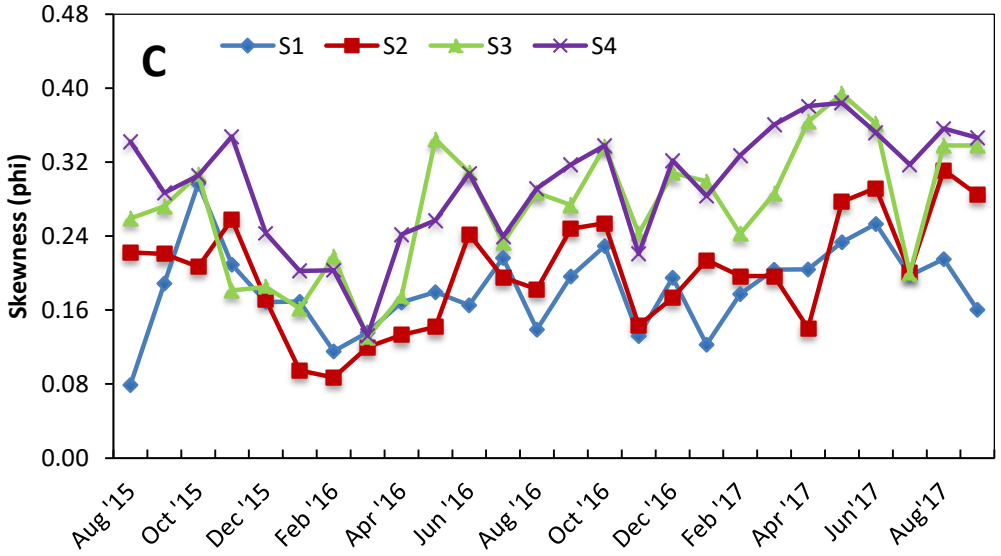
C
S1
S2
S3
S4
Skewness (phi)
0.48
0.40
0.32
0.24
0.16
0.08
0.00
Aug '15
Oct '15
Dec '15
Feb '16
Apr '16
Jun '16
Aug '16
Oct '16
Dec '16
Feb '17
Apr '17
Jun'17
Aug'17

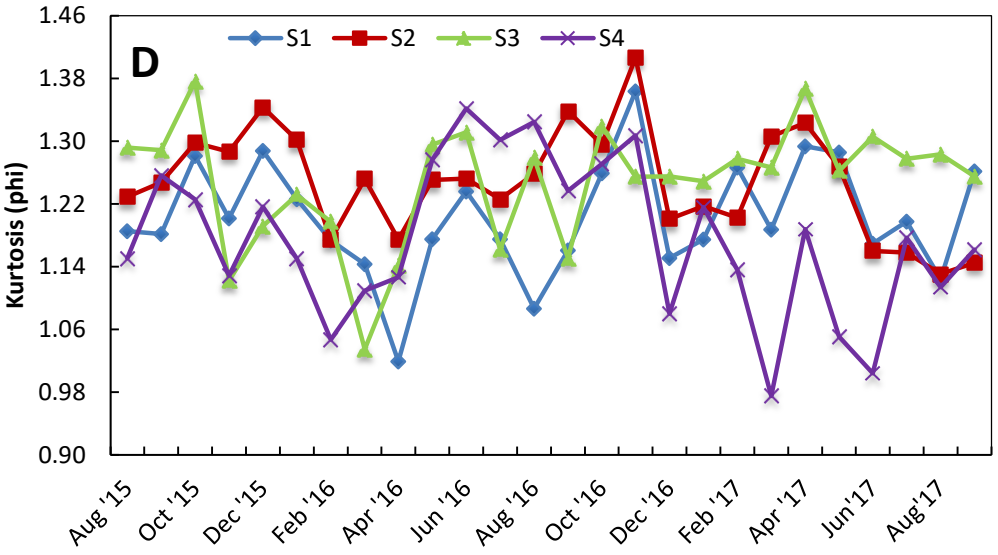

Figure 4.6: A) mean, B) sorting, C) skewness and D) kurtosis at S1, S2, S3 and S4 on RYD23 over 26 month period from August 2015 to October 2017.

4.4.3 Relationship between sediment characteristics and elevation

Figure 4.7 A shows that there is no overall correlation between elevation of the sandflat and the mean grain size, although there are indications of a positive relationship as elevation alters at each station with seasonal sediment movements. Overall, the mean grain size has the largest range at the lower foreshore station (S4). A scatter plot of the mean grain size versus sorting (Figure 4.7 B) shows that mean grain size was significantly correlated with the sorting of sediments (r = 0.87, $p < 0.0001$), as finer sediments in the area tend to be better sorted. A scatter plot of sorting versus skewness (Figure 4.7 C) shows that better sorted samples were positively skewed (r = 0.56, $p < 0.0001$), with the most finely skewed and well-sorted samples being those from lower foreshore area (S4).

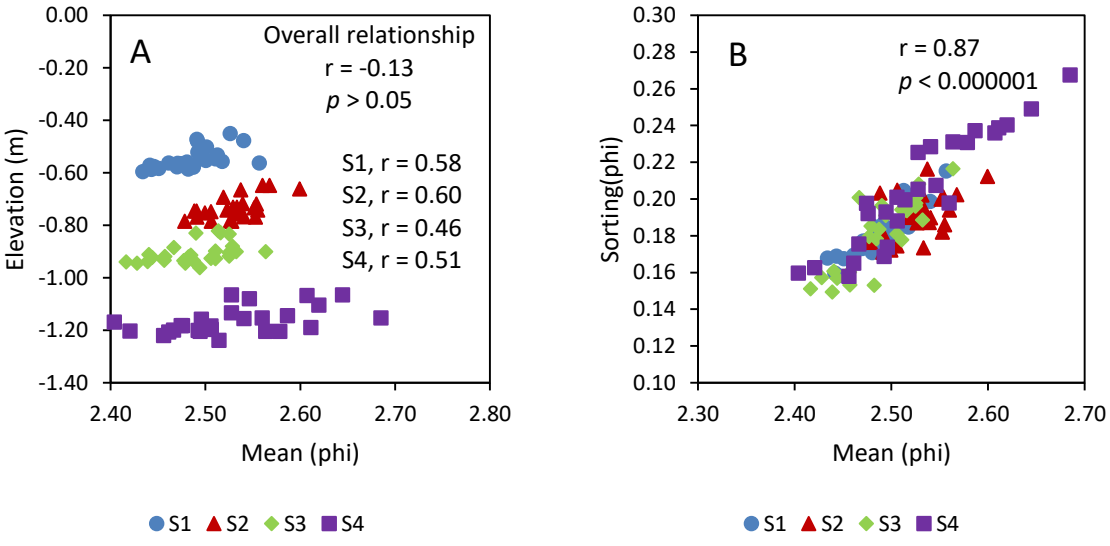

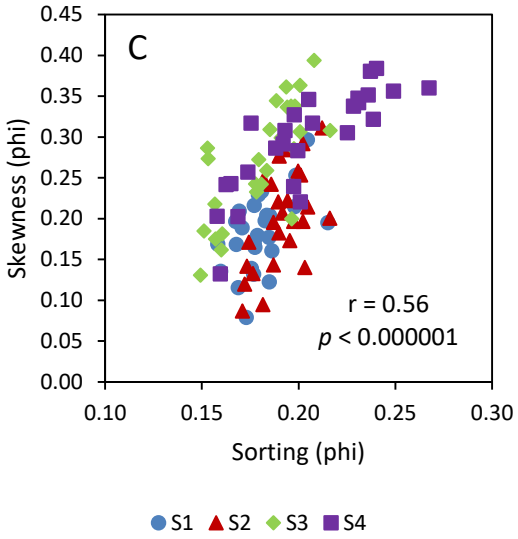

Figure 4.7: Relationship between A) mean grain size and elevation; B) mean and sorting and C) sorting and skewness on RYD23.

4.4.4 Relationships between seagrass shoots density and sediment parameters

Increases in Cross Sectional Area (CSA) at S1 – S4 correspond to the seasonal seagrass density as shown in Figure 4.8. Shoots densities at all stations were positively correlated to the CSA ($p < 0.05$). The highest cumulative CSA was in summer and the lowest cumulative CSA was in winter at all stations. The mean shoot densities at the most landward station (S1) were 1652 m^{-2}, 769 m^{-2}, 105 m^{-2}, 168 m^{-2}, while the mean CSA were 1.38 m^2, 1.34 m^2, 1.33 m^2 and 1.35 m^2 in summer, autumn, winter and spring, respectively. The most seaward station (S4) showed a similar pattern where the mean shoot densities were 3370 m^{-2}, 1925 m^{-2}, 1264 m^{-2} and 1118 m^{-2} while the CSA were 0.77 m^2, 0.72 m^2, 0.70 m^2 and 0.74 m^2, respectively.

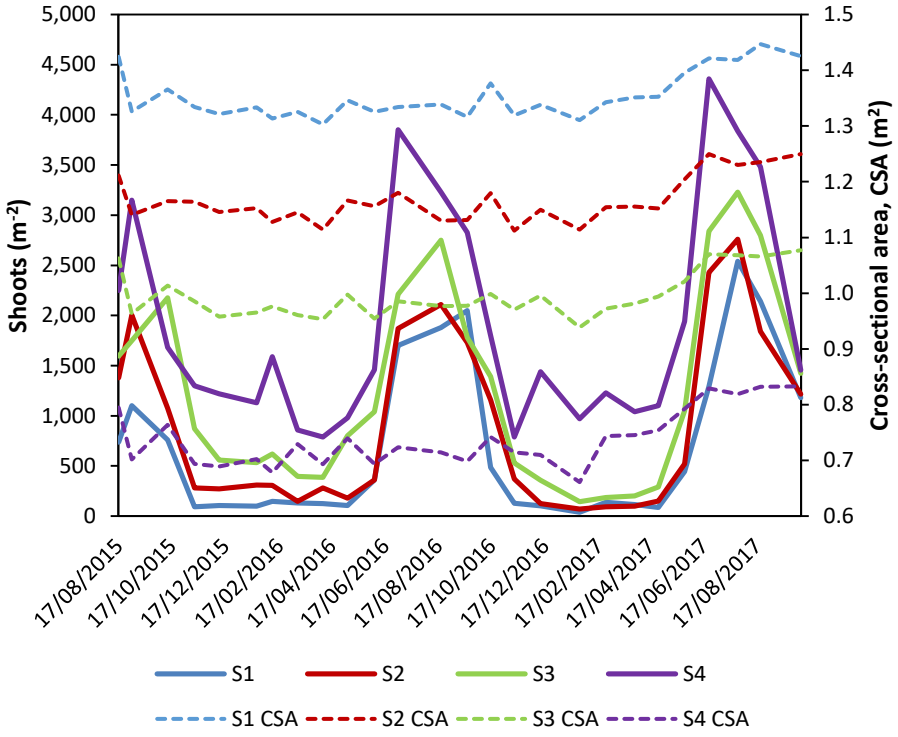

Figure 4.8: Shoot density (m^{-2}) in solid lines and cross-sectional area (m^2) in dashed lines on RYD23.

Sediment characteristics were related to the structural parameters of the *Zostera noltii* on profile RYD23 (Figure 4.9). Figure 4.9 A shows the positive overall correlation between the elevation of the sand flat and the surface area of the plants (LAI). LAI has a higher spread as the elevation decreases, being significantly correlated with the elevation of the seabed ($r = -0.42$, $p < 0.00001$) (Figure 4.9 A), thus indicating denser seagrass canopy in the lower foreshore zone. Mean grain size shows a positive correlation with LAI ($r = 0.22$, $p < 0.05$) (Figure 4.9 B). LAI from the study area was positively correlated with sorting ($r = 0.33$, $p < 0.001$) (Figure 4.9 C) and skewness ($r = 0.45$, $p < 0.001$) (Figure 4.9 D), whereas LAI shows no correlation with kurtosis (Figure 4.9 E).

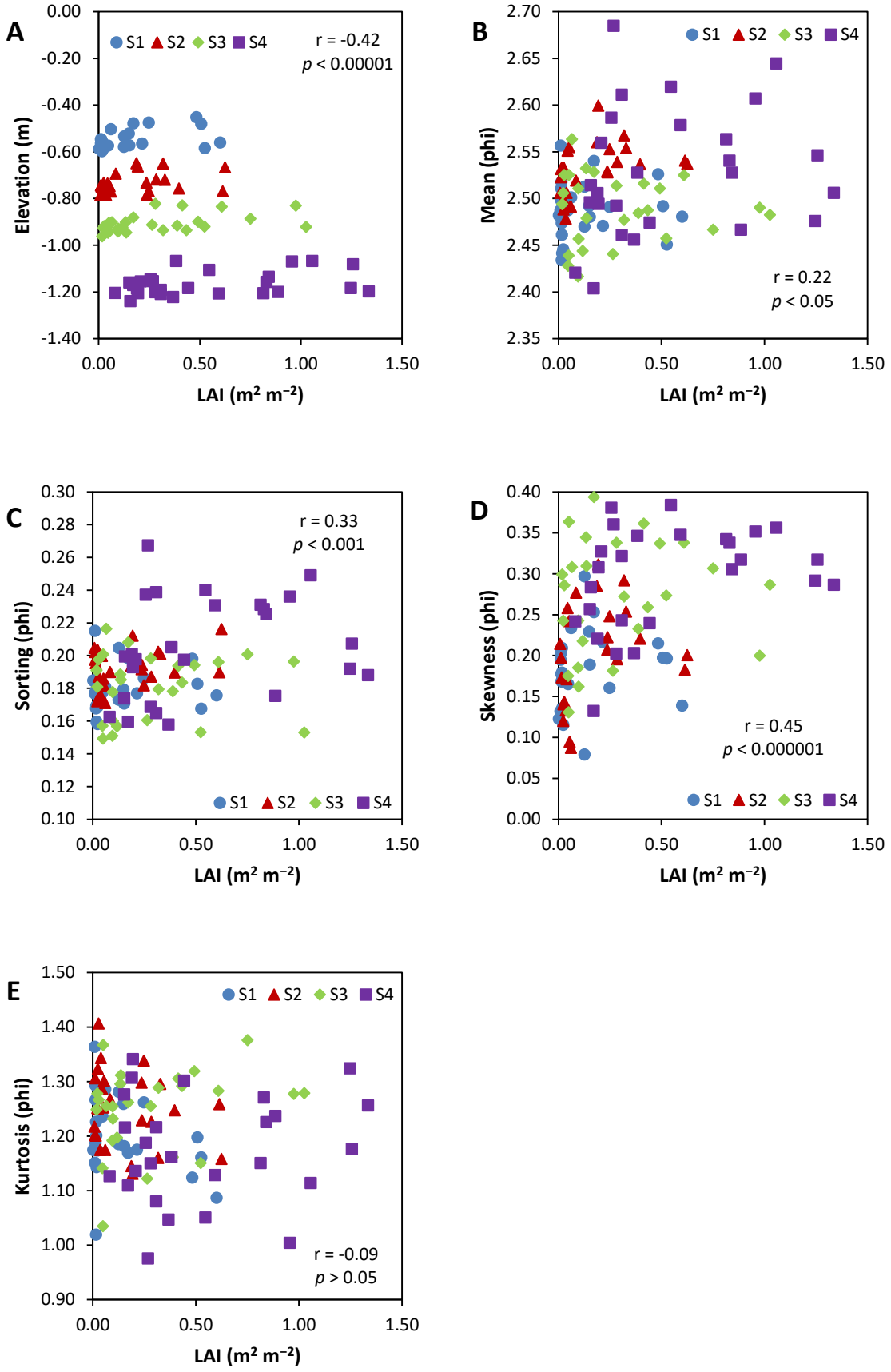

Figure 4.9 : Relationship between A) Elevation and Leaf Area Index, LAI; B) mean and LAI; B) sorting and LAI; D) skewness and LAI; E) kurtosis and LAI on RYD23.

4.4.5 Cross-shore profiles of Ryde intertidal flats (monthly)

The difference in cross-sectional area of the beach profiles inhabited by seagrass, *Zostera noltii* were measured focusing on RYD19 and RYD23. The intertidal flat volume changes for 2 surveyed profiles between August 2015 and October 2017 are summarised in Table 4.2. Figure 4.10 to Figure 4.17 show the comparison of monthly seabed morphology in relation to these two transect lines across the study sites.

Sediment accretion was recorded on lines RYD19 and RYD23 from the beginning of the survey in August 2015 to October 2017, with a cross-sectional area (CSA) increase of 5.6 % and 9.9 %, respectively. Largest erosion on RYD19 was recorded during the period between December 2016 and January 2017 at 2.2% while the least erosion occurred in between July and August 2016 and June and July 2017, both at 0.1%. On RYD23, the highest increase in CSA was in the autumn during the peak seasonal growth of seagrass (3.8%).

There was a good agreement between CSA and density of seagrass meadows. In Ryde, peak seagrass biomass growth was generally in summer while the meadows lose most of their biomass in autumn and recorded their lowest biomass in winter months. Highest average CSA was also recorded in summer while the lowest average CSA was recorded in winter season.

Table 4.2: Monthly survey data on RYD23. Negative values indicate erosion and are in italics. Blue boxes indicate percentage change of higher than 5 %.

		RYD19			RYD23		
	Date	Cross-sectional Area (m^2)	Area Change (m^2)	% change	Cross-sectional Area (m^2)	Area Change (m^2)	% change
Profile 1	17/08/2015	592	0.0	0.0	498	0.0	0.0
Profile 2	01/09/2015	596	4.9	0.8	504	6.8	1.4
Profile 3	12/10/2015	613	16.2	2.7	523	18.2	3.6
Profile 4	12/11/2015	602	*-10.2*	*-1.7*	507	*-15.3*	*-2.9*
Profile 5	10/12/2015	597	*-5.6*	*-0.9*	501	*-5.9*	*-1.2*
Profile 6	22/01/2016	594	*-2.8*	*-0.5*	513	11.9	2.4
Profile 7	09/02/2016	595	0.5	0.1	505	*-8.0*	*-1.6*
Profile 8	09/03/2016	595	0.3	0.0	510	4.2	0.8
Profile 9	07/04/2016	589	*-6.3*	*-1.1*	501	*-8.7*	*-1.7*
Profile 10	05/05/2016	602	13.2	2.2	518	17.3	3.5
Profile 11	05/06/2016	596	*-6.0*	*-1.0*	510	*-8.2*	*-1.6*
Profile 12	02/07/2016	601	5.1	0.9	510	0.0	0.0
Profile 13	20/08/2016	600	*-0.9*	*-0.1*	505	*-5.0*	*-1.0*
Profile 14	19/09/2016	588	*-11.5*	*-1.9*	502	*-3.1*	*-0.6*
Profile 15	16/10/2016	604	15.6	2.6	521	19.0	3.8
Profile 16	12/11/2016	593	*-11.1*	*-1.8*	504	*-16.6*	*-3.2*
Profile 17	12/12/2016	595	2.3	0.4	521	17.2	3.4
Profile 18	26/01/2017	582	*-13.2*	*-2.2*	504	*-17.2*	*-3.3*
Profile 19	25/02/2017	593	10.6	1.8	520	16.0	3.2
Profile 20	30/03/2017	595	2.1	0.4	519	*-1.0*	*-0.2*
Profile 21	26/04/2017	593	*-2.0*	*-0.3*	522	2.8	0.5
Profile 22	26/05/2017	605	12.0	2.0	539	16.7	3.2
Profile 23	23/06/2017	625	19.8	3.3	548	9.7	1.8
Profile 24	26/07/2017	624	*-0.4*	*-0.1*	546	*-2.4*	*-0.4*
Profile 25	21/08/2017	625	0.6	0.1	547	1.5	0.3
Profile 26	06/10/2017	624	*-0.4*	*-0.1*	547	*-0.6*	*-0.1*
Total change (m^2)			32.8	5.7		49.2	10.0
% change in CSA Baseline August 2015 to October 2017				**5.6**			**9.9**

4.4.5.1 RYD19

Over the two years period, intertidal flat profiles of transect line RYD19 (375 m long) (Figure 4.10 A) were evaluated and 32.8 m^2 (5.6 %) of sediment accretion was recorded from the baseline profile in August 2015 (Figure 4.10 B). Surveys in autumn, winter, spring and summer recorded a cumulative change of 8.3 m^2, 14.0 m^2, 31.4 m^2 and -4.5 m^2, respectively. Largest sediment accretion was recorded in June 2017 with 19.8 m^2 (3.3 %) increase of volume from the previous month (Figure 4.10 C); while the largest sediment erosion was -13.18 m^2 (-2.2 %) in January 2017 (Figure 4.10 D). Evolution rate of the profile ranged

between -15.7 cm and 5.6 cm with an average increase of approximately 2 cm per year (Figure 4.11) indicating a depositional bed. The first 10 m of the profile however, were experiencing an erosion up to 15.7 cm per year. Profiles during late winter were generally lower as compared to late summer profiles (Figure 4.12). Figure 4.13 shows the monthly evolution of CSA. The periodic rise and fall suggest alternating phases of deposition and erosion. The average CSA was lowest in winter (592.57 m^2) and highest during summer (611.67 m^2). Autumn and spring CSA were 603.04 m^2 and 596.25 m^2, respectively.

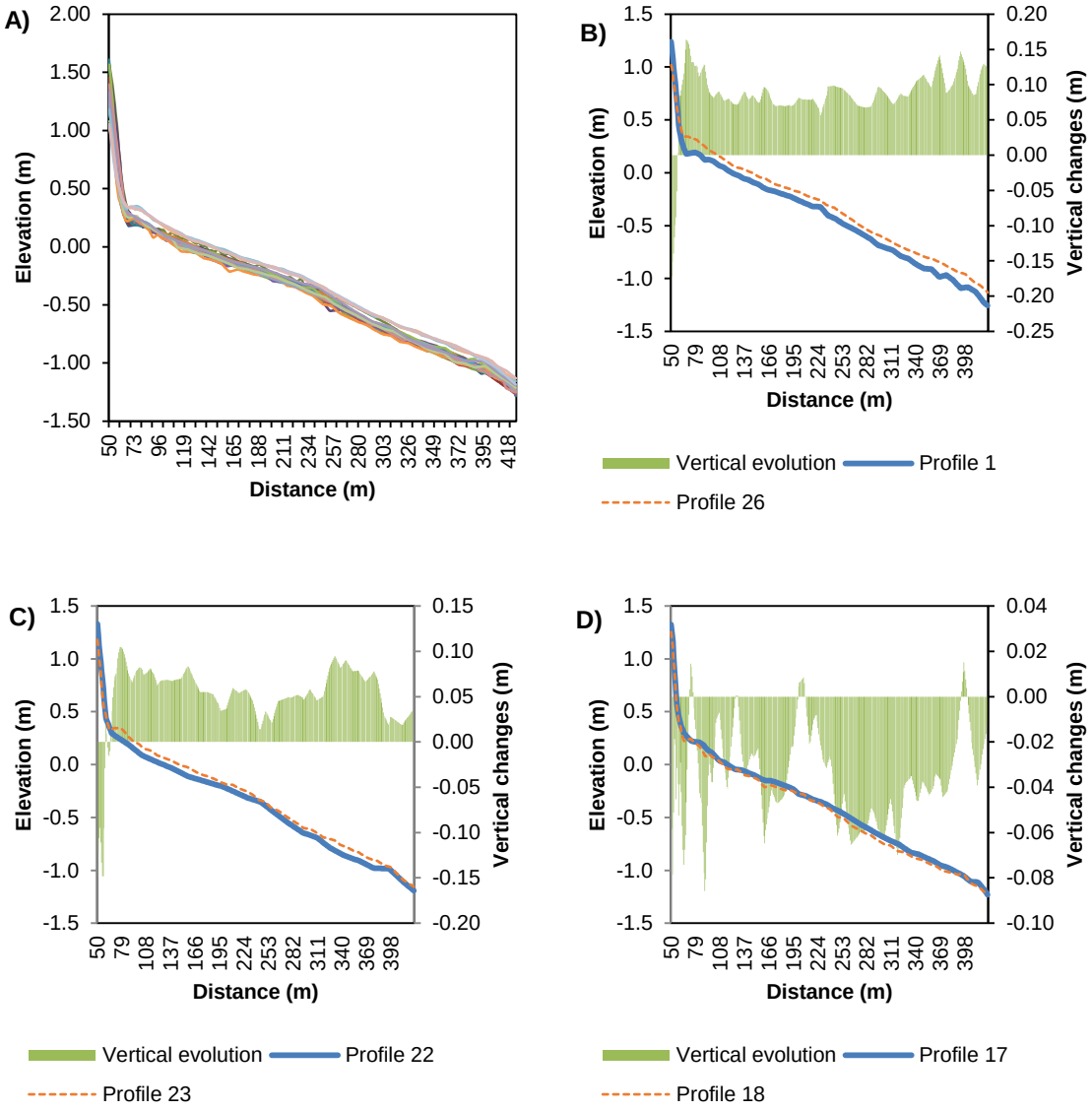

Figure 4.10: A) RYD19 profile envelope from August 2015 – October 2017, B) baseline (August 2015) and most recent profile (October 2017), C) biggest accretion between successive surveys, D) biggest erosion between successive surveys and their vertical evolutions respectively.

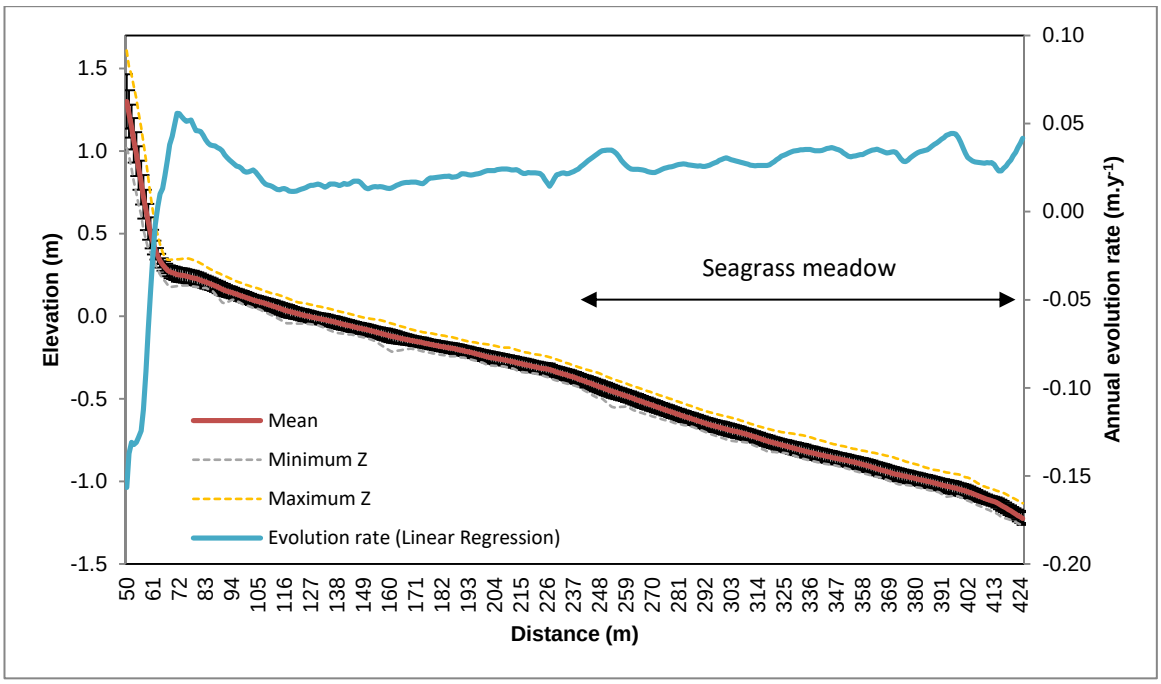

Figure 4.11: Mean, median, standard-deviation, minimum, maximum and evolution rates of profile RYD19. The vertical bars represent the standard-deviation of each point related to its mean.

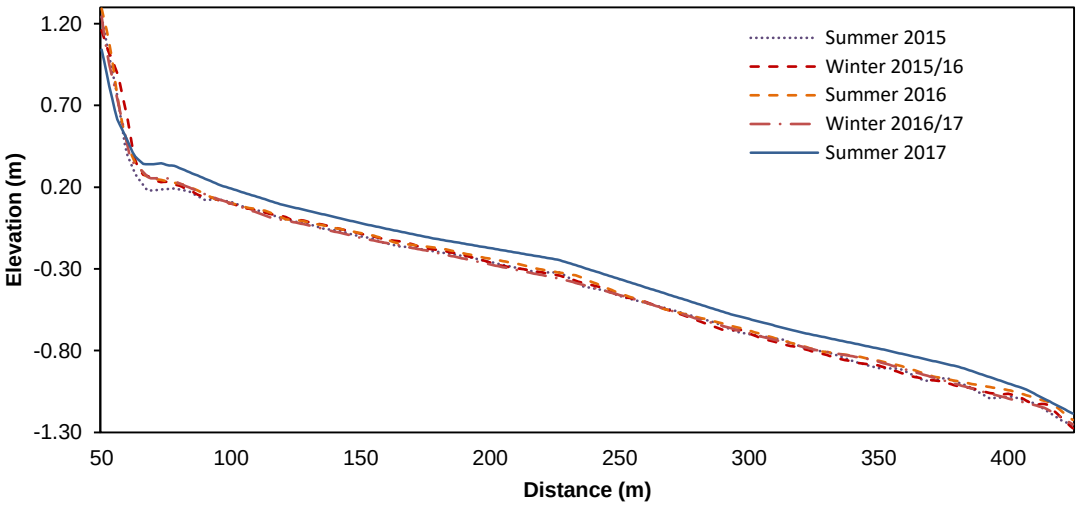

Figure 4.12: Summer and winter profiles of RYD19 (2015-2017).

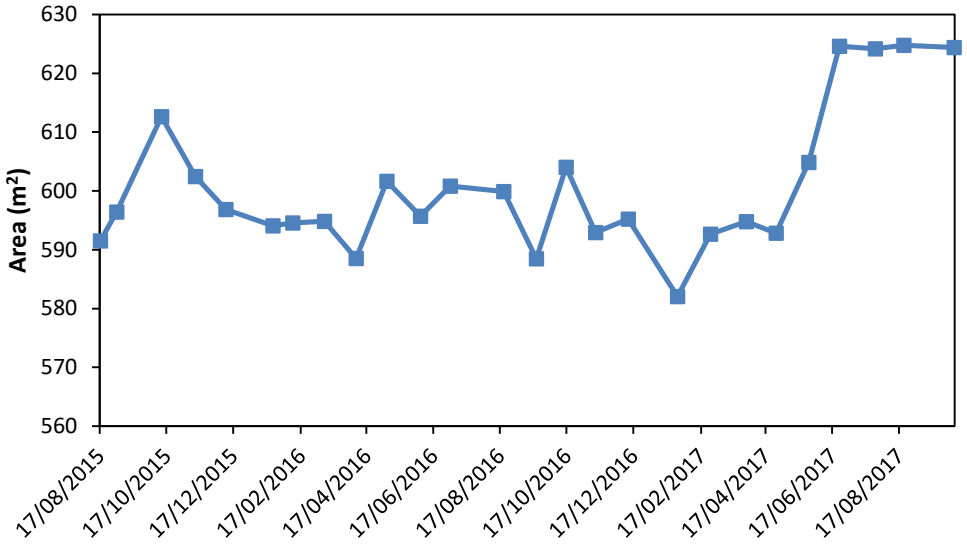

Figure 4.13: Monthly cross sectional area (CSA) of each profiles on RYD19.

4.4.5.2 RYD23

Over the two year period, intertidal flat profiles of transect line RYD23 (482 m long) (Figure 4.14 A) were evaluated and 49.2 m^2 (9.9 %) of sediment accretion was recorded from the baseline profile in summer 2015 (Figure 4.14 B). Surveys in autumn, winter, spring and summer recorded a cumulative change of 8.3 m^2, 14.0 m^2, 31.4 m^2, -4.5 m^2, respectively. Largest sediment accretion was recorded in October 2016 with 19.02 m^2 (%) increase of volume from the previous month (Figure 4.14 C), while the largest sediment erosion was -17.19 m^2 (-2.31 %) in January 2017 (Figure 4.14 D). The evolution rate on the profile ranged between 0.8 cm and 15.9 cm with an average increase of approximately 5 cm per year (Figure 4.15) suggesting a depositional bed. Profiles during late winter were generally lower as compared to late summer profiles (Figure 4.16). Figure 4.17 shows the monthly evolution of CSA with rise and fall suggesting alternating phases of deposition and erosion. The average CSA was lowest in winter (510.98 m^2) and highest during summer (527.79 m^2). Autumn and spring CSA were 515.44 m^2 and 518.08 m^2 respectively.

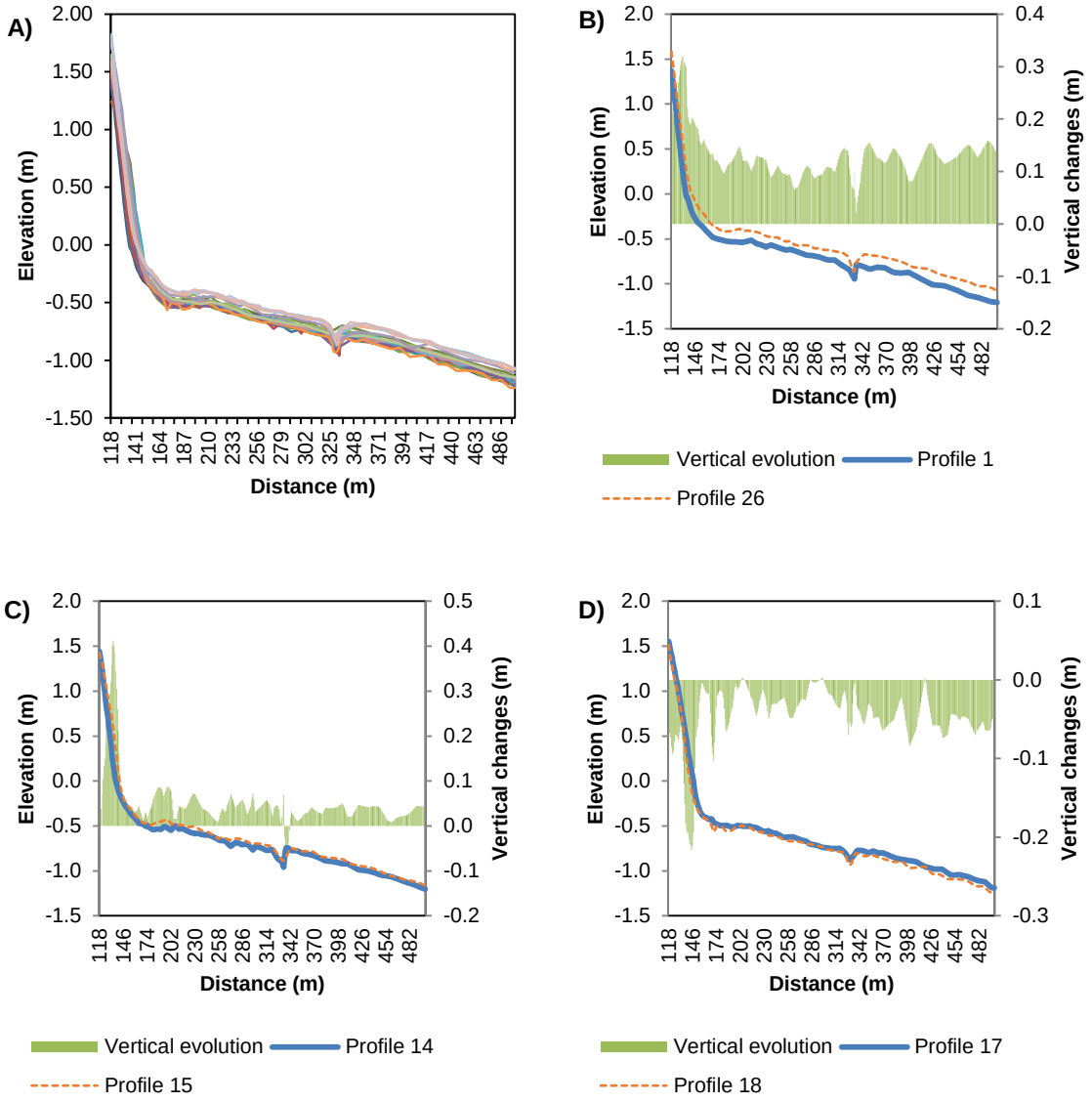

Figure 4.14: A) RYD23 profile envelope from August 2015 – October 2017, B) baseline (August 2015) and most recent profile (October 2017), C) biggest accretion between successive surveys, D) biggest erosion between successive surveys and their vertical evolutions respectively.

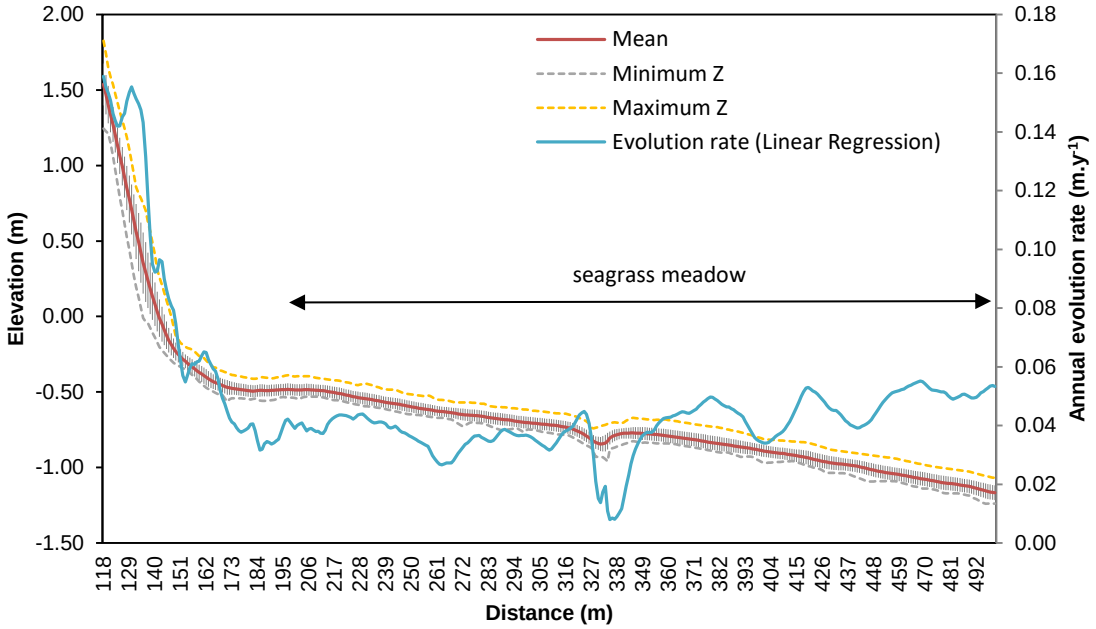

Figure 4.15: Mean, median, standard-deviation, minimum, maximum and evolution rates of profile RYD23. The vertical bars represent the standard-deviation of each point related to its mean.

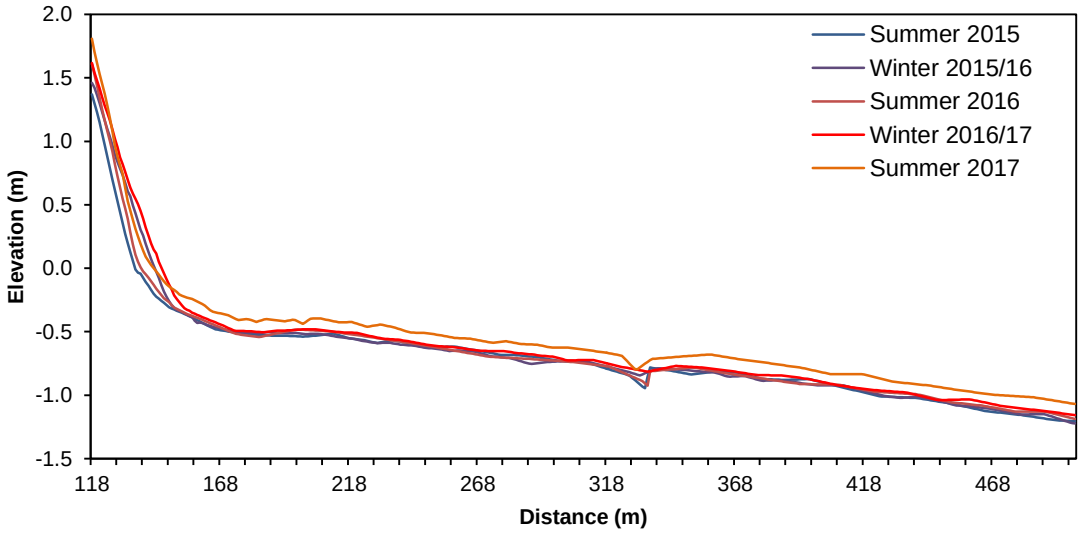

Figure 4.16: Summer and winter profiles of RYD23.

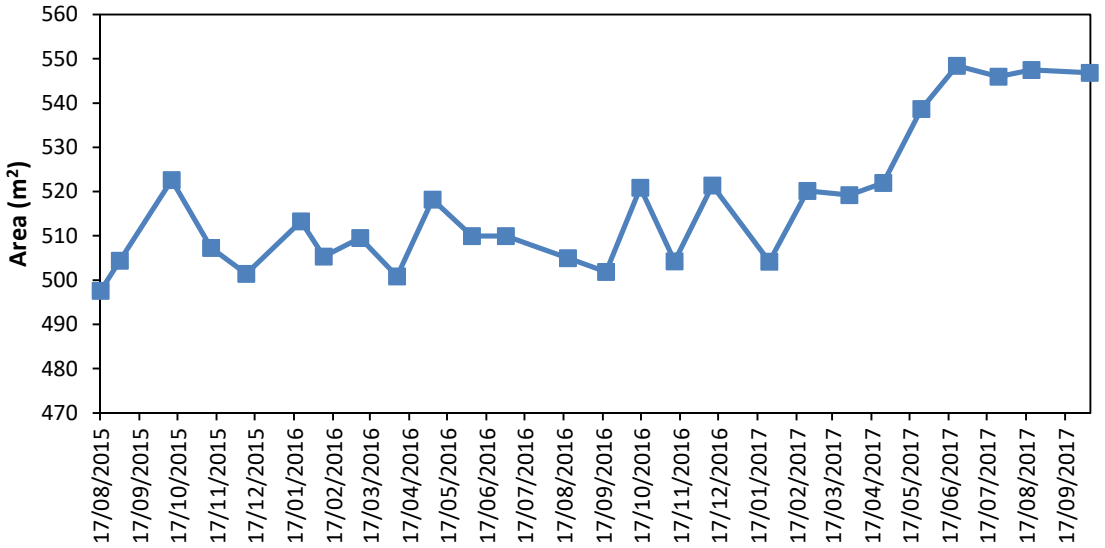

Figure 4.17 :Cross-sectional area (m²) from Baseline August 2015 to October 2017.

4.4.6 Cross-shore profiles of Ryde intertidal flats (CCO survey)

The intertidal flat volume changes of the 17 surveyed profiles between 2004 and 2017 are summarised in Table 4.3, with the morphological changes of these profiles being shown in Figure 4.18. Out of 17 lines analysed, only 4 lines were inhabited by seagrass namely line RYD15, RYD19, RYD23 and IOW217. At each transect line, cross-shore profiles of the same length were compared. However, profiles at different transects differ in length therefore large changes in cross-sectional area (CSA) can correspond to relatively minor % changes in CSA. All baseline profiles were recorded in autumn 2004 except for three transect lines (RYD70, RYD76 and IOW230), which were recorded earlier in winter 2004. The profiles on the east and the west of Ryde have been stable since 2004. Central profiles, IOW217, RYD34 and RYD37 showed the highest CSA changes. Profile IOW217 and RYD34 showed marked accretion towards the seaward limit of the profile due to the westward movement of the sand bank and growth of an offshore bar. In comparison RYD37 showed significant erosion. The central section was generally eroding.

There was accretion at both ends of the study area with erosion through the middle section. Lines IOW217 and RYD34 were having the biggest changes since the baseline survey in autumn 2004 with accretion of 61.6 % and 14.2 %, respectively. To the east of these lines, lines RYD37- IOW225 recorded net erosion up to 8.7 %. At Ryde West where the seagrass meadows were most abundant, minimal changes were recorded on all three lines.

The evolution rates over the whole study area over the 14 years period ranged from -5.6 cm y^{-1} to +16.9 cm.y^{-1}. All three transect lines on Ryde West had a low mean annual evolution rates of -0.1, -0.2 and 0.5 cm.y^{-1}. On Ryde East, annual evolution rate was the highest on

transect line IOW217 at -3.1 cm.y^{-1}, RYD37 decreased by -1.3 cm.y^{-1} and RYD76 increased by 0.8 cm.y^{-1} while the rest of the lines changes between -1 cm.y^{-1} to 1.3 cm. y^{-1}.

Due to the different length of the transect lines, large changes in CSA may correspond to relatively minor percentage changes. In Ryde West most of the profiles show minor erosion. The centre and the east of the Ryde shoreline showed erosion and accretion with the highest increase in CSA being evident along profiles IOW217 and RYD34 while RYD37 showed the biggest decrease in CSA.

Table 4.3: Percentage change in cross-sectional area. Negative values are in italic. Erosion is indicated in red and accretion in blue, no change is grey (Dates of profiles are available in Table 4.1)

	Area percentage, %																
	RYD15	**RYD19**	**RYD23**	**IOW217**	**RYD34**	**RYD37**	**RYD40**	**RYD43**	**RYD48**	**RYD53**	**RYD57**	**IOW225**	**RYD65**	**RYD70**	**RYD76**	**IOW230**	**RYD85**
Profile 1	Baseline profile																
Profile 2	0.9	*-1.7*	*-0.7*	*-1.2*	*-1.8*	*-2.3*	*-0.1*	*-1.0*	*-2.2*	*-1.1*	0.1	*-1.4*	0.3	*-0.7*	2.5	2.2	*-6.1*
Profile 3	*-0.4*	2.0	*-0.3*	11.1	*-0.2*	*-0.6*	*-1.5*	*-0.6*	0.1	1.0	0.8	*-0.4*	*-1.2*	0.4	1.0	0.0	*-1.6*
Profile 4	0.0	*-1.5*	0.6	*-2.0*	2.1	*-0.3*	*-1.3*	0.7	*-0.8*	*-0.2*	1.2	*-1.7*	*-0.8*	*-1.5*	7.7	0.0	*-2.0*
Profile 5	0.5	1.1	1.1	1.6	*-0.3*	0.2	-0.3	*-0.5*	0.6	1.2	*-2.0*	0.2	0.8	*-1.0*	*-2.5*	0.1	8.5
Profile 6	*-1.9*	*-1.4*	*-2.2*	4.0	*-1.3*	0.4	*-1.5*	1.1	*-0.7*	*-0.4*	*-0.6*	0.4	*-0.4*	2.1	0.1	4.6	*-5.0*
Profile 7	2.0	0.2	*-0.5*	1.2	*-0.4*	0.6	1.8	0.9	0.6	*-1.4*	*-0.6*	0.3	0.7	1.3	1.8	*-1.7*	*-5.0*
Profile 8	*-0.1*	0.7	1.6	6.6	1.7	*-1.1*	1.2	0.7	*-0.6*	0.0	*-0.3*	0.7	*-1.7*	1.0	1.6	0.1	0.0
Profile 9	*-0.5*	*-0.7*	*-0.1*	*-3.1*	2.6	*-1.1*	1.1	*-0.5*	*-0.1*	0.9	0.7	*-0.8*	1.9	*-1.4*	*-2.1*	*-1.0*	*-4.8*
Profile 10	1.7	0.2	0.9	7.3	*-1.9*	*-0.2*	*-0.7*	*-0.7*	*-0.4*	*-1.5*	*-2.8*	*-2.5*	*-1.6*	2.4	1.6	*-3.8*	3.0
Profile 11	*-1.1*	*-0.6*	0.1	*-1.0*	2.1	*-2.2*	*-1.0*	*-0.6*	*-0.7*	*-1.4*	*-0.8*	0.6	4.3	*-1.9*	*-2.3*	*-1.1*	6.3
Profile 12	0.2	0.3	0.9	1.0	*-0.8*	0.4	0.1	0.1	*-0.8*	0.3	*-1.2*	0.8	*-1.3*	4.4	5.9	5.0	4.6
Profile 13	*-0.8*	1.8	0.6	*-0.1*	4.2	*-0.9*	1.6	0.4	1.7	*-0.1*	2.6	*-1.5*	*-0.7*	*-3.2*	*-1.8*	*-2.6*	*-0.3*
Profile 14	*-0.3*	*-1.2*	*-0.7*	1.1	0.7	*-2.9*	0.0	*-2.5*	*-0.9*	*-1.1*	*-2.1*	0.3	0.1	1.0	*-2.9*	1.7	3.9
Profile 15	0.1	*-0.2*	-1.0	1.5	1.3	0.5	1.1	1.3	-0.7	1.0	0.4	*-1.3*	0.4	*-1.4*	5.0	*-0.5*	*-7.2*
Profile 16	*-0.1*	0.5	1.4	6.0	0.4	0.5	-1.0	-2.4	0.3	0.6	*-1.7*	*-1.9*	1.2	0.5	*-4.7*	*-0.6*	6.1
Profile 17	1.2	*-1.0*	0.9	3.3	-1.5	-1.1	0.6	0.4	-1.3	*-0.4*	*-0.9*	*-0.1*	*-1.3*	0.0	3.5	1.1	*-3.1*
Profile 18	*-0.6*	*-0.7*	1.2	2.3	2.9	0.9	1.0	*-1.8*	*-3.4*	*-0.8*	1.0	4.6	*-2.1*	*-0.7*	*-4.6*	*-0.5*	5.2
Profile 19	0.3	1.1	0.6	0.3	0.2	*-1.1*	*-0.6*	*-0.5*	6.9	0.9	*-1.5*	*-7.6*	3.5	*-1.3*	4.8	*-4.3*	*-9.5*
Profile 20	*-1.2*	*-1.7*	*-2.3*	*-1.8*	*-1.8*	*-1.4*	*-0.7*	*-0.8*	*-4.4*	*-2.3*	3.1	1.1	*-0.5*	1.7	7.4	2.2	0.9
Profile 21	*-0.1*	0.1	*-0.8*	2.2	0.4	0.3	*-0.5*	*-1.6*	*-0.2*	0.2	*-0.1*	0.2	1.4	*-1.2*	*-15.5*	*-1.7*	9.4
Profile 22	*-1.2*	*-0.6*	0.0	2.9	2.7	0.8	*-0.7*	0.6	*-0.8*	*-1.8*	-0.2	0.1	-2.4	*-0.9*	6.4	*-1.1*	*-9.1*
Profile 23	0.8	0.3	1.2	6.5	*-0.1*	0.1	*-0.7*	0.2	0.4	0.9	0.3	1.4	1.2	*-0.9*	1.4	*-0.4*	*-0.4*
Profile 24	1.6	1.9	5.0		2.3	1.6	*-0.9*	2.1	*-0.2*	*-1.0*	0.6		1.1	1.0	*-1.5*	*-0.2*	6.3
Profile 25														1.8	2.1	6.3	11.3
Profile 26																	1.2
Average	0.0	0.0	0.3	2.3	0.6	*-0.4*	*-0.1*	*-0.2*	*-0.3*	*-0.3*	*-0.2*	*-0.4*	0.1	0.1	0.6	0.2	0.5
Change from Baseline	**0.9**	***-1.2***	**7.5**	**61.6**	**14.2**	***-8.7***	***-3.1***	***-5.1***	***-7.9***	***-5.6***	**-4.1**	***-8.7***	**2.5**	**1.2**	**12.8**	**3.3**	**9.1**

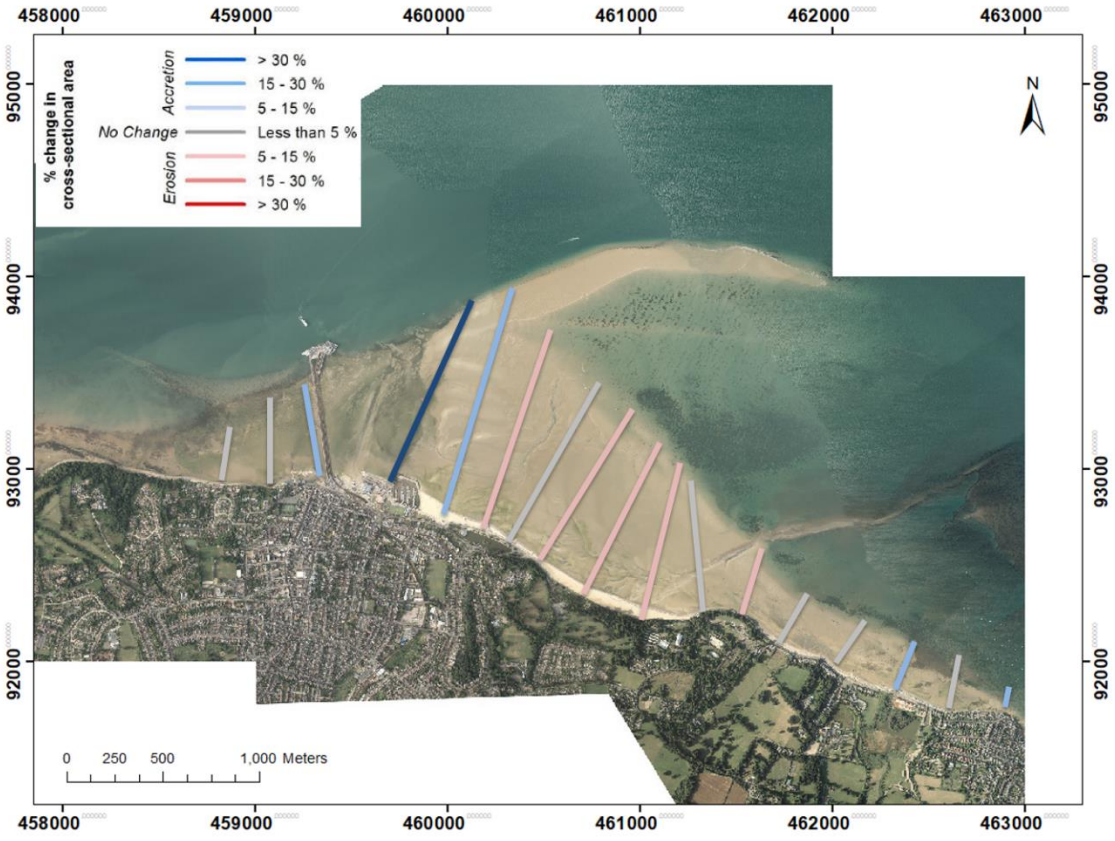

Figure 4.18: % change in cross-sectional area (CSA) from Baseline 2004 to March 2017 along various profiles. Erosion is indicated in red/pinks and accretion in blue, no change is grey.

4.4.6.1 Transect line RYD23

Four transect lines were chosen to represent the longer-term geomorphic changes in the area. Over a 14 years period, intertidal flat profiles of transect line RYD23 (482 m long) (Figure 4.19 A) were evaluated and 41.64 m^2 (7.5 %) of sediment accretion was recorded from the baseline profile in autumn 2004 (Figure 4.19 B). Surveys in both seasons, autumn and spring recorded a cumulative of 24.37 m^2 (4.44 %) and 17.27 m^2 (3.08 %) of sediment accretion, respectively.

Largest sediment accretion was recorded in spring 2017 with 28.14 m^2 (5 %) increase of volume from the previous survey in autumn 2016 (Figure 4.19 C), while the largest sediment erosion was 13.29 m (-2.31 %) in spring 2015 (Figure 4.19 D). Evolution rate of the profile is below 0.02 m per year (Figure 4.20) suggesting minimal changes on the transect line.

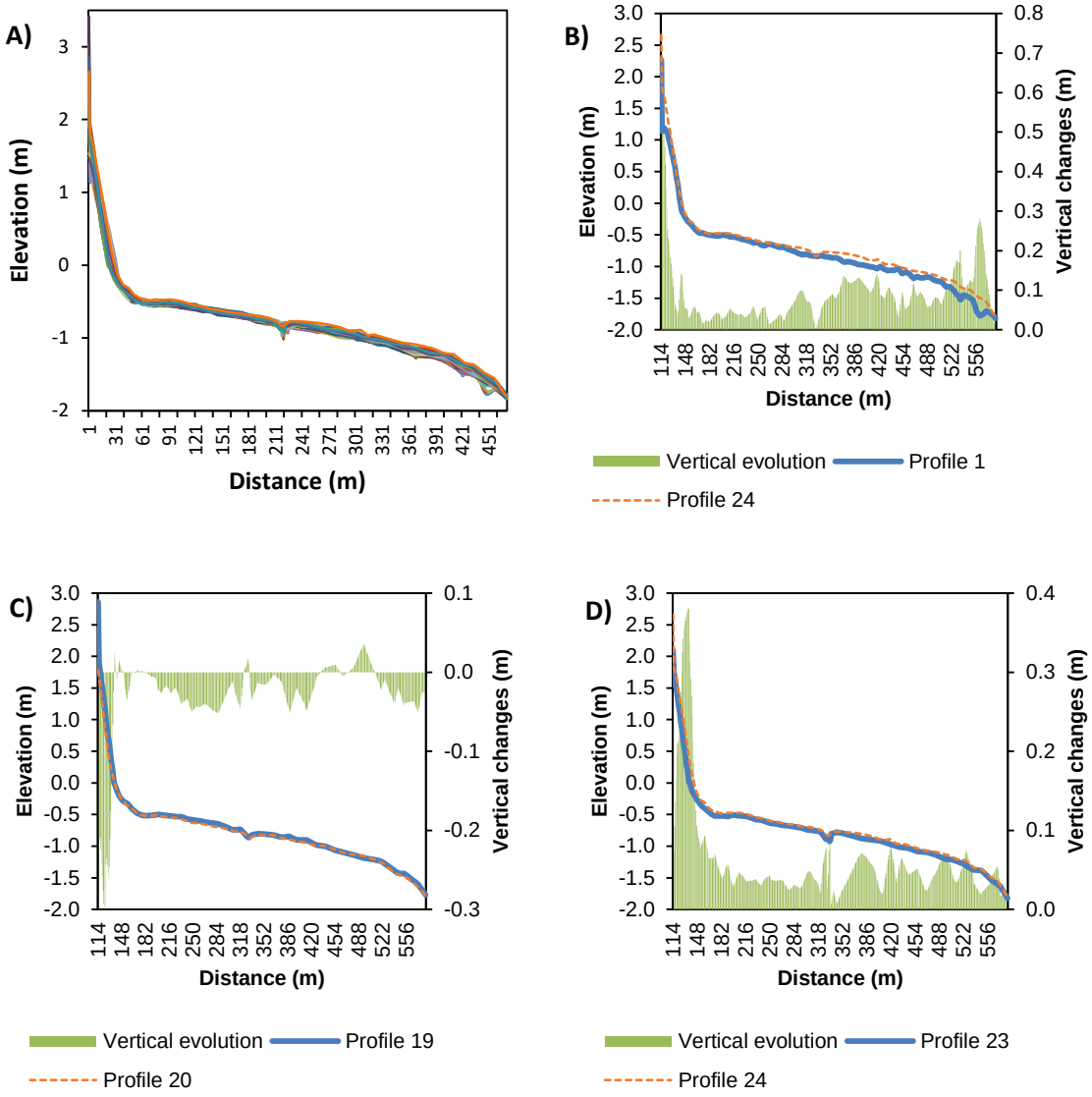

Figure 4.19: A) Profile envelope of transect line RYD23, B) baseline (October 2004) and most recent profile (March 2017), C) biggest erosion between successive surveys, D) biggest accretion between successive surveys and their vertical evolutions respectively.

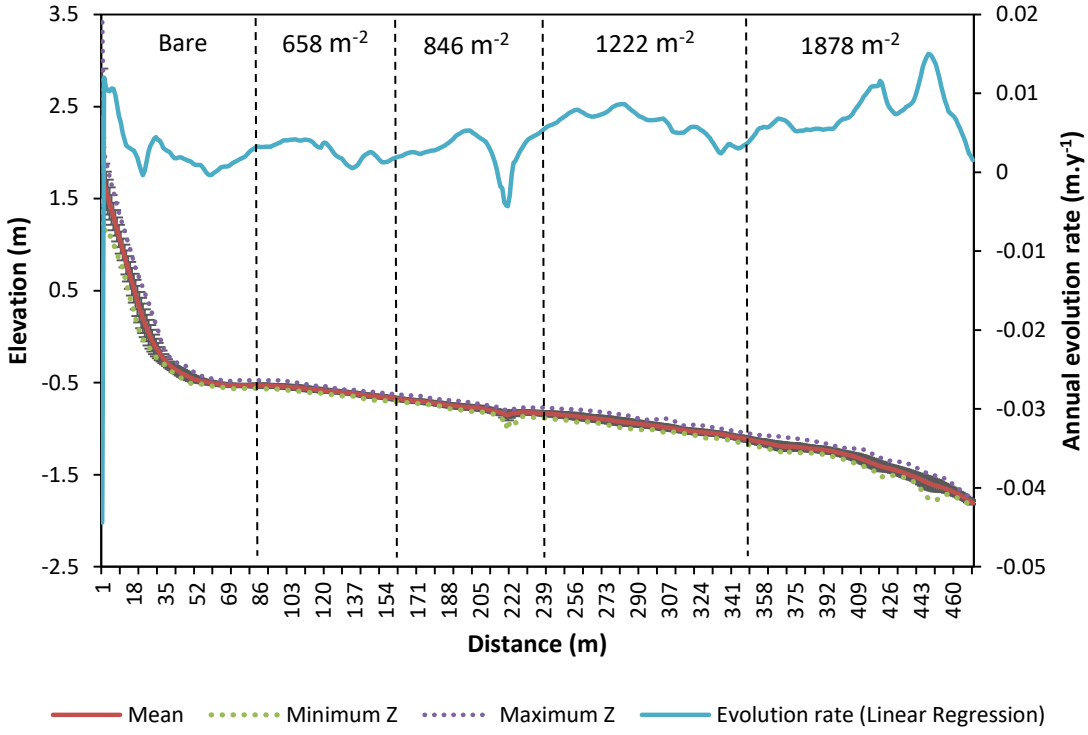

Figure 4.20: Mean, median, standard-deviation, minimum, maximum and evolution rates of profile RYD23. The vertical bars represent the standard-deviation of each point related to its mean.

4.4.6.2 Transect line IOW217

The IOW217 transect line consisted of 25 profiles measured from 2004 – 2017 (Figure 4.21 A). The profile is 858 m long and with seagrass covering approximately 40 % of the line. This transect line experienced the biggest increase in sediment volume with an accretion of 365.78 m^2 (61 %) over the baseline profile (Figure 4.21 B). Accretion over the seagrass area was 119.06 m^2 (54 %). Average standard deviation along the transect line was 0.28, while the standard deviation on the seagrass area was 0.14, suggesting it confers greater stability.

The increase in bed profile was mostly recorded during the winter/ spring survey with a net accretion of 315.15 m^2 (44.1 %). Summer/ autumn survey recorded 49.63 m^2 (5.7 %). Biggest increase in the surface elevation was from May 2005 to May 2006, with an accretion of 65.33 m^2 (11.1 %) (Figure 4.21 C). The biggest loss of sediment (-22.86 m^2) was between March 2009 and September 2009 (Figure 4.21 D). Comparing the IOW217 profiles, significant changes of accretion were found in the seaward area near the sandbank spit. Evolution rate in this area ranged between -1.2 and 7.6 $cm.y^{-1}$ (Figure 4.22) with an average of 3.1 $cm.y^{-1}$ suggesting it as an accretion zone.

Largest increase of sediment volume was near the sand spit where material from the sand bank migrated westward. The seagrass meadows can be divided into two areas separated by

a water way. The seagrass patches occupied areas from 183 m to 380 m and 435 m to 592 m from the shoreline. The volume change on the first patch, which was denser and closer to the shoreline, was 15.16 % while on the second patch was 136.26 %. The standard deviation from the mean in the vegetated areas were 0.04 and 0.17, respectively, smaller compared to bare sands. Volume changes on bare sand were 4.81 %, 85.38 %, 137.07 % with standard deviations of 0.08, 0.13, and 0.25, respectively.

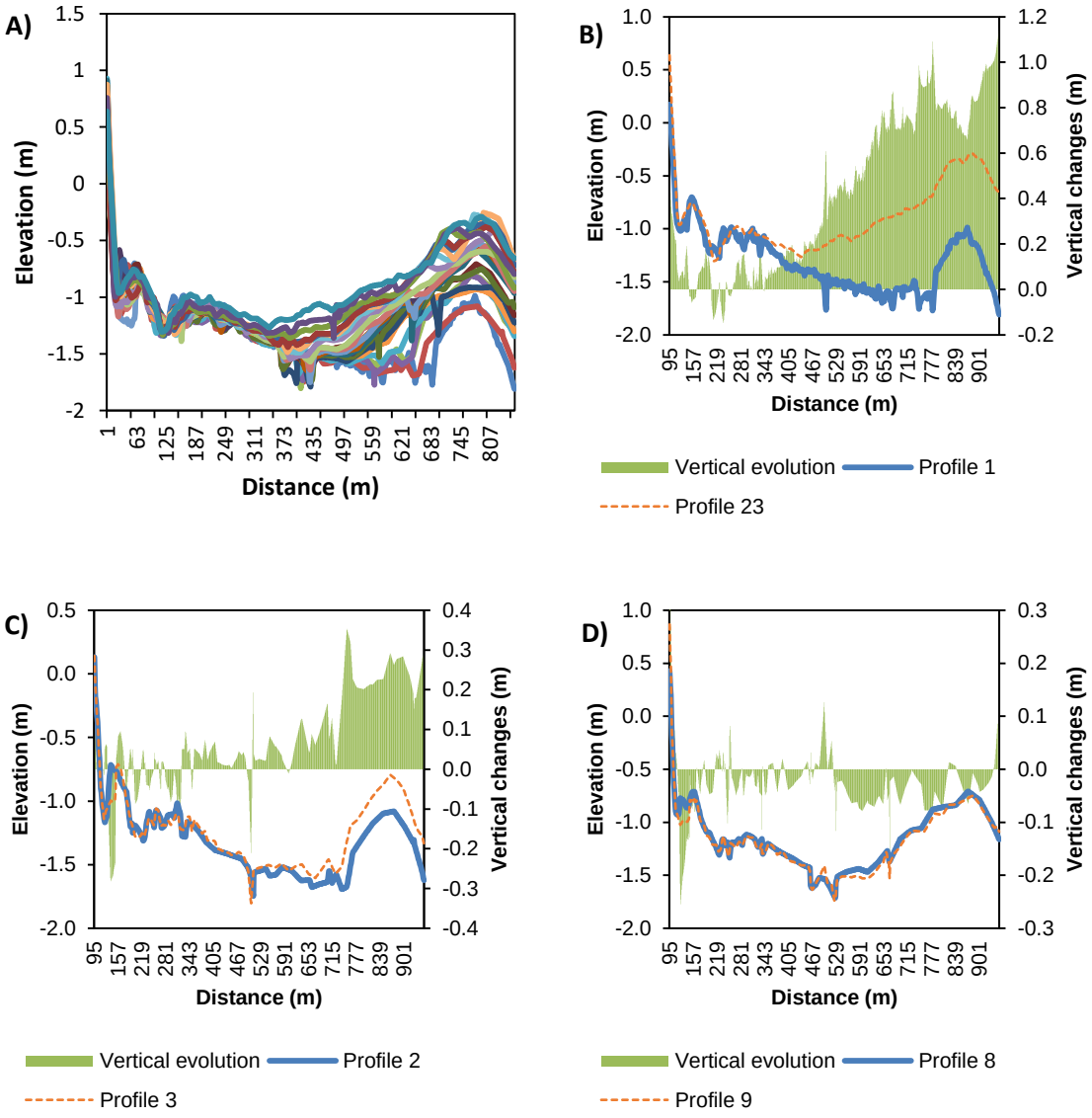

Figure 4.21: A) Profile envelope of transect line IOW217, B) baseline (October 2004) and most recent profile (March 2017), C) biggest accretion between successive surveys, D) biggest erosion between successive surveys and their vertical evolutions respectively.

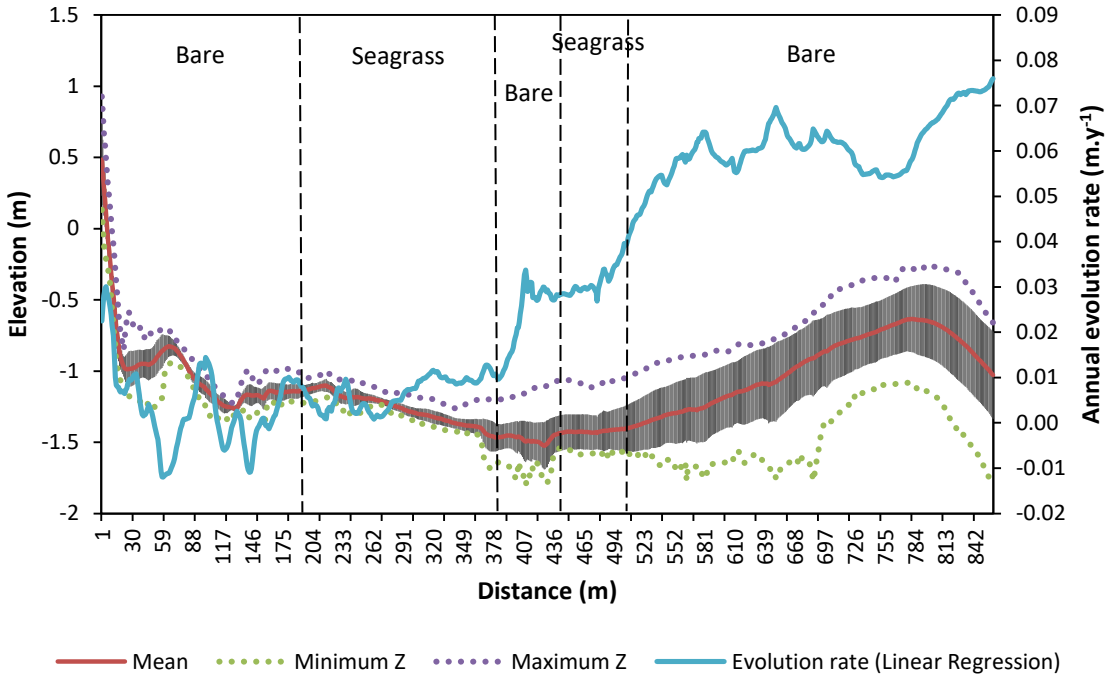

Figure 4.22: Mean, standard-deviation, minimum, maximum and evolution rates of profile IOW217. The vertical bars represent the standard-deviation of each point related to its mean. The vertical dashed-lines separate between the bare and seagrass covered area.

4.4.6.3 Transect line RYD37

Transect line RYD37 consisted of 24 profiles measured from 2004 – 2017 (Figure 4.23 A). It is 1040 m long with no seagrass meadow on any part of the transect line. Change from the baseline survey were recorded at -8.7 % indicating the highest sediment erosion in the study area (Figure 4.23 B). Net sediment loss from the baseline profile were recorded on RYD37 was continual during the whole period of survey. Higher rate of sediment loss was recorded in summer/ autumn at -80.69 m^2 (-5.56 %) compared to winter/ spring -53.87 m^2 (-3.44 %). Biggest loss of sediment was recorded in late summer 2011 with 2.9 % (-41.39 m^2) loss of volume from the previous survey in autumn 2016 (Figure 4.23). Average standard deviation along RYD37 line is 0.10. The data indicate that the nearshore bars migrated landward consistently during this 16-year span. A large amount of the sediment loss on this part of the sand bank was migrating westward, resulting in accretion on the IOW217 transect line. The evolution rates over the study period of the transect range from -0.04 to +0.05 m per year (Figure 4.24). An alternation of bigger and smaller erosion zones can be seen on Figure 4.24.

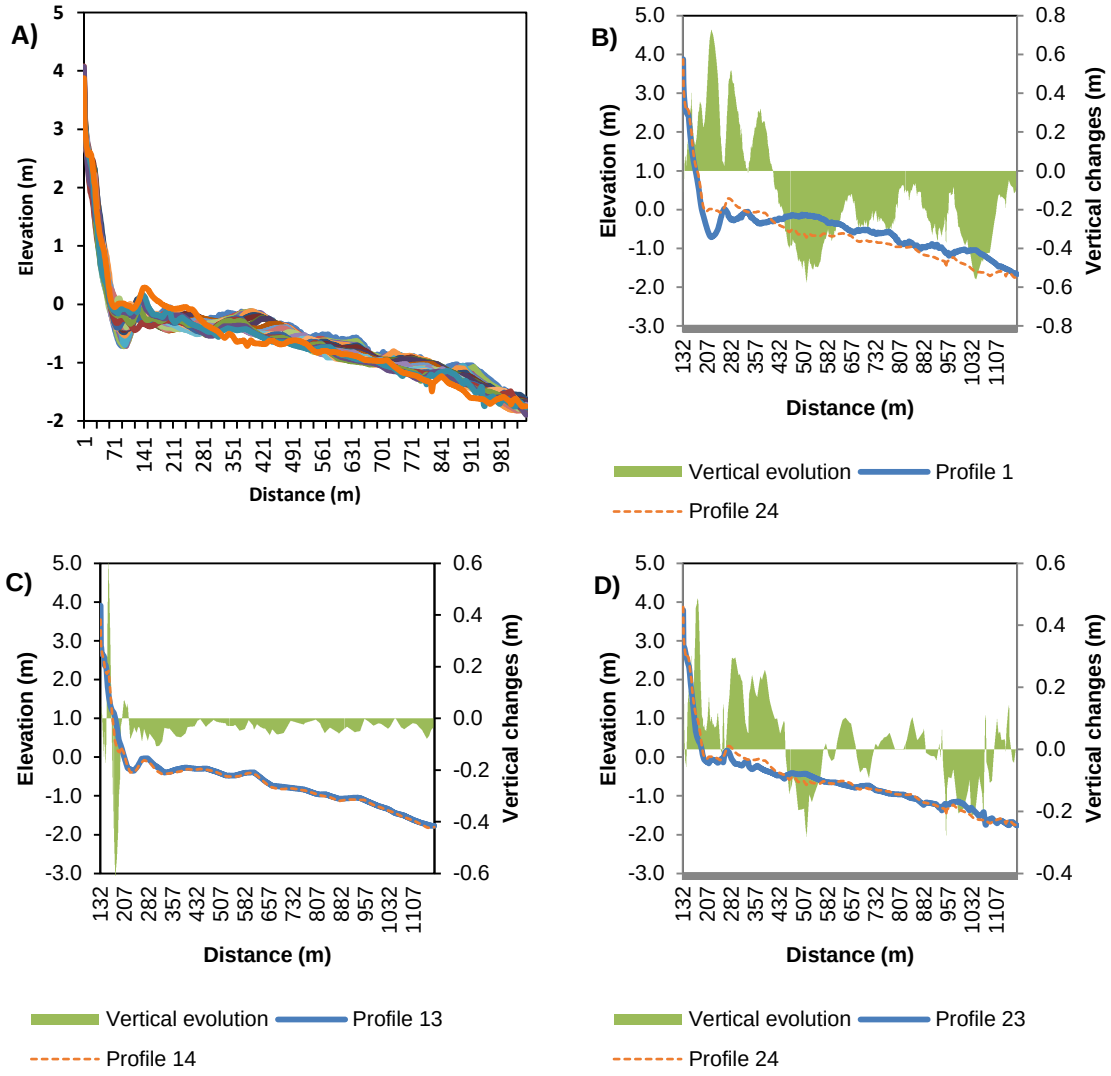

Figure 4.23: Profile envelope of transect line RYD37, B) baseline (October 2004) and most recent profile (March 2017), C) biggest accretion between successive surveys, D) biggest erosion successive between surveys and their vertical evolutions respectively.

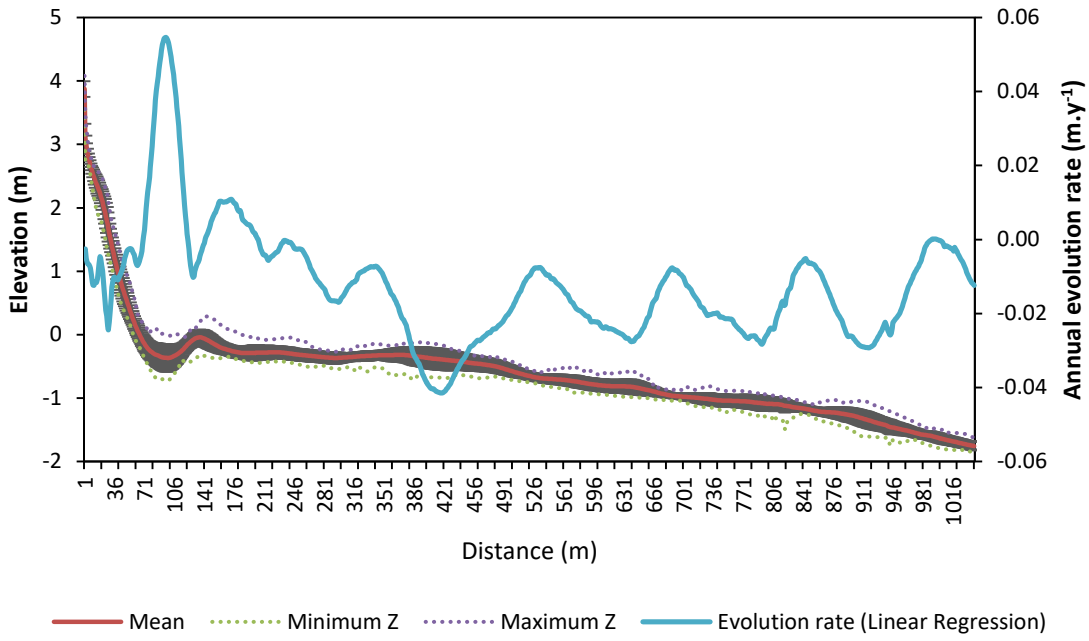

Figure 4.24: Mean, standard-deviation, minimum, maximum and evolution rates of profile IOW217. The vertical bars represent the standard-deviation of each point related to its mean.

4.4.6.4 Transect line RYD76

Transect line RYD76 consisted of 25 profiles measured from 2004 – 2017 (Figure 4.25 A). It is 260 m long and experienced an increase in surface elevation with 41.53 m^2 (12.8 %) (Figure 4.25 B) of sediment accretion over the course of the surveys, despite being without any vegetation. This transect is in line with a groyne which trapped the westward longshore drift. A higher rate of sediment gained was recorded in spring, with an increase of 37.11 m^2 (13.08 %) compared to autumn -4.42 m^2 (-2.02 %). However, the biggest sediment erosion was recorded from August 2014 to March 2015 with -15.54 % (-61.96 m^2) loss of volume from the previous survey (Figure 4.25 D). Evolution rates over the study period of the transect was up to +0.04 m per year (Figure 4.26) at the steeper part of the beach. Average standard deviation along RYD76 line was 0.11.

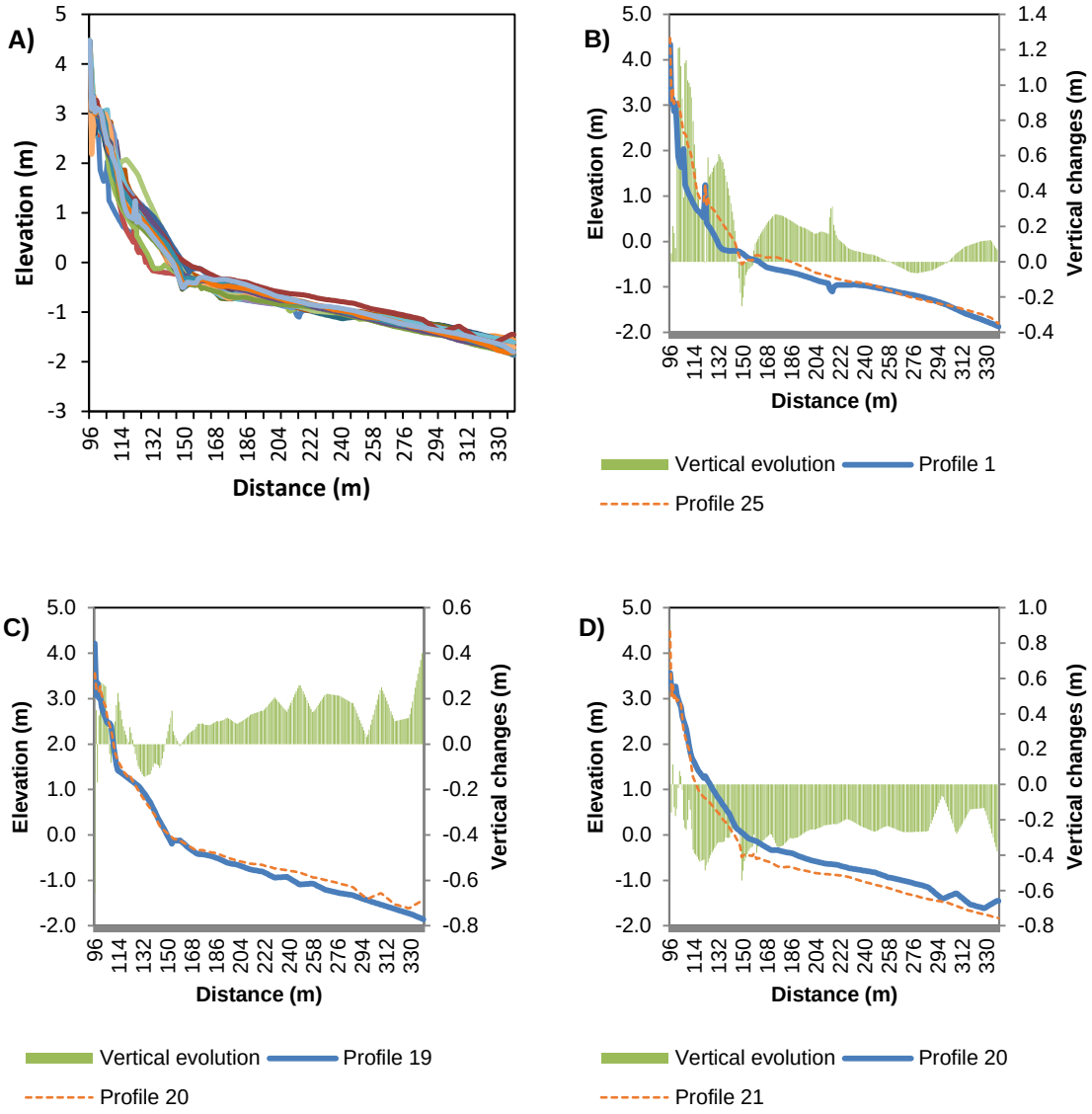

Figure 4.25: A) Profile envelope of transect line RYD76, B) baseline (October 2004) and most recent profile (March 2017), C) biggest accretion between successive surveys, D) biggest erosion between successive surveys and their vertical evolutions respectively.

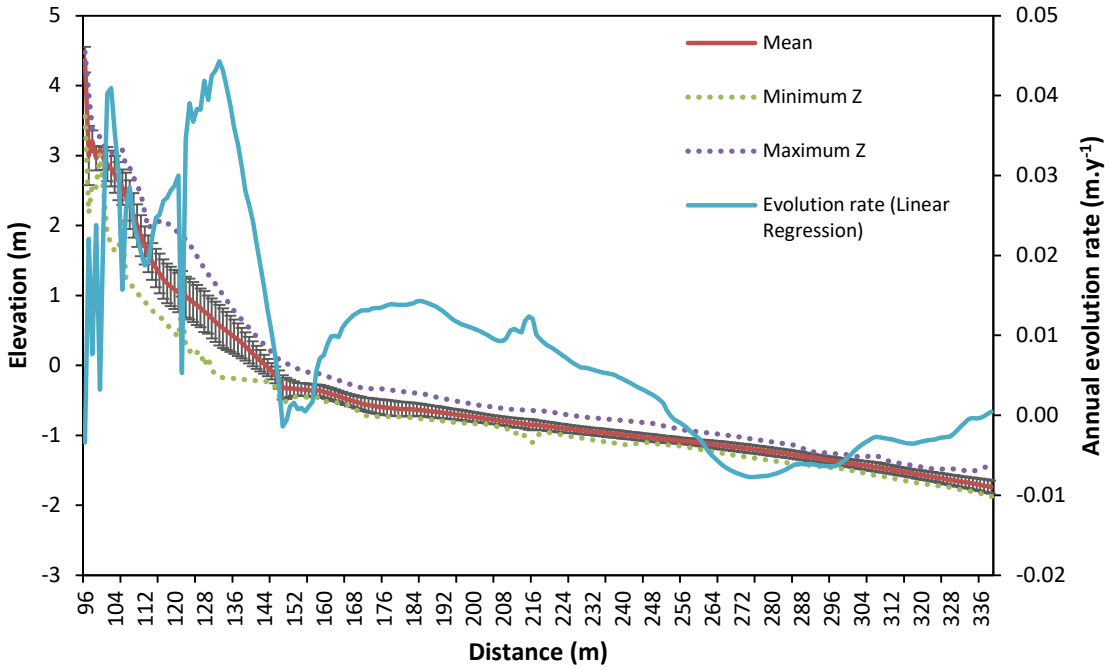

Figure 4.26: Mean, standard-deviation, minimum, maximum and evolution rates of profile RYD76. The vertical bars represent the standard-deviation of each point related to its mean.

4.5 Discussion

This section is divided into two parts. The first part discusses the results related to the sand flat spatial and temporal variation. The second part relates to the seagrass temporal variation and its relation to sand flat profile evolution.

4.5.1 Sediment spatial and temporal variation at Ryde

The composition of Ryde Sands intertidal flat inhabited by *Zostera noltii* was found to be formed of fine sand. More fine-grained sediments are associated with this species as recorded in other areas such as the Oka estuary (Valle et al., 2011) and Archachon lagoon (Ganthy et al., 2013). This type of sediment is usually found in lower energy environments. The samples show mean grain size between 2.69 to 2.40 phi. The mean grain size was reasonably uniform over the sand flat with a small trend of fining towards the foreshore. On average, mean grain size was slightly finer (2.52 phi) in the summer months compared to the winter months (2.50 phi). The finer mean grain size at the most seaward station can be attributed to the denser seagrass meadow entrapping bed load grains and suspended matter (Hendriks et al., 2010; Ward et al., 2003). In the summer months, the increase of seagrass density as well as the reduction in wave and current intensity promoted sediment deposition.

Very well sorted sediment within the seagrass bed is unusual, however, it could be attributed to the low wave energy in the study area. Moreover, the whole area of the sand flat Ryde consisted of well sorted to very well sorted sediment (Chapter 3). Sorting was poorest when the seagrass meadows were most abundant at the lowest shore station as sediments were more protected within the meadow and less influenced by hydrodynamic forces. There was a slight increase in sorting during the winter months. Coarser and better sorting of sediment occurred due to the winnowing of sediment as the seagrass biomass significantly reduced in winter.

Over the 26 month period, highest skewness values at S1, S2, S3 and S4 were 0.30, 0.31, 0.39 and 0.38 phi, respectively. Positive skewness at all stations indicates a depositional environment (Duane, 1964). High skewness values correspond to the period of high seagrass shoot density. Sediments were more positively skewed (finer skewed) during the peak growth of seagrass season at all stations indicating the increase of finer particles. Sediment were also finer skewed with increasing seaward distance across the sand flat. Overall, finer grains tend to be better sorted and more positively (fine) skewed. During the degeneration period of the seagrass, the reduction in both, above-ground and below-ground biomass allowed the removal of fine sand, causing the sand to become coarser. Generally, beach sands are known to have negative skewness, while positive skewness are more common in dune and river sands (Martins, 1965). The dominance of positive skewed sediment in the study area thus indicate the prevalence of low wave activity and alongshore currents (Bramha et al., 2017), as also shown by the long-term deposition in the area.

It has been reported that platykurtic to very platykurtic and leptokurtic to very leptokurtic sedimentary environments are due to extremely low and high energy environments, respectively (Friedman, 1962). Thus, mesokurtic sediments usually dominates areas with a more uniform energy environment. Generally, Ryde Sands shows a dominance within the mesokurtic to leptokurtic range, and an absence of platykurtic distribution. Finer sized and dominant leptokurtic nature of sediments typically reflect maturity of the sand (Prabakhara, 2001). In this study, S1 and S4 showed a flatter sediment distribution as compared to the midshore stations. A temporal trend could not be found as mesokurtic grains were recorded in all seasons. The dominance of leptokurtic sediment in the *Zostera noltii* bed of Ryde Sands intertidal flat follows the *Halodule wrightii* and *Thalassia testudinum* bed in St Andrews Bay, Florida (Grady, 1981).

In general, the positive skewness of sediment reflect the low energy in the area. The leptokurtic distribution of sediment indicating higher energy environments were restricted to the area inhabited by the seagrass.

4.5.2 Spatial and temporal variation on Ryde Sands intertidal flat

The shape and size of the sand flat has evolved over the years, as well as the volume of sand on the sand flat. Changes in the sand volume that makes up the profiles can be seen to vary on a monthly, seasonally and yearly basis. Modifications on the sand volumes also proved to be spatially variable. Sediment accumulation above the sea bed results from an equilibrium between two opposing processes, accretion and erosion. My results indicate that these interchanging processes control the bed level, with bare flats varying more as compared to the areas where seagrass meadows were present. Generally, winter profiles were associated with the loss of beach sediment possibly due to the incidence of higher waves during the winter months. On the contrary, calmer period usually in the summer contributes to beach recovery (de Alegría-Arzaburu & Vidal-Ruiz, 2018; Scott et al., 2016).

Ryde West is seen to be more stable as compared to Ryde East. The evolution rates over the total study period on the three transect lines in Ryde West were small at -0.1, -0.2 and 0.5 cm per year, respectively. All three transect lines covered by the seagrass meadow on Ryde West recorded less than -0.4 % change from the baseline survey indicating slight erosion during late winter/ early spring surveys, with the exception of line RYD23 which showed deposition. This could be due to the location of the transect line being close to Ryde Pier, providing protection to the area from waves and boat wakes. The erosive behaviour on two out of three transect lines on Ryde West were probably due to stronger wave incidence and largely reduced *Zostera noltii* shoot densities in winter, thus limiting the role of the seagrass shoots in protecting the inshore through wave attenuation. Summer/autumn surveys showed an average increase up to 0.4 % change from the baseline survey indicating accretion. This increase is related to the lower waves reaching the area and allowing the beach to recover. Furthermore, the stable bed elevation over 14 years showed that the seabed is more resistant to both, accretion and erosion due to the presence of the seagrass meadow. In the seagrass occupied areas, despite losing most of the above-ground biomass during winter season, the below-ground biomass was likely to play an important role in binding the subsurface sediments and increase grain cohesion thus reducing the changes in bed level (Feagin et al., 2015).

Ryde East can be divided into three sections depending on changes on the bed level. The first section is furthest west, closest to the pier with an accretion rate of approximately 2-3 cm per year suggesting this area as an accretion zone. Two transect lines in this section (IOW217 and RYD34) showed the biggest change from the baseline survey in autumn 2004 with accretion of 61.6 % and 14.2 %, respectively. The middle section showed an evolution rate of around -1 cm per year indicating erosion. As shown in Chapter 3, sediment distribution patterns indicate that transport of sediment on the sand flat occurs due to longshore currents in a

north-west direction. A second longshore drift in a south-east direction was suggested in a study by SCOPAC (2012); however, this is believed to be going further offshore around Ryde West, converging with the opposing direction of transport to form the sand spit at Ryde East. The eastern most section recorded an accretion rate of approximately 0.3 cm per year. This part of the sand flat receives an active supply of sediment from the offshore to onshore transport as well as from erosion on the east-side of the Isle of Wight (SCOPAC, 2012).

The transect line IOW217 in the first section of Ryde East provided an interesting finding as it was mostly bare sand with two separate patches of seagrass meadows. Changes on transect line IOW217 were high on the bare sand meanwhile areas colonised by seagrass showed much less change as demonstrated in the annual evolution rate. Average annual evolution rate on the bare sand was an accretion of 3.6 cm per year compared to 2.3 cm per year on the seagrass meadow. The transect line can be divided into two seagrass meadow areas with the evolution rate of 0.7 $cm.y^{-1}$ on the first section and 4.3 cm per year on the second section. There is a big increase in the evolution rate just after the first seagrass section where the rate was 2.7 cm per year. The foreshore section with most bare sand recorded 6.3 cm per year increase in elevation, a 2 cm per year increase as compared to the seagrass area. The difference of fluctuation in the seabed elevation variations were also clear as the standard deviation of the vegetated and unvegetated area were 0.10 cm and 0.17 cm, respectively.

4.5.3 Implications of the seasonal growth cycle of seagrass meadows on bed stability and sediment dynamics

There is a good agreement between CSA and density of seagrass meadows. In Ryde, peak seagrass biomass growth was generally in summer while the meadows lose most of their biomass in autumn, recording their lowest biomass in winter months. Highest average CSA was also recorded in summer while the lowest average CSA was recorded in winter season. The increase in CSA indicates a net sediment deposition during the summer months due to the increased seagrass biomass and reduction in resuspension of the freshly deposited sediments. Evaluation of the topographic data discovered strong trends in sediment accretion during the seagrass meadow growth season, and a tendency of surficial sediments to become finer.

Peak seagrass distribution differs among years as seagrass density was most abundant in September, August and June in 2015, 2016 and 2017, respectively. The density variation was reflected in the vegetated profiles CSA. In summer 2015, peak seagrass density was 3150 shoots m^{-2} at the foreshore site (S4) and the CSA was 504.37 m^2. In summer 2016 a slight increase in peak seagrass density at 2.5 % and an increase in CSA by 0.1 % was recorded. In

summer 2017, seagrass density further increased by 35 % (4360 shoots m^{-2}) and this was reflected in a 5 % increase in CSA (547.47 m^2).

Measurements showed that surface elevation at station S1 and S2 decreased and increased alternatively, although the overall tendency was accretion at a rate of about 0.3 cm per year. Moving seaward to the lower intertidal zone, there was an increase in fine sediment fraction following the seagrass growth season and the accretion rate also increased up to 0.5 and 0.7 cm per year in station S3 and S4, respectively. The increase in accretion rate in this highly vegetated zone can be attributed to the domination of particle trapping leading to centimetric accretion. The accretion rates were, however, lower as compared to some unvegetated beds in the area. Lower rates of accretion on seagrass beds can be attributed to easier resuspension of materials that settle on the bended leaves of *Zostera noltii* allowing the particles to be transported away.

My analysis shows that seagrass meadows stabilise sediment and help in facilitating surface elevation in Ryde. The stabilisation services provided by seagrass meadows also occurs in different settings of subtidal and intertidal zones as well as in tropical and temperate regions by a variety of seagrass species. More importantly, my results show that seagrass meadows regulate surface elevation in an area with a higher rate of erosion and accretion and bigger fluctuation between these two processes. Stabilisation of sediments in turn leads to other services such as carbon sequestration by seagrass meadows (Fourqurean et al., 2012; Marbà et al., 2015).

4.5.3.1 Sediment retention by seagrass meadows

The accretion rates obtained in this study, range from 3 to 7 mm per year, in the upper intertidal zone with lower shoot densities and higher shoot densities respectively. These rates are comparable to another study on the same species in Arcachon lagoon (8 to 32 mm per year; Ganthy et al., 2013) and those obtained for a similar but larger-sized species, *Zostera marina,* in mainly subtidal meadows in Wadden Sea where the accretion rate did not exceed 5 to 7 mm/year (Bos et al., 2007). However these values were higher than other subtidal, perennial *Posidonia oceanica* beds (2 mm per year; (Gacia & Duarte, 2001; Gacia et al., 1999)). Furthermore, despite the differences in sediment supply and environmental characteristics, the difference in accretion rates were of the same order of magnitude between these different environments.

In a low energy environment, it would be expected that fewer larger particles would be lost as it takes more energy to reach their threshold of motion, moving them over the bed or into suspension, compared to the smaller ones. During a typically higher wave energy in winter, this is evident in the coarsening of sediment on Ryde intertidal flat as finer sediments were

transported away. Sediment trapped by *Zostera noltii* also decreases with increasing flow. In laboratory experiments (Chapter 5), increased flow speeds over vegetated beds showed more complex vertical flow profiles, with the development of skimming flow at higher shoot densities and higher flow velocities, which was indicated by accelerated flow above the canopy. Many particles would have remained in suspension and carried over the bed through the canopy by this skimming flow.

The lower standard deviation in surface elevation across vegetated beds also suggests a greater particle retention as compared to bare sediment. This quality is demonstrated in other seagrass beds, *Zostera noltii* (Wilkie et al., 2012), *Thalassia testudinum* (Koch, 1999) and *Posidonia oceanica* (Gacia & Duarte, 2001) in low energy environment.

4.5.3.2 The balance between accretion and erosion

Sediment accumulation on an intertidal flat results from the balance between accretion and erosion. The presence of seagrass reduces the bed-load transport, increases deposition of suspended sediments (Chen et al., 2007; Gacia & Duarte, 2001; Hendriks et al., 2008) and decreases resuspension (Gacia & Duarte, 2001; Gacia et al., 1999; Jorge Terrados & Duarte, 2000), as flow energy was reduced near the bed (Hendriks et al., 2010, 2008; Widdows et al., 2008). On the contrary, the increased local turbulence may cause resuspension due to the presence of the shoots (Fonseca & Koehl, 2006; Pujol et al., 2013). One of these processes (deposition or resuspension) will dominate depending on other factors such as the seagrass development stage, sediment composition and the hydrodynamics.

My analysis showed a time-varying pattern, correlated to the seasonal development of the seagrass meadows. Accretion and the fining of sediment in the summer may be correlated with a decrease in turbulence near the bed due to higher shoot densities (Gambi et al., 1990; Lefebvre et al., 2010). This may contribute to lower depositional rates within the meadows compared to the unvegetated bed. From autumn to winter, the significant decrease in meadow density exposed the surficial sediment leading to erosion. There was also an increase in sand fraction and improved sorting that may have resulted from the erosion of fine particles. Finer particles are more likely to be resuspended as turbulence increases during this declining and low meadow densities season (van Katwijk et al., 2010).

Previous studies often found an increase in suspended sediment deposition (Gacia & Duarte, 2001; Ganthy et al., 2015), decrease in resuspension (Gacia & Duarte, 2001; Jorge Terrados & Duarte, 2000) as a result of flow energy reduction near the bed (Hendriks et al., 2010; Lefebvre et al., 2010; Widdows et al., 2008). However, there were reported cases of increased resuspension due to the presence of the shoots causing locally increased turbulence (Fonseca & Koehl, 2006; Hendriks et al., 2010; Widdows et al., 2008). One of these processes will

prevail depending on the development stage of the vegetation, sediment composition and hydrodynamics of an area.

As unvegetated areas were found to be having higher variation in surface elevation and less resistant to erosion compared to vegetated areas, the decline of meadows can lead to higher erosion of bed sediments.

4.6 Conclusions

A combination of 2-year field survey and my analysis of a 14-year dataset collected by Channel Coastal Observatory (CCO), UK at Ryde, Isle of Wight were used to quantify and characterise the spatial and temporal variability of the intertidal flat. Bed topography was recorded at sites with different densities and coverage of *Zostera noltii* meadows. Surficial sediments and seagrass development characteristics were recorded monthly during the field surveys. This dataset allows the understanding of short-term long-term evolution of the sand flat. The following conclusions can be drawn from this study:

- The short-term alternation of erosion and accretion are seen in the monthly and annual beach profile surveys, however the sand flat are stable over long time periods. Different areas of the sand flat experienced different changes depending on the seagrass presence and hydrodynamic forces.
- Seagrass meadows are abundant in Ryde West where CSA fluctuation were less in relative to Ryde East indicating that the seagrass confers stability. The presence of meadows modifies the balance between particle trapping and protection against erosion processes, depending upon the seasonal growth stage of the seagrass. During the growth period (spring to summer), particle trapping dominates and is linked with finer particles on the surficial sediments, thus leading to centimetric accretion of vegetated areas. During the degeneration period (autumn to winter), erosion occurs, but less than in unvegetated areas. Protection against erosion dominates and is related to the increase to the mean grain size of the surficial sediments. This may be caused the resuspension of finer particles on the surface, while larger sediments remain trapped in the meadows.
- There were unvegetated areas of the sand flat recorded as having accretion during both winter and summer surveys, however, this can be explained by the longshore drift in the study area. Longshore drift in the north-west direction creates an area of sand accumulation at the west edge of the spit. Previous studies indicated a second longshore drift in the south-east direction causing the formation of the spit and creating a convergence zone at the edge of the sand flat on Ryde East.

Seagrass provide vital protection to the coast as a natural alternative or complementary to artificial structures. It is recommended to create or restore their habitats in order to safeguard the coastline. My study represents an important first step in assessing the role of seagrasses in controlling sediment surface elevation. The ability of one the smallest eelgrass, *Zostera noltii* to provide sediment stabilisation suggests the need for a more comprehensive monitoring of seagrass across all geographical settings. Furthermore, this emphasises the need to protect and restore seagrass meadows due to their continued provision of biodiversity and ecosystem services especially in the face of sea level rise.

Chapter 5: The influence of seagrass, *Zostera noltii* on benthic boundary layer structure and sediment transport under unidirectional currents

5.1 Introduction

Coastal vegetation in subtidal and intertidal ecosystems directly contribute to coastal protection by acting as barriers to wave and tidal flow (Möller, 2006; Paul et al., 2012). Their above-ground biomass enhances sedimentary deposition through particle trapping and reducing re-suspension, as well as attenuating waves and current flow. Furthermore, it has been suggested that below-ground biomass of rhizomes and roots can bind and stabilise sediments by altering the erodibility (Christianen et al., 2013; Le Hir et al., 2000).

Zostera noltii meadows are recognized as playing an important role in protecting and stabilising the coast (Potouroglou et al., 2017; Wilkie et al., 2012). This species is a common intertidal species along European and North African coasts (Coyer et al., 2004). They offer coastal protection by attenuating waves (Paul & Amos, 2011) and create a lower energy environment that promotes deposition of particles (Ganthy et al., 2015). In recent studies, *Zostera noltii* was utilised in seagrass restoration and transplantation projects as part of a mitigation programme for dike reinforcement (Suykerbuyk et al., 2016), due to its ability to rapidly recover through clonal growth after moderate sediment disturbance (Han et al., 2012). The meadows are highly seasonal (see Chapter 4) with high shoot densities (1460 – 4360 shoots per m^2) in summer and low shoot densities (790 – 1940 shoots per m^2) in winter and spring (see also Auby & Labourg, 1996; Harrison, 1993; Paul & Amos, 2011). The ability of seagrass meadows to modify benthic boundary structure and unidirectional currents have been described using various flume studies (Ganthy et al., 2015; Lefebvre et al., 2010). However, knowledge of the influence of this on sediment transport, particularly bed-load transport, associated with this habitat are limited. Moreover, in the same way that roots of terrestrial plants reduce soil erosion (Vannoppen et al., 2017), below-ground biomass of seagrasses are expected to have an influence on sediment stability in marine environment (Feagin et al., 2015; Möller et al., 2014). This prompted my study on the influence of both above and below-ground biomass on boundary layer structure (including flow-velocity and

turbulence) and bed load sediment transport in controlled laboratory flume experiments, using a combination of mimics and natural meadow sections.

5.1.1 Hydrodynamics and sediment dynamics within and around vegetated beds

5.1.1.1 Benthic boundary layers

Sediment transport in coastal regions is induced by steady currents and wave motion. It is mostly influenced by the region of the water column known as the benthic boundary layer (Figure 5.1) where the flow is subjected to bed friction and form drag. Here, the sea bed exerts a frictional drag force on currents and waves that is expressed as a bed shear stress. In this layer, the mean flow velocity therefore increases from a minimum (zero) at the bed to its maximum in the free stream (Soulsby, 1997). The bed shear stress, τ_0, can be described as a frictional force exerted on a unit area of seabed. The bed shear stress acting on the bed is made up of 1) skin friction related to sediment grain size, and 2) form drag produced by the pressure drag on bed irregularities.

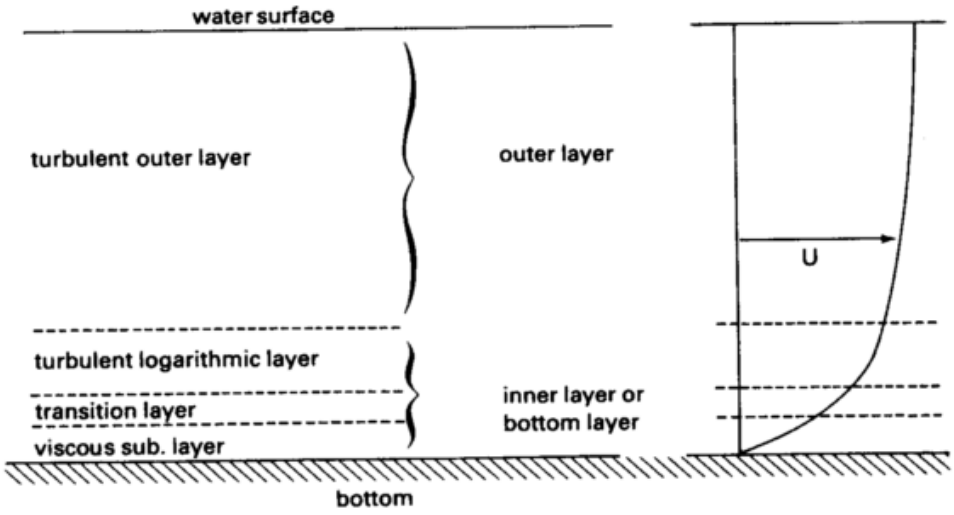

Figure 5.1: Current velocity with height above the bed and benthic boundary layers (van Rijn, 1993).

In a turbulent boundary layer typical of natural marine habitats, the benthic boundary layer is usually divided into four different layers (van Rijn, 1993). Closest to the bed is the viscous sub layer, where the viscous stresses dominate (only present when the roughness elements are smaller than the viscous sub layer thickness). Above that layer is the transition layer, where the viscous and turbulence influence are equal. Next is the turbulent logarithmic layer, where the viscous shear stress can be neglected. Within this logarithmic layer, the shear stress is assumed to be nearly constant with height above the bed and equal to the bed shear stress. The turbulent outer layer is where the flow velocities are almost constant (Z. Liu,

2001). The turbulent layer is described by the von Karman-Prandtl equation referred to as the Law of the Wall:

$$\overline{U}(z) = \frac{U_*}{\kappa} ln\left(\frac{z}{z_0}\right)$$

Equation 5.1

Where $\overline{U}(z)$ is the velocity at height z above the bed, U_* is the friction velocity, k is von Karman's constant (0.4), and z_0 is the roughness length. This equation is only applicable to turbulent rough flow where the viscous sub-layer is absent.

The friction velocity, U_* is a measure of the momentum flux to the bed. The friction velocity is related to bed shear stress by:

$$\tau_0 = \rho {U_*}^2$$

Equation 5.2

$$U_* = (\tau_0/\rho)^{1/2}$$

Equation 5.3

The shear stress may be evaluated through analysis of turbulence using the Turbulence Kinetic Energy (TKE) method. Roughness of the seabed and speed of the flow influence the bed shear stress. This roughness can be determined using the roughness length, z_0 (measurement of the height above the bed at when the velocity, U, goes to zero) or by a physical bed roughness, k_b, that is related to the bed form and grain size. The empirical relationship between roughness length and bed roughness is written as below:

$$z_0 = \frac{k_b}{30}$$

Equation 5.4

The presence of seagrass on the seabed changes z_0 and k_b, thus influencing the dynamics of the benthic boundary layer. Seagrass beds are also associated with various benthic organisms as well as epiphytes that may contribute towards bed stability/instability (Ganthy et al., 2015). Seagrass bed morphology also influences the creation of turbulence and eddy dissipation within the flow (Neumeier & Amos, 2006; Thompson et al., 2004). More knowledge on the magnitude, flow direction and stresses in the benthic boundary layer is required to quantify the morphological alterations by seagrass and improve prediction of sediment transport.

5.1.2 Flow modifications inside and around vegetated beds

The effects of submerged vegetation on the flow differ under either unidirectional flows or waves. Vegetation modification of the flow is normally discussed in terms of the influence on 1) the steady unidirectional currents, and 2) the attenuance of wave energy (Figure 5.2). The magnitude of the effects caused by vegetation also differs between species according to plant morphology and growth stage (Yager & Schmeeckle, 2013). Depending on the vegetation flexibility, leaves are bent under unidirectional flows and create a closed canopy, resulting in reduced mixing between the flow above the canopy and the flow within it thus reducing bed shear stress applied by the flow. On the other hand, leaves move back and forth under the orbital motion of waves. These movements allow mixing across the canopy (Paul, 2011), but flow velocities are reduced compared to the free stream velocity inside a *Zostera marina* canopy, (Gambi et al., 1990; Fonseca & Koehl, 2006; Lefebvre et al., 2010), and *Posidonia oceanica* (Manca et al., 2012; Stratigaki et al., 2011).

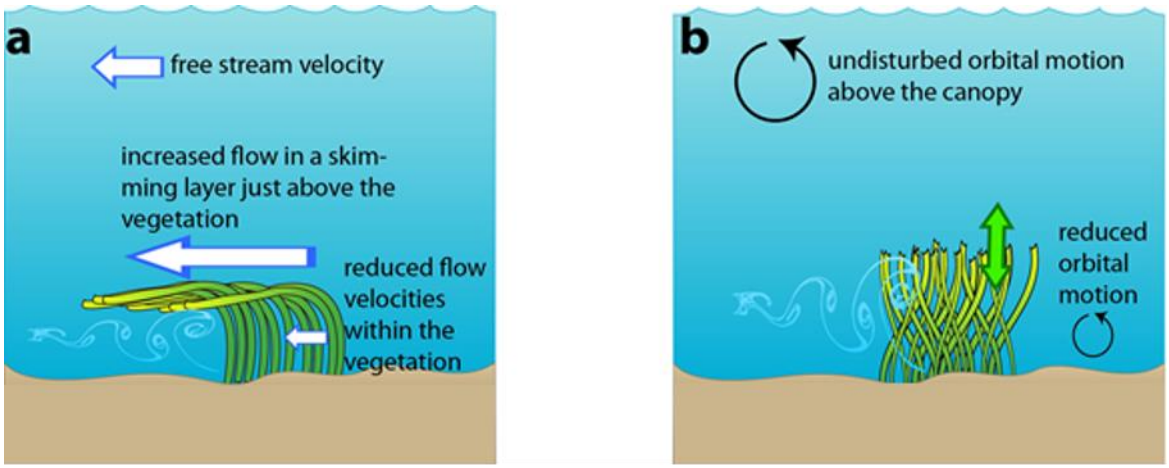

Flexible vegetation bends under flow and creates a closed canopy. As a result the exchange between water bodies within and above the canopy is reduced

Flexible vegetation moves back and forth under orbital wave motion, the canopy is open and allows exchange between water bodies within and above the canopy

Figure 5.2: Conceptual diagram of vegetation influence on A) unidirectional flow and B) waves (from Paul, 2011).

5.1.2.1 Effects of submerged vegetation on unidirectional flow

It is generally accepted that two layers develop in a flow over submerged vegetation: one inside the canopy, exhibiting a reduced flow and the second one, above the canopy, exhibiting skimming flow (Gambi et al., 1990; Lefebvre et al., 2010; Neumeier & Amos, 2006; Wilkie et al., 2012). This response, however, depends on the density of the canopy and the flow velocity (Figure 5.3). Essentially, there are two drag forces acting on the flow over submerged vegetation: the bed drag and the canopy drag. The velocity profile behaves like a normal turbulent boundary layer if the bed drag is larger than the canopy drag, as in the case of a

sparse canopy (Figure 5.3 A). In this case, the vegetation is considered as part of the bed roughness. On the other hand, above a dense canopy, a layer of strong shear develops. Under this condition, the canopy drag is larger than the bed drag (Figure 5.3 A and B) (Nepf, 2012). Above the canopy, the flow usually follows a classic logarithmic profile (Lefebvre et al., 2010; Neumeier & Amos, 2006).

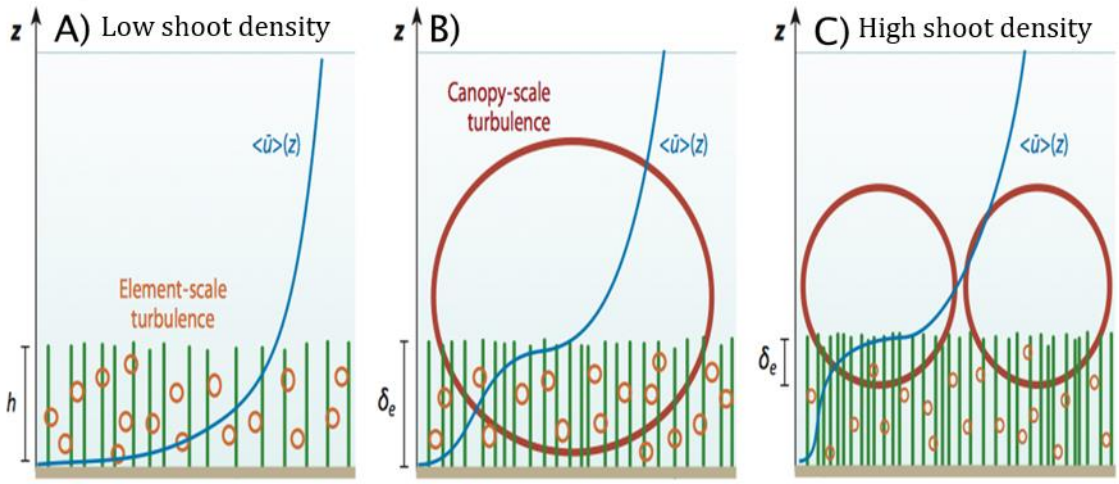

Figure 5.3: Modification of flow structure in relation to shoot density. $\langle\bar{u}\rangle(z)$ is the profile of longitudinal velocity (adapted from Nepf, 2012).

5.1.2.2 Turbulence associated with submerged vegetation

Turbulence within submerged vegetation plays an important role as it influences the particle settling rate and bed erosion through the bed shear stress (Neumeier & Amos, 2006). Under unidirectional flows, turbulence intensities over submerged vegetation were found to increase at the canopy-water interface and further increase with distance from the leading edge of the meadow in the direction of the flow (Gambi et al., 1990; Paul & Gillis, 2015). The morphology of the vegetation also influences the turbulence of the boundary layer. For instance, Zhang et al. (2015) compared the TKE of the flow between two submerged seagrass species, *Vallisneria natans* and *Potamogeton malaianus* and found that due to lower frontal area at the lower part of the canopy, the latter seagrass species have a lower Reynolds stress and TKE.

5.1.3 Sediment transport

5.1.3.1 Initiation of sand mobilisation

Steady currents, waves or their combined effects generate shear stresses that move sediments (Soulsby, 1997). Sediment transport on the bed is initiated at a critical shear stress (τ_{cr}) when the applied shear is greater than the stabilising forces of the sediment grains (Z.

Liu, 2001). The particular velocity at which the fluid force starts to move sediment from a stationary position is known as critical or threshold velocity. The movement of sediment can occur either as bed load by rolling, sliding and saltation or as suspended load (van Rijn, 1993). The mode of sediment transport depends on the magnitude of the forces that act upon a grain.

There are three main forces involved in sediment transport. These are: the lift forces (F_L), the drag forces (F_D), and the gravitational force (W'). These forces operate around the contact points between grains of sediment, known as the pivotal angle. The pivotal angle (ϕ_i), or angle of repose, is the angle at which a single grain rotates about its neighbour as it moves (Figure 5.4). At threshold, the drag force can be written as:

$$F_L + F_D = W' \tan \emptyset_i$$

Equation 5.5

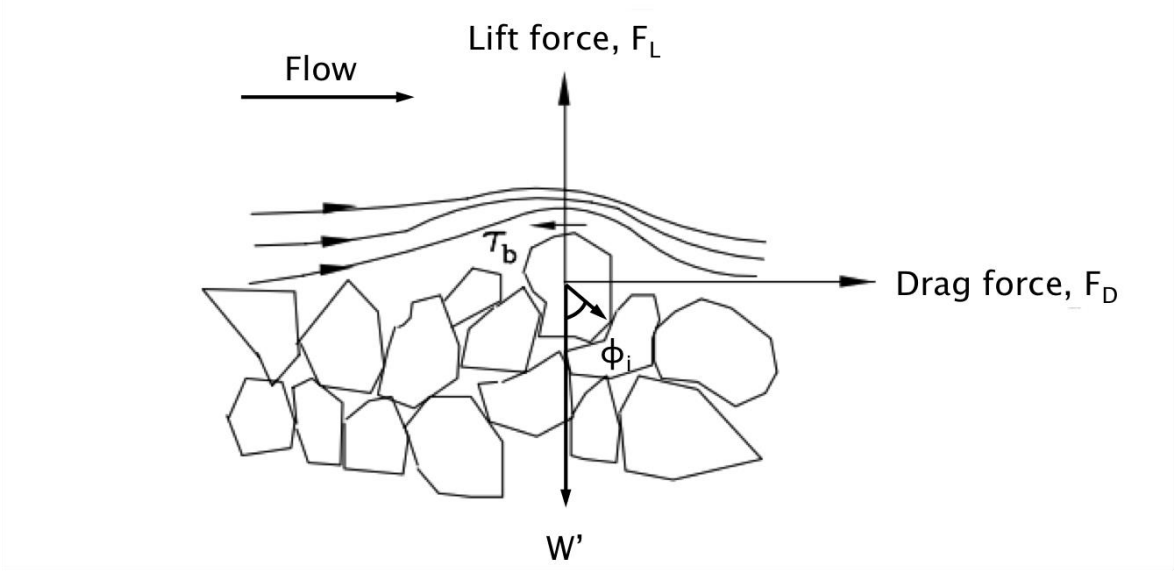

Figure 5.4: Forces acting on grains on the bed (modified from Liu, 2001).

The threshold of motion can be measured in terms of the bed shear stress, τ_b where:

$$\tau_b = (F_L + F_D)/Area$$

Equation 5.6

At threshold, τ_b is equal to τ_{cr}. The shear stress approach was introduced by Shields (1936), who plotted initial-movement data from flume experiments by dividing the critical bed shear stress by the submerged weight of the grain counteracting this. The resulting dimensionless variable is known as the Shields parameter, θ_{cr} defined as:

$$\theta_{cr} = \frac{\tau_{cr}}{g(\rho_s - \rho)d}$$

Equation 5.7

Where, τ_{cr} is the threshold/ critical bed shear stress, g is the acceleration due to gravity (9.81 m s^{-1}), ρ_s is the grain density (kg/m^3), ρ is the water density (kg/m^3) and d is the grain diameter (m).

Hydraulic conditions are often measured by the flow Reynolds number (Re), a dimensionless indicator used to categorise the flow state. The Reynolds number is the ratio of inertial forces to viscous forces. Inertial force involves force due to the momentum of the mass of flowing fluid and viscous forces deal with the friction of a flowing fluid. The Reynolds number describes the nature of the flow, the turbulence level and hence, the critical bed shear stress (van Rijn, 1993). It categorises whether the flow is steady (laminar) or on the average steady with small unsteady fluctuations (turbulent). Shields divided the flow response to Re into four regions as shown in Figure 5.5. Region I is defined as laminar flow, where Re < 2. Region II is considered as transitional flow, between laminar and turbulent, where 2 < Re < 10. In Region III, the thickness of the viscous sub-layer is comparable to the particle diameter, where 10 < Re < 1000. This flow is thus defined as turbulent smooth. In Region IV, the flow is considered hydrodynamically rough (Re > 1000). The viscous sub-layer in this region is absent and the logarithmic layer is considered to extend to the bed.

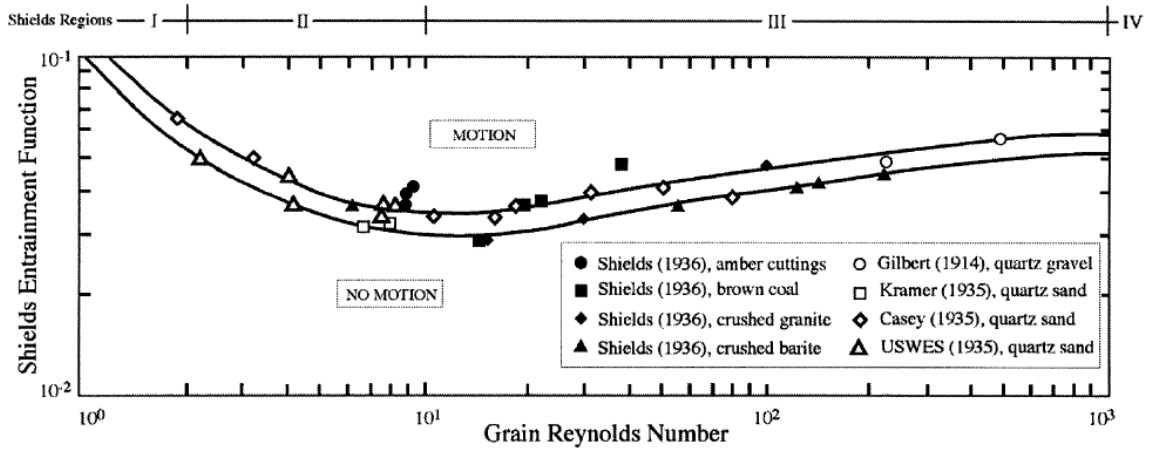

Figure 5.5: The Shield's curve for the initiation of sediment motion (from Paphitis, 2001).

The movement of sediment of various grain sizes and at different flow velocities is non-linear. Silts and clays are harder to mobilise due to their cohesive nature, though they tend to be transported further than coarser grains once they are in motion. Silts and clays are generally transported in suspension due to their low settling velocities. As a result, they are deposited at low flow speeds (Winterwerp, 2011).

5.1.4 Sediment transport in seagrass meadows

The presence of seagrass generally stabilizes the bed though a combination of the reduction of the bed shear stress and an increase in the threshold for sediment motion (Fonseca & Fisher, 1986; Lefebvre et al., 2010; Thompson et al., 2004).

Flow deflection by the meadow leads to reduced/low mixing between the water column above and within the canopy (Koch, 1999). The dampening of hydrodynamic energy, and reduction of bed shears stress, creates a region of net deposition with increased sediment deposition and reduced suspension (Ganthy et al. 2015). It has been reported that beds colonised by seagrasses and other vegetation are characterised by finer sediment compared to their adjacent areas due the mechanical trapping of fine particles by the meadows (De Falco et al., 2000). The role of seagrasses in the retention of sediments can therefore be divided into their ability to enhance deposition and to reduce resuspension (Gacia & Duarte, 2001).

The below-ground properties of the seagrass (roots and rhizomes) have also been demonstrated to help bind the sediment and reduce resuspension. However, due to the lack of vertical rhizomes, *Zostera* species have limited sediment-fixing capacity (Lefebvre et al., 2010).

The density of seagrass plays an important role in sediment stabilisation of the seabed. Van Katwijk et al. (2010) mention that low density or low biomass seagrass meadows have low sediment trapping efficiencies. However, Paquier et al. (2014) and Christianen et al. (2013) recorded accretion of sediment even in low shoot density meadows. Low densities of seagrass stems were also reported to enhance turbulence resulting in resuspension of sediment even at low current velocities (Koch, 1999). In conditions of low flow speed and high leaf density, deposition is increased because the seagrass leaves usually bend less. Therefore, there is a greater canopy height wherein suspended particles can be trapped (Ganthy et al., 2015).

5.1.5 Aim and objectives

My overall aim was to study velocity attenuation, flow structure, bed shear stress and sediment transport associated with real and mimic *Zostera noltii* canopies, including the role of below-ground biomass in controlled flume experiments. In *Zostera noltii* beds, up to 95% of the plant's biomass lie below ground. For the first time, the role of In *Zostera noltii* meadows in reducing bed load transport is quantified compared with the effects of hydrodynamic alteration at a seasonal time scale.

The flow characteristics, turbulence, roughness of the bed and sediment movement around and within *Zostera noltii* beds of different densities were simulated in a straight recirculating flume and an annular flume (the Lab Carousel). The straight flume enabled characterisation of the flow within and above canopies using mimics. The Lab Carousel was used to investigate the flow upstream, within and downstream of transplanted natural seagrass clumps; it also allowed the use of real seagrass and a mobile sand layer and thus enabling the study of bed load transport through ripple migration. The specific objectives of this chapter were;

1. To characterise the flow structure and turbulence inside and above seagrass canopies of different densities and applied velocities;
2. to characterise the bed shear stress and bed roughness associated with the canopy;
3. to measure bed load transport within and around seagrass canopies of different densities and velocities as well as bed load transport on below-ground biomass only bed.

5.2 Material and methods

5.2.1 Assessment of field conditions

Prior to experiments in the laboratory, hydrodynamics conditions were assessed in Ryde, Isle of Wight in order to create similar conditions in the flumes (Paul, 2011). Seagrass densities were counted within a 0.5 m x 0.5 m quadrat with five replicates of seagrass percentage cover monthly for 26 months at lowest low water on Ryde tidal flats (N 50.7369°, W 01.1619°) (detailed in chapter 2). The shoot density increased closer to the water line where small patches of subtidal seagrass species, *Zostera marina* can also be found (-1.5 m OD). Seagrass densities of 500 (late winter), 1000 (early spring and late autumn) and 4000 (peak late summer densities) shoots m^{-2} were therefore chosen to represent the different phases of the seagrass seasonal growth. This also allows comparison with the work of Paul et al. (2012) who investigated wave attenuation through the same species over the same shoot densities. Sediment samples were collected around the seagrass bed in Ryde, and analysed for grain size as described in Chapter 2 (section 2.2.1). The sediment samples were composed of more than 95% sand. The median grain diameter was 0.18 mm (fine sand).

Horizontal flow velocities were measured using an Electromagnetic Current Meters (EMCM, Valeport Model 808) and water depth was measured by a pressure transducer on the instrument. It was deployed from 31 August to 4 September 2015 as described in Chapter 2 (section 2.2). The tidal flow showed that the tide was a progressive wave type over the tidal flats. The maximum current values were around 0.2 m s^{-1} and took place over high water (Figure 5.6). The main flow was from East to West during flood tide and West to East during

the ebb tide. The tidal flow rotates clockwise over the flats during tidal inundation. Current velocity in the area have been reported with values up to 0.3 m s^{-1} (Paul, 2011).

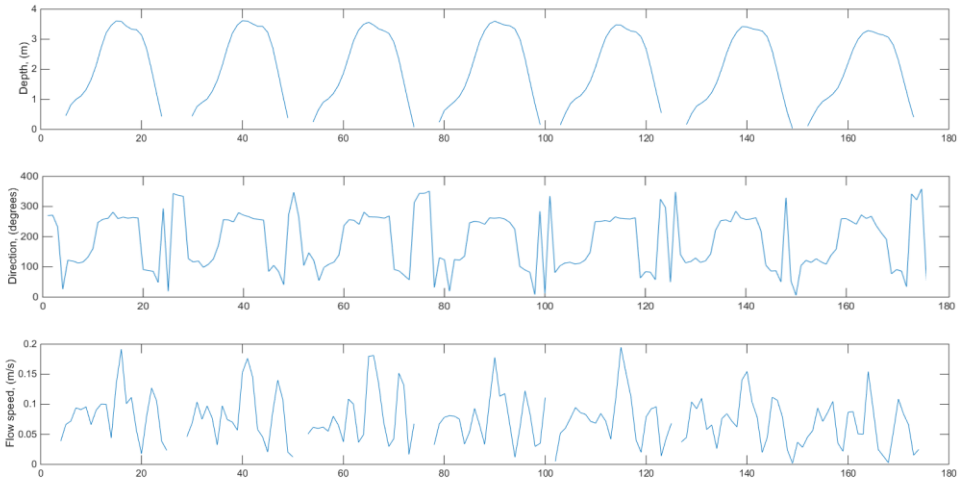

Figure 5.6: Tidal flow conditions from 31 August to 3 September 2015 representing A) the tidal elevation, B) the direction, where 0 degree is the North and C) the flow speed.

5.2.2 Laboratory experiments in recirculating and annular flume

Laboratory experiments were carried out in two types of flumes, a recirculating flume and an annular flume (Lab Carousel). The advantage of carrying out experiments in the recirculating flume is the flume has greater depth, allowing better assessment of above seagrass canopy velocity. It is also straight sided, therefore 2D flow was achieved. The flume, however, has a limited working length due to the entrance and exit conditions. It also does not allow the use of seawater and not kept submerged, which led to the use of seagrass mimics. On the other hand, Lab Carousel has an infinite flow length, thus, better for investigation of sediment transport and upstream/ downstream effects of seagrass. Seawater can be used in the flume and the meadow was kept submerged during the experiments. However, the annular flume is shallower with limited potential for above canopy measurements. Secondary flows usually develop in annular flumes due to the curved shape of the flume (Amos et al., 1992).

5.2.3 Recirculating flume experimental setup

A set of experiments was conducted in a recirculating flume at NOCS, UK in order to investigate the flow structure above and within *Zostera noltii* canopies. The open top recirculating flume (Paphitis & Collins, 2001) is 5 m long, 0.3 m wide and 0.45 m deep (Figure 5.7). The base of the flume is painted metal and the side-walls are made of toughened glass.

When in use, freshwater stored in the reservoir tanks is pumped into the upstream constant-head inlet tank through an adjustable gate valve. The water flows into the working section through a honeycomb baffle structure (to reduce eddy sizes) and over a hinged weir into the reservoir tank on the downstream. Opening the gate valve increases the flow speed and water level while lowering the hinged weir increases flow speed but reduces the water level. A 25 cm-long gravel section was added at the flume entrance and together with the honeycomb-like structure, ensured a fully rough turbulent flow in the working section (Nowell & Jumars, 1987).

An Acoustic Doppler Velocimeter (ADV) manufactured by Nortek was used to take flow velocity measurements. The ADV was mounted on a carriage that enabled it to be moved horizontally along the centre line of the flume. The ADV probe was attached to a mechanism that can be adjusted vertically enabling measurement at a specific height above the bed. The current velocities were recorded in three dimensions; tangential (x), radial (y) and vertical (z) at 5 cm below the sensor head.

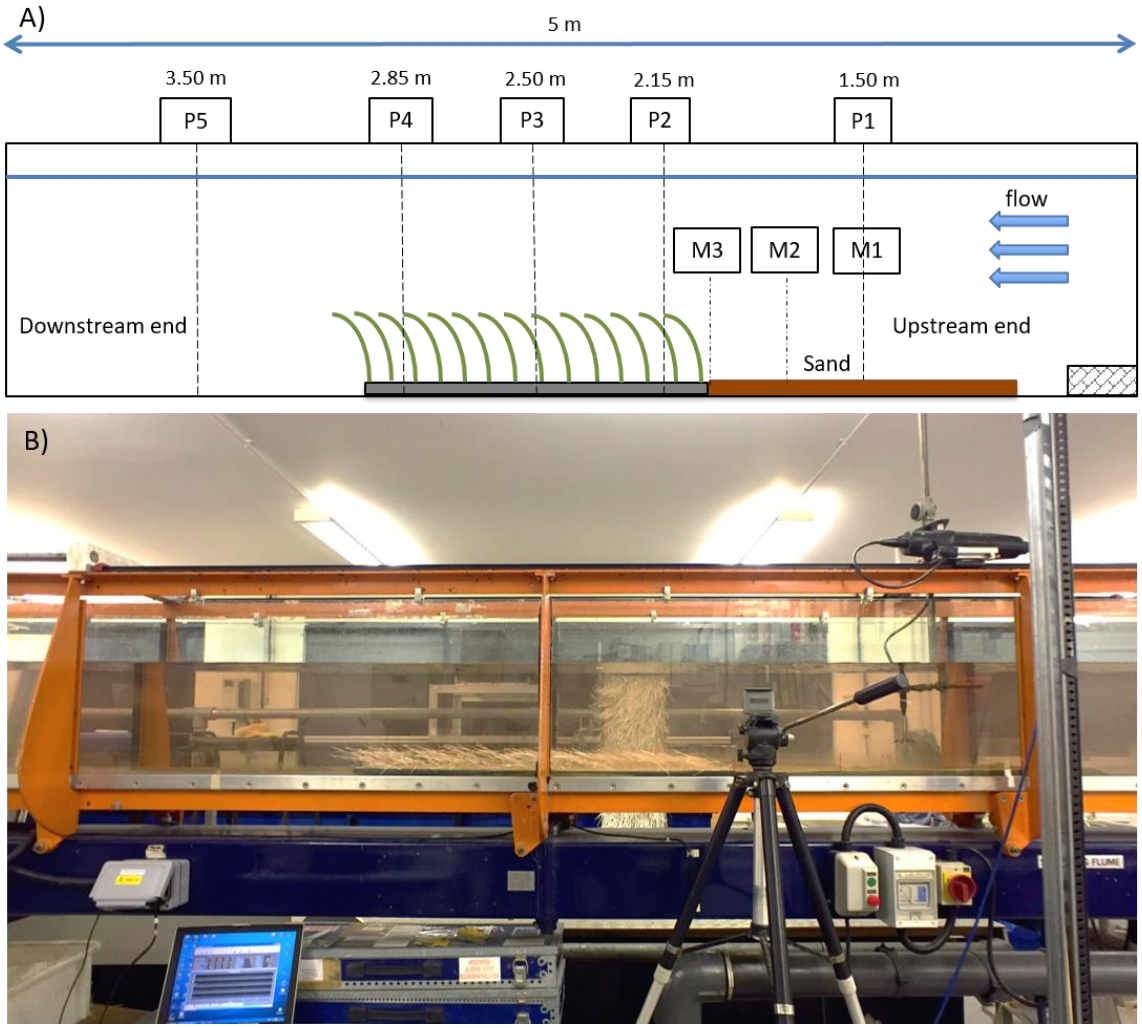

Figure 5.7: (A) Schematic diagram of the recirculating flume and positions of profile measurement (not to scale). P1 to P5 mark the location of flow measurements and M1 to M3 mark the location of sediment transport measurements (B) Photograph of the working section of the flume.

Several different seagrass arrangements were used in this experiment to investigate the effect of seagrass density on unidirectional flow. Mimics of *Zostera noltii,* created based on field measurements of the seagrass density, leaf length and leaf width, were used to investigate the effect of seagrass on the flow and sediment mobilisation. These were attached to a plate which could be inserted into the flume, and allowed easy modification of the shoot density. Control experiements were undertaken to assess any effect of the plate on the flow in the absence of the mimics. The *Zostera noltii* mimics were then tied to a mesh and attached to the plate using thread. A reference point was set 1 m from the flume entrance at 0.3 m height above the bed (free-stream) to ensure consistent flow speed in repeat runs. Consistency between runs was achieved by maintaining a constant water level and constant weir position, as well as taking velocity measurement at the reference point before each run. Flow velocity profiles were measured at five positions along the centre line of the flume to obtain measurement upstream (x: -0.5 m), inside (x: 0.15 m, 0.5 m, 0.85 m), and downstream (x: 1.5

m) of the leading edge of the seagrass mimic canopy (Figure 5.7). Water depth was kept constant at 0.41 m throughout the 0.1 m s^{-1} flow velocity runs and at 0.38 m during the 0.2 m s^{-1} runs.

At each location, flow velocities were measured at 10 heights (1, 2, 3, 5, 7.5, 10, 15, 20, 25 and 30 cm) above the bed. Each velocity measurement was recorded at 25 Hz for 120 seconds. Twelve runs were carried out in the recirculating flume to test the effect of the mimics with varying shoot densities and different flow velocities (Table 5.1). During runs 9-12, sediment was placed upstream of the meadow from one meter into the flume until the leading edge of the canopy. Placing sediment only in the upstream of the meadow avoids any damage to the flume pump, which is not designed for sediment load. There were no sediment movement observed under a flow velocity of 0.1 m s^{-1} and 0.2 m s^{-1}. Therefore, flow velocity was increased to 0.25 m s^{-1} in order to measure the bedload transport rate. In the field, the higher velocity normally occurs during high tide.

Table 5.1: Details of runs undertaken in the recirculating flume.

Experiment	Run number	Free-stream velocity (m s^{-1})	Patch length (m)	Shoot density (shoots m^{-2})	Sediment
R1	1 and 2	0.1 and 0.2	1	Bare	None
R2	3 and 4	0.1 and 0.2	1	500	None
R3	5 and 6	0.1 and 0.2	1	1000	None
R4	7 and 8	0.1 and 0.2	1	4000	None
R5	9	0.25	1	Bare	Upstream
R6	10	0.25	1	500	Upstream
R7	11	0.25	1	1000	Upstream
R8	12	0.25	1	4000	Upstream

5.2.3.1 Vegetation characteristics

Zostera noltii mimics used in this experiment were made of polypropylene ribbon. The mimics have a similar stiffness and motion to *Zostera noltii*. It was designed based on the size and density of *Zostera noltii* found in the natural environment (Paul, 2011). The number of shoots per sample was counted before each run, providing the shoot density (D_{shoot}, in m^{-2}). Leaves were cut to approximately 0.12 m in length (average *Zostera noltii* length in Ryde during winter) to enable the evaluation of flow structure above the canopy. Mean leaf area index (LAI), was calculated as leaf length x leaf width x shoot density. Air-dried leaves were weighed to calculate the above-ground biomass. The vegetation configurations tested during the experiment in the recirculating flume are detailed in Table 5.2.

Table 5.2: Vegetation characteristics in recirculating flume experiment with seagrass mimics.

Experiment	**R1**	**R2**	**R3**	**R4**	**R5**	**R6**	**R7**	**R8**
Density of shoot (m^{-2}), D_{shoot}	Bare	500	1000	4000	Bare	500	1000	4000
Leaf Area Index, LAI	-	0.12	0.24	0.96	-	-	-	-
Leaf length (cm) L_{leaf}	-	12.00	12.00	12.00	-	-	-	-
Leaf width (cm), W_{leaf}	-	0.20	0.20	0.20	-	-	-	-
Above-ground biomass (g m^{-2})	-	12.65 ± 0.61	25.1 ± 1.21	100.4 ± 4.85	-	-	-	-
Below-ground biomass (g m^{-2})	-	-	-	-	-	-	-	-
Height of canopy (U = 0.1) (cm)	-	P2 = 5, P3 = 7.5, P4 = 7.5	P2 = 5, P3 = 7.5, P4 = 7.5	P2 = 7.5, P3 = 7.5, P4 = 7.5	-	-	-	-
Height of canopy (U = 0.2) (cm)	-	P2 = 3, P3 = 3, P4 = 5	P2 = 3, P3 = 5, P4 = 5	P2 = 5, P3 = 5, P4 = 5	-	-	-	-

5.2.3.2 Sediment used in the flume experiments

The sediments used in the flume were obtained from the upper shore of the study area in Ryde, Isle of Wight. The sediments were wet sieved using a 63µm sieve to remove any fines. The fine, very well-sorted sands have a negative skewness and a very leptokurtic distribution (mean, Mz: 2.43 phi; sorting, σ: 0.27 phi; skewness, Sk: -0.33 phi; kurtosis, K_G: 1.84 phi) (Figure 5.8).

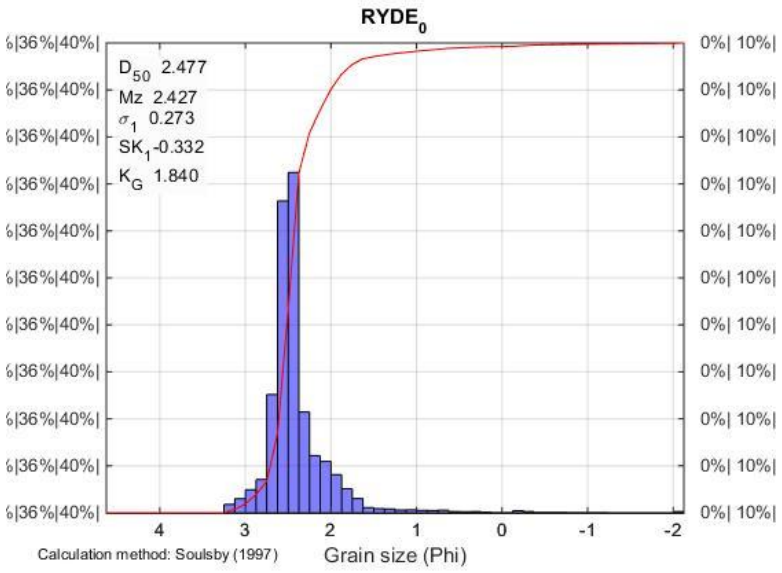

Figure 5.8: Grain size distribution used in the recirculating flume.

Theoretically, the sand used in the experiments has a threshold mean current velocity of 0.25 m s^{-1}, calculated using the Soulsby (1997) formula to measure threshold current speed for non-cohesive sediment and water conditions for which $D_* > 0.1$. The threshold current velocity, $\overline{\boldsymbol{U}}_{\boldsymbol{cr}}$ is calculated as follows:

$$\overline{U}_{cr} = 7\left(\frac{h}{d_{50}}\right)^{\frac{1}{7}}[g(s-1)d_{50}f(D_*)]^{\frac{1}{2}}$$

Equation 5.8

$$f(D_*) = \frac{0.30}{1+1.2D_*} + 0.055[1-\exp(-0.02D_*)]$$

Equation 5.9

Where h is the total water depth and D*, the dimensionless grain size, is equation (2.2).

5.2.4 Annular flume, Lab Carousel experimental setup

A second set of experiments was carried out using an annular flume (Lab Carousel) at NOCS, UK, to characterise flow structure and sediment transport inside *Zostera noltii* canopies. The Lab Carousel (Thompson et al., 2006) is an annular flume constructed of smooth acrylic with a diameter of 2 m, with a 0.15 m wide by 0.45 m deep channel. The current is generated within the channel using a rotating lid, fitted with 8 equidistant paddles. The speed of rotation of the lid is controlled by a motor controller, with velocity being measured using an Vectrino ADV by Nortek. The ADV used is similar to the one used in the recirculating flume, except the transducer's shaft is shaped to allow measurements in the middle of the channel allowing for the rotating lid. Due to the paddles, velocity measurements are limited to 19 cm above an empty bed. The flume was filled with sediments collected in Ryde, Isle of Wight to approximately 6.5 cm (±1.5) deep. It is then filled with seawater of 34 ppt (±1) salinity and 19°C (±2) temperature.

Flow velocity profiles were measured at five positions along the centre of the flume to obtain one measurement upstream (x: -0.3 m), three inside (x: 0.1 m, 0.4 m, 0.7 m), and one downstream (x: 1.1 m) from the leading edge of the *Zostera noltii* canopy (Figure 5.10). Water depth was kept at 0.40 m on all runs. Flow velocities were recorded vertically every 0.5 cm within and just above the canopy and every 1 cm thereafter. Each velocity profile consisted of 13 to 17 instantaneous velocity measurements recorded at 25 Hz for 120 seconds.

A total of eighteen runs were carried out in the Lab Carousel to test the effect of shoot density on the flow and measure sediment bed load transport (Table 5.3). *Zostera noltii* plants were collected on Ryde tidal flat (N 50.73692°, W 1.1619°) during low water on spring tides during different phases of its annual growth. The canopy was cut into four 0.2 x 0.15 x 0.08 m blocks and was inserted into the flume (Figure 5.9), this maintained the above and below bed structure. Any gaps between the blocks were filled with sediment from the same area. Bedforms developed after each run were levelled before the start of the following run. At the end of runs with both, above and below-ground biomass intact, the above-ground biomass were removed by cutting the shoots, leaving only the roots and rhizomes of the below-ground biomass. Further experiments were carried out to test the effect of below-ground biomass on the flow and measure sediment bed load transport.

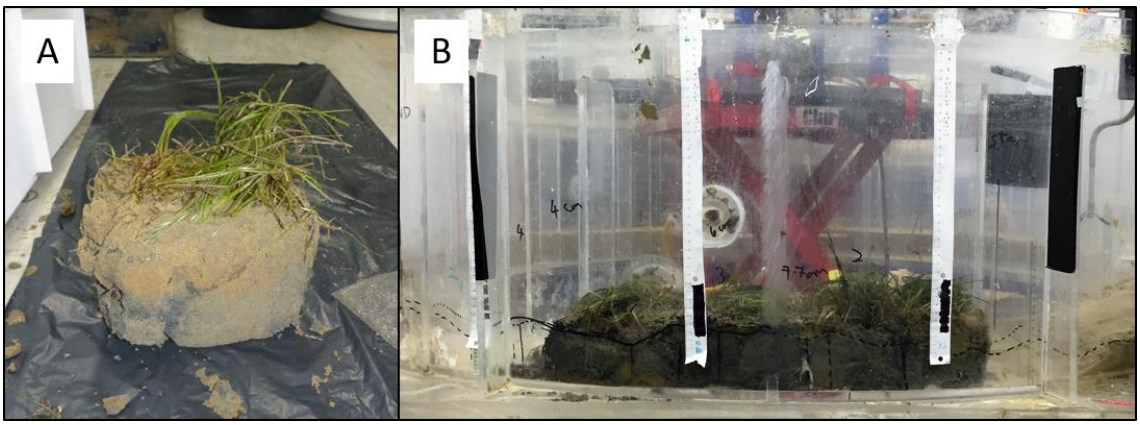

Figure 5.9: Pictures of *Zostera noltii* in; (A) small block; (B) arranged in the annular flume.

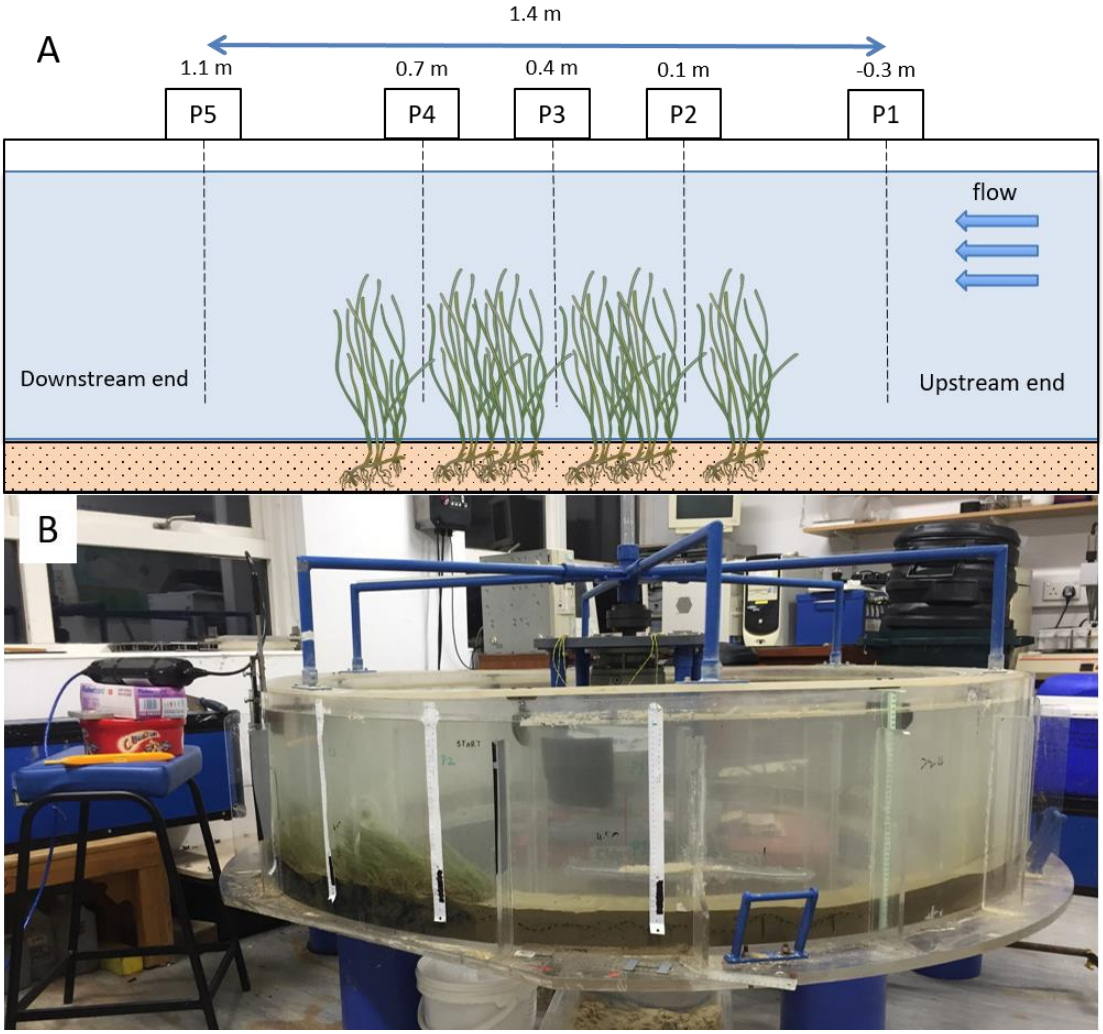

Figure 5.10: (A) Schematic diagram of the Lab Carousel experimental setup and positions of profile measurements (P1 to P5). (B) Photograph of the working section of the flume.

Table 5.3: Details of runs undertaken in the annular flume.

Experi-ment	Run number	Free-stream velocity (m s^{-1})	Patch length (m)	Shoot density (shoots m^{-2})	Biomass
A1	1, 2, 3	0.1, 0.2, 0.3	0.8	Bare	None
A2	4, 5, 6	0.1, 0.2, 0.3	0.8	672	Above and below-ground
A3	7, 8, 9	0.1, 0.2, 0.3	0.8	1100	Above and below-ground
A4	10, 11, 12	0.1, 0.2, 0.3	0.8	2850	Above and below-ground
A5	13, 14, 15	0.1, 0.2, 0.3	0.8	1100	Below-ground
A6	16, 17, 18	0.1, 0.2, 0.3	0.8	2850	Below-ground

5.2.4.1 Vegetation characteristics

The number of shoots per sample was counted before each run, providing the shoot density (D_{shoot}, in m^{-2}). The length and width of 5 randomly selected leaves were measured and used to calculate the mean leaf length, mean leaf width and mean leaf area index (LAI), calculated as leaf length * leaf width * shoot density. LAI is used to compare the influence of canopy on the flow as this measurement accounts the variety in leaf length and width as well as the density. The canopy height (H_{cm}, in cm) was measured manually from the outside of the flume wall. After each experiment, the 0.15 m x 0.8 m seagrass blocks were washed with fresh water on 2 mm and 1 mm sieves to separate the roots and rhizomes from sediments and shell fragments. Above-ground and below-ground biomass were weighed after both were dried at 60°C for 24 hours. The characteristics of vegetation tested in the lab carousel are presented in Table 5.4.

Table 5.4: Vegetation characteristics in the annular flume experiment with real seagrass.

Experiment	**A1**	**A2**	**A3**	**A4**	**A5**	**A6**
Sampling date	-	26/01/2017	26/04/2017	21/08/2017	26/04/2017	21/08/2017
Density of shoot (m^{-2}), D_{shoot}	0	672	1100	2850	0	0
Leaf Area Index, LAI	-	0.16	0.26	0.87	-	-
Leaf length (cm) L_{leaf}	-	16.10	19.40	20.24	-	-
Leaf width (cm), W_{leaf}	-	0.10	0.12	0.15	-	-
Above-ground biomass (g m^{-2})	-	6.98	11.42	89.00	-	-
Below-ground biomass (g m^{-2})	-	294.58	239.42	486.30	239.42	486.30
Height of canopy (U = 0.1) (cm)	-	P2 = 6, P3 = 6, P4 = 6	P2 = 5, P3 = 6, P4 = 7	P2 = 7, P3 = 6, P4 = 7	-	-
Height of canopy (U = 0.2) (cm)	-	P2 = 4, P3 = 4, P4 = 4	P2 = 2, P3 = 4, P4 = 4	P2 = 5, P3 = 7, P4 = 6	-	-
Height of canopy (U = 0.3) (cm)	-	P2 = 3, P3 = 3, P4 = 3	P2 = 2, P3 = 2, P4 = 1.5	P2 = 2, P3 = 5, P4 = 4	-	-

5.2.5 Data processing

The ADVs record three velocity components (x, y and z), three signal strengths and three correlation values for each sample. Signal strength and correlation values indicate the quality of the velocity measurement. All the velocity records were processed using a Matlab code by removing records with low signal-to-noise ratio and a correlation below 70 % (Kassem et al., 2015). Any spikes in the data were removed using a despiking function by Mori et al. (2007). The data were then smoothed using the method applied by Kassem et al. (2015) by using a moving average algorithm (Thompson et al., 2012), and an axes rotation algorithm, to eliminate the effects of sensor misalignment (Elgar et al., 2001). An example plots of the raw, despiked and smoothed and axes rotated mean is shown in Figure 5.11.

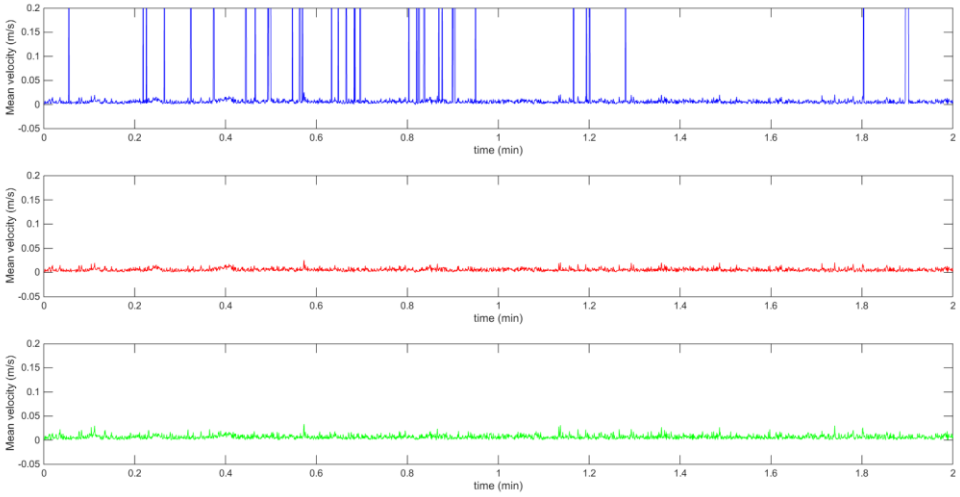

Figure 5.11: The mean velocity, $\bar{u}$ before processing, after despiking and smoothing and after axes rotation, measured at z = 0.02 m, x = 2.85 m at 0.1 m s^{-1}.

For the turbulence analysis, instantaneous velocities in the x-direction (u) are defined as:

$$u = \bar{u} + u'$$

Equation 5.10

Where, ($\bar{u}$) is the mean velocity and the instantaneous velocity fluctuation is (u'). This calculation is applied to the other two components of the flow in y-direction (v) and z-direction (w). The depth-averaged velocity is then calculated using:

$$\overline{U} = \sqrt{\overline{u}^2 + \overline{v}^2 + \overline{w}^2}$$

Equation 5.11

The Turbulent Kinetic Energy (TKE), is computed as follows:

$$TKE = 1/2\rho(\overline{u'^2} + \overline{v'^2} + \overline{w'^2})$$

Equation 5.12

The turbulence intensity, U_{rms} is defined as the ratio of the root-mean-square of the velocity fluctuations, u' to the mean flow velocity, $\overline{U}$. These turbulence measurements are calculated as follow:

Turbulence intensity,

$$U_{rms} = \frac{rmsu'}{\overline{U}}100$$

Equation 5.13

The two-dimensional Reynolds stress was measured as:

$$\tau_{rs} = -\rho(\overline{u'w'})$$

Equation 5.14

Velocity attenuation coefficient inside the canopy (VA, in %) was calculated as the depth-averaged velocity attenuation inside the canopy in order to compare the effects of seagrass canopy on near-bed velocities. The velocity attenuation is calculated as:

$$VA = \frac{1}{N}\sum_{1}^{H_C}\left[\frac{100\big(U_s(z) - U_v(z)\big)}{U_s(z)}\right]$$

Equation 5.15

Where, N is the number of vertical measurements within the canopy, H_C is the measured canopy height in m, $U_s(z)$ is the velocity at height z above the bed in the bare bed run for experiments in recirculating flume, and velocity at height z above the bed at the upstream profile (P1) for experiments in the Lab Carousel. $U_v(z)$ is the velocity at height z above the bed in the vegetated bed tests.

5.3 Results

5.3.1 Flow structure within and around *Zostera noltii* mimics (An experiment in a recirculating flume).

In this section, results from measurements recorded in the recirculating flume experiment with *Zostera noltii* mimics are presented. Vertical profiles of mean velocity, TKE and turbulence intensity were compared for two flow velocities and three different seagrass annual growth phases observed at Ryde, Isle of Wight. The mean velocity, TKE and turbulence intensity were calculated using equations (5.6), (5.7), (5.8) and (5.9), respectively. Figure 5.12 and Figure 5.13 presents the parameters mentioned above, plotted against height above the bed for the three seagrass densities and one control tested at the free stream velocity of 0.2 m s^{-1} and 0.1 m s^{-1}. The Reynolds number, $Re = \bar{U}d/\nu$, calculated for the flow velocities tested was above 1000. This value shows that the flow is turbulent rough throughout the water column.

Generally, the velocity profile over the unvegetated bed in the control experiment was characterised by an approximately constant velocity throughout the water columns, which reduced closer to the bed similar to a typical log profile. On the other hand, the velocity profiles with vegetated beds showed a more complex structure, which varied with seagrass densities. Two zones were evident within the profiles: a within canopy zone characterised by low velocities and high turbulence and above it characterised by higher velocity and lower turbulence compared to the upstream of the canopy. In the densest canopy tests, the flow can be divided into two distinct flow profiles, one from the free-stream until the top of the canopy and another one from the top of the canopy to the bed. In a sparse canopy, the profile presents an increasing flow reduction, approaching the bed.

The time-averaged mean velocity showed an increase with height above the bed and reduced drastically within the canopy. The TKE and turbulence intensities were high at the canopy/ water interface. Profiles of the TKE (Figure 5.12) were characterised by a maximum value at the top of the canopy on the vegetated bed. Below this maximum, the TKE value decreased towards the bed and is even smaller than over the bare bed for the high-density canopy. Meanwhile for the unvegetated and bare beds, the maximum value was measured close to the bed.

The current flow was slowest and the TKE and turbulence intensity were highest in test R4 which has the highest LAI value at 0.96. As an example, the depth-averaged velocity along P4 at 0.2 m s^{-1} was 0.17 m s^{-1}, 0.16 m s^{-1}, 0.15 m s^{-1} and 0.12 m s^{-1} in tests, R1, R2, R3 and R4, respectively. The turbulence intensity was 11% with the bare bed and increased to 45% with the highest shoot density. The average velocity decreased from P1 to P4 before accelerating at P5 to almost the same value as at P1 (i.e. the flow has almost recovered).

The velocity profile was observed to be consistent for all shoot densities tested in the first profile (P1), located in the upstream of the canopy, indicating no influence of the meadow. TKE were low and constant throughout the profile while turbulence intensities were slightly higher as compared to profiles within and downstream of the canopy. The flow velocity was reduced to approximately 13 % of the initial free stream flow velocity within the canopy (R4) in the second profile (P2). The canopy height was the shortest at this profile as a result of leaf bending. The flow velocity was observed to accelerate in the free stream above the canopy. Turbulence was reduced above the canopy while it increased within the canopy. Turbulence intensities in the region above the canopy were reduced with increasing distance from the leading meadow edge. Along this profile and within the canopy, flow velocity decelerated while turbulence and TKE increased.

At the third (P3) and fourth profile (P4), the mean flow velocity decreased further while turbulence increased to its highest just below the top of the canopy. For the densest canopy, which was 4000 shoots m^{-2}, the TKE was highest at the top of the canopy while in the less dense canopies, peak TKE was observed lower within the canopy. A fifth profile (P5) showed that the flow accelerated after it exits the canopy but was still influenced by the canopy. This was confirmed by the high TKE values near the bed along this profile.

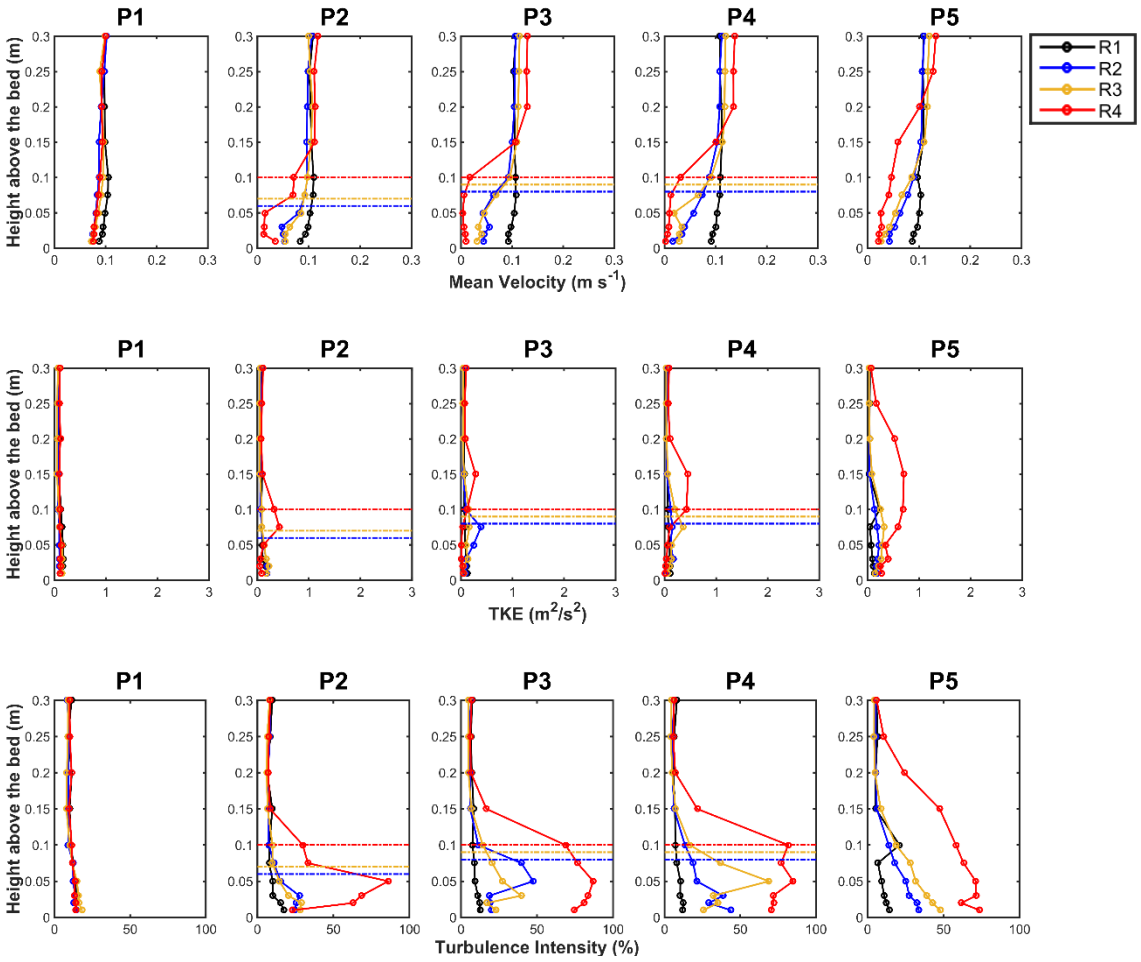

Figure 5.12: Mean velocity, TKE and turbulence intensity at different seagrass growth phase along 5 positions (P1 to P5) on bed at 0.1 m s^{-1}. R1, R2, R3 and R4 represent 0, 500 (late winter), 1000 (early spring and late autumn) and 4000 (summer) shoot density/m^2, respectively. Dotted horizontal lines refer to the average canopy (mimics) height of the tested density.

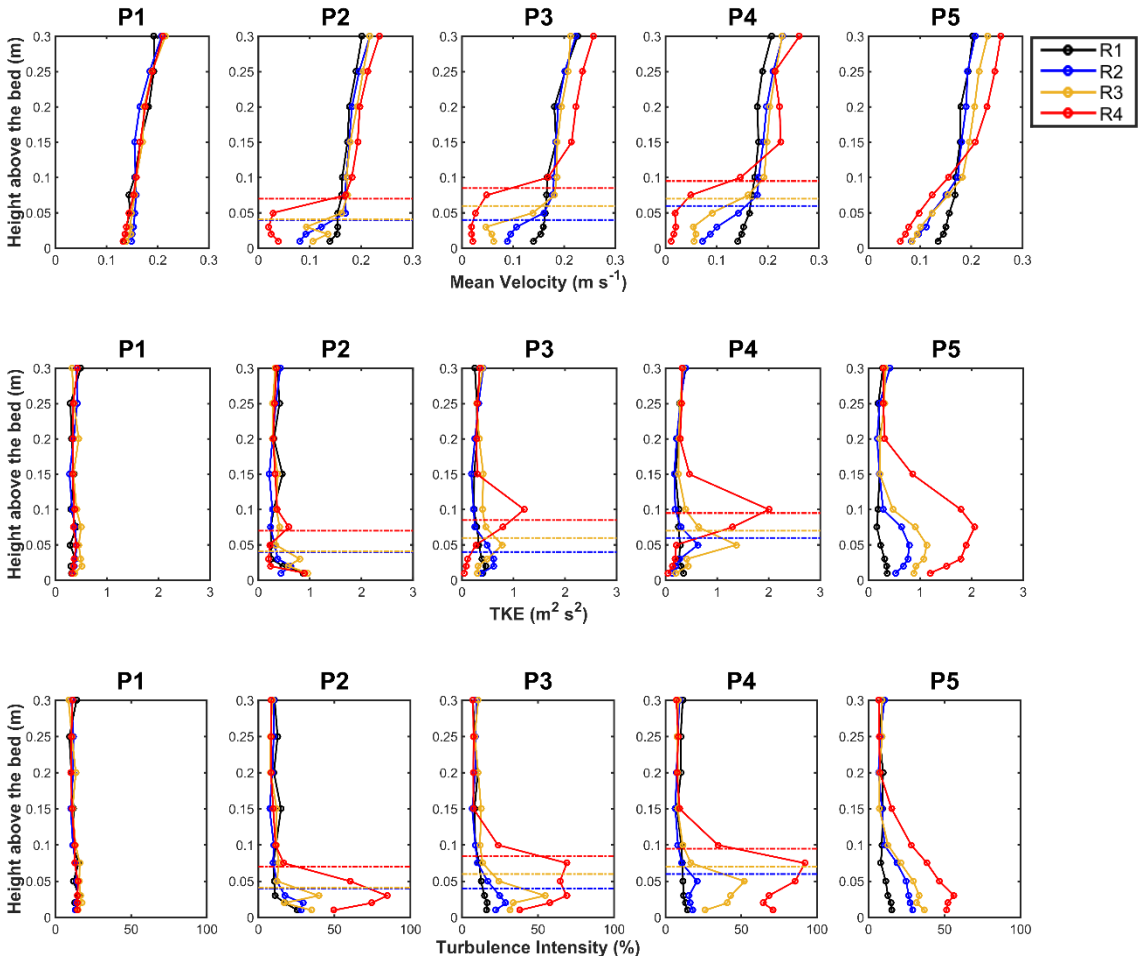

Figure 5.13: Mean velocity, TKE and turbulence intensity at different densities reflecting seagrass seasonal growth phases along 5 positions (P1 to P5) on bed at 0.2 m s^{-1}. R1, R2, R3 and R4 represent 0, 500 (late winter), 1000 (early spring and late autumn) and 4000 (summer) shoot density/m^2, respectively. Dotted horizontal lines refer to the average canopy height of the tested density.

Velocity attenuation coefficients (Equation 5.17) within the canopy were highest for the highest density tested (R4) at 71 to 93 % on both 0.1 m s-1 and 0.2 m s^{-1} free-stream velocity (Figure 5.14). Lower density canopies (R2 and R3) show that VA increases with increasing shoot density except for R3, where the attenuations were 5 and 9 % lower than R2 at 0.1 and 0.2 m s^{-1} free stream velocity, respectively. Generally, VA increases with distance into the canopy.

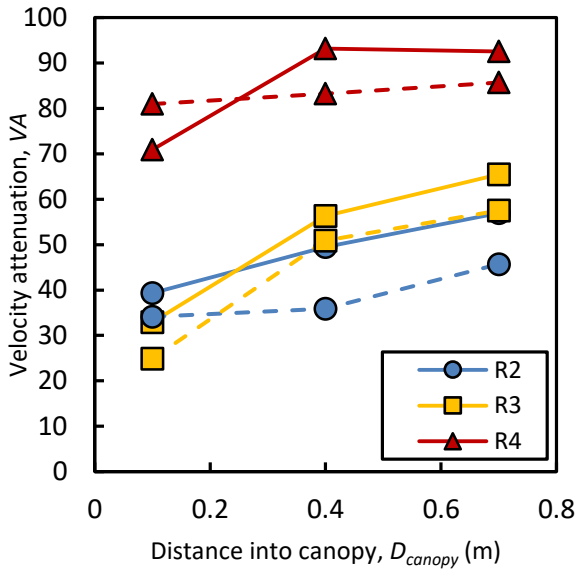

Figure 5.14: Velocity attenuation coefficient by *Zostera noltii* canopy with increasing distance into the canopy. R2, R3 and R4 represent 500 (late winter), 1000 (early spring and late autumn) and 4000 (summer) shoot density/m^2, respectively. Solid line and dashed line refer to tests at 0.1 m s^{-1} and 0.2 m s^{-1} free stream velocity, respectively.

5.3.1.1 Roughness length and bed shear stress

There are several methods used to estimate shear stress from measured instantaneous current velocities. In this section, bed shear stress (τ_0), roughness length (z_0) and friction velocity (U^*), values were calculated using law of the wall from velocity profiles measured upstream and above the canopy (Table 5.5). Velocity profiles within and downstream of the canopy departed from the classical log profile, therefore the law of the wall could not be applied. Shear stress ranged from 0.01 to 1.16 Pa. Shear stress was found to be higher above the canopy than at the upstream position and increased with distance into the canopy. Roughness lengths in the upstream of the canopy were small (0.0001 - 0.0265 mm), relative to roughness length above the canopy (0.0004 – 14.2086 mm). Roughness length increases by at least two-fold from the upstream of the canopy. Friction velocity ranged from 0.003 – 0.034 m s^{-1}. Friction velocity shows an increasing

trend with increasing distance into the canopy. Within vegetated beds, bed shear stress values were at least twice as high as in the unvegetated bed. The values show a similar increase with higher LAI value and distance into the canopy.

Table 5.5: Summary of R^2, z_0, U* and τ_0 calculated by fitting profiles upstream and above the canopy to the Law of the Wall.

Profile	Distance from leading edge	R^2	z_0 (mm)	U* (m s^{-1})	τ_0 (Pa)
Run 1: Unvegetated bed, 0.1 m s^{-1}					
P1	-0.65	0.96	0.0575	0.0050	0.03
P2	0.15	0.88	0.0573	0.0053	0.03
P3	0.5	0.85	0.0021	0.0037	0.01
P4	0.85	0.97	0.0029	0.0040	0.02
Run 2: Unvegetated bed, 0.2 m s^{-1}					
P1	-0.65	0.84	0.0147	0.008	0.06
P2	0.15	0.87	0.0016	0.006	0.04
P3	0.5	0.80	0.0108	0.008	0.07
P4	0.85	0.93	0.0030	0.007	0.05
Run 3: LAI: 0.12, 500 shoots m^{-2}, 0.1 m s^{-1}					
P1	-0.65	0.87	0.0007	0.003	0.01
P2	0.15	0.78	0.0107	0.004	0.02
P3	0.5	0.94	0.0712	0.011	0.03
P4	0.85	0.89	1.2604	0.011	0.07
Run 4: LAI: 0.12, 500 shoots m^{-2}, 0.2 m s^{-1}					
P1	-0.65	0.53	0.0001	0.005	0.02
P2	0.15	0.71	0.0412	0.009	0.09
P3	0.5	0.84	0.1449	0.011	0.13
P4	0.85	0.87	1.0677	0.016	0.26
Run 5: LAI: 0.24, 1000 shoots m^{-2}, 0.1 m s^{-1}					
P1	-0.65	0.93	0.0025	0.004	0.01
P2	0.15	0.87	0.0670	0.005	0.03
P3	0.5	0.87	0.2636	0.007	0.05
P4	0.85	0.80	1.9821	0.010	0.10
Run 6: LAI: 0.24, 1000 shoots m^{-2}, 0.2 m s^{-1}					
P1	-0.65	0.85	0.0073	0.007	0.05
P2	0.15	0.88	0.1671	0.011	0.13
P3	0.5	0.85	0.5345	0.014	0.19
P4	0.85	0.91	0.4217	0.016	0.27
Run 7: LAI: 0.96, 4000 shoot m^{-2}, 0.1 m s^{-1}					
P1	-0.65	0.93	0.0004	0.003	0.01
P2	0.15	0.73	11.2291	0.015	0.23
P3	0.5	0.72	4.5393	0.013	0.17
P4	0.85	0.74	18.2441	0.021	0.44
Run 8: LAI: 0.96, 4000 shoots m^{-2}, 0.2 m s^{-1}					
P1	-0.65	0.83	0.0265	0.008	0.07
P2	0.15	0.91	1.3292	0.017	0.29
P3	0.5	0.96	9.6348	0.030	0.92
P4	0.85	0.74	14.2086	0.034	1.16

5.3.2 Sediment movement upstream and within the canopy

Bed load transport rate was estimated from observed bed form migration (i.e. ripples). Ripple migration measurements were taken at three positions, M1, M2 and M3, upstream of the canopy (Figure 5.7, x: -0.5 m, -0.25 m and 0 m, respectively). The volumetric bed load transport rate, Q_b was calculated as follows:

$$Q_b = \frac{1}{2} hLV_{mig} \tag{5.18}$$

Where h and L are the height and length of a ripple, respectively. V_{mig} is the ripple migration speed. The method assumes no sediment by-passing of the ripples which was confirmed by observation during the experiment.

Table 5.6 presents the overall results obtained from four runs with varied seagrass densities. The highest volume bed load transport rate was observed in the position furthest from the leading edge of the canopy, M1 (x: 1.5 m). The transport rate in this position slightly decrease with the increase of seagrass density except for the densest canopy where the bed load transport was found to be close to the bare bed. At M2, 1.75 m into the flume and 0.25 m from the leading edge of the canopy, the volume of bed load transport reduced by more than 30 % for all shoots densities. The lowest transport rate was measured directly at the leading edge of the canopy in M3 (x: 2.0 m). In general, the bed load transport rates showed an inverse relation with proximity to the seagrass canopy, regardless of the density (Figure 5.15). On the bare bed, after an hour, sediment had travelled 0.13 m into the seagrass canopy. The distance of sediment transported within the canopy reduced with increasing seagrass density from 0.11 m, 0.10 m and 0.06 m on tests R2, R3 and R4, respectively.

Table 5.6: Sand transport based on ripple migration and the sediment penetration rate into seagrass canopies.

Volumetric bed load transport rate, Q_b (g hr^{-1})				
Test	M1	M2	M3	Canopy penetration rate (m/hr)
R1	0.091	0.036	0.024	0.13
R2	0.055	0.021	0.015	0.11
R3	0.043	0.028	0.007	0.10
R4	0.070	0.044	0.013	0.06

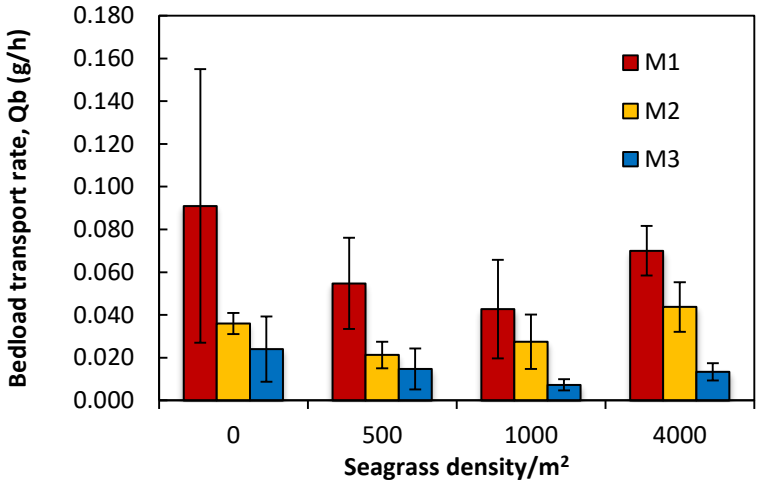

Figure 5.15: Volumetric bed load transport rate over bare, 500 (late winter), 1000 (early spring and late autumn) and 4000 (summer) shoots m^{-2} at 3 different positions (M1, red; M2; yellow; M3, blue) upstream of the canopy.

5.3.3 Flow structure within and around live *Zostera noltii* (An experiment in an annular flume).

The profiles of mean velocity, TKE and turbulence intensity recorded in the Lab Carousel are presented in this section (Figure 5.16, Figure 5.17 and Figure 5.18). These parameters were compared at three flow velocities for three different seagrass beds collected at different phases of its annual growth in Ryde, Isle of Wight. Vertical profiles over bare beds with shoots trimmed off but with complete with below-ground biomass left in place were also recorded to evaluate its influence on the flow structure. Velocity profiles were recorded at 5 positions, 1 upstream (P1, 0.4 m before the leading edge of the canopy), 3 positions within (P2 to P4, 0.1, 0.4 and 0.7 m from the leading edge) and 1 position downstream (P5), 0.3 m after the last *Zostera noltii* shoots. The patch length was 0.8 m for each run. The vertical ADV measurement positions started close to the bed (z = 0.005 m) up to the highest possible height where the ADV probe was not obstructing the paddle rotation (z = 0.11 m). The step size was set at 0.005 m near the bed (from 0.005 to 0.075 m) and at 0.01 m in the upper part of the profile (from 0.075 to 0.11 m). The areas where the ADV probe was placed to measure vertical profile velocity were clear from seagrass leaves. After each run, a few unattached leaves were removed, slightly reducing the number of shoots when the experiment started and the bed was re-flattened after each run at 0.3 m s^{-1}.

The velocity profile over unvegetated bed was characterised by a typical log profile with an approximately constant velocity throughout most of the water column and a slight decrease in velocity near the bed. In the vegetated bed runs, two zones were evident within the profiles: a within canopy zone characterised by low velocities and high turbulence and above it characterised by higher velocity and lower turbulence than upstream of the canopy. In the densest canopy tests, the flow was observed to have 2 boundary layers; one above the canopy and one within it.

The velocity profile was observed to be consistent for all shoot density at the first profile (P1), location upstream of the canopy, indicating no influence of the canopy. Current velocity measured over the vegetated beds showed strong velocity reduction within the *Zostera noltii* canopy compared to unvegetated bed, because flow was obstructed by the shoots. In the free stream zone above all vegetated beds, the average velocity was observed to increase relative to the average velocity over unvegetated bed in all tests. Canopy height was observed to decrease with increasing free-stream velocity and distance into the canopy. Depth averaged velocity along the first profile (P1) in all free-stream velocity tested was faster than the second profile (P2) with an exception for the sparse canopy. At the highest free stream velocity tested, an average velocity of 0.282 and 0.292 were recorded at P1 and 0.244, 0.255 m s^{-1} for tests A3 (LAI: 0.26) and A4 (LAI: 0.87). In test A2 (LAI: 0.16), depth-averaged velocity increased from 0.284 m s^{-1} at P1 to 0.290 m s^{-1} at P2 for an average free-stream velocity of 0.29 m s^{-1}. At free stream velocity of 0.1 m s^{-1}, depth averaged velocity at P2 to P4 were significantly lower than P1 as the canopy covers the entire vertical profile. Downstream of the canopy (P5) was characterised by an increase of depth-averaged velocity from the velocity within the canopy; however, this velocity was still lower than in P1. The flow accelerated once it exited the canopy section.

TKE and turbulence intensities were always larger inside the canopy as compared to unvegetated and bare beds. Highest TKE values were below the top of canopy for the densest canopy and closer to the bed in the sparse canopy. The TKE value decreased towards the bed below the peak value. The TKE values close to the bed were generally lower than values over the unvegetated bed. In the unvegetated and below-ground biomass test, the peak value was measured close to the bed.

Overall, results from the experiments using mimics were replicated when using natural plants. Acceleration of flow was observed above the canopy. Within the canopy, deceleration of flow and an increase of turbulence was observed. Differences between the shoot densities tested can be

seen in the TKE profiles. In the highest shoot density tested, the peak TKE was at the top half of the canopy height while it is much closer to the bed in a sparse canopy.

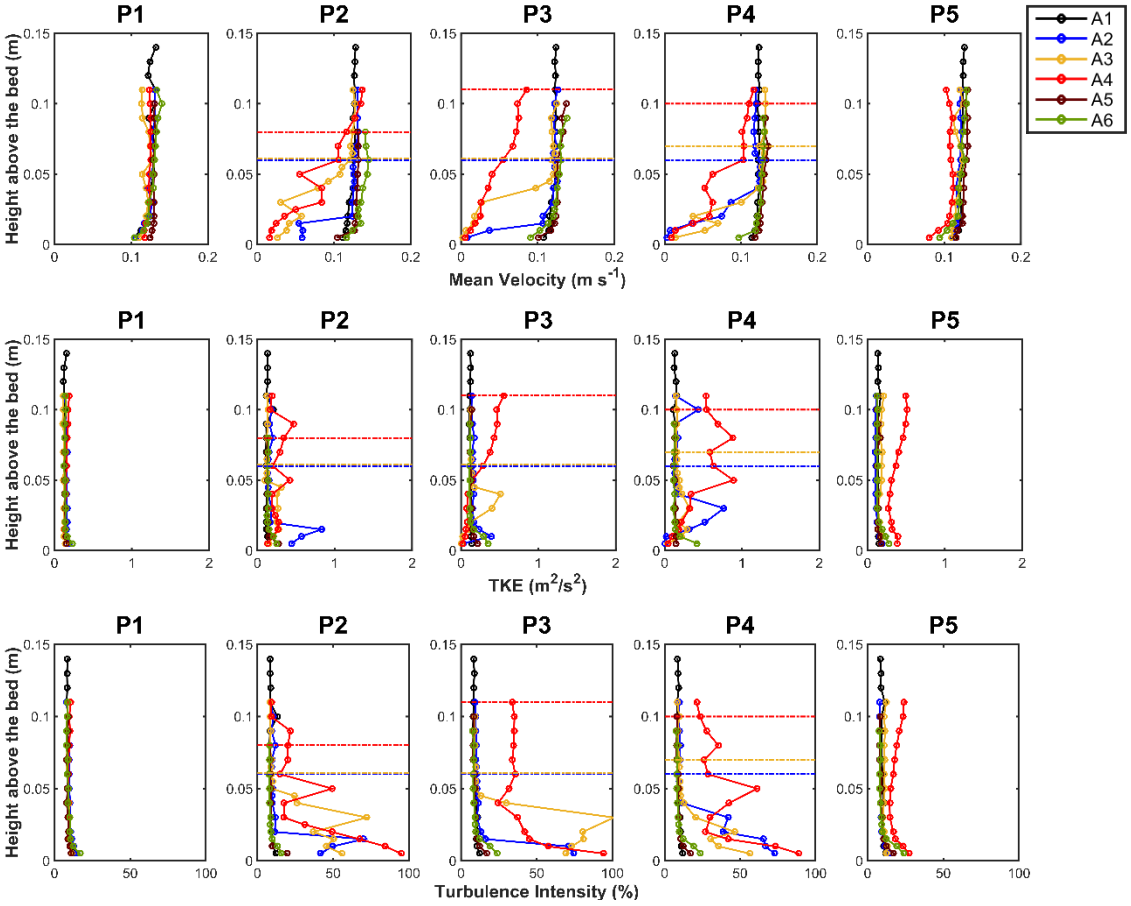

Figure 5.16: Mean velocity, TKE and turbulence intensity at different seagrass growth phase along 5 positions (P1 to P5) on bed at 0.1 m s^{-1}. A1, A2, A3 and A4 represent 0, 672 (late winter), 1100 (early spring and late autumn) and 2850 (summer) shoot density/m^2, respectively. A5 and A6 represent below-ground biomass only of 1100 and 2850 shoot density/m^2, respectively. Dotted horizontal lines refer to the average canopy height of the tested density. Description of A1 – A6 can be found at Table 5.4.

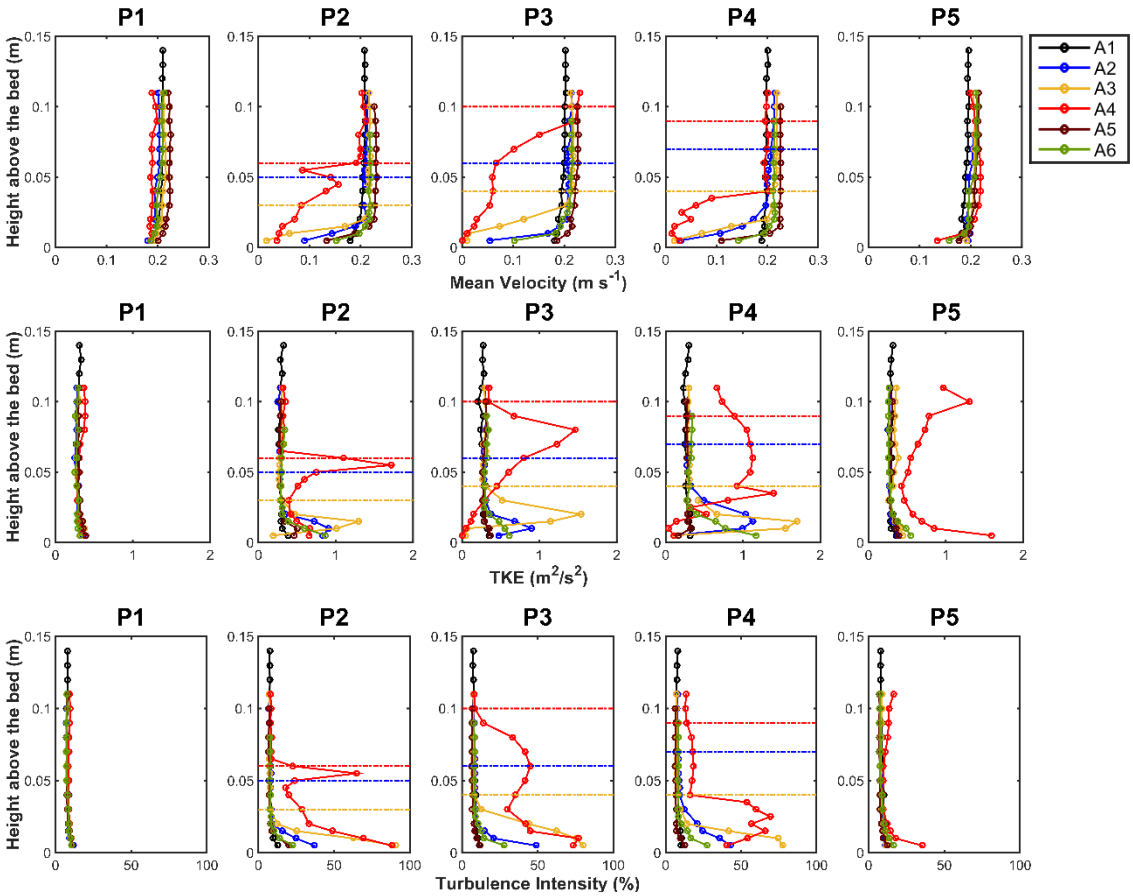

Figure 5.17: Mean velocity, TKE and turbulence intensity at different seagrass growth phase along 5 positions (P1 to P5) on bed at 0.2 m s^{-1}. A1, A2, A3 and A4 represent 0, 672 (late winter), 1100 (early spring and late autumn) and 2850 (summer) shoot density/m^2, respectively. A5 and A6 represent below-ground biomass only of 1100 and 2850 shoot density/m^2, respectively. Dotted horizontal lines refer to the average canopy height of the tested density. Description of A1 – A6 can be found at Table 5.4.

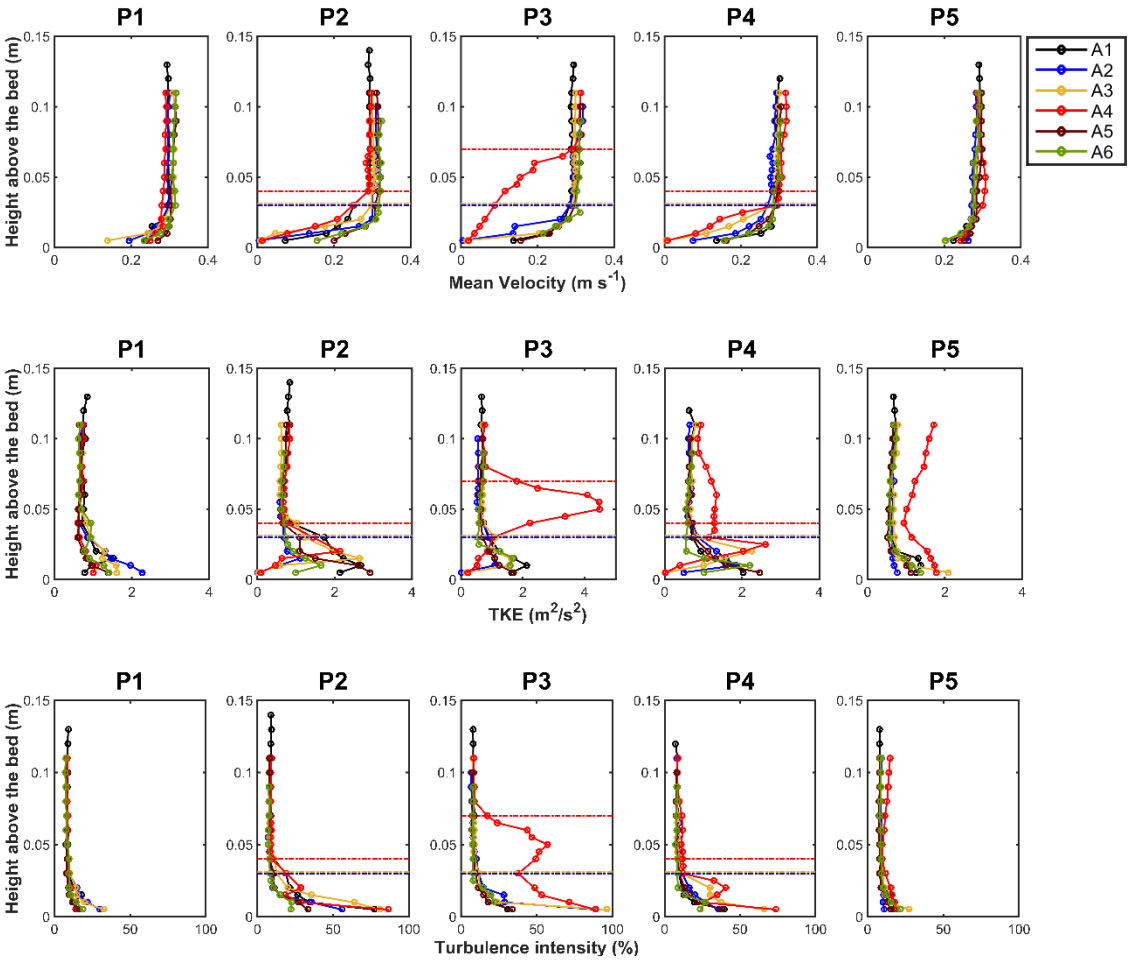

Figure 5.18: Mean velocity, TKE and turbulence intensity at different seagrass growth phase along 5 positions (P1 to P5) on bed at 0.3 m s^{-1}. A1, A2, A3 and A4 represent 0, 672 (late winter), 1100 (early spring and late autumn) and 2850 (summer) shoot density/m^2, respectively. A5 and A6 represent below-ground biomass only of 1100 and 2850 shoot density/m^2, respectively. Dotted horizontal lines refer to the average canopy height of the tested density. Description of A1 – A6 can be found at Table 5.4.

Figure 5.19 presents the velocity attenuation coefficients within *Zostera noltii* canopy. Velocity attenuation coefficients (Equation 5.17) within the canopy were highest in test A4 representing test with the highest LAI value of 0.87, ranged from 55 % to 78 % at all free-stream velocities. In the lower LAI value tests, (A2, LAI: 0.16 and A3, LAI: 0.26), VA ranged from 16 % to 55 %. VA increases with distance into the canopy in test A2 and A3 with an exception of A3 at 0.1 m s^{-1} where VA coefficient dropped. Meanwhile in the test with highest LAI value, VA coefficient values continue to increase up to P2 but were noticed to decrease at P3.

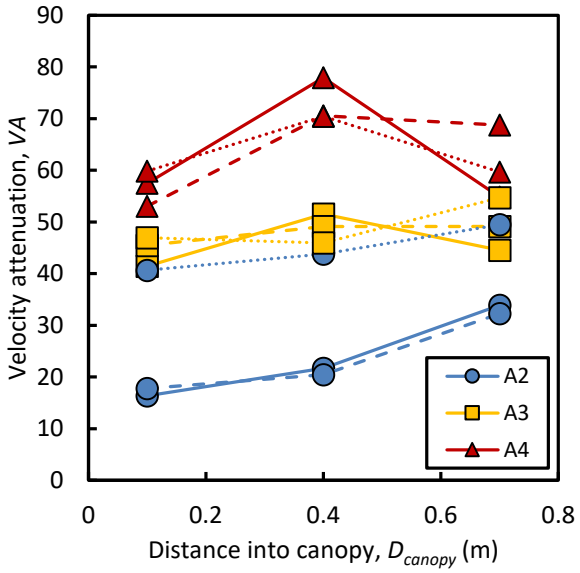

Figure 5.19: Velocity attenuation coefficient by *Zostera noltii* canopy with increasing distance into the canopy. Solid line, dashed line and dotted line refer to tests at 0.1 m s^{-1}, 0.2 m s^{-1} and 0.3 m s^{-1} free stream velocity, respectively. Description of A2 – A4 can be found at Table 5.4.

5.3.4 Sediment characteristics

Sediment used in the annular flume were clean sand collected in the area around the seagrass bed in Ryde, Isle of Wight. Grain-size distributions of the initial bed sediments were unimodal in all the tests, consisting of a narrow primary mode corresponding to fine sands (0.18 mm). The sediment bed with seagrass were observed to be anoxic, identified visually by dark-colouration, approximately 1 cm underneath the surface.

5.3.5 Sediment movement upstream, within and downstream of the canopy

Investigation on the effect of vegetation on bed load transport under steady unidirectional flow was carried out in the lab carousel. Bed load transport rate was estimated from the bed-form migration (i.e. ripples) computed using Equation 5.18. Sediment transport was not observed during the 0.1 and 0.2 m s^{-1} free-stream velocity runs. Ripples started forming at approximately 0.26 m s^{-1} and therefore for this experiment, ripple migration was recorded at free-stream velocity of 0.3 m s^{-1}. Ripple migration measurements were taken at five positions around the seagrass canopy, P1 (upstream), P2-P4 (within), P5 (downstream), similar to the vertical velocity profile measurements. Bed load transport rates were normalised to the upstream (P1) values in order to compare between different runs. The normalised rate is calculated as,

$$Q_{normalised} = \frac{Q_{Px}}{Q_{P1}} \cdot 100 \tag{5.19}$$

Where Q_{P1} is the bed load transport rate at P1, Q_{Px} is the bed load transport rate at the other profiles.

The results show that bed load sediment transport was highly influenced by the presence of vegetation. Bed load transport rate ranged from 0.001 to 1.278 g s^{-1} with the highest rate recorded in test A1 and the least in A4 (Figure 5.20). In test A1 (bare bed control), bed load transport rate was observed to be increasing or at least similar to the first profile. In all other runs, most of the transport was taking place in the upstream and downstream of the canopy. Within the vegetated beds, transport rate reduces significantly compared to the upstream of the canopy. The cumulative transport rate along the three profiles in the two densest vegetated beds and the densest below-ground biomass bed (A3, A4 and A6) were less than transport in the upstream at 0.271, 0.134 and 0.176 g s^{-1} compared to 0.274, 0.168 and 0.270 g s^{-1}, respectively. In tests A4 and A6, no transport was observed at P3 and P4. In the below-ground biomass only bed, the bed load transport rates in the downstream of the bare sediment with roots system are similar or reduced relative to the rates upstream.

Bed load transport rate normalised to the upstream profile (P1), shows that in a vegetated bed, most transport was taking place in the upstream and downstream of the canopy (Figure 5.21). Bed load transport rate reduced by almost 50% as the flow entered the canopy (P2) and

continued to reduce until the end of the canopy (P4). Bed load transport rate reduction within the canopy can be related to the reduction of bed shear stress calculated as 0.19 * TKE in the vegetated bed (Figure 5.22). Bed shear stresses within the canopy were reduced by at least approximately 50%. The average bed shear stress reduced with increasing shoot density from 0.35 Pa in the unvegetated bed (A1) to 0.17, 0.11 and 0.10 Pa in A2, A3 and A4, respectively.

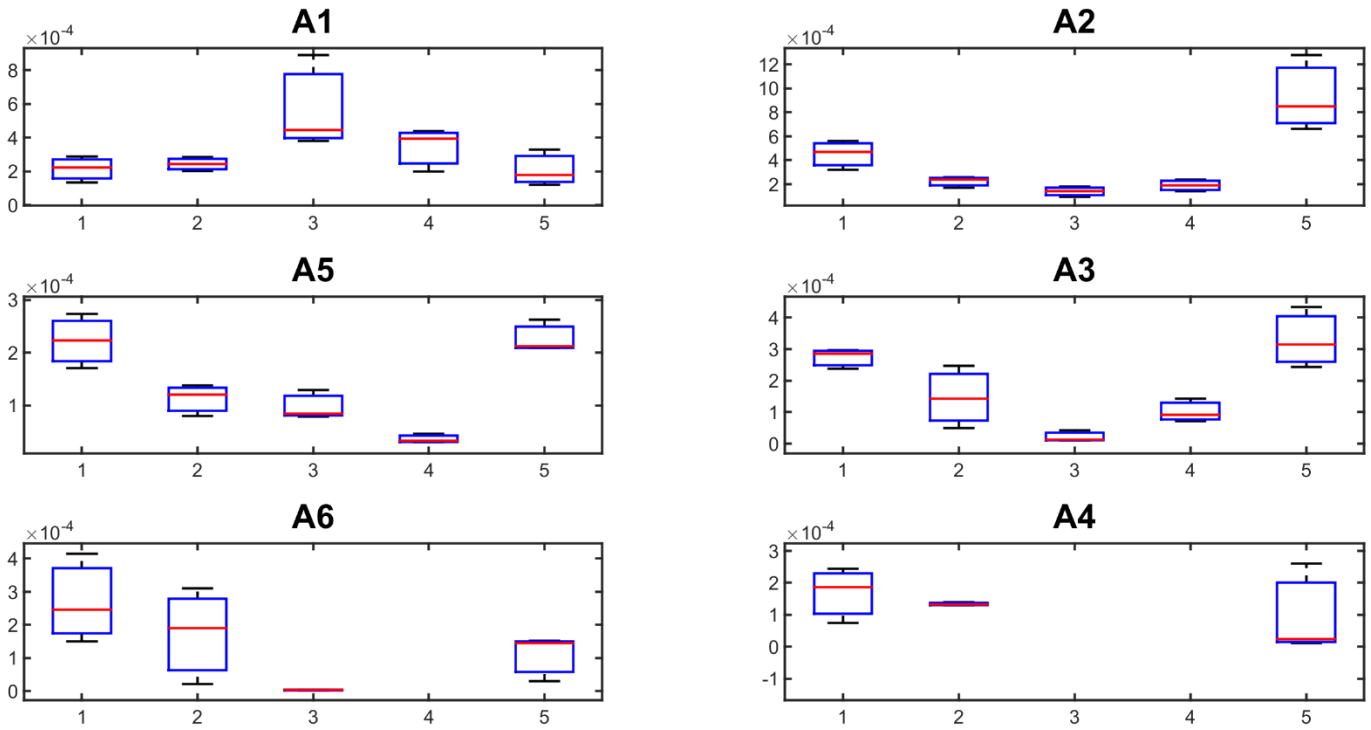

Figure 5.20: Boxplots showing the sediment bed load transport rate at 5 profiles across the lab carousel, profiles 2 – 4 covered by *Zostera noltii* canopy. A1 is the control bed (bare). A2, A3 and A4 represent 672 (late winter), 1100 (early spring and late autumn) and 2850 (summer) shoot density/m², respectively. A5 and A6 represent below-ground biomass only of 1100 and 2850 shoot density/m², respectively. Note that the vertical axes are different on each plot.

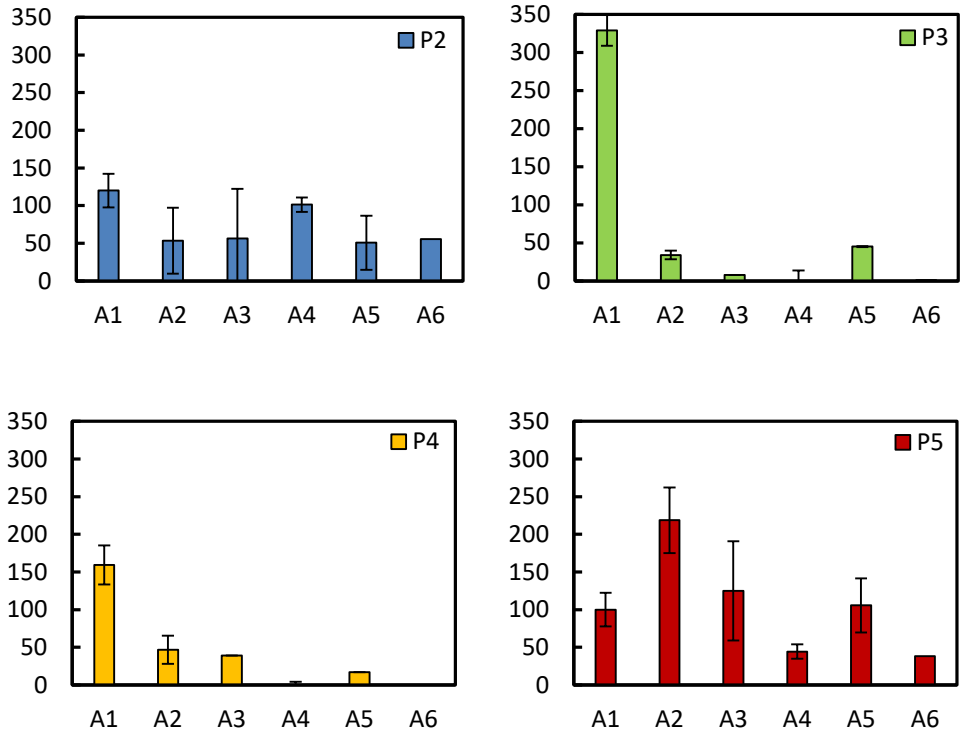

Figure 5.21: Normalised bed load transport rate on bare bed (A1) vegetated beds (A2 – A4) and beds with below-ground biomass only (A5-A6). P2 – P5 refer to positions along the flume (Figure 5.10).

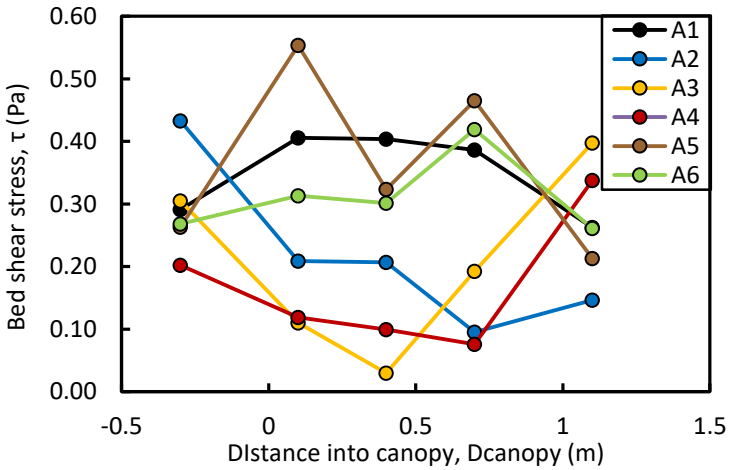

Figure 5.22: Bed shear stress calculated in all tests at 0.3 m s^{-1} free stream velocity. Canopy starts from 0 to 0.8 m. Description of A1 – A6 can be found at Table 5.4.

5.4 Discussion

5.4.1 Flow structure with *Zostera noltii* canopy

The effect of seagrass on the flow was investigated using both mimics and natural *Zostera noltii* in a laboratory study. The results showed that *Zostera noltii* above-ground biomass strongly influence the benthic boundary layer dynamics by altering the velocity, turbulence and bed shear stress. Subsequently it affects the transport of sediment as the leading canopy edge reduces bed load movement into the canopy. The reduction of flow within the canopy was observed in all tests, however, it varied with the stages of the plant seasonal growth. *Zostera noltii* canopies responds to its surrounding by deflecting the flow as the canopy height decreased with increasing free stream velocity (Figure 5.23).

Results from both sets of experiments in the recirculating and annular flumes showed that the water column can be divided into two or three layers depending on the density of the canopy, comparable to zones found in a flow associated with *Zostera marina* canopies (Gambi et al., 1990; Lefebvre et al., 2010). In a dense canopy, there is (1) an above canopy region, where current velocity was equal to or greater than the velocity upstream of the canopy, and turbulence intensities and TKE are low; (2) a transition region; a high stress region at the canopy/ water interface, where current velocity increased, turbulence intensities decreased but TKE was high and (3) the inner canopy region associated with low and relatively constant current velocity, high turbulence intensities and moderately high but decreasing TKE. In a sparse canopy, there is a similar above canopy region with high current velocity, low turbulence and low TKE. The transition region however disappears as the high stress region and peak TKE is at the inner canopy region. The differences between dense and sparse canopy has been highlighted by Nepf (2012) who found that in a dense canopy, the canopy drag is larger than the bed shear stress.

These experiments show that the influence of seagrass on near-bed hydrodynamics increases with an increase of canopy density and with distance from the leading edge of the seagrass canopy. Velocity profiles described in this study have a similar trend to other studies investigating flow structure around *Zostera noltii* canopies (Ganthy et al., 2015) and other *Zostera* species (Fonseca et al., 1982; Gambi et al., 1990; Lefebvre et al., 2010). Velocities were found to be relatively constant within the canopy or slightly increasing from the bed to the top of the canopy. The enhanced TKE observed at the canopy/water interface suggests that large-scale oscillations develop at the canopy surface. These oscillations are related to the canopy wave motion known as monami (Ackerman & Okubo, 1993; Nepf, 2012) that was observed during the experiments. Large-frequency turbulence is then broken down within the canopy and becomes even smaller near the bed. In the region just above the canopy,

turbulence intensity increases with distance into the seagrass indicating patch length influences the flow. Peak turbulence was above the densest canopy and within it for less dense canopies. This is caused by the reduction of porosity within the denser canopy causing deflection of the flow (Ganthy et al., 2015). There is less bending of leaves in the denser canopy due to increased contact between the leaves.

Higher stress was observed on the bare beds compared to the vegetated beds, indicating that higher canopy densities enhance protection against erosion (Neumeier & Amos, 2006). The presence of the skimming flow above the canopy increase the bed protection against erosion (Ganthy et al., 2015).

Whilst Paul & Amos (2011) suggested that there is a minimum shoot density required for the meadow to attenuate wave energy, flow velocity reduction was observed even at the lowest seagrass density tested, although small (approximately 20%)(Figure 5.23). The increase of LAI leads to the increase in velocity attenuation (Figure 5.19). The configuration of the seagrass also plays an important role in influencing the flow modification. In the experiment using the seagrass mimics, the shoots were arranged at an approximately regular distance along the 1 metre patch. In their natural state, *Zostera noltii* configuration is less uniform and very patchy.

My study did not take into account orbital velocity as the study on the effect of *Zostera noltii* on waves has been carried out previously by Paul (2011) in the same location. Waves has been reported as greatly affected by the presence of vegetation especially for short-period waves with smaller wave heights (Lara et al., 2016; Paul & Amos, 2011). During storm events, the wave damping capabilities of vegetation reduces. However, they still provide local shelter by reducing the orbital velocities close to the bed (Manca et al., 2012). In a natural environment, both waves and currents affect the flow. Attenuation by vegetation is more efficient when current is acting in the opposing direction to wave propagation as compared to when it is acting in the same direction. However, it is proven that even with the decline of the above-ground biomass during winter time, below-ground biomass was able to reduce local sediment transport.

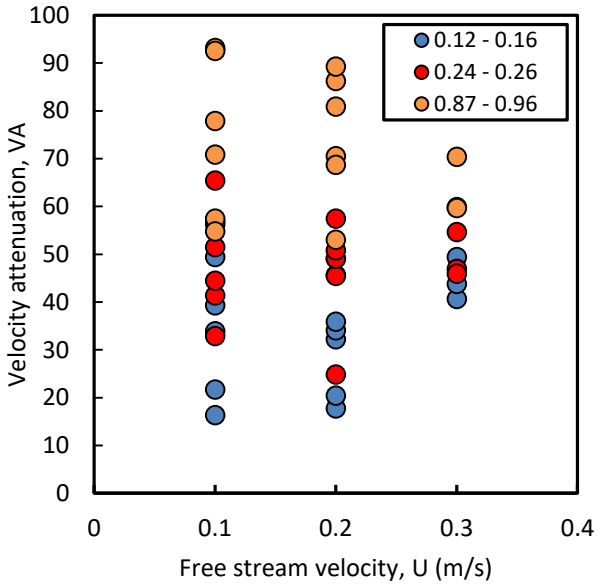

Figure 5.23: Relation between the attenuation of velocity inside the canopy and the depth-averaged velocity (U) for different seagrass LAI values.

5.4.2 Sediment movement

The use of sampled *Zostera noltii* complete with intact sediment beds enabled the assessment of the effect of the natural seagrass bed condition and the binding effects of below-ground biomass on sediment stabilisation. Bed load transport is caused by applied bed-shear stress. Sediment mobilisation starts when the bed shear stress is above a critical value at the threshold of motion. In an unvegetated bed, the critical shear stress follows the Shields criterion where the applied bed-shear stress is usually calculated from a relationship derived from the balance of shear force at the bed and the downslope weight component of the flow. In a vegetated bed, both the above-ground and the below-ground biomass play a role in reducing sediment transport by reducing the bed-shear stress and increasing soil cohesion.

5.4.2.1 Sediment transport into a seagrass meadow

In my study, sediment was placed in the upstream region of the canopy and a free stream velocity of 0.25 m s^{-1} applied. Sediment movement was observed as migrating sand ripples. Ripple migration was measured at positions -0.5 m (M1), -0.25 m (M2) and at the leading edge of the canopy (M3) into the flume. In general, bed load transport rate shows a closer relation to position in the flume rather than density of the canopy. A reduction in bed load transport rate was observed closer to the leading edge of the meadow. This is due to the flow sheltering caused by the formation of larger ripples in the upstream (Baas, 1999). The movement of sediment in the upstream of the canopy was observed to be unrelated to the density of the meadow. This agrees with the flow structure in P1 (Figure 5.12 and Figure 5.13) that shows low and consistent TKE for all shoot densities tested. On the other hand,

sediment moved into the meadow was found to be influenced by the canopy LAI value. Longer, larger and denser leaves were more efficient in obstructing the transport of sediment along the bed and are more likely to produce deposition within and behind the vegetation patch (Le Bouteiller & Venditti, 2014). Seasonal growth of *Zostera noltii* suggests that its ability to reduce sediment movement into the meadow decreases as the LAI value reduces however the persistence of below-ground biomass during winter slows down sediment transport along the bed as shown in the experiment with natural seagrass (Figure 5.21).

5.4.2.2 Bed-load transport through submerged seagrass canopy

In the presence of vegetation, quantifying the bed shear stress is challenging and predicting sediment transport from the bed shear stress can be misleading (Nepf, 2012). In a scarcely vegetated bed, the shear stress on the bed is higher than the shear stress of the canopy. While in a densely vegetated bed, the canopy acts as a macro roughness element where shear stress caused by the canopy is higher than the shear stress at the actual bed.

In my study, sediment movement on the bed was observed on the upstream, inside and downstream of the canopy at a typical free-stream velocity of 0.3 m s^{-1}. Although the work presented here confirms that sediment mobilisation occur within seagrass beds, the sediment movement rate is reduced by half as soon as it reaches the leading edge of the canopy. Bed load transport rates within the canopy were reduced significantly, up to no movement at all, in the highest canopy density tested. This is consistent with the lack of bed load transport reported in another flume experiment with *Zostera noltii* by Ganthy et al. (2015) where the lowest shoot density tested was 7960 shoots m^{-2}. The bed shear stress was observed to be lower in a sparsely vegetated bed compared to the unvegetated bed. In a densely vegetated bed, the shear stress reduced significantly leading to reduced sediment transport on the bed. Even though it is not specifically tested in my experiment, plant characteristics such as the frontal area and flexilibity are believed to play important roles in influencing the sediment transport.

In order to investigate the influence of below-ground biomass in stabilising or destabilising the sediment, above-ground biomass was removed, leaving the below-ground biomass intact. It should be noted that there were incidents of tubeworms surfacing from the subsurface during the experiment. In a below-ground biomass only bed, the bed was observed to be very stable with a significant reduction of bed load transport within the bed where the section of below-ground biomass exists compared to clean, unvegetated sand bed covering the rest of the flume. This shows that plant roots and rhizomes were efficient in reducing sediment movement on a sandy bed as compared to root-free bed. The fine roots and rhizomes of *Zostera noltii* may increase soil cohesion and attach to shell fragments. Consequently, the

reduced or lack of bed load transport within below-ground biomass beds suggests that long-term intertidal flat evolution is more influenced by the below-ground biomass than the above-ground biomass which is the first order of defense against bed load sediment transport.

In a natural *Zostera noltii* bed, surface roughness is enhanced by particles trapped within the canopy and other organisms associated with the habitat (Folkard & Bouma, 2016) and may further reduce the transport of sediment. However, my experiment does not take into account the sediment transport in the form of suspension that is often reported in a vegetated bed due to the increased turbulence levels lifting finer sediment into suspension (Ganthy et al., 2015).

5.4.3 Limitations of the experimental setup

Laboratory experiments using flumes presents some constraints due to the flume design. Flow around submerged vegetation is deflected and accelerated around the vegetation. In the lab carousel, the flow was generated from the top by eight paddles fixed on a rotating lid. High turbulence was found at this area. Measurements were taken at least 19 cm below the water surface. The flow was also found to be faster closer to the outer wall of the flume and slower closer to the inner wall. This produced variable canopy height across the vegetation. Leaves closer to the outer wall of the flume were bent more acutely. This phenomena influences the sediment transport as well. Larger ripples were observed to form closer to the outer wall when compared to the inner wall. In order to address this issue, ripple dimensions in the middle of the flume were measured instead. On the other hand, the use of the Lab Carousel allows experiments using live seagrass complete with its root-sediment system in seawater. There are also no entrance and exit condition of the flow as experienced in a recirculating flume.

In the recirculating flume, the exit condition was influenced by the weir which creates an obstacle to the flow. Furthermore, the flume is not rated for seawater use, and thus did not allow the use of live seagrass plants for the experiment. On the other hand, instantaneous velocities can be measured above the canopy as well as within it, allowing the application of the Law of the Wall and the estimation of roughness lengths and shear velocities above the canopy.

The measurements of instantaneous current velocities were taken using an intrusive technique. In this study, the use of an ADV means that a probe was inserted into the flume thus affecting the ambient flow. In order to enable the acoustical measurement of the flow velocity, vegetation underneath the ADV probe had to be trimmed therefore creating an

artificial gap within the canopy. The increase in canopy bending during the higher free stream velocity runs meaning further trimming was needed for the vegetation, reducing the canopy density. Flow velocity measurements were recorded 5 cm below the instrument probe which reduces the effect of flow disturbance on the measurement volume itself.

Calculation of bed load transport rate through ripple migration provides a good estimate of sediment transport within the seagrass. However, the measurements of the ripples in the Lab Carousel can only be taken after paddles forcing the flow were stopped resulting in some slight movement of sediment while the flow is slowing down. The recirculating flume available in NOCS was not designed for sediment movement studies, therefore only the upstream of the canopy was filled with sediment for ripple migration measurements.

The use of both living seagrass plants and artificial mimics presents different challenges. Mimics had the advantage of a more uniform canopy that does not deteriorate with time. However reproducing living plant flexibility and morphology with mimics are difficult (Fonseca & Koehl, 2006). Live plants comprise of a more varied leaf lengths according to the season they were collected. Furthermore, the plant health may decline after a few days and repeated runs in the flume as observed in other flume experiments using live plants (Möller et al., 2014). A loss of biomass was also recorded due to leaf trimming and decay.

5.5 Conclusions

Laboratory-based experiments were conducted in a straight recirculating flume using *Zostera noltii* mimics and in annular flume using canopy transplanted from their natural bed in densities reflecting four different stages of their seasonal growth cycle. A mobile sand layer was used on the upstream of the canopy in the former experiment while the latter consist of mobile layer over the entire bed. These experiments aimed to investigate the influence of *Zostera noltii* canopies on hydrodynamics and sediment mobilisation, with emphasis on flow structure upstream, within and downstream of canopies of different densities. These experiments quantified the impact of seagrass development on unidirectional flow, bed load sediment transport and the bed stability of intertidal areas. Several conclusions can be drawn from this work.

Current flow is affected by the presence of *Zostera noltii* canopy. The affect varies seasonally according to the growth cycle of the canopy. The seasonality of *Zostera noltii* means most of the above-ground biomass die in winter thus providing the bed less protection against the hydrodynamic forcing. Shoot density was found to accentuate flow reduction, increase turbulence in the outer canopy and reduce it in the inner canopy. Higher shoot density and

flow velocity results in greater velocity attenuation. It is found that velocity attenuation is more dependent on seagrass characteristics rather than the hydrodynamics.

Above the canopy, depending on the density, flow was generally found to follow a logarithmic profile. Friction velocity increased with increasing distance into the canopy and free-stream velocity. Roughness length was higher above the canopy than over bare sand. It also increased with increasing distance from the leading edge of the canopy and vary with shoot density.

Either two or three layers can be distinguished within the water column depending on the density of the canopy. In a dense canopy, the first region is above the canopy where the flow velocity is equal or higher than the free stream velocity and the turbulence is low. Second region is the transitional region where the turbulence is increasing but the stress did not change too much. In the third region, the high stress region where the flow and turbulence increased as compared to before it reaches the canopy. Whereas in a sparse canopy, there are only two layers present; one above the canopy characterised by an accelerating flow, faster than before it reaches the canopy and low turbulence and TKE. The second region is the inner canopy, where the flow velocity was greatly reduced and turbulence and TKE were high.

Sediment transport is affected by the seagrass canopy in the upstream on a vegetated bed. The efficiency of sediment trapping by seagrass canopy at its leading edge was found to be dependent on the shoot density. Sediment movement was observed to reduce within the canopy with the increase of shoot density. Below-ground biomass were efficient in reducing erosion compared to root and rhizome free bed. Despite the reduction in seagrass canopy influence on the hydrodynamic forcing, the persistent presence of below-ground biomass all year round reduces sediment transport hence providing stability to the bed

Chapter 6: General discussion and conclusions

In this concluding chapter I briefly summarise my main findings, before discussing in turn sediment transport at Ryde, spatial and temporal variation in profiles, the influence of *Zostera noltii* on unidirectional flow, sediment transport around the *Zostera* canopy, limitations and suggestions for further work. I then make some concluding remarks.

6.1 Summary of approach and findings

Seagrass studies in temperate coastal waters have been mostly carried out in France (Ganthy et al., 2015; Kombiadou et al., 2013; Laugier et al., 1999; Paquier et al., 2014) and the Wadden Sea of Netherlands or Germany (Bouma et al., 2009; Peralta et al., 2008; Widdows et al., 2008). In the UK, research on seagrass has been more limited. Lefebvre et al. (2010) studied the influence of seagrass canopies on unidirectional flow and sediment movement, however, it was carried out on a larger mainly subtidal eelgrass species, *Zostera marina*. Research on intertidal *Zostera noltii* at Ryde, Isle of Wight has been carried out, focusing solely on wave attenuation, but not including influences of seagrass on the transport of sediment (Paul & Amos, 2011). Therefore, my project was undertaken to fill the gap of knowledge on the evolution of the Ryde seagrass bed in general, to investigate sediment transport and quantify the effects of *Zostera noltii* on unidirectional flow resulting primarily from tidal currents and bed stability. This was achieved by quantifying sediment characteristics, surface elevation and seagrass parameters affecting sediment transport and current flow. Furthermore, my study highlighted the importance of below-ground biomass in reducing sediment transport thus suggesting its role in bed stabilisation all year round despite the reduction in above-ground biomass in the winter months.

The sediment characteristics (mean grain size, sorting, skew and kurtosis) and transport direction were investigated to understand the dynamics of Ryde intertidal flat mainly by the means of Grain Size Trend Analysis, a statistical model developed to determine sediment transport direction. The model is based on spatial distribution patterns of sediment characteristics (Chapter 3). The study site was visited monthly for two years to obtain sediment characteristics and information on seagrass size, density and cover. The sediment type present in the entirety of intertidal sand fiat of Ryde was fine, well sorted grained sand. However, the characteristics of sediment on the *Zostera noltii* seagrass beds can be differentiated from bare beds. Sediments on vegetated beds tend to be finer, poorer sorted and more positively fine-skewed than the sediments of unvegetated beds. The overall transport direction suggested by GSTA is towards west direction. A second direction of

transport towards east and south-east was derived by the model to the east of Ryde Pier. This finding is supported by the south-east longshore current suggested by SCOPAC (2012), creating a convergence zone forming a sand spit at Ryde East. *Zostera noltii* shows high seasonality with an increase of up to five-fold during peak distribution in summer. Normalised Difference Vegetation Index (NDVI) derived from satellite images was used to quantify seagrass coverage; this parameter proved effective for seagrass monitoring, revealing a 13.5 % growth of the seagrass bed from 2013 to 2016.

The combination of my medium-term two -year field study and analyses of past publically available data collected by the Channel Coastal Observatory (CCO) described in Chapter 4 showed the evolution of surface elevation on the vegetated and unvegetated area of the intertidal flat. *Zostera noltii* is capable of stabilising the bed by reducing current flow, decreasing bed load transport and preventing resuspension of sediment. The effect of *Zostera noltii* above and below-ground biomass on unidirectional flow was investigated in detail in a laboratory study (Chapter 5) where both mimics and natural seagrass were used to determine the effect of leaf length, shoot density as well as roots and rhizomes on benthic boundary layer under unidirectional and bed load transport. Overall, my work improves our knowledge of bed stabilisation and how seagrass, particularly *Zostera noltii* affects unidirectional flow and contributes to the understanding of sediment transport, mainly bed load transport on a vegetated bed.

6.2 Sediment transport at Ryde

Sediment transport patterns have been evaluated through GSTA and image analysis. The GSTA suggests that the general movement of sediment is a longshore transport in a westward direction. Analysis of LIDAR data and aerial photographs indicate that the spit formed in a north easterly direction. Tonks (2008) reported that the end of the spit had remained stable from 1975 to 1995, whereas the west side was growing further offshore. From the derived transport model, it can be seen that there is a sediment transport pathway that goes towards the east. This transport direction has a low reliability, but it could provide an explanation for the spit location and growth on this side.

According to the results from Grain Size Trend Analysis (GSTA) in Chapter 3, sediments on the sand bank on Ryde east is transporting to the west where the seagrass meadows are present. The westward transport of sediment may cause sediment burial on the seagrass meadow. As the transport of sediment is a natural event occurring on intertidal flats, this may allow the recovery and/or adaptation of seagrasses to burial. The extent of the effects of burial on seagrasses is species-specific and strongly size-dependent (Cabaço et al., 2008).

6.3 Variation in intertidal flat profiles

6.3.1 Spatial and temporal changes on intertidal flat profiles

The sand flat shape and size has evolved over the years, as well as the volume of sand on the sand flat. Changes in the sand volume that makes up the profiles can be seen to vary monthly, seasonally and among years. Modifications on the sand volumes also proved to be spatially variable. The majority of the erosion appears to take place over the winter months, as would be expected due to the storm waves and higher winds (Scott et al., 2016) causing more sediment movement (Boudet et al., 2017). The impact of seagrass on Ryde intertidal flat was quite easy to observe as the intertidal flat is almost fully covered by the seagrass meadows on the west side of Ryde Pier. On the east of the pier, seagrass meadow only covered the area closest to the pier. Over 14 years, Ryde West recorded less than -0.4 % change from the baseline survey in summer 2004. Two out of three transect lines in the showed insignificant erosion. The transect line with the most abundant seagrass showed continuous deposition during all seasons.

Ryde East can be divided into three sections depending on changes on the bed level. The first section is furthest west, closest to the pier with an accretion rate of approximately 2-3 cm per year suggesting this area as an accretion zone. Two transect lines in this section (IOW217 and RYD34) showed the biggest change from the baseline survey in autumn 2004, with accretion of 61.6 % and 14.2 %, respectively. The middle section showed an evolution rate of around -1 cm per year indicating erosion. As shown in Chapter 3, sediment distribution patterns indicate that transport of sediment on the sand flat occurs due to longshore currents in a north-west direction. A second longshore drift in a south-east direction was suggested in a study by SCOPAC (2012); however, this transport of sediment is believed to be going above Ryde West and converges with the opposing direction of transport at the sand spit on Ryde East (Tonks, 2008). My findings agree with the previous study by Tonks (2008) focusing on the east of Ryde Pier. The eastern most section recorded an accretion rate of approximately 0.3 cm per year. This part of the sand flat receives an active supply of sediment from the offshore to onshore transport as well as from erosion on the east-side of the Isle of Wight (SCOPAC, 2012).

6.3.2 Intertidal flat surface elevation regulation by seagrass

Seagrass, *Zostera noltii* affects hydrodynamic conditions, in addition to trapping sediment, reducing resuspension and raising the intertidal profile, thus directly contributing to coastal protection. Changes in surface elevation of vegetated intertidal flats are driven by superficial processes of sediment deposition and erosion (Hendriks et al., 2008), as well as subsurface

processes such as subsidence and root expansion (Christianen et al., 2013). Ganthy et al. (2013) reported that accretion rates in a *Zostera noltii* bed in Arcachon Bay, France ranged from 8 to 32 mm/year. In another *Zostera noltii* bed in Berre lagoon, France, accretion rates ranged from 10 to 30 mm/year (Paquier et al., 2014).

Long-term morphological monitoring of Ryde intertidal flat by Channel Coastal Observatory (CCO) provided a unique opportunity to assess the morphological influence of seagrass, *Zostera noltii* on the dynamics of the sand flat. The survey of intertidal seagrass habitat (Chapter 3) revealed that there was a huge overall coverage of *Zostera* in Ryde intertidal flat, with around 40 ha of *Zostera noltii.* The total area of the sand flat at Ryde is ~300 ha, thus seagrass covers approximately 13% of the shore. From these figures it could be assumed that seagrass play a significant role in coastal stability in the sand flat. In the vegetated bed of Ryde Sands, seagrasses are facilitating sediment surface elevation with an accretion rates ranging from 8 to 55 mm/year, greater than those found elsewhere cited above.

Evaluation of the topographic data discovered strong trends in sediment accretion during the seagrass meadow growth season. Further evidence is the good agreement between Cross-sectional Area (CSA) and density of seagrass meadows. Highest average CSA recorded was in summer corresponding to the peak seagrass biomass growth. The meadows lose most of their biomass in autumn, with lowest biomass recorded in winter months when the lowest average CSA was recorded. The increase in CSA indicates a net sediment deposition during the summer months due to the increased seagrass biomass and reduction in resuspension of the freshly deposited sediments. During the winter months, vegetated beds generally showed erosion however at a much lower rate compared to the un-vegetated areas of Ryde Sands.

In conclusion, surface elevation was regulated by seagrass by increasing deposition in the summer months through modification of the benthic boundary layer by the above-ground biomass. In the winter months, the bed resists erosion through increased cohesiveness of the bed due to the sediment binding provided by the below-ground biomass.

6.4 The effect of *Zostera noltii* on unidirectional flow

Plant morphology of seagrass of temperate or higher latitude coastal waters have shown variation between populations (Peralta et al., 2000). However the biggest factor affecting variation in leaf length, leaf width and shoot density is the seasonal changes (Auby & Labourg, 1996; Laugier et al., 1999; Philippart, 1995; Vermaat & Verhagen, 1996). Therefore it is important to understand how these seasonal changes affect current flow by seagrass over the annual cycle in order to predict sediment transport correctly. *Zostera noltii* shows large variation in above ground biomass throughout the year which can be observed in changing

shoot densities as well as leaf lengths. Previous studies (Fonseca and Cahalan, 1992; Bouma et al., 2005; Chen et al., 2007; Augustin et al., 2009; Prinos et al., 2010) showed that changes in shoot density and leaf length can affect wave attenuation by vegetation.

Beds of *Zostera noltii* at various shoot densities and current velocities were tested. Unidirectional flows were reduced by *Zostera noltii* bed (both natural and simulated with mimics) confirming previous findings cited above. At the highest current velocity tested, flow was fast enough for skimming flow to develop and the leaves will have reconfigured, forming a faster current layer above the bended seagrass leaves.

Measurements of various instantaneous velocity profiles in the laboratory revealed three layers that can be distinguished along the profiles (Figure 6.1): first layer within the canopy, with low and relatively constant current velocity, high turbulence and moderately high TKE; second layer at the canopy/water interface, where current velocity increased, turbulence decreased and TKE was high; and third layer above the canopy, where current velocity was equal or greater than upstream of the canopy, and turbulence and TKE were low. Depth-averaged flow velocity was seen to be reduced when entering the canopy and accelerated before exiting it, however the downstream velocity were still lower than the upstream. The enhanced TKE observed at the canopy/water interface suggests that large-scale oscillations at the canopy surface related to the waving of canopy leaves known as *monami* (Ackerman & Okubo, 1993; Nepf, 2012) that was observed during the experiments.

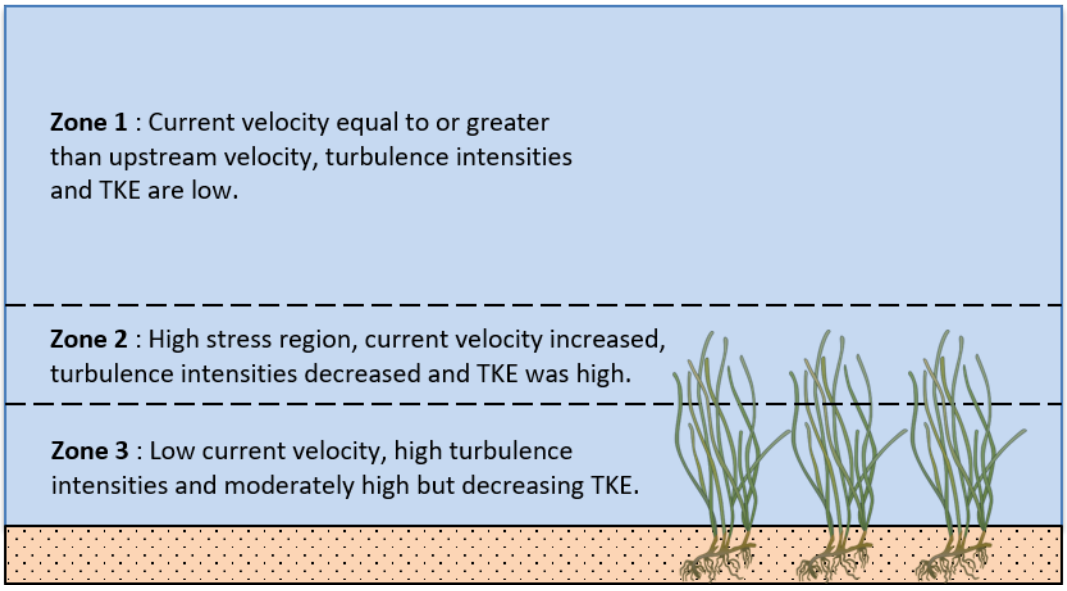

Figure 6.1: Different layers within the flow profile in the presence of *Zostera noltii.*

Sediment moved into the meadow was found to be influenced by the plant morphology. Longer, larger and denser leaves were more efficient in obstructing the transport of sediment along the bed and are more likely to produce deposition within and behind the vegetation patch (Le Bouteiller & Venditti, 2014). Seasonal growth of *Zostera noltii* suggests that its

ability to reduce sediment movement into the meadow decreases as the LAI value reduces. However, the persistence of below-ground biomass during winter slows down sediment transport along the bed as shown in the experiment with natural seagrass.

6.5 Sediment transport around seagrass canopy

My work presented here also confirms that sediment mobilisation occurs within seagrass beds. However, the sediment movement rate is reduced by half as soon as it reaches the leading edge of the canopy. Bed load transport rates within the canopy were reduced significantly, up to no movement at all, in the highest canopy density tested. This is consistent with the lack of bed load transport reported in another flume experiment with *Zostera noltii* by Ganthy et al. (2015). The bed shear stress was observed to be lower in a sparsely vegetated bed compared to the unvegetated bed. In a densely vegetated bed, the shear stress reduced significantly leading to reduced sediment transport on the bed. Even though it was not specifically tested in my experiments, plant characteristics such as the frontal area and flexilibity are believed to play important roles in influencing the flow, thus sediment transport (Nepf, 2012a).

The influence of below-ground biomass in stabilising or destabilising the sediment was also tested. The bed was observed to be very stable with a significant reduction of bed load transport within the bed where the section of below-ground biomass exists compared to clean, unvegetated sand bed suggesting that plant roots and rhizomes were efficient in reducing sediment movement by increasing soil cohesion (Vannoppen et al., 2017). Therefore, the reduced sediment transport within roots and rhizome strengthened beds suggests that the below-ground biomass influence on long-term vegetated intertidal flat evolution is as important as the above-ground biomass, if not bigger.

On a seasonal scale, the influence of *Zostera noltii* on sediment movement varied due to increased growth of the above-ground biomass as well as the below-ground biomass in the spring and summer period and their subsequent degeneration in autumn and winter (see Chapter 4). Experimental results showed that erosion was higher in bare beds than in vegetated beds, and that the development of both above and below-ground biomass promotes deposition and increased protection against erosion. Moreover, despite the significant reduction in the above-ground biomass in winter (the lowest shoot density were often measured in late winter and early spring), the seagrass leaves still provide a considerable protection to the seabed throughout the winter months. In the winter months, below-ground biomass is likely to play a more significant role as above-ground biomass decreases.

6.6 Limitation of works

The Grain Size Trend Analysis (GSTA) model used in this study represents the average transport pattern; but it does not identify transport mechanisms, transport events or changes in transport patterns due to storm events. This model also assumes that the likelihood of a particular grain size being transported is independent of any other grain transportation.

All flume-based experiments are constrained by design and operation of the flume itself. Experiments carried out in a straight recirculating flume often cite redirection of flow around the meadow caused by the flume walls despite plants occupying the entire width of the flume (Fonseca et al., 1982; Lefebvre et al., 2010). Gambi et al. (1990) reported deflection and acceleration of the flow around the canopy as constant flow is forced through the canopy between the flume walls. Furthermore, there are constraints created by entrance and exit condition in this type of flume. The use of the Lab Carousel solves this issue, allowing measurements to be taken upstream, within and downstream without these effect. It also allows the use of live *Zostera noltii* meadows in their natural bed sediments. However in the carousel, water movement was generated by paddles fixed on a rotating flume lid. This action causes high turbulence near the water surface. Therefore, measurement had to be taken 25 cm from the water surface.

Instruments used to measure instantaneous current velocities usually affect the flow being measured as they are positioned within the water column. In this study, the use of ADV means vegetation had to be cut around its sensor head to enable acoustical measurement of flow velocity creating artificial gaps in the vegetation around the ADV head.

Finally, as the seagrass, *Zostera noltii* is listed as Least Concern under the IUCN Red List of Threatened Species, only limited amount of samples were allowed to be collected by the authorities therefore limiting the scope of the study. Limited duration of survey was supplemented by CCO data analysed to provide understanding of longer-term changes on Ryde Sands.

6.7 Future work

My study helped to better estimate of the directions of sediment transport and seagrass distribution over Ryde intertidal flat as well as flow structure and sediment movement within and around *Zostera noltii* beds. However, further research is needed to fully comprehend these processes. Key recommendations for future research are:

- Survey a larger area than just the sand flat itself. A larger area would allow more samples to be collected and provide more reliable transport vectors. Higher sampling

resolution would allow a better analysis of the spatial variability on the on the intertidal sand flat, which will improve the accuracy of the grain size trend analysis. Additionally, a larger study area especially on the west side of Ryde Pier would allow better understanding and verification of the north-east sediment transport direction suggested by SCOPAC, (2012). Furthermore, mineralogical analysis of sediments from Ryde and Sandown would allow the origin of the sand flat to be analysed and provided validation of the transport pathways in the area.

- Field measurements to validate the results observed in the flume. Turbulence structure within the canopy was found to differ in the flume and in the field and therefore additional research is needed to understand where the differences come from. A thorough investigation of the dominant currents speeds and directions around the sand bank and within the seagrass meadow. This would allow a better understanding of the influence of wave and tide driven currents, and could involve hydrodynamic field measurements and numerical modelling. It is also worth to examine the transport of both bed load and suspended sediment through direct measurement in the field.
- Measuring short-time fluctuations in sediment level, such as those occurring within hours or within tidal cycles during different stages of seagrass growth.
- More work should be done to understand the below ground biomass influence on the binding and increasing sediment strength and thus reducing sediment transport due to extensive root and rhizome network.
- In a flume study, a better characterization of how seagrass species characteristics (e.g. biomass, shoot density, stiffness or morphology) influence the dynamics involved in wave and current attenuation and sediment transport is required.
- Investigation on performance of seagrass versus artificial structures as coastal defence
- The effect of climate change on seagrass structure, functioning and how it will influence the bed morphology.
- Work on other services provided by seagrass meadows and ultimately driven by sediment characteristics, particularly influence of sediment profiles with depth on redox, remineralisation of nutrients and carbon sequestration.

6.8 Conclusions

A combination of two-year field survey and analysis of publically available data was conducted in Ryde intertidal flat. Surficial sediments and seagrass development characteristics were recorded monthly. Flume experiments were conducted using mimics

and boxes of *Zostera noltii* meadows in their natural bed sediments sampled at contrasting density from different areas of the intertidal flat. In the laboratory experiments conducted in an annular and a straight recirculating flume using live *Zostera noltii* plants, mimics and a mobile sand layer, the influence of *Zostera noltii* canopies on unidirectional flow and sediment mobilization was investigated, with emphasis on flow structure upstream, within and downstream of patches of different density

Several conclusions can be made from my study:

1. Ryde sand flat was found to be composed of fine sands. Finer sediments are found to the west of the sand flat and coarser sediment to the east. The short term effects of erosion and accretion are seen in the annual beach profile surveys. However the sand flat has been deemed to be stable over long time periods (2004 to 2017). Statistical parameters indicate clear sediment transport trends on Ryde West. Ryde East shows a more complex trend. The spit is accumulating to the north-west with sediment that is most likely originating from the west of Ryde.
2. GSTA along with the spatial distribution patterns and bed forms indicates transport on the central sand flat occurs due to longshore currents generated by waves travelling north-west. The reliability of these transport vectors varied depending on the closeness of the surrounding sample sites. The spit, however, is formed from a second longshore transport current generated by waves travelling south-east. Previous studies have indicated a convergence zone occurring on Ryde sand flat. From the results of my study, it would appear that the convergence zone, rather than being to the west of the pier, could be in a north-east direction along the edge of the sand flat to the end of the spit.
3. Either two or three layers can be distinguished within the water column depending on the density of the canopy. In a dense canopy, the first layer is above the canopy where the flow velocity is equal or higher than the free stream velocity and the turbulence is low. The second is a transitional layer where the turbulence is increasing but the stress did not change too much. In the third layer, the high stress region where the flow and turbulence increased as compared to before it reaches the canopy. Whereas in a sparse canopy, there are only two layers present; one above the canopy characterised by an accelerating flow, faster than before it reaches the canopy and low turbulence and TKE. The second layer is the inner canopy, where the flow velocity was greatly reduced and turbulence and TKE were high.
4. Sediment transport is affected by the seagrass canopy in the upstream on a vegetated bed as well as within it. The efficiency of sediment trapping by seagrass canopy at its leading edge was found to be dependent on the shoot density. Sediment movement

was observed to be reduced within the canopy with the increase of shoot density. The transport rate reduced by almost 50% as the flow enters the canopy and continues to reduce until the end of the canopy. In the downstream of the canopy, sediment movement increases. Below-ground biomass were efficient in reducing erosion compared to root and rhizome free bed. Despite the reduction in seagrass canopy influence on the hydrodynamic forcing, the persistent presence of below-ground biomass all year round reduces sediment transport hence providing stability to the bed.

Appendices

Appendix A Field data (spatial): sediment and seagrass

ID	Eastings	Northings	Elevation	'Mz'	sigma'	'SK1'	'Kg'	'D50'	Cover (%)	LOI (%)
1	459315.00	92983.99	1.53	2.43	0.20	-0.09	1.31	2.44	0	0.06
2	459204.63	93008.32	-0.23	2.15	0.22	0.01	1.12	2.14	0	0.22
3	459129.16	92941.85	0.28	2.27	0.18	-0.04	1.13	2.27	0	0.24
4	459056.55	92934.36	0.23	2.53	0.21	0.03	1.48	2.52	0	0.19
5	458989.45	92938.05	0.47	2.05	0.20	0.37	1.70	2.02	0	0.24
6	458922.34	92943.97	0.10	2.11	0.18	0.12	1.14	2.10	0	0.19
7	458855.97	92945.45	0.20	2.24	0.23	0.21	1.01	2.21	0	0.25
8	458786.12	92943.55	-0.06	2.28	0.19	0.01	1.17	2.28	0	0.22
9	458574.50	92995.67	-0.46	2.82	0.36	-0.25	0.88	2.88	0	0.42
10	458642.21	92999.77	-0.67	2.40	0.24	0.07	1.34	2.39	20	0.28
11	458709.92	93003.86	-0.30	2.36	0.20	0.15	1.39	2.35	8	0.26
12	458778.34	93007.97	-0.31	2.36	0.19	0.00	1.21	2.36	4	0.22
13	458846.75	93012.07	-0.28	2.34	0.17	0.08	1.24	2.33	0	0.30
14	458914.45	93017.28	-0.12	2.38	0.20	-0.07	1.31	2.38	0	0.26
15	458982.87	93021.39	-0.13	2.35	0.18	0.04	1.08	2.34	0	0.23
16	459051.29	93024.39	-0.12	2.33	0.18	0.02	1.10	2.33	0	0.26
17	459117.60	93027.36	-0.52	2.36	0.17	0.07	1.17	2.35	0	0.18
18	459186.73	93030.36	-0.52	2.50	0.23	0.04	1.43	2.49	0	0.26
19	459293.46	93078.27	-0.55	2.48	0.16	0.16	1.30	2.47	4	0.25
20	459289.17	93146.07	-0.71	2.54	0.19	0.17	1.41	2.52	12	0.27
21	459284.16	93213.85	-0.82	2.59	0.15	0.21	1.38	2.58	4	0.26
22	459280.55	93283.87	-0.99	2.52	0.17	0.20	1.48	2.51	4	0.36
23	459276.25	93351.66	-1.19	2.48	0.18	0.06	1.40	2.47	16	0.30
24	459271.93	93421.68	-1.40	2.51	0.22	0.13	1.36	2.49	12	0.29
25	459204.94	93416.47	-1.40	2.51	0.21	0.41	1.22	2.46	NaN	0.22
26	459204.98	93350.86	-1.25	2.47	0.15	0.14	1.25	2.45	16	0.22
27	459137.20	93353.43	-1.60	2.48	0.20	0.24	1.33	2.46	24	0.29
28	459070.14	93354.90	-1.63	2.43	0.25	0.01	1.35	2.43	32	0.14
29	459069.46	93290.39	-1.36	2.33	0.19	-0.08	1.14	2.34	0	0.22
30	459004.38	93304.11	-1.43	2.42	0.28	0.03	1.35	2.42	28	0.19
31	458939.29	93317.83	-1.51	2.26	0.30	-0.01	1.28	2.26	28	0.25
32	458930.83	93254.35	-1.61	2.45	0.26	0.16	1.53	2.43	28	0.23
33	458866.71	93245.84	-1.60	2.50	0.29	0.20	1.38	2.45	12	0.30
34	458803.22	93242.90	-1.61	2.43	0.45	0.06	1.20	2.39	0	0.28

35	458809.56	93181.81	-1.48	2.58	0.30	0.23	0.95	2.52	0	0.27
36	458745.40	93175.53	-1.35	2.71	0.26	0.06	0.97	2.70	0	0.29
37	458684.74	93172.62	-1.55	2.57	0.29	0.13	1.12	2.54	12	0.26
38	458699.54	93111.62	-1.14	2.91	0.30	-0.09	1.24	2.92	0	0.84
39	458636.75	93109.81	-1.63	2.65	0.26	-0.01	1.29	2.64	12	0.28
40	458573.99	93104.65	-1.63	2.54	0.26	0.09	1.02	2.53	32	0.28
41	458527.48	93035.18	-1.07	2.29	0.53	-0.29	1.36	2.38	0	0.37
42	458592.39	93037.02	-1.16	2.61	0.37	0.14	0.94	2.56	12	0.30
43	458658.70	93039.99	-1.29	2.34	0.26	-0.13	1.22	2.36	12	0.24
44	458723.61	93041.83	-0.44	2.35	0.20	-0.04	1.28	2.35	16	0.30
45	458787.82	93043.66	-0.50	2.35	0.19	0.17	1.23	2.34	8	0.28
46	458853.45	93044.40	-0.50	2.38	0.17	0.02	1.17	2.38	4	0.26
47	458919.07	93046.25	-0.57	2.38	0.17	0.06	1.12	2.37	4	0.25
48	458983.98	93048.09	-0.11	2.34	0.19	0.07	1.10	2.33	0	0.26
49	459048.90	93048.82	-0.15	2.38	0.16	-0.05	1.12	2.38	0	0.24
50	459047.45	93114.42	-0.45	2.45	0.19	-0.06	1.19	2.46	4	0.25
51	459045.99	93181.13	-0.81	2.43	0.17	0.18	1.17	2.42	12	0.33
52	458980.43	93174.83	-0.73	2.41	0.19	0.30	1.37	2.38	12	0.27
53	458975.51	93110.28	-0.39	2.39	0.16	0.08	1.15	2.39	8	0.21
54	458971.99	93046.85	-0.11	2.35	0.19	0.05	1.25	2.34	0	0.25
55	459261.99	93115.73	-0.64	2.47	0.18	0.17	1.24	2.45	16	0.25
56	459203.96	93129.53	-0.70	2.58	0.17	0.34	1.40	2.55	20	0.25
57	459140.32	93139.94	-0.61	2.41	0.14	0.14	1.11	2.41	16	0.23
58	459075.37	93142.54	-0.64	2.38	0.15	0.10	1.12	2.38	12	0.25
59	459076.06	93205.94	-0.87	2.34	0.16	0.09	1.13	2.34	16	0.25
60	459137.38	93213.30	-0.97	2.56	0.22	0.36	1.78	2.51	32	0.25
61	459200.77	93224.03	-0.93	2.43	0.15	0.15	1.17	2.42	20	0.30
62	459261.34	93234.72	-0.87	2.47	0.16	0.24	1.36	2.46	28	0.34
63	459321.95	93242.08	-0.93	2.51	0.14	0.13	1.17	2.50	0	0.24
64	459251.36	93305.78	-1.04	2.42	0.16	0.06	1.23	2.41	28	0.36
65	459252.07	93368.07	-1.21	2.48	0.19	0.23	1.35	2.46	68	0.33
66	459191.35	93370.72	-1.40	2.44	0.19	0.17	1.36	2.42	56	0.29
67	459128.55	93370.01	-1.65	2.42	0.21	0.10	1.27	2.41	4	0.28
68	459062.89	93372.61	-1.88	2.44	0.28	0.15	1.44	2.42	40	0.32
69	459061.50	93308.09	-1.58	2.58	0.27	0.28	1.35	2.52	52	0.65
70	459129.13	93318.86	-1.53	2.42	0.22	0.10	1.72	2.41	0	0.26
71	459193.28	93325.15	-1.15	2.64	0.28	0.42	1.11	2.55	80	0.35
72	459258.14	93330.33	-1.20	2.65	0.26	0.42	1.06	2.57	68	0.27
73	459263.84	93263.66	-0.94	2.62	0.24	0.44	1.21	2.55	32	0.34
74	459197.57	93257.36	-1.01	2.59	0.24	0.45	1.42	2.52	24	0.23

75	459131.97	93254.39	-1.20	2.53	0.22	0.30	1.59	2.50	44	0.24
76	459063.58	93249.17	-0.73	2.45	0.19	0.22	1.66	2.44	32	0.25
77	459063.64	93181.33	-0.81	2.34	0.12	-0.04	1.23	2.33	24	0.26
78	458995.93	93177.23	-0.73	2.38	0.18	0.26	1.54	2.35	44	0.32
79	458930.41	93166.49	-1.41	2.34	0.18	0.00	1.55	2.35	40	0.27
80	458859.20	93160.12	-1.28	2.13	0.16	-0.13	1.12	2.14	24	0.24
81	458789.39	93154.89	-1.20	2.57	0.32	-0.05	0.89	2.57	68	0.38
82	458792.14	93223.87	-1.60	2.58	0.38	0.17	0.84	2.53	4	0.54
83	458863.44	93222.45	-1.74	2.54	0.33	0.22	0.97	2.47	20	0.35
84	458935.41	93224.37	-1.42	2.41	0.20	0.35	1.42	2.38	8	0.32
85	459007.37	93226.30	-1.01	2.34	0.15	-0.11	1.37	2.34	48	0.23
86	459077.25	93225.97	-1.01	2.35	0.18	0.17	1.70	2.35	12	0.24
87	459063.07	93293.65	-1.45	2.43	0.19	0.20	1.40	2.41	76	0.29
88	459132.21	93295.54	-1.36	2.37	0.17	0.05	1.22	2.37	68	0.49
89	459202.06	93297.44	-1.06	2.41	0.20	0.38	1.69	2.38	72	0.29
90	459187.91	93362.90	-1.32	2.36	0.19	0.25	2.32	2.35	56	0.29
91	459257.05	93364.79	-1.25	2.52	0.25	0.57	1.83	2.42	84	0.29
92	459256.47	93291.38	-1.02	2.47	0.17	0.19	1.34	2.45	48	0.32
93	459262.24	93155.77	-0.75	2.52	0.24	0.40	1.47	2.45	8	0.25
94	459258.09	93085.66	-0.60	2.47	0.18	0.13	1.29	2.45	20	0.25
95	459257.36	93087.88	-0.58	2.46	0.16	0.12	1.25	2.45	12	0.27
96	459257.41	93083.43	-0.58	2.44	0.17	0.09	1.30	2.43	20	0.25
97	459260.21	93085.68	-0.58	2.44	0.17	0.09	1.26	2.43	4	0.26
98	459254.56	93085.62	-0.58	2.40	0.16	0.07	1.17	2.39	4	0.37
99	458749.00	93096.00	-1.10	2.53	0.18	0.11	1.20	2.52	16	0.21
100	458824.00	93096.00	-0.73	2.32	0.16	0.11	1.14	2.31	0	0.26
101	458899.00	93096.00	-0.63	2.29	0.17	0.08	1.17	2.28	0	0.24
102	459124.00	93096.00	-0.37	2.49	0.17	0.17	1.20	2.47	0	0.27
103	459420.84	92986.30	1.35	2.53	0.20	0.11	1.32	2.52	0	0.23
104	459421.23	93076.38	-0.50	2.68	0.20	0.20	1.13	2.65	16	0.33
105	459436.41	93168.86	-0.70	2.72	0.24	0.00	0.97	2.72	28	0.42
106	459432.55	93260.01	-0.90	2.79	0.21	0.09	1.08	2.78	24	0.41
107	459456.93	93350.37	-1.12	2.85	0.24	0.06	1.09	2.84	68	0.64
108	459464.32	93444.98	-1.57	2.48	0.18	0.20	1.37	2.46	8	0.26
109	459476.66	93538.54	-1.66	2.58	0.21	0.21	1.17	2.55	40	0.30
110	459571.98	93534.06	-1.58	2.56	0.20	0.17	1.29	2.54	8	0.29
111	459665.17	93530.67	-1.63	2.55	0.25	-0.07	1.38	2.54	24	0.33
112	459650.02	93621.70	-1.56	2.70	0.21	0.11	1.11	2.68	0	0.34
113	459738.03	93639.38	-1.68	2.60	0.21	0.06	1.22	2.58	0	0.40
114	459830.43	93642.66	-1.39	2.66	0.18	0.16	1.08	2.65	60	0.43

115	459910.68	93660.25	-1.11	2.50	0.17	0.05	1.04	2.50	0	0.24
116	460000.13	93674.62	-0.55	2.47	0.16	0.04	1.09	2.47	0	0.20
117	460091.69	93690.13	-0.77	2.43	0.16	0.04	1.08	2.43	0	0.22
118	460185.42	93701.21	-0.95	2.56	0.21	0.07	0.81	2.55	0	0.18
119	460187.21	93606.70	-0.96	2.49	0.16	0.08	1.17	2.49	0	0.19
120	460096.23	93602.32	-0.49	2.49	0.13	0.16	1.11	2.48	0	0.21
121	460007.59	93577.95	-0.58	2.46	0.14	0.17	1.04	2.45	0	0.20
122	459917.60	93549.12	-0.78	2.44	0.16	0.12	1.07	2.43	0	0.24
123	459823.81	93542.49	-0.89	2.62	0.18	0.09	1.16	2.61	0	0.30
124	459736.37	93537.04	-0.98	2.49	0.23	-0.05	1.22	2.49	8	0.26
125	459718.35	93446.76	-1.17	2.48	0.26	-0.02	1.29	2.48	16	0.27
126	459625.94	93443.48	-1.22	2.53	0.19	0.08	1.24	2.52	24	0.30
127	459535.77	93429.11	-1.32	2.73	0.25	0.05	0.97	2.71	40	0.38
128	459535.40	93337.91	-0.99	2.58	0.20	0.21	1.22	2.55	28	0.42
129	459611.22	93310.97	-1.24	2.53	0.24	0.13	1.30	2.51	20	0.30
130	459691.87	93294.09	-1.27	2.63	0.21	0.14	1.09	2.60	36	0.41
131	459778.85	93278.40	-1.28	2.65	0.20	0.07	1.28	2.64	52	0.42
132	459865.56	93286.06	-1.41	2.55	0.18	0.17	1.17	2.53	16	0.26
133	459955.10	93293.76	-1.22	2.45	0.14	0.11	1.13	2.44	0	0.22
134	460043.92	93302.56	-0.57	2.41	0.17	0.08	1.12	2.40	0	0.22
135	460134.98	93301.38	-0.67	2.40	0.16	0.08	1.16	2.38	0	0.22
136	460167.90	93384.05	-0.68	2.47	0.16	0.10	1.07	2.46	0	0.20
137	460077.40	93398.58	-0.68	2.38	0.20	0.05	1.19	2.37	0	0.21
138	459982.67	93413.07	-1.08	2.41	0.18	0.09	1.23	2.40	0	0.24
139	459890.77	93426.48	-0.88	2.52	0.15	0.24	1.10	2.50	20	0.28
140	459537.93	93054.35	-0.95	2.59	0.24	0.29	1.17	2.53	4	0.35
141	459631.78	93055.42	-0.59	2.51	0.21	0.12	1.25	2.50	8	0.31
142	459719.31	93054.19	-1.19	2.43	0.26	0.21	1.13	2.39	12	0.27
143	459811.27	93035.22	-1.21	2.49	0.21	0.10	1.25	2.47	0	0.22
144	459908.64	93037.44	0.12	2.48	0.19	-0.02	1.20	2.48	0	0.20
145	460006.74	93037.45	-0.15	2.46	0.14	0.08	1.19	2.45	0	0.23
146	460103.49	93031.88	-0.15	2.38	0.18	0.00	0.99	2.38	0	0.22
147	460195.35	93022.93	-0.20	2.31	0.24	-0.15	1.35	2.32	0	0.21
148	460289.37	93009.55	-0.28	2.42	0.21	-0.15	1.61	2.42	0	0.25
149	460274.96	92912.63	-0.33	2.47	0.14	0.11	1.14	2.47	0	0.25
150	460178.19	92919.30	-0.30	2.44	0.26	-0.22	1.69	2.46	0	0.25
151	460080.80	92918.18	0.10	2.41	0.23	-0.14	1.30	2.42	0	0.20
152	459983.43	92915.96	0.15	2.52	0.17	-0.05	1.28	2.52	0	0.20
153	459886.07	92912.62	0.30	2.51	0.19	0.03	1.32	2.50	0	0.27
154	459484.23	93307.31	-0.93	2.78	0.25	0.02	0.93	2.77	72	0.57

155	459345.40	93414.72	-1.43	2.55	0.20	0.24	1.26	2.52	68	0.27
156	459328.95	93433.44	-1.48	2.43	0.18	0.10	1.22	2.42	36	0.27
157	459348.75	93305.77	-0.99	2.55	0.21	0.36	1.14	2.50	76	0.32
158	459371.05	93144.77	-0.65	2.68	0.23	0.22	1.10	2.64	16	0.35
159	459394.02	93048.27	-0.51	2.60	0.24	0.16	1.26	2.58	16	0.30
160	459397.54	93049.42	-0.51	2.58	0.24	0.13	1.35	2.56	16	0.32
161	459393.28	93051.60	-0.51	2.59	0.20	0.17	1.21	2.57	0	0.31
162	459394.05	93046.05	-0.51	2.58	0.22	0.15	1.28	2.55	0	0.28
163	459391.20	93048.24	-0.51	2.61	0.23	0.14	1.22	2.58	4	0.32
164	460168.00	93146.00	-0.49	2.46	0.19	-0.02	1.35	2.45	0	0.21
165	460068.00	93146.00	-0.47	2.52	0.16	0.05	1.38	2.50	0	0.39
166	459968.00	93146.00	-0.70	2.47	0.16	0.02	1.35	2.46	0	0.19
167	459868.00	93146.00	-0.98	2.46	0.17	0.01	1.26	2.46	0	0.22
168	459768.00	93146.00	-1.18	2.60	0.22	0.18	1.18	2.57	0	0.32
169	459668.00	93146.00	-1.10	2.30	0.17	0.08	1.08	2.30	0	0.29
170	459568.00	93146.00	-1.05	2.50	0.18	-0.01	1.25	2.49	52	0.23

Appendix B Field data: seagrass attributes (temporal)

Date	Point ID	Eastings	Northings	Seagrass density (m^{-2})	LAI (m^2 m^{-2})
17/08/2015	S1	459287.5	93093.78	738	0.13
17/08/2015	S2	459272.6	93177.02	1380	0.24
17/08/2015	S3	459255.3	93268.02	1596	0.43
17/08/2015	S4	459237.9	93370.14	2250	0.81
01/09/2015	S1	459287.5	93093.78	1100	0.15
01/09/2015	S2	459272.6	93177.02	2004	0.40
01/09/2015	S3	459255.3	93268.02	1750	0.32
01/09/2015	S4	459237.9	93370.14	3150	1.34
12/10/2015	S1	459287.5	93093.78	760	0.13
12/10/2015	S2	459272.6	93177.02	1075	0.24
12/10/2015	S3	459255.3	93268.02	2175	0.75
12/10/2015	S4	459237.9	93370.14	1683	0.84
12/11/2015	S1	459287.5	93093.78	92	0.02
12/11/2015	S2	459272.6	93177.02	280	0.04
12/11/2015	S3	459255.3	93268.02	870	0.26
12/11/2015	S4	459237.9	93370.14	1300	0.59
10/12/2015	S1	459287.5	93093.78	106	0.02
10/12/2015	S2	459272.6	93177.02	272	0.04
10/12/2015	S3	459255.3	93268.02	560	0.10
10/12/2015	S4	459237.9	93370.14	1220	0.31
22/01/2015	S1	459287.5	93093.78	98	0.02
22/01/2015	S2	459272.6	93177.02	310	0.05
22/01/2015	S3	459255.3	93268.02	532	0.10
22/01/2015	S4	459237.9	93370.14	1130	0.28
09/02/2016	S1	459287.5	93093.78	146	0.02
09/02/2016	S2	459272.6	93177.02	308	0.06
09/02/2016	S3	459255.3	93268.02	620	0.12
09/02/2016	S4	459237.9	93370.14	1590	0.37
09/03/2016	S1	459287.5	93093.78	130	0.02
09/03/2016	S2	459272.6	93177.02	148	0.02
09/03/2016	S3	459255.3	93268.02	396	0.05
09/03/2016	S4	459237.9	93370.14	860	0.17
07/04/2016	S1	459287.5	93093.78	126	0.02
07/04/2016	S2	459272.6	93177.02	280	0.04
07/04/2016	S3	459255.3	93268.02	386	0.05
07/04/2016	S4	459237.9	93370.14	790	0.08
05/05/2016	S1	459287.5	93093.78	106	0.02
05/05/2016	S2	459272.6	93177.02	178	0.02
05/05/2016	S3	459255.3	93268.02	800	0.13
05/05/2016	S4	459237.9	93370.14	980	0.15
05/06/2016	S1	459287.5	93093.78	360	0.05
05/06/2016	S2	459272.6	93177.02	362	0.05
05/06/2016	S3	459255.3	93268.02	1040	0.14
05/06/2016	S4	459237.9	93370.14	1460	0.19
02/07/2016	S1	459287.5	93093.78	1700	0.21
02/07/2016	S2	459272.6	93177.02	1870	0.28
02/07/2016	S3	459255.3	93268.02	2210	0.39

02/07/2016	S4	459237.9	93370.14	3850	0.44
20/08/2016	S1	459287.5	93093.78	1880	0.60
20/08/2016	S2	459272.6	93177.02	2110	0.61
20/08/2016	S3	459255.3	93268.02	2750	1.03
20/08/2016	S4	459237.9	93370.14	3230	1.25
19/09/2016	S1	459287.5	93093.78	2050	0.53
19/09/2016	S2	459272.6	93177.02	1730	0.25
19/09/2016	S3	459255.3	93268.02	1780	0.52
19/09/2016	S4	459237.9	93370.14	2826	0.89
16/10/2016	S1	459287.5	93093.78	486	0.15
16/10/2016	S2	459272.6	93177.02	1160	0.33
16/10/2016	S3	459255.3	93268.02	1392	0.49
16/10/2016	S4	459237.9	93370.14	1800	0.83
12/11/2016	S1	459287.5	93093.78	128	0.01
12/11/2016	S2	459272.6	93177.02	370	0.03
12/11/2016	S3	459255.3	93268.02	530	0.10
12/11/2016	S4	459237.9	93370.14	790	0.19
12/12/2016	S1	459287.5	93093.78	102	0.01
12/12/2016	S2	459272.6	93177.02	126	0.01
12/12/2016	S3	459255.3	93268.02	358	0.07
12/12/2016	S4	459237.9	93370.14	1440	0.31
26/01/2017	S1	459287.5	93093.78	40	0.00
26/01/2017	S2	459272.6	93177.02	70	0.01
26/01/2017	S3	459255.3	93268.02	144	0.02
26/01/2017	S4	459237.9	93370.14	972	0.16
25/02/2017	S1	459287.5	93093.78	138	0.01
25/02/2017	S2	459272.6	93177.02	94	0.01
25/02/2017	S3	459255.3	93268.02	186	0.02
25/02/2017	S4	459237.9	93370.14	1230	0.21
30/03/2017	S1	459287.5	93093.78	114	0.01
30/03/2017	S2	459272.6	93177.02	100	0.01
30/03/2017	S3	459255.3	93268.02	202	0.03
30/03/2017	S4	459237.9	93370.14	1040	0.27
26/04/2017	S1	459287.5	93093.78	88	0.01
26/04/2017	S2	459272.6	93177.02	150	0.02
26/04/2017	S3	459255.3	93268.02	292	0.05
26/04/2017	S4	459237.9	93370.14	1100	0.26
26/05/2017	S1	459287.5	93093.78	444	0.06
26/05/2017	S2	459272.6	93177.02	520	0.08
26/05/2017	S3	459255.3	93268.02	1050	0.17
26/05/2017	S4	459237.9	93370.14	1940	0.55
23/06/2017	S1	459287.5	93093.78	1291.6	0.17
23/06/2017	S2	459272.6	93177.02	2430	0.32
23/06/2017	S3	459255.3	93268.02	2840	0.41
23/06/2017	S4	459237.9	93370.14	4360	0.96
23/07/2017	S1	459287.5	93093.78	2540	0.51
23/07/2017	S2	459272.6	93177.02	2760	0.62
23/07/2017	S3	459255.3	93268.02	3230	0.98
23/07/2017	S4	459237.9	93370.14	3837.5	1.26
21/08/2017	S1	459287.5	93093.78	2140	0.48
21/08/2017	S2	459272.6	93177.02	1840	0.19
21/08/2017	S3	459255.3	93268.02	2800	0.61
21/08/2017	S4	459237.9	93370.14	3480	1.06
06/10/2017	S1	459287.5	93093.78	1180	0.25

06/10/2017	S2	459272.6	93177.02	1215	0.19
06/10/2017	S3	459255.3	93268.02	1425	0.28
06/10/2017	S4	459237.9	93370.14	1455	0.38

Appendix C Field data: seagrass percentage cover

Date	Station ID	% cover 1	% cover 2	% cover 3	% cover 4	% cover 5	Average %
17/08/2015	S1	67	n/a	n/a	n/a	n/a	67
17/08/2015	S2	69	n/a	n/a	n/a	n/a	69
17/08/2015	S3	78	n/a	n/a	n/a	n/a	78
17/08/2015	S4	100	n/a	n/a	n/a	n/a	100
01/09/2015	S1	75	n/a	n/a	n/a	n/a	75
01/09/2015	S2	67	n/a	n/a	n/a	n/a	67
01/09/2015	S3	89	n/a	n/a	n/a	n/a	89
01/09/2015	S4	97	n/a	n/a	n/a	n/a	97
12/10/2015	S1	69	n/a	n/a	n/a	n/a	69
12/10/2015	S2	78	n/a	n/a	n/a	n/a	78
12/10/2015	S3	92	n/a	n/a	n/a	n/a	92
12/10/2015	S4	100	n/a	n/a	n/a	n/a	100
12/11/2015	S1	19	22	14	19	19	19
12/11/2015	S2	22	31	28	25	17	25
12/11/2015	S3	69	81	72	64	44	66
12/11/2015	S4	89	89	92	83	81	87
10/12/2015	S1	14	11	6	9	14	11
10/12/2015	S2	31	19	14	14	17	19
10/12/2015	S3	47	36	33	31	33	36
10/12/2015	S4	89	86	75	72	69	78
22/01/2016	S1	9	9	14	6	14	10
22/01/2016	S2	25	14	22	25	14	20
22/01/2016	S3	39	36	33	36	44	38
22/01/2016	S4	69	83	69	67	47	67
09/02/2016	S1	17	14	14	6	9	12
09/02/2016	S2	19	22	12	12	17	16
09/02/2016	S3	47	31	28	36	25	33
09/02/2016	S4	64	75	86	64	58	69
09/03/2016	S1	11	3	6	6	3	6
09/03/2016	S2	6	6	6	3	9	6
09/03/2016	S3	25	12	9	19	19	17
09/03/2016	S4	42	31	39	19	31	32
07/04/2016	S1	17	14	8	8	17	13
07/04/2016	S2	33	25	14	14	22	22
07/04/2016	S3	47	36	28	31	31	35
07/04/2016	S4	86	69	72	81	83	78
05/05/2016	S1	14	22	17	8	19	16
05/05/2016	S2	19	14	22	17	25	19
05/05/2016	S3	53	42	36	58	64	51
05/05/2016	S4	78	56	67	58	44	61

05/06/2016	S1	28	16	20	22	19	21
05/06/2016	S2	29	23	30	25	26	27
05/06/2016	S3	53	57	49	50	60	54
05/06/2016	S4	70	68	76	64	70	70
02/07/2016	S1	53	33	36	36	44	40
02/07/2016	S2	42	50	47	39	44	44
02/07/2016	S3	50	44	50	53	36	47
02/07/2016	S4	86	94	92	92	81	89
20/08/2016	S1	53	56	58	50	56	55
20/08/2016	S2	56	58	56	56	58	57
20/08/2016	S3	75	64	69	72	69	70
20/08/2016	S4	92	94	86	89	89	90
19/09/2016	S1	67	72	78	75	58	70
19/09/2016	S2	64	69	72	75	61	68
19/09/2016	S3	61	75	78	75	70	72
19/09/2016	S4	100	100	94	92	89	95
16/10/2016	S1	33	36	33	22	39	33
16/10/2016	S2	31	47	44	36	47	41
16/10/2016	S3	56	61	61	56	69	61
16/10/2016	S4	94	78	89	89	75	85
12/11/2016	S1	19	8	11	11	14	13
12/11/2016	S2	31	33	19	17	28	26
12/11/2016	S3	39	56	39	67	42	49
12/11/2016	S4	69	75	83	89	89	81
12/12/2016	S1	6	8	6	3	8	6
12/12/2016	S2	11	14	14	17	6	12
12/12/2016	S3	36	33	31	44	31	35
12/12/2016	S4	78	75	92	69	83	79
26/01/2017	S1	3	0	3	3	0	2
26/01/2017	S2	3	11	3	14	14	9
26/01/2017	S3	19	17	6	14	17	15
26/01/2017	S4	67	72	47	61	50	59
25/02/2017	S1	6	14	8	6	3	7
25/02/2017	S2	11	14	6	11	6	10
25/02/2017	S3	17	33	28	28	22	26
25/02/2017	S4	83	78	86	83	72	80
30/03/2017	S1	11	3	8	14	3	8
30/03/2017	S2	14	11	6	11	14	11
30/03/2017	S3	19	22	44	17	17	24
30/03/2017	S4	79	89	89	89	72	84
26/04/2017	S1	17	11	6	8	11	11
26/04/2017	S2	17	11	17	33	31	22
26/04/2017	S3	47	25	25	39	44	36
26/04/2017	S4	86	89	92	83	83	87

26/05/2017	S1	19	17	22	11	17	17
26/05/2017	S2	22	19	25	19	36	24
26/05/2017	S3	44	44	64	28	47	45
26/05/2017	S4	89	92	64	86	89	84
23/06/2017	S1	25	39	42	28	22	31
23/06/2017	S2	42	44	39	39	36	40
23/06/2017	S3	61	56	64	53	61	59
23/06/2017	S4	92	94	97	89	94	93
26/07/2017	S1	50	33	44	42	44	43
26/07/2017	S2	69	50	47	58	47	54
26/07/2017	S3	69	67	78	75	78	73
26/07/2017	S4	92	94	97	89	92	93
21/08/2017	S1	69	56	50	67	61	61
21/08/2017	S2	64	67	72	64	69	67
21/08/2017	S3	78	56	67	64	83	70
21/08/2017	S4	94	97	83	89	94	91
06/10/2017	S1	56	53	50	39	47	49
06/10/2017	S2	69	72	56	56	58	62
06/10/2017	S3	67	78	64	83	72	73
06/10/2017	S4	92	94	92	86	83	89

Appendix D Field data: sediment characteristics (temporal)

Date	Point ID	Elevation (m)	LOI (%)	Mean (phi)	Sorting (phi)	Skew (phi)	Kurtosis (phi)	D50 (phi)
17/08/2015	S1	-0.578	0.14	2.47	0.17	0.08	1.19	2.46
17/08/2015	S2	-0.785	0.10	2.53	0.19	0.22	1.23	2.51
17/08/2015	S3	-0.935	0.14	2.49	0.18	0.26	1.29	2.47
17/08/2015	S4	-1.205	0.16	2.56	0.23	0.34	1.15	2.52
01/09/2015	S1	-0.572	0.15	2.48	0.17	0.19	1.18	2.46
01/09/2015	S2	-0.757	0.15	2.54	0.19	0.22	1.25	2.51
01/09/2015	S3	-0.935	0.17	2.48	0.18	0.27	1.29	2.46
01/09/2015	S4	-1.197	0.16	2.51	0.19	0.29	1.26	2.48
12/10/2015	S1	-0.533	0.19	2.51	0.20	0.30	1.28	2.48
12/10/2015	S2	-0.732	0.21	2.53	0.19	0.21	1.30	2.51
12/10/2015	S3	-0.885	0.18	2.47	0.20	0.31	1.38	2.44
12/10/2015	S4	-1.134	0.20	2.53	0.23	0.31	1.23	2.49
12/11/2015	S1	-0.564	0.23	2.46	0.17	0.21	1.20	2.44
12/11/2015	S2	-0.735	0.21	2.55	0.20	0.26	1.29	2.52
12/11/2015	S3	-0.913	0.23	2.44	0.16	0.18	1.12	2.42
12/11/2015	S4	-1.205	0.24	2.58	0.23	0.35	1.13	2.53
10/12/2015	S1	-0.576	0.20	2.45	0.16	0.17	1.29	2.43
10/12/2015	S2	-0.749	0.20	2.51	0.17	0.17	1.34	2.49
10/12/2015	S3	-0.941	0.14	2.42	0.15	0.19	1.19	2.40
10/12/2015	S4	-1.208	0.16	2.46	0.16	0.24	1.22	2.44
22/01/2015	S1	-0.566	0.20	2.47	0.18	0.17	1.23	2.46
22/01/2015	S2	-0.747	0.21	2.49	0.18	0.09	1.30	2.48
22/01/2015	S3	-0.934	0.19	2.46	0.16	0.16	1.23	2.45
22/01/2015	S4	-1.201	0.19	2.49	0.17	0.20	1.15	2.48
09/02/2016	S1	-0.587	0.17	2.44	0.17	0.12	1.17	2.43
09/02/2016	S2	-0.770	0.18	2.49	0.17	0.09	1.17	2.48
09/02/2016	S3	-0.923	0.14	2.44	0.16	0.22	1.20	2.43
09/02/2016	S4	-1.221	0.15	2.46	0.16	0.20	1.05	2.44
09/03/2016	S1	-0.572	0.18	2.44	0.16	0.14	1.14	2.43
09/03/2016	S2	-0.753	0.15	2.50	0.17	0.12	1.25	2.49
09/03/2016	S3	-0.939	0.16	2.44	0.15	0.13	1.03	2.43
09/03/2016	S4	-1.170	0.16	2.40	0.16	0.13	1.11	2.39
07/04/2016	S1	-0.596	0.23	2.43	0.17	0.17	1.02	2.42
07/04/2016	S2	-0.785	0.21	2.48	0.18	0.13	1.17	2.46
07/04/2016	S3	-0.946	0.21	2.43	0.16	0.17	1.14	2.41
07/04/2016	S4	-1.204	0.21	2.42	0.16	0.24	1.13	2.40
05/05/2016	S1	-0.554	0.26	2.50	0.18	0.18	1.18	2.48
05/05/2016	S2	-0.732	0.25	2.53	0.17	0.14	1.25	2.52
05/05/2016	S3	-0.901	0.27	2.53	0.19	0.34	1.30	2.50
05/05/2016	S4	-1.159	0.28	2.50	0.17	0.26	1.28	2.48
05/06/2016	S1	-0.573	0.30	2.49	0.18	0.17	1.24	2.47
05/06/2016	S2	-0.743	0.31	2.56	0.19	0.24	1.25	2.53
05/06/2016	S3	-0.946	0.29	2.48	0.19	0.31	1.31	2.45
05/06/2016	S4	-1.205	0.29	2.49	0.19	0.31	1.34	2.47
02/07/2016	S1	-0.564	0.22	2.47	0.18	0.22	1.18	2.45
02/07/2016	S2	-0.718	0.23	2.54	0.19	0.20	1.23	2.52

02/07/2016	S3	-0.915	0.22	2.48	0.18	0.23	1.16	2.47
02/07/2016	S4	-1.183	0.26	2.47	0.20	0.24	1.30	2.44
20/08/2016	S1	-0.560	0.29	2.48	0.18	0.14	1.09	2.47
20/08/2016	S2	-0.769	0.27	2.54	0.19	0.18	1.26	2.52
20/08/2016	S3	-0.921	0.26	2.48	0.15	0.29	1.28	2.46
20/08/2016	S4	-1.183	0.26	2.48	0.19	0.29	1.32	2.45
19/09/2016	S1	-0.584	0.28	2.45	0.17	0.20	1.16	2.43
19/09/2016	S2	-0.769	0.27	2.55	0.18	0.25	1.34	2.53
19/09/2016	S3	-0.920	0.25	2.46	0.15	0.27	1.15	2.44
19/09/2016	S4	-1.200	0.23	2.47	0.18	0.32	1.24	2.44
16/10/2016	S1	-0.522	0.39	2.49	0.18	0.23	1.26	2.47
16/10/2016	S2	-0.720	0.38	2.55	0.20	0.25	1.30	2.53
16/10/2016	S3	-0.899	0.35	2.51	0.19	0.34	1.32	2.48
16/10/2016	S4	-1.156	0.42	2.54	0.23	0.34	1.27	2.49
12/11/2016	S1	-0.580	0.42	2.49	0.18	0.13	1.36	2.47
12/11/2016	S2	-0.783	0.39	2.53	0.19	0.14	1.41	2.51
12/11/2016	S3	-0.928	0.35	2.51	0.18	0.24	1.25	2.49
12/11/2016	S4	-1.185	0.39	2.51	0.20	0.22	1.31	2.48
12/12/2016	S1	-0.563	0.43	2.56	0.22	0.19	1.15	2.53
12/12/2016	S2	-0.750	0.13	2.53	0.20	0.17	1.20	2.51
12/12/2016	S3	-0.902	0.28	2.56	0.22	0.31	1.26	2.53
12/12/2016	S4	-1.190	0.33	2.61	0.24	0.32	1.08	2.56
26/01/2017	S1	-0.587	0.26	2.48	0.18	0.12	1.17	2.47
26/01/2017	S2	-0.785	0.27	2.51	0.20	0.21	1.22	2.48
26/01/2017	S3	-0.962	0.23	2.49	0.19	0.30	1.25	2.47
26/01/2017	S4	-1.239	0.24	2.51	0.20	0.28	1.22	2.49
25/02/2017	S1	-0.557	0.25	2.52	0.18	0.18	1.27	2.50
25/02/2017	S2	-0.743	0.24	2.52	0.20	0.20	1.20	2.50
25/02/2017	S3	-0.927	0.26	2.51	0.18	0.24	1.28	2.49
25/02/2017	S4	-1.154	0.28	2.56	0.20	0.33	1.14	2.53
30/03/2017	S1	-0.547	0.27	2.51	0.19	0.20	1.19	2.49
30/03/2017	S2	-0.743	0.28	2.53	0.20	0.20	1.31	2.51
30/03/2017	S3	-0.918	0.25	2.53	0.20	0.29	1.27	2.50
30/03/2017	S4	-1.153	0.32	2.69	0.27	0.36	0.98	2.62
26/04/2017	S1	-0.546	0.39	2.50	0.18	0.20	1.29	2.48
26/04/2017	S2	-0.746	0.38	2.49	0.20	0.14	1.32	2.47
26/04/2017	S3	-0.904	0.47	2.53	0.20	0.36	1.37	2.49
26/04/2017	S4	-1.145	0.49	2.59	0.24	0.38	1.19	2.53
26/05/2017	S1	-0.503	0.47	2.50	0.18	0.23	1.29	2.48
26/05/2017	S2	-0.693	0.42	2.52	0.19	0.28	1.27	2.49
26/05/2017	S3	-0.880	0.43	2.53	0.21	0.39	1.26	2.49
26/05/2017	S4	-1.105	0.48	2.62	0.24	0.38	1.05	2.56
23/06/2017	S1	-0.478	0.46	2.54	0.20	0.25	1.17	2.51
23/06/2017	S2	-0.649	0.46	2.57	0.20	0.29	1.16	2.53
23/06/2017	S3	-0.829	0.39	2.52	0.19	0.36	1.31	2.48
23/06/2017	S4	-1.069	0.44	2.61	0.24	0.35	1.00	2.56
23/07/2017	S1	-0.480	0.23	2.49	0.18	0.20	1.20	2.47
23/07/2017	S2	-0.666	0.29	2.54	0.22	0.20	1.16	2.51
23/07/2017	S3	-0.831	0.24	2.49	0.20	0.20	1.28	2.47
23/07/2017	S4	-1.080	0.26	2.55	0.21	0.32	1.18	2.51
21/08/2017	S1	-0.451	0.36	2.53	0.20	0.21	1.12	2.50
21/08/2017	S2	-0.663	0.38	2.60	0.21	0.31	1.13	2.56
21/08/2017	S3	-0.834	0.37	2.53	0.20	0.34	1.28	2.49
21/08/2017	S4	-1.066	0.37	2.64	0.25	0.36	1.11	2.59

06/10/2017	S1	-0.474	0.25	2.49	0.19	0.16	1.26	2.48
06/10/2017	S2	-0.648	0.25	2.56	0.19	0.28	1.15	2.53
06/10/2017	S3	-0.822	0.25	2.51	0.20	0.34	1.26	2.48
06/10/2017	S4	-1.066	0.25	2.53	0.21	0.35	1.16	2.49

Bibliography

Abuodha, J. O. Z. (2003). Grain size distribution and composition of modern dune and beach sediments, Malindi Bay coast, Kenya. *Journal of African Earth Sciences*, *36*(1–2), 41–54.

Ackerman, J. D., & Okubo, A. (1993). Reduced Mixing in a Marine Macrophyte Canopy. *Functional Ecology*, *7*(3), 305–309.

Adriano, S., Chiara, F., & Antonio, M. (2005). Sedimentation rates and erosion processes in the lagoon of Venice. *Environment International*, *31*(7 SPEC. ISS.), 983–992.

Airoldi, L., Abbiati, M., Beck, M. W., Hawkins, S. J., Jonsson, P. R., Martin, D., … Åberg, P. (2005). An ecological perspective on the deployment and design of low-crested and other hard coastal defence structures. *Coastal Engineering*, *52*(10–11), 1073–1087.

Amos, C. L., J.Grant, Daborn, G. R., & Black, K. (1992). Sea Carousel - A Benthic, Annular Flume. *Estuarine, Coastal and Shelf Science*, *34*, 557–577.

Anderson, M. E., & Smith, J. M. (2014). Wave attenuation by flexible, idealized salt marsh vegetation. *Coastal Engineering*, *83*, 82–92.

Arkema, K. K., Guannel, G., Verutes, G., Wood, S. A., Guerry, A., Ruckelshaus, M., … Silver, J. M. (2013). Coastal habitats shield people and property from sea-level rise and storms. *Nature Clim. Change*, *3*(10), 913–918.

Auby, I., & Labourg, P.-J. (1996). Seasonal dynamics of Zostera noltii hornem. In the bay of arcachon (France). *Journal of Sea Research*, *35*(4), 269–277.

Augustin, L. N., Irish, J. L., & Lynett, P. (2009). Laboratory and numerical studies of wave damping by emergent and near-emergent wetland vegetation. *Coastal Engineering*, *56*(3), 332–340.

Baas, J. H. (1999). An empirical model for the development and equilibrium morphology of current ripples in fine sand. *Sedimentology*, *46*(1), 123–138.

Balsinha, M., Fernandes, C., Oliveira, A., Rodrigues, A., & Taborda, R. (2014). Sediment transport patterns on the Estremadura Spur continental shelf: Insights from grain-size trend analysis. *Journal of Sea Research*, *93*, 28–32.

Bargain, A., Robin, M., Méléder, V., Rosa, P., Le Menn, E., Harin, N., & Barillé, L. (2013). Seasonal spectral variation of Zostera noltii and its influence on pigment-based Vegetation Indices. *Journal of Experimental Marine Biology and Ecology*, *446*, 86–94.

Barillé, L., Robin, M., Harin, N., Bargain, A., & Launeau, P. (2010). Increase in seagrass distribution at Bourgneuf Bay (France) detected by spatial remote sensing. *Aquatic Botany*, *92*(3), 185–194.

Blott, S. J., & Pye, K. (2001). GRADISTAT: a grain size distribution and statistics package for the analysis of unconsolidated sediments. *Earth Surface Processes and Landforms*, *26*(11), 1237–1248.

Borum, J., Duarte, C. M., Krause-Jensen, D., & Greve, T. M. (2004). *European seagrasses: an introduction to monitoring and management*. (J. Borum, C. M. Duarte, D. Krause-Jensen, & T. M. Greve, Eds.)*The (M&MS) project* (Vol. EVK3-CT-20). The M&MS project.

Bos, A. R., Bouma, T. J., de Kort, G. L. J., & van Katwijk, M. M. (2007). Ecosystem engineering by annual intertidal seagrass beds: Sediment accretion and modification. *Estuarine, Coastal and Shelf Science*, *74*(1–2), 344–348.

Bos, A. R., & Van Katwijk, M. M. (2007). Planting density, hydrodynamic exposure and mussel beds affect survival of transplanted intertidal eelgrass. *Marine Ecology Progress Series*, *336*, 121–129.

Boudet, L., Sabatier, F., & Radakovitch, O. (2017). Modelling of sediment transport pattern in the mouth of the Rhone delta: Role of storm and flood events. *Estuarine, Coastal and Shelf Science*, *198*(October), 568–582.

Bouma, T. J., De Vries, M. B., Low, E., Peralta, G., Tánczos, I. C., Van De Koppel, J., & Herman, P. M. J. (2005). Trade-offs related to ecosystem engineering: A case study on stiffness of emerging macrophytes. *Ecology*, *86*(8), 2187–2199.

Bouma, T. J., Friedrichs, M., Klaassen, P., Van Wesenbeeck, B. K., Brun, F. G., Temmerman, S., … Herman, P. M. J. (2009). Effects of shoot stiffness, shoot size and current velocity on scouring sediment from around seedlings and propagules. *Marine Ecology Progress Series*, *388*, 293–297.

Bradley, K., & Houser, C. (2009). Relative velocity of seagrass blades: Implications for wave attenuation in low-energy environments. *Journal of Geophysical Research: Earth Surface*, *114*(1), 1–13.

Bramha, S. N., Mohanty, A. K., Samantara, M. K., Panigrahi, S. N., & Satpathy, K. K. (2017). Textural characteristics of beach sediments along kalpakkam, south east coast of India. *Indian Journal of Geo-Marine Sciences*, *46*(8), 1562–1574.

Bulmer, R. H., Townsend, M., Drylie, T., & Lohrer, A. M. (2018). Elevated turbidity and the

nutrient removal capacity of seagrass. *Frontiers in Marine Science*, *5*(DEC), 1–9.

Cabaço, S., & Santos, R. (2007). Effects of burial and erosion on the seagrass Zostera noltii. *Journal of Experimental Marine Biology and Ecology*, *340*(2), 204–212.

Cabaço, S., Santos, R., & Duarte, C. M. (2008). The impact of sediment burial and erosion on seagrasses: A review. *Estuarine, Coastal and Shelf Science*, *79*(3), 354–366.

Cardoso, P. G., Raffaelli, D., & Pardal, M. A. (2008). The impact of extreme weather events on the seagrass Zostera noltii and related Hydrobia ulvae population. *Marine Pollution Bulletin*, *56*(3), 483–492.

Charbonneau, B. R., Wnek, J. P., Langley, J. A., Lee, G., & Balsamo, R. A. (2016). Above vs. belowground plant biomass along a barrier island: Implications for dune stabilization. *Journal of Environmental Management*, *182*, 126–133.

Cheikh, M. A. S., Govers, L. L., van der Heide, T., Olff, H., van Belzen, J., van Gils, J. A., … van de Koppel, J. (2018). A facultative mutualistic feedback enhances the stability of tropical intertidal seagrass beds. *Scientific Reports*, *8*(1), 1–10.

Chen, S.-N., Sanford, L. P., Koch, E. W., Shi, F., & North, E. W. (2007). A nearshore model to investigate the effects of seagrass bed geometry on wave attenuation and suspended sediment transport. *Estuaries and Coasts*, *30*(2), 296–310.

Christianen, M. J. A., van Belzen, J., Herman, P. M. J., van Katwijk, M. M., Lamers, L. P. M., van Leent, P. J. M., & Bouma, T. J. (2013). Low-Canopy Seagrass Beds Still Provide Important Coastal Protection Services. *PLoS ONE*, *8*(5).

Cloern, J. E., Abreu, P. C., Carstensen, J., Chauvaud, L., Elmgren, R., Grall, J., … Yin, K. (2016). Human activities and climate variability drive fast-paced change across the world's estuarine-coastal ecosystems. *Global Change Biology*, *22*(2), 513–529.

Cohen, O. (2014). Profiler 3.1 XL, un logiciel gratuit pour la construction et l'analyse de profils topographiques dans Microsoft Excel©. In *13ÈMES JOURNÉES NATIONALES GÉNIE CÔTIER - GÉNIE CIVIL* (pp. 557–564). Dunkirk.

Costanza, R., d'Arge, R., de Groot, R., Farber, S., Grasso, M., Hannon, B., … van den Belt, M. (1997). The value of the world's ecosystem services and natural capital. *Nature*, *387*(6630), 253–260.

Coyer, J. A., Diekmann, O. E., Serrão, E. A., Procaccini, G., Milchakova, N., Pearson, G. A., … Olsen, J. L. (2004). Population genetics of dwarf eelgrass Zostera noltii throughout its biogeographic range. *Marine Ecology Progress Series*, *281*, 51–62.

Cullen-Unsworth, L. C., Nordlund, L. M., Paddock, J., Baker, S., McKenzie, L. J., & Unsworth, R. K. F. (2014). Seagrass meadows globally as a coupled social-ecological system: Implications for human wellbeing. *Marine Pollution Bulletin*, *83*(2), 387–397.

Curiel, D., Bellato, A., Rismondo, A., & Marzocchi, M. (1996). Sexual reproduction of Zostera noltii Hornemann in the lagoon of Venice (Italy, north Adriatic). *Aquatic Botany*, *52*(4), 313–318.

de Alegría-Arzaburu, A. R., & Vidal-Ruiz, J. A. (2018). Beach recovery capabilities after El Niño 2015–2016 at Ensenada Beach, Northern Baja California. *Ocean Dynamics*, *68*(6), 749–759.

De Falco, G., Ferrari, S., Cancemi, G., & Baroli, M. (2000). Relationship between sediment distribution and Posidonia oceanica seagrass. *Geo-Marine Letters*, *20*(1), 50–57.

De Falco, G., Molinaroli, E., Baroli, M., & Bellacicco, S. (2003). Grain size and compositional trends of sediments from Posidonia oceanica meadows to beach shore, Sardinia, western Mediterranean. *Estuarine, Coastal and Shelf Science*, *58*(2), 299–309.

den Hartog, C. (1970). *The seagrasses of the world*. Amsterdam: North-Holland Publication Company.

Dennison, W. C. (1987). Effects of Light On Seagrass Photosynthesis, Growth and Depth Distribution. *Aquatic Botany*, *27*, 15–26.

Dolch, T., Buschbaum, C., & Reise, K. (2013). Persisting intertidal seagrass beds in the northern Wadden Sea since the 1930s. *Journal of Sea Research*, *82*, 134–141.

Duane, D. B. (1964). Significance of Skewness in Recent Sediments, Western Pamlico Sound, North Carolina. *Journal of Sediment Petrology*, *34*(4), 864–874.

Duarte, C. M. (1991). Allometric scaling of seagrass form and productivity. *Marine Ecology Progress Series*, *77*(2–3), 289–300.

Duarte, Carlos M., Merino, M., Agawin, N. S. R., Uri, J., Fortes, M. D., Gallegos, M. E., … Hemminga, M. A. (1998). Root production and belowground seagrass biomass. *Marine Ecology Progress Series*, *171*, 97–108.

Duarte, Carlos M, Kennedy, H., Marbà, N., & Hendriks, I. (2013). Assessing the capacity of seagrass meadows for carbon burial: Current limitations and future strategies. *Ocean & Coastal Management*, *83*, 32–38.

Dyer, K. R. (1980). Sedimentation and Sediment Transport. In *The Solent Estuarine System: An*

Assessment of Present Knowledge (pp. 20–24). Swindon: NERC.

Elgar, S., Raubenheimer, B., & Guza, R. T. (2001). Current meter performance in the surf zone. *Journal of Atmospheric and Oceanic Technology*, *18*(10), 1735–1746.

Feagin, R. A., Figlus, J., Zinnert, J. C., Sigren, J., Martínez, M. L., Silva, R., … Carter, G. (2015). Going with the flow or against the grain? The promise of vegetation for protecting beaches, dunes, and barrier islands from erosion. *Frontiers in Ecology and the Environment*, *13*(4), 203–210.

Ferrario, F., Beck, M. W., Storlazzi, C. D., Micheli, F., Shepard, C. C., & Airoldi, L. (2014). The effectiveness of coral reefs for coastal hazard risk reduction and adaptation. *Nature Communications*, *5*(May), 1–9. http://doi.org/10.1038/ncomms4794

Firth, L. B., Browne, K. A., Knights, A. M., Hawkins, S. J., & Nash, R. (2016). Eco-engineered rock pools: A concrete solution to biodiversity loss and urban sprawl in the marine environment. *Environmental Research Letters*, *11*(9).

Folk, R., & Ward, W. (1957). Brazos River Bar: A Study in the Significance of Grain Size Parameters. *Journal of Sedimentary Petrology*.

Folkard, A., & Bouma, T. (2016). Flow interactions with blue mussel patches: hydrodynamic and ecological implications. In *11th International Symposium on Ecohydraulics* (pp. 1–10). Melbourne, Australia: The University of Melbourne.

Fonseca, M. S. (1989). Sediment stabilization by Halophila decipiens in comparison to other seagrasses. *Estuarine, Coastal and Shelf Science*, *29*(5), 501–507.

Fonseca, M. S., & Cahalan, J. A. (1992). A Preliminary Evaluation of Wave Attenuation by Four Species of Seagrass. *Estuarine, Coastal and Shelf Science*, *35*, 565–576.

Fonseca, M. S., & Fisher, J. S. (1986). A comparison of canopy friction and sediment movement between four species of seagrass with reference to their ecology and restoration. *Marine Ecology Progress Series*, *29*, 15–22.

Fonseca, M. S., Fisher, J. S., Zieman, J. C., & Thayerd, G. W. (1982). Influence of the Seagrass, Zostera marina L ., on Current Flow ". *Estuaries and Coasts*, *15*, 351–364.

Fonseca, M. S., & Koehl, M. A. R. (2006). Flow in seagrass canopies: The influence of patch width. *Estuarine, Coastal and Shelf Science*, *67*(1–2), 1–9.

Fonseca, M. S., Koehl, M. A. R., & Kopp, B. S. (2007). Biomechanical factors contributing to self-organization in seagrass landscapes. *Journal of Experimental Marine Biology and Ecology*,

340(2), 227–246.

Fourqurean, J. W., Duarte, C. M., Kennedy, H., Marbà, N., Holmer, M., Mateo, M. A., … Serrano, O. (2012). Seagrass ecosystems as a globally significant carbon stock. *Nature Geoscience*, *5*(7), 505–509.

Friedman, G. M. (1961). DISTINCTION BETWEEN DUNE, BEACH, AND RIVER SANDS FROM THEIR TEXTURAL CHARACTERISTICS. *Journal of Sediment Petrology*, *31*(4), 514–529.

Friedman, G. M., & Sanders, J. E. (1978). *Principles of Sedimentology*. New York: Wiley.

Friedman, Gerald M. (1962). On Sorting, Sorting Coefficients, and the Lognormality of the Grain-Size Distribution of Sandstones. *The Journal of Geology*, *70*(6), 737–753.

Gacia, E., & Duarte, C. M. (2001). Sediment Retention by a Mediterranean Posidonia oceanica Meadow: The Balance between Deposition and Resuspension. *Estuarine, Coastal and Shelf Science*, *52*(4), 505–514.

Gacia, E., Granata, T. ., & Duarte, C. . (1999). An approach to measurement of particle flux and sediment retention within seagrass (Posidonia oceanica) meadows. *Aquatic Botany*, *65*(1–4), 255–268.

Gambi, M. C., Nowell, A. R. M., & Jumars, P. A. (1990). Flume observations on flow dynamics in Zostera marina (eelgrass) beds. *Marine Ecology Progress Series*, *61*(1984), 159–169.

Ganthy, F., Soissons, L., Sauriau, P.-G., Verney, R., & Sottolichio, A. (2015). Effects of short flexible seagrass Zostera noltei on flow, erosion and deposition processes determined using flume experiments. *Sedimentology*, *62*, 997–1023.

Ganthy, F., Sottolichio, A., & Verney, R. (2013). Seasonal modification of tidal flat sediment dynamics by seagrass meadows of Zostera noltii (Bassin d'Arcachon, France). *Journal of Marine Systems*, *109–110*, S233–S240.

Gao, S. (1996). A Fortran Program for Grain-Size Trend Analysis To Define Net Sediment Transport Pathways. *Computers & Geoscience*, *22*(4), 449–452.

Gao, S. (2019). Geomorphology and Sedimentology of Tidal Flats. In Gerardo M. E. Perillo, E. Wolanski, D. R. Cahoon, & M. M. Brinson (Eds.), *Coastal Wetlands: An Integrated Ecosystem Approach* (pp. 295–312). Elsevier.

Gao, S., & Collins, M. (1992). Net sediment transport patterns inferred from grain-size trends, based upon definition of "transport vectors." *Sedimentary Geology*, *80*, 47–60.

Gomes, A. C. C., Bernardo, N., & Alcântara, E. (2017). Accessing the southeastern Brazil 2014

drought severity on the vegetation health by satellite image. *Natural Hazards*, *89*(3), 1401–1420.

Gong, Z., Jin, C., Zhang, C., Zhou, Z., Zhang, Q., & Li, H. (2017). Temporal and spatial morphological variations along a cross-shore intertidal profile, Jiangsu, China. *Continental Shelf Research*, *144*, 1–9.

Grady, J. R. (1981). Properties of Sea Grass and Sand Flat Sediments from the Intertidal Zone of St. Andrew Bay, Florida. *Estuaries*, *4*(4), 335–344.

Han, Q., Bouma, T., Brun, F., Suykerbuyk, W., & van Katwijk, M. (2012). Resilience of Zostera noltii to burial or erosion disturbances. *Marine Ecology Progress Series*, *449*, 133–143.

Harrison, P. G. (1993). Variations in demography of Zostera marina and Z. noltii on an intertidal gradient. *Aquatic Botany*, *45*(528), 63–77.

Heiss, W. M., Smith, A. M., & Probert, P. K. (2000). Influence of the small intertidal seagrass Zostera novazelandica on linear water flow and sediment texture. *New Zealand Journal of Marine and Freshwater Research*, *34*(4), 689–694.

Hendriks, I. E., Olsen, Y. S., Ramajo, L., Basso, L., Steckbauer, A., Moore, T. S., … Duarte, C. M. (2014). Photosynthetic activity buffers ocean acidification in seagrass meadows. *Biogeosciences*, *11*(2), 333–346.

Hendriks, Iris E., Bouma, T. J., Morris, E. P., & Duarte, C. M. (2010). Effects of seagrasses and algae of the Caulerpa family on hydrodynamics and particle-trapping rates. *Marine Biology*, *157*(3), 473–481.

Hendriks, Iris E., Sintes, T., Bouma, T. J., & Duarte, C. M. (2008). Experimental assessment and modeling evaluation of the effects of the seagrass Posidonia oceanica on flow and particle trapping. *Marine Ecology Progress Series*, *356*(March), 163–173.

Hillman, K., McComb, a. J., & Walker, D. I. (1995). The distribution, biomass and primary production of the seagrass Halophila ovalis in the Swan/Canning Estuary, Western Australia. *Aquatic Botany*, *51*(1–2), 1–54.

Hu, Z., van der Wal, D., Cai, H., van Belzen, J., & Bouma, T. J. (2018). Dynamic equilibrium behaviour observed on two contrasting tidal flats from daily monitoring of bed-level changes. *Geomorphology*, *311*, 114–126.

Hu, Z., Yao, P., van der Wal, D., & Bouma, T. J. (2017). Patterns and drivers of daily bed-level dynamics on two tidal flats with contrasting wave exposure. *Scientific Reports*, *7*(1), 7088.

Hughes, S. A. (2005). *Use of Sediment Trend Analysis (STA ®) for Coastal Projects*. *US Army Corps of Engineers*.

Isle of Wight Council, & Haskoning, R. (2010). *Isle of Wight Shoreline Management Plan 2 (Review Sub-cell 5d+e)*.

IUCN. (2016). The IUCN Red List of Threatened Species. Version 2015-4. <www.iucnredlist.org>.

Kadlec, R. H. (1990). Overland flow in wetlands: vegetation resistance. *Journal of Hydraulic Engineering*, *116*(5), 691–706.

Kakeh, N., Coco, G., & Marani, M. (2015). On the morphodynamic stability of intertidal environments and the role of vegetation. *Advances in Water Resources*, *93*, 303–314.

Kassem, H., Thompson, C. E. L., Amos, C. L., & Townend, I. H. (2015). Wave-induced coherent turbulence structures and sediment resuspension in the nearshore of a prototype-scale sandy barrier beach. *Continental Shelf Research*, *109*, 78–94.

Kinyanjui, M. J. (2011). NDVI-based vegetation monitoring in Mau forest complex, Kenya. *African Journal of Ecology*, *49*(2), 165–174.

Kirwan, M. L., & Megonigal, J. P. (2013). Tidal wetland stability in the face of human impacts and sea-level rise. *Nature*, *504*(7478), 53–60.

Kobayashi, N., Raichle, A., & Asano, T. (1993). Wave Attenuation by Vegetation. *Journal of Waterway, Port, Coastal, and Ocean Engineering*, *119*(1), 30–48.

Koch, E. W. (1999). Sediment resuspension in a shallow Thalassia testudinum banks ex König bed. *Aquatic Botany*, *65*(1–4), 269–280.

Koch, E. W., Verduin, J. J., Keulen, M. Van, & Orth, R. J. (2006). Fluid Dynamics in Seagrass Ecology — from Molecules to Ecosystems. In *Seagrasses: biology, ecology and conservation* (pp. 193–225). Dordrecht, The Netherlands: Springer.

Kombiadou, K., Verney, R., Plus, M., & Ganthy, F. (2013). Modelling the effects of Zostera Noltii meadows on the sediment dynamics: applicatio to the Arcachon Lagoon. *Coastal Dynamics*, 991–1002.

Krumbien, W. C. (1934). Size Frequency Distributions of Sediments. *Journal of Sedimentary Petrology*, *4*(2), 65–77.

Krumbien, W. C. (1938). Size Frequency Distributions of Sediments and the Normal Phi Curve. *Journal of Sediment Petrology*, *8*(December), 84–90.

Lara, J. L., Maza, M., Ondiviela, B., Trinogga, J., Losada, I. J., Bouma, T. J., & Gordejuela, N. (2016). Large-scale 3-D experiments of wave and current interaction with real vegetation. Part 2: Experimental analysis. *Coastal Engineering*, *106*, 73–86.

Laugier, T., Rigollet, V., & De Casabianca, M. L. (1999). Seasonal dynamics in mixed eelgrass beds, Zostera marina L. and Z. noltii Hornem., in a Mediterranean coastal lagoon (Thau lagoon, France). *Aquatic Botany*, *63*(1), 51–69.

Le Bouteiller, C., & Venditti, J. G. (2014). Vegetation-driven morphodynamic adjustments of a sand bed. *Geophysical Research Letters*, *41*(11), 3876–3883.

Le Hir, P., Roberts, W., Cazaillet, O., Christie, M., Bassoullet, P., & Bacher, C. (2000). Characterization of intertidal flat hydrodynamics. *Continental Shelf Research*, *20*(12–13), 1433–1459.

Le Roux, J. P., & Rojas, E. M. (2007). Sediment transport patterns determined from grain size parameters: Overview and state of the art. *Sedimentary Geology*, *202*(3), 473–488.

Lefebvre, A., Thompson, C. E. L., & Amos, C. L. (2010). Influence of Zostera marina canopies on unidirectional flow, hydraulic roughness and sediment movement. *Continental Shelf Research*, *30*(16), 1783–1794.

Lefebvre, A., Thompson, C. E. L., Collins, K. J., & Amos, C. L. (2009). Use of a high-resolution profiling sonar and a towed video camera to map a Zostera marina bed, Solent, UK. *Estuarine, Coastal and Shelf Science*, *82*(2), 323–334.

Leonard, L. a., & Luther, M. E. (1995). Flow hydrodynamics in tidal marsh canopies. *Limnology and Oceanography*, *40*(8), 1474–1484.

Liu, X., Wang, Y., Costanza, R., Kubiszewski, I., Xu, N., Gao, Z., … Yuan, M. (2019). Is China's coastal engineered defences valuable for storm protection? *Science of The Total Environment*, *657*, 103–107.

Liu, Z. (2001). *SEDIMENT TRANSPORT*. Aalborg.

Lo, V. B., Bouma, T. J., van Belzen, J., Van Colen, C., & Airoldi, L. (2017). Interactive effects of vegetation and sediment properties on erosion of salt marshes in the Northern Adriatic Sea. *Marine Environmental Research*, *131*(September), 32–42.

Lowe, J. A., & Gregory, J. M. (2005). The effects of climate change on storm surges around the United Kingdom. *Philosophical Transactions. Series A, Mathematical, Physical, and Engineering Sciences*, *363*(1831), 1313–1328.

Lugendo, B. R., Nagelkerken, I., Van Der Velde, G., & Mgaya, Y. D. (2006). The importance of mangroves, mud and sand flats, and seagrass beds as feeding areas for juvenile fishes in Chwaka Bay, Zanzibar: Gut content and stable isotope analyses. *Journal of Fish Biology*, *69*(6), 1639–1661.

Madsen, J. D. D., Chambers, P. A. A., James, W. F. F., Koch, E. W., & Westlake, D. . F. (2001). The interaction between water movement, sediment dynamics and submersed macrophytes. *Hydrobiologia*, *444*, 71–84.

Malarkey, J., Baas, J. H., Hope, J. a, Aspden, R. J., Parsons, D. R., Peakall, J., … Thorne, P. D. (2015). The pervasive role of biological cohesion in bedform development. *Nature Communications*, *6*(February), 6257.

Manca, E., Cáceres, I., Alsina, J. M., Stratigaki, V., Townend, I., & Amos, C. L. (2012). Wave energy and wave-induced flow reduction by full-scale model Posidonia oceanica seagrass. *Continental Shelf Research*, *50–51*, 100–116.

Marbà, N., Arias-Ortiz, A., Masque, P., Kendrick, G. A., Mazarrasa, I., Bastyan, G. R., … Duarte, C. M. (2015). Impact of seagrass loss and subsequent revegetation on carbon sequestration and stocks. *Journal of Ecology*, *103*, 296–302.

Marsden, A. L., & Chesworth, J. C. (2015). *Inventory of eelgrass beds in Hampshire and the Isle of Wight 2015, Section One: Report. Version 7 : May 2015*. Hampshire.

Marsden, A. L., & Scott, A. L. (2015). *Inventory of eelgrass beds in Hampshire and the Isle of Wight 2015, Section Two: Data. Version 7: May 2015*. Hampshire.

Martins, L. R. (1965). Significance of skewness and kurtosis in environmental interpretation. *Journal of Sedimentary Research*, *35*(3), 768–770. d

McCave, I. N. (1978). Grain-size trends and transport along beaches: Example from eastern England. *Marine Geology*, *28*(1–2), M43–M51.

McLaren, P. (1981). An interpretation of trends in grain size measures. *Journal of Sedimentary Research*, *51*(2).

McLaren, P., & Bowles, D. (1985). The effects of sediment transport on grain size distributions. *Journal of Sedimentary Petrology*, *55*(4), 457–470.

McLaren, P., & Teear, G. (2013). A Sediment Trend Analysis (STA®) in Support of Dredged Material Management in Lyttelton Harbour, Christchurch, New Zealand. *Journal of Coastal Research*, 438–447.

McMahon, K., van Dijk, K., Ruiz-Montoya, L., Kendrick, G. A., Krauss, S. L., Waycott, M., … Duarte, C. (2014). The movement ecology of seagrasses. In *Proceedings of the Royal Society of London B: Biological Sciences* (Vol. 281). Royal Society.

McNinch, J. E. (2004). Geologic control in the nearshore: shore-oblique sandbars and shoreline erosional hotspots, Mid-Atlantic Bight, USA. *Marine Geology*, *211*(1–2), 121–141.

Mcskimming, C., Connell, S. D., Russell, B. D., & Tanner, J. E. (2016). Habitat restoration: early signs and extent of faunal recovery relative to seagrass recovery. *Estuarine, Coastal and Shelf Science*, *171*, 51–57.

Meinesz, A., Lefevre, J. R., & Astier, J. M. (1991). Impact of coastal development on the infralittoral zone along the southeastern Mediterranean shore of continental France. *Marine Pollution Bulletin*, *23*, 343–347.

Mendez, F. J., Losada, I. J., & Losada, M. A. (1999). Hydrodynamics induced by wind waves in a vegetation field. *Journal of Geophysical Research*, *104*(C8), 18383–18396.

Messori, G., Caballero, R., & Gaetani, M. (2016). On cold spells in North America and storminess in western Europe, (section 2), 6620–6628.

Mitchell, J. F. B., Lowe, J., Wood, R. A., & Vellinga, M. (2006). Extreme events due to human-induced climate change. *Philosophical Transactions of the Royal Society A: Mathematical, Physical and Engineering Sciences*, *364*(1845), 2117–2133.

Möller, I. (2006). Quantifying saltmarsh vegetation and its effect on wave height dissipation: Results from a UK East coast saltmarsh. *Estuarine, Coastal and Shelf Science*, *69*(3–4), 337–351.

Möller, Iris, Kudella, M., Rupprecht, F., Spencer, T., Paul, M., van Wesenbeeck, B. K., … Schimmels, S. (2014). Wave attenuation over coastal salt marshes under storm surge conditions. *Nature Geoscience*, *7*(10), 727–731.

Montgomery, J. M., Bryan, K. R., Horstman, E. M., & Mullarney, J. C. (2018). Attenuation of tides and surges by mangroves: Contrasting case studies from New Zealand. *Water (Switzerland)*, *10*(9).

Mori, N., Suzuki, T., & Kakuno, S. (2007). Noise of Acoustic Doppler Velocimeter Data in Bubbly Flows. *Journal of Engineering Mechanics*, *133*(1), 122–125.

Morris, R. L., Strain, E. M. A., Konlechner, T. M., Fest, B. J., Kennedy, D. M., Arndt, S. K., & Swearer, S. E. (2019). Developing a nature-based coastal defence strategy for Australia.

Australian Journal of Civil Engineering, *17*(2), 167–176.

Nagalakshmi, K., Kumar, M. P., Prasad, T. L., Jayaraju, N., Lakshmanna, M., & Sreenivasulu, G. (2018). A study on textural parameters of beach sands along some parts of the Nellore coast, east coast of India: Implications to Depositional Environment. *Journal of Indian Geophysical Union*, *22*(September), 558–567.

Narayan, S., Beck, M. W., Reguero, B. G., Losada, I. J., Van Wesenbeeck, B., Pontee, N., … Burks-Copes, K. A. (2016). The effectiveness, costs and coastal protection benefits of natural and nature-based defences. *PLoS ONE*, *11*(5), 1–17.

National Biodiversity Network. (2017). Retrieved November 16, 2017, from http://www.iobis.org/explore/#/taxon/763279

Nepf, H. M. (1999). Drag, turbulence, and diffusion in flow through emergent vegetation. *Water Resource Research*, *35*(2), 479–489.

Nepf, Heidi M. (2012a). Flow and Transport in Regions with Aquatic Vegetation. *Annual Review of Fluid Mechanics*, *44*, 123–142. http://doi.org/10.1146/annurev-fluid-120710-101048

Nepf, Heidi M. (2012b). Hydrodynamics of vegetated channels. *Journal of Hydraulic Research*, *50*(3), 262–279.

Neumeier, U., & Amos, C. L. (2006). The influence of vegetation on turbulence and flow velocities in European salt-marshes. *Sedimentology*, *53*(2), 259–277.

Neumeier, U., & Ciavola, P. (2004). Flow Resistance and Associated Sedimentary Processes in a Spartina maritima Salt-Marsh. *Journal of Coastal Research*, *20*(2), 435–447.

Nicholls, R. J., Wong, P. P., Hay, J., McLean, R., Ragoonaden, S., & Woodroffe, C. D. (2007). *Coastal systems and low-lying areas. Climate Change 2007: Impacts, Adaptation and Vulnerability. Contribution of Working Group II to the Fourth Assessment Report on the Intergovernmental Panel on Climate Change*. Cambridge, UK: Cambridge University Press.

Nordlund, Lina M., Unsworth, R. K. F., Gullström, M., & Cullen-Unsworth, L. C. (2018). Global significance of seagrass fishery activity. *Fish and Fisheries*, *19*(3), 399–412.

Nordlund, Lina Mtwana, Jackson, E. L., Nakaoka, M., Samper-Villarreal, J., Beca-Carretero, P., & Creed, J. C. (2018). Seagrass ecosystem services – What's next? *Marine Pollution Bulletin*, *134*(April 2017), 145–151.

Nordlund, Lina Mtwana, Koch, E. W., Barbier, E. B., & Creed, J. C. (2016). Seagrass ecosystem services and their variability across genera and geographical regions. *PLoS ONE*, *11*(10), 1–23.

Nowell, A. R. M., & Jumars, P. A. (1987). Flumes : theoretical and experimental consideration for simulation of benthic environments. *Oceanography Marine Biology Annual Revision*, *25*, 91–112.

Ondiviela, B., Losada, I. J., Lara, J. L., Maza, M., Galván, C., Bouma, T. J., & van Belzen, J. (2014). The role of seagrasses in coastal protection in a changing climate. *Coastal Engineering*, *87*, 158–168.

Paphitis, D., & Collins, M. B. (2001). The 5 m Long Recirculating Flume, at the School of Ocean and Earth Science (SOES), University of Southampton (UK). Part I: Descriptive Manual. National Oceanographic Library, Southampton Oceanography Centre, *a*, 22.

Paquier, A.-E., Meulé, S., Anthony, E. J., & Bernard, G. (2014). Sedimentation and erosion patterns in a low shoot-density Zostera noltii meadow in the fetch-limited Berre lagoon, Mediterranean France. *Journal of Coastal Research*, (Special Issue No. 70), 563–567.

Park, S. R., Kim, S., Kim, Y. K., Kang, C. K., & Lee, K. S. (2016). Photoacclimatory responses of Zostera marina in the intertidal and subtidal zones. *PLoS ONE*, *11*(5), 1–16.

Passarelli, C., Olivier, F., Paterson, D. M., Meziane, T., & Hubas, C. (2014). Organisms as cooperative ecosystem engineers in intertidal flats. *Journal of Sea Research*, *92*(September 2014), 92–101.

Paul, M., Bouma, T. J., & Amos, C. L. (2012). Wave attenuation by submerged vegetation: Combining the effect of organism traits and tidal current. *Marine Ecology Progress Series*, *444*(January), 31–41.

Paul, Maike. (2011). *The role of Zostera noltii in wave attenuation*. University of Southampton.

Paul, Maike, & Amos, C. L. (2011). Spatial and seasonal variation in wave attenuation over Zostera noltii. *Journal of Geophysical Research*, *116*(C8), C08019.

Paul, Maike, & Gillis, L. G. (2015). Let it flow: how does an underlying current affect wave propagation over a natural seagrass meadow? *Marine Ecology Progress Series*, *523*, 57–70.

Paul, Maike, Rupprecht, F., Möller, I., Bouma, T. J., Spencer, T., Kudella, M., … Schimmels, S. (2016). Plant stiffness and biomass as drivers for drag forces under extreme wave loading: A flume study on mimics. *Coastal Engineering*, *117*, 70–78.

Pedreros, R., Howa, H. L., & Michel, D. (1996). Application of grain size trend analysis for the determination of sediment transport pathways in intertidal areas. *Marine Geology*, *135*(1–4), 35–49.

Peralta, G., Pérez-Lloréns, J. L., Hernández, I., Brun, F., Vergara, J. J., Bartual, A., … García, C. M. (2000). Morphological and physiological differences between two morphotypes of Zostera noltii Hornem. from the south-western Iberian Peninsula. *Helgoland Marine Research*, *54*, 80–86.

Peralta, G., Van Duren, L. A., Morris, E. P., & Bouma, T. J. (2008). Consequences of shoot density and stiffness for ecosystem engineering by benthic macrophytes in flow dominated areas: A hydrodynamic flume study. *Marine Ecology Progress Series*, *368*(September), 103–115.

Pethick, J. (2001). Coastal management and sea-level rise. *Catena*, *42*(2–4), 307–322. http://doi.org/10.1016/S0341-8162(00)00143-0

Pettijohn, F. J., & Ridge, J. D. (1932). A textural variation series of beach sands from Cedar Point, Ohio. *Journal of Sedimentary Research*, *2*(2).

Philippart, C. J. M. (1995). Seasonal variation in growth and biomass of an intertidal Zostera noltii stand in the Dutch wadden sea. *Netherlands Journal of Sea Research*, *33*(2), 205–218.

Plomaritis, T. A., Paphitis, D., & Collins, M. (2008). The use of grain size trend analysis in macrotidal areas with breakwaters: Implications of settling velocity and spatial sampling density. *Marine Geology*, *253*(3–4), 132–148.

Poizot, E., Mear, Y., Thomas, M., & Garnaud, S. (2006). The application of geostatistics in defining the characteristic distance for grain size trend analysis. *Computers and Geosciences*, *32*(3), 360–370.

Poizot, Emmanuel, Anfuso, G., Méar, Y., & Bellido, C. (2013). Confirmation of beach accretion by grain-size trend analysis: Camposoto beach, Cádiz, SW Spain. *Geo-Marine Letters*, *33*(4), 263–272.

Poizot, Emmanuel, Méar, Y., & Biscara, L. (2008). Sediment Trend Analysis through the variation of granulometric parameters: A review of theories and applications. *Earth-Science Reviews*, *86*(1–4), 15–41.

Polte, P., & Asmus, H. (2006). Intertidal seagrass beds (Zostera noltii) as spawning grounds for transient fishes in the Wadden Sea. *Marine Ecology Progress Series*, *312*, 235–243.

Potouroglou, M., Bull, J. C., Krauss, K. W., Kennedy, H. A., Fusi, M., Daffonchio, D., … Huxham, M. (2017). Measuring the role of seagrasses in regulating sediment surface elevation. *Scientific Reports*, *7*(1), 1–11.

Poulos, S. E., & Ballay, A. (2010). Grain-Size Trend Analysis for the Determination of Non-Biogenic Sediment Transport Pathways on the Kwinte Bank (southern North Sea), in Relation to Sand Dredging. *Journal of Coastal Research*, (51), 87–92.

Prabakhara, R. A. (2001). Grain size parameters in the interpretation of depositional environments of coastal sediments between Bendi Creek and Vamsadhara river, East Coast, India. *Jour. Indian Assoc. Sedimentologists*, *20*, 106–116.

Prager, E. J., & Halley, R. B. (1999). The Influence of Seagrass on Shell Layers and Florida Bay Mudbanks. *Journal of Coastal Research*, *15*(4), 1151–1162.

Pujol, D., Casamitjana, X., Serra, T., & Colomer, J. (2013). Canopy-scale turbulence under oscillatory flow. *Continental Shelf Research*, *66*, 9–18.

Raffaelli, D., & Hawkins, S. J. (1996). *Intertidal Ecology*. London: Chapman & Hall. http://doi.org/10.1007/978-94-009-1489-6

Rasheed, M. a., McKenna, S. a., Carter, A. B., & Coles, R. G. (2014). Contrasting recovery of shallow and deep water seagrass communities following climate associated losses in tropical north Queensland, Australia. *Marine Pollution Bulletin*, *83*(2), 491–499.

Reidenbach, M. A., & Thomas, E. L. (2018). Influence of the Seagrass , Zostera marina, on Wave Attenuation and Bed Shear Stress Within a Shallow Coastal Bay. *Frontiers in Marine Science*, *5*(October), 1–16.

Rodríguez-Salinas, P., Riosmena-Rodríguez, R., Hinojosa-Arango, G., & Muñiz-Salazar, R. (2010). Restoration experiment of Zostera marina L. in a subtropical coastal lagoon. *Ecological Engineering*, *36*(1), 12–18.

Román, J. M. P., & Achab, M. (1999). Grain-size trends associated with sediment transport patterns in Cadiz Bay (southwest Iberian Peninsula). *Boletino Del Instituto Espanol De Oceanografia*, *15*((1-4)), 269–282.

Rouse, J. W., Haas, R. H., Schell, J. A., & Deering, D. W. (1974). Monitoring vegetation systems in the Great Plains with ERTS. In *3rd ERTS Symposium, NASA SP-351 I* (pp. 309–317).

Ruberti, D., Vigliotti, M., Di Mauro, A., Chieffi, R., & Di Natale, M. (2018). Human influence over 150 years of coastal evolution in the Volturno delta system (southern Italy). *Journal of Coastal Conservation*, *22*(5), 897–917.

Rupprecht, F., Möller, I., Paul, M., Kudella, M., Spencer, T., van Wesenbeeck, B. K., … Schimmels, S. (2017). Vegetation-wave interactions in salt marshes under storm surge conditions. *Ecological Engineering*, *100*, 301–315.

Salvador de Paiva, J. N., Walles, B., Ysebaert, T., & Bouma, T. J. (2018). Understanding the conditionality of ecosystem services: The effect of tidal flat morphology and oyster reef characteristics on sediment stabilization by oyster reefs. *Ecological Engineering*, *112*(October 2016), 89–95.

Schanz, A., & Asmus, H. (2003). Impact of hydrodynamics on development and morphology of intertidal seagrasses in the Wadden Sea. *Marine Ecology Progress Series*, *261*(August), 123–134.

SCOPAC. (2012). Sediment Transport Study. Retrieved September 29, 2015, from https://www.scopac.org.uk/sts/ne-iow.html

Scott, T., Masselink, G., O'Hare, T., Saulter, A., Poate, T., Russell, P., … Conley, D. (2016). The extreme 2013/2014 winter storms: Beach recovery along the southwest coast of England. *Marine Geology*, *382*, 224–241.

Shi, Z., Pethick, J. S., & Pye, K. (1995). Flow structure in and above the various heights of a saltmarsh canopy: a laboratory flume study. *Journal of Coastal Research*, 1204–1209.

Sholihah, R. I., Trisasongko, B. H., Shiddiq, D., Iman, L. O. S., Kusdaryanto, S., Manijo, & Panuju, D. R. (2016). Identification of Agricultural Drought Extent Based on Vegetation Health Indices of Landsat Data: Case of Subang and Karawang, Indonesia. *Procedia Environmental Sciences*, *33*, 14–20.

Short, F. T., Coles, R., Fortes, M. D., Victor, S., Salik, M., Isnain, I., … Seno, A. (2014). Monitoring in the Western Pacific region shows evidence of seagrass decline in line with global trends. *Marine Pollution Bulletin*, *83*(2), 408–416. h

Sillmann, J., & Roeckner, E. (2008). Indices for extreme events in projections of anthropogenic climate change. *Climatic Change*, *86*(1–2), 83–104. http://doi.org/10.1007/s10584-007-9308-6

Soulsby, R. (1997). *Dynamics of marine sands: a manual for practical applications*. Thomas Telford.

Stratigaki, V., Manca, E., Prinos, P., Losada, I. J., Lara, J. L., Sclavo, M., … Sánchez-Arcilla, A. (2011). Large-scale experiments on wave propagation over Posidonia oceanica. *Journal of Hydraulic Research*, *49*(sup1), 31–43.

Sundblad, G., & Bergström, U. (2014). Shoreline development and degradation of coastal fish reproduction habitats. *Ambio*, *43*(8), 1020–1028.

Suykerbuyk, W., Govers, L. L., Bouma, T. J., Giesen, W. B. J. T., de Jong, D. J., van de Voort, R., … van Katwijk, M. M. (2016). Unpredictability in seagrass restoration: analysing the role of positive feedback and environmental stress on Zostera noltii transplants. *Journal of Applied Ecology*, *53*(3), 774–784.

Temmerman, S., Meire, P., Bouma, T. J., Herman, P. M. J., Ysebaert, T., & De Vriend, H. J. (2013). Ecosystem-based coastal defence in the face of global change. *Nature*, *504*(7478), 79–83.

Terrados, J, Duarte, C. ., Kamp-Nielsen, L., Agawin, N. S. R., Gacia, E., Lacap, D., … Greve, T. (1999). Are seagrass growth and survival constrained by the reducing conditions of the sediment? *Aquatic Botany*, *65*(1–4), 175–197.

Terrados, Jorge, & Duarte, C. M. (2000). Experimental evidence of reduced particle resuspension within a seagrass (Posidonia oceanica L.) meadow. *Journal of Experimental Marine Biology and Ecology*, *243*, 45–53.

Thompson, C. E. L., Amos, C. L., Angelaki, M., Jones, T. E. R., & Binks, C. E. (2006). An evaluation of bed shear stress under turbid flows. *Journal of Geophysical Research*, *111*(C4), C04008.

Thompson, C. E. L., Williams, J. J., Metje, N., Coates, L. E., & Pacheco, A. (2012). Turbulence based measurements of wave friction factors under irregular waves on a gravel bed. *Coastal Engineering*, *63*(January), 39–47.

Thompson, Charlotte E. L., Amos, C. L., & Umgiesser, G. (2004). A comparison between fluid shear stress reduction by halophytic plants in Venice Lagoon , Italy and Rustico Bay , Canada — analyses of in situ measurements. *Journal of Marine Systems*, *51*, 293–308.

Thompson, R. C., Crowe, T. P., & Hawkins, S. J. (2002). Rocky intertidal communities: past environmental changes, present status and predictions for the next 25 years. *Environmental Conservation*, *29*(2), 168–191.

Tonks, V. L. (2008). *An Investigation Into The Sediment Processes On Ryde Sandflat Using Grain Trend Analysis*. University of Southampton.

Tucker, M. E. (2009). *Sedimentary petrology: an introduction to the origin of sedimentary rocks*. John Wiley & Sons.

Udden, J. A. (1914). Mechanical composition of clastic sediments. *Bulletin of the Geological Society of America*, *25*, 655–744.

Valle, M., Borja, Á., Chust, G., Galparsoro, I., & Garmendia, J. M. (2011). Modelling suitable estuarine habitats for Zostera noltii, using Ecological Niche Factor Analysis and Bathymetric LiDAR. *Estuarine, Coastal and Shelf Science*, *94*(2), 144–154.

Valle, M., Chust, G., del Campo, A., Wisz, M. S., Olsen, S. M., Garmendia, J. M., & Borja, Á. (2014). Projecting future distribution of the seagrass Zostera noltii under global warming and sea level rise. *Biological Conservation*, *170*, 74–85.

van Katwijk, M. M., Bos, A. R., de Jonge, V. N., Hanssen, L. S. A. M., Hermus, D. C. R., & de Jong, D. J. (2009). Guidelines for seagrass restoration: Importance of habitat selection and donor population, spreading of risks, and ecosystem engineering effects. *Marine Pollution Bulletin*, *58*(2), 179–188.

van Katwijk, M. M., Bos, A. R., Hermus, D. C. R., & Suykerbuyk, W. (2010). Sediment modification by seagrass beds: Muddification and sandification induced by plant cover and environmental conditions. *Estuarine, Coastal and Shelf Science*, *89*(2), 175–181.

Van Lancker, V., Lanckneus, J., Hearn, S., Hoekstra, P., Levoy, F., Miles, J., … Whitehouse, R. (2004). Coastal and nearshore morphology, bedforms and sediment transport pathways at Teignmouth (UK). *Continental Shelf Research*, *24*(11), 1171–1202.

van Rijn, L. C. (1993). *Principles of Sediment Transport in Rivers, Estuaries and Coastal Seas*. Amsterdam: Aqua Publications.

Vannoppen, W., De Baets, S., Keeble, J., Dong, Y., & Poesen, J. (2017). How do root and soil characteristics affect the erosion-reducing potential of plant species? *Ecological Engineering*, *109*(January), 186–195.

Vermaat, J. E., & Verhagen, F. C. A. (1996). Seasonal variation in the intertidal seagrass Zostera noltii Hornem.: coupling demographic and physiological patterns. *Aquatic Botany*, *52*(4), 259–281.

Wang, Y. P., Gao, S., Jia, J., Thompson, C. E. L., Gao, J., & Yang, Y. (2012). Sediment transport over an accretional intertidal flat with influences of reclamation, Jiangsu coast, China. *Marine Geology*, *291–294*, 147–161.

Ward, K., Callaway, J. C., & Zedler, J. B. (2003). Episodic colonization of an intertidal mudflat by cordgrass (Spartina foliosa) at Tijuana Estuary. *Estuaries*, *26*(1), 116–130.

Ward, L. G., Kemp, W. M., & Boynton, W. R. (1984). The Influence of Waves and Seagrass Communities On Suspended Particulates In An Estuarine Embayment. *Marine Geology*, *59*, 85–103.

Waycott, M., Duarte, C. M., Carruthers, T. J. B., Orth, R. J., Dennison, W. C., Olyarnik, S., … Williams, S. L. (2009). Accelerating loss of seagrasses across the globe threatens coastal ecosystems. *Proceedings of the National Academy of Sciences of the United States of America*, *106*(30), 12377–12381.

Wentworth, C. K. (1922). A Scale of Grade and Class Terms for Clastic Sediments Author (s): Chester K . Wentworth Published by : The University of Chicago Press Stable URL : http://www.jstor.org/stable/30063207 . *The Journal of Geology*, *30*(5), 377–392.

Whitfield, A. K. (2017). The role of seagrass meadows, mangrove forests, salt marshes and reed beds as nursery areas and food sources for fishes in estuaries. *Reviews in Fish Biology and Fisheries*, *27*(1), 75–110.

Widdows, J., Pope, N. D., & Brinsley, M. D. (2008). Effect of Spartina anglica stems on near-bed hydrodynamics, sediment erodability and morphological changes on an intertidal mudflat. *Marine Ecology Progress Series*, *362*(2005), 45–57.

Wilkie, L., O'Hare, M. T., Davidson, I., Dudley, B., & Paterson, D. M. (2012). Particle trapping and retention by Zostera noltii: A flume and field study. *Aquatic Botany*, *102*, 15–22.

Winterwerp, J. C. (2011). *Treatise on Estuarine and Coastal Science*. *Treatise on Estuarine and Coastal Science*. Elsevier.

Yager, E. M., & Schmeeckle, M. W. (2013). The influence of vegetation on turbulence and bed load transport. *Journal of Geophysical Research: Earth Surface*, *118*(3), 1585–1601.

Zhang, W., Zheng, J., Xiaomei, J., Hoitink, A. J. F., van der Vegt, M., & Zhu, Y. (2013). Surficial sediment distribution and the associated net sediment transport pattern in the Pearl River Estuary, South China. *Continental Shelf Research*, *61–62*, 41–51.

Zhang, Y., Lai, X., & Jiang, J. (2015). The impact of plant morphology on flow structure: comparative analysis of two types of submerged flexible macrophyte. *Hydrological Sciences Journal*, (October).